Engineering new approaches for pathogen separation and detection to tackle antimicrobial resistance

Andrew G. Farthing, MBiochem

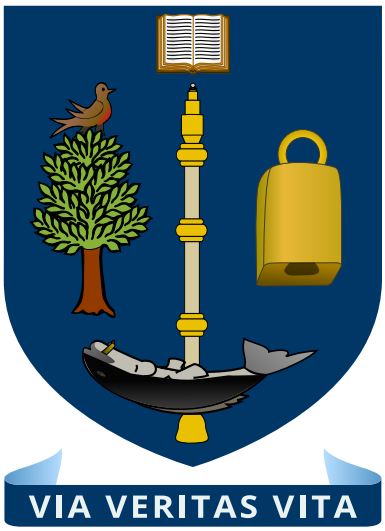

James Watt School of Engineering

College of Science and Engineering

University of Glasgow

Submitted in fulfilment of the requirements for the degree of

Doctor of Philosophy

February 2024

Abstract

Sepsis and antimicrobial resistance are global health crises. Sepsis, defined as a life-threatening, dysregulated host response to infection, is responsible for one fifth (11 million) of all global deaths. The importance of immediate antimicrobial therapy in sepsis management is well documented, with 80% of patients surviving if they receive adequate antimicrobial therapy within one hour of documented hypotension. For each hour of subsequent delay for the following 6 hours there is an associated decrease in survival of 7.6%; at this rate, the chance of surviving more than 30 hours is less than 10%. This reliance on rapid, broad spectrum antimicrobial therapy necessary to treat sepsis accelerates the spread of resistance which is predicted to result in one death every 3 seconds due to a drug-resistant infection by 2050, resulting in 10 million more global deaths each year. Rapid and accurate pathogen identification remains a significant challenge in sepsis management due to the low concentration of pathogens in the bloodstream (1-1000 colony forming units/ml). This necessitates a lengthy blood culture step which typically takes 1-5 days. This thesis addresses the diagnostic bottleneck in sepsis treatment by exploring innovative methods for pathogen detection and separation. Focusing on the Glasgow Royal Infirmary's clinical diagnostics workflow, I aimed to develop a novel sample preparation assay for blood samples by leveraging Toll-like Receptors 2, 4 and 9. These receptors, known for their broad pathogen recognition capabilities, were investigated for their potential to bind and detect Gram-positive bacteria, Gram-negative bacteria, and microbial DNA directly from blood samples. By exploiting the advantages of imaging flow cytometry for high-throughput detection of small particles, I developed and optimised assays to accurately quantify the binding capacity of TLRs to whole bacteria, and pathogen DNA. This work highlights the diagnostic and therapeutic potential of Toll-like receptors to be used, not only for pathogen detection, but also as possible biomarkers for the sepsis immune response, offering a novel, double-edged approach to diagnostics. Further optimisation may one day reduce the need for lengthy blood cultures, facilitating antimicrobial stewardship and helping pave the way for more effective sepsis management.

Contents

List of Tables

List of Figures

Acknowledgements

This journey would not have been possible without the support and contributions of many, for which I am deeply grateful. Firstly, I extend my sincere thanks to Dr. Melanie Jimenez, whose dedication to this project was undeniable. Her commitment provided me with invaluable opportunities to present our work at conferences, enriching my research experience and academic growth. I am thankful for the rigorous engagement and the high standards she set, which, while challenging, have undoubtedly contributed to my development as a researcher.

I am also grateful to Professor Carl Goodyear for giving me the opportunity to work within his lab over the past five years. The lab environment, alongside the camaraderie and collaboration with the group members, was highly conducive to my research. Access to such a resourceful setting has been instrumental in the progression of my work, and for that, I am truly appreciative.

Special thanks are owed to Professor Alasdair Clark, who, upon Dr. Jimenez's departure from the University of Glasgow, kindly welcomed me into his group. Professor Clark's support, especially during the extended phases of my project, were crucial in maintaining my momentum and morale.

I would also like to express my gratitude to the Division of Biomedical Engineering and the School of Infection and Immunity at the University of Glasgow for providing a stimulating academic environment. I would like to thank the LKAS fellowship for financial support; their backing has been essential in the pursuit and fulfilment of my research objectives.

The interdisciplinary nature of this project benefited immensely from the technical expertise and support across many different fields. This support was provided by a number of specific individuals to whom I would like to take this opportunity to thank.

I am particularly thankful to Dr. Will Peveler, for his invaluable support in chemistry. His insightful feedback on key results chapters gave a fresh perspective when it was needed most and this greatly enhanced my motivation during the

final stages of writing. My appreciation extends to Professor Rick Maizels, who generously welcomed me into his group during the initial months of my project. I cannot thank Nic Britton and Dr. Danielle Smyth enough for their unmatched help during those first few months. Their expertise was pivotal in overcoming early challenges in the lab.

Special thanks go to Dr. Michael Murphy and Dr. Simon Pybus, whose collaboration made our work at the Glasgow Royal Infirmary feasible. Their assistance in planning and executing clinical experiments laid the groundwork for the subsequent phases of my research. I am grateful to Professor Julien Reboud and Dr. Ngo Tat Trung for the wonderful opportunity to test LFT/LAMP devices at the 108 Central Military Hospital in Hanoi, Vietnam. This greatly enjoyable experience was instrumental in broadening the application of our findings.

Alana Hamilton and Diane Vaughan provided an enormous amount of help with planning and executing flow cytometry experiments during my final few months in the lab. Our time at the CYTO conference was unforgettable, thanks to Alana's great company. I also want to express my gratitude to Dr. Jenny Gracie, with whom I thoroughly enjoyed working on the quantum dot experiments. Our collaboration was one of the highlights of my research journey. An important mention to Dana Aghabi, whose invaluable assistance with TLRs and beads during the summer of 2019 was indispensable to our progress. Her contribution to our project was beyond what could be expected and added significant value to our research. I am thankful for Alex Harrison, a summer student whose help was much appreciated.

Finally, John Cole deserves a special thank you for providing me with opportunities to develop my programming skills through demonstrating for his R course, sparking an interest I plan to pursue further. The trip to the BSI conference and the evenings spent discussing our research and future aspirations in the pub were both enriching and memorable.

Each of you has played a pivotal role in the success of this project. Thank you.

The support, camaraderie, and friendship I have received from my colleagues have been a cornerstone of my PhD experience, making my journey not just productive but also enjoyable. I am profoundly grateful to the members of Carl's group: Dr. Yuriko Yamamura, Dr. Shatakshi Sood, Dr. Cecilia Ansalone, Dr. Aysin Tulunay Virlan and Dr. Lauren Kelly, for their support and help. Dr. Kieran Woolcock, Patricia Riedlová, Maria-Laura Vieri, and Annie Peacock also deserve special mention for contributing to the vibrant and supportive atmosphere of our group, which also extended to the pub.

Lastly to the members of the Jimenez lab: Jessie Howell has been a true friend during our time working in Melanie's group. Her unforgettable company shone during the hilarity of the CYTO conferences, coupled with her help and support throughout, made those experiences significantly better. Jessie, thank you for the laughter, drinks, insights, and enduring friendship. Sulo Omwenga's kindness was greatly appreciated when it came to those cake vouchers; they were a much-needed boost during the long days. To Alex Dobrea, Rui Sousa, Nicole Hall, and Kimberley Jordan - your support has made all the difference.

My journey through the PhD would have been significantly harder and less joyful without the presence and support of my friends, who have provided companionship, perspective, and unwavering support.

Nik Panayotov and Lina Panayotova, your ability to provide me with a sense of perspective during challenging times has been a gift, and I am deeply grateful for it. Dr. Kieran Woolcock, thank you for the friendship that has sustained me, the bike rides that offered much-needed breaks from the rigours of research and your insightful feedback during the final push at the end. Dr. Hannah Craven, not just the best flatmate one could ask for but also a constant source of hilarity and laughter. Living together has been one of the highlights of my PhD life. To Dev Sanders, Dani Rosati, Thomas Bartlome, Liv Lynch, Rhona Macfarlane, Dr. Chris Bigley, Dr. George Finney, Dr. Holly Webster, Hannah Bialic, Dr. Sara Bartlome, Dr. Joe Jones, and Dr. Hannah Baer - our trips, dinners, beers, and laughs provided an essential balance, reminding me of the world beyond academia. Dr. Alfonso Martinez Carmena, from long lunches to even longer hikes, your unforgettable companionship has been a source of joy and adventure. Ryan Glossop, one of my oldest friends, our moaning sessions in the pub have been therapeutic, providing a space to vent and laugh about our struggles. Hannah Johnson, thank you for your persistent Skype catch-ups, the surprise visits and the hikes, especially during the most taxing times. You're always welcome in Glasgow. Gaynor Evans MBE, your friendship, laughter support and delicious meals during the final stages of the writing process, were nothing short of a lifeline.

To each of you, and to those not named but who have been part of this journey, thank you from the bottom of my heart.

To my family, whose love and support have been my anchor throughout this journey, I owe an immeasurable debt of gratitude.

To Mum and Dad, Liz and Chris Farthing, your unconditional support has been the foundation of everything I am today. You have always encouraged me to pursue my passions, aim for the top, and never settle for anything less than my best. Your belief in me has been a constant source of strength and motivation, especially during the most difficult times. To my sister, Rebecca, your support has been unwavering, and I hope to inspire you just as much as you've inspired me. Josh, your support through this journey has been invaluable. Gwyneth Thompson, you have been part of my academic journey since you got your first computer around the time I went to York 10 years ago. My pen friend and great aunty, from the memories we made during your visit to Glasgow in 2019 with Uncle Ron and Big Alex, to the unforgettable times we spent together last year in Kingston after the conference in Montreal. To Lorrie, Hannah, Tom, Jade, and Jack, thank you for welcoming me into your family with open arms, making me feel at home. Brian, Andrea, Hayley, your warmth and inclusion have made every holiday, birthday, and celebration even more special. I look forward to making many more memories with all of you.

Lou, words cannot fully capture the depth of my gratitude towards you. You've been my rock, bearing the brunt of this PhD journey more than anyone else. Your limitless support, understanding, and love have been the essence of my ability to persevere. Now, as I close this chapter, it's my turn: It's finally done, and we can now look forward to moving on with our lives.

To my entire family, your love has been the most precious resource throughout my PhD. Thank you for everything.

Andrew Farthing
University of Glasgow
2024

Author's Declaration

I declare that, except where explicit reference is made to the contribution of others, that this dissertation is the result of my own work and has not been submitted for any other degree at the University of Glasgow or any other institution.

.....

A. Farthing

List of Abbreviations

ACPA . . . . . Anti-Citrullinated Protein Antibodies

AF647 . . . . . Alexa-Fluor 647 nm

AFM . . . . . Atomic Force Microscopy

AMR . . . . . Antimicrobial Resistance

APC . . . . . Antigen Presenting Cell

ARDS . . . . . Acute Respiratory Damage Syndrome

AST . . . . . Antimicrobial Susceptibility Test

BA . . . . . Blood Agar

BC . . . . . Blood Culture

BF . . . . . Brightfield

BSA . . . . . Bovine Serum Albumin

BSI . . . . . Bloodstream Infection

BSL . . . . . Biological Safety Level

CDS . . . . . Coding Sequence

CFC . . . . . Conventional Flow Cytometry

CFU . . . . . Colony Forming Units

Ch . . . . . Channel (**e.g.** Ch05)

CHCA . . . . . α-Cyano-4-Hydroxycinnamic Acid

CLED . . . . . Cystine Lactose Electrolyte Deficient

CMI . . . . . Cell-Mediated Immunity

COPD . . . . . Chronic Obstructive Pulmonary Disease

CpG . . . . . Cytosine-phosphate-Guanine

CRE . . . . . Carbapenem-Resistant *Enterobacteriaceae*

CT . . . . . Cycle Threshold

CTD . . . . . C-Terminal Domain

DAMP . . . . Damage-Associated Molecular Pattern

DAPI . . . . . 4',6-diamidino-2-phenylindole

DC . . . . . Dendritic Cell

DIC . . . . . Disseminated Intravascular Coagulation

DIT . . . . . Disseminated Intravascular Microthrombosis

DMSO . . . . . Dimethylsulfoxide

ECDC . . . . . European Centre for Disease Prevention and Control

EDTA . . . . . Ethylenediamine Tetra-acetic Acid

EIS . . . . . Electronic Impedance Spectroscopy

ELISA . . . . . Enzyme-Linked Immunosorbent Assay

EMSA . . . . . Electromobility Shift Assay

ER . . . . . Endoplasmic Reticulum

EUCAST . . . European Committee Antimicrobial Susceptibility Testing

FBS . . . . . Foetal Bovine Serum

GFP . . . . . Green Fluorescent Protein

GRI . . . . . Glasgow Royal Infirmary

GSH . . . . . Glutathione (reduced)

HC . . . . . Healthy Control

HO . . . . . Hydroxide

HRP . . . . . Horse Raddish Peroxidase

ICU . . . . . Intensive Care Unit

IDT . . . . . Integrated DNA Technologies

IFC . . . . . Imaging Flow Cytometry

IFN . . . . . Interferon

IgG . . . . . Immunoglobulin G

IL . . . . . Interleukin

IMS . . . . . Immunomagnetic Separation

IRAK . . . . . Interleukin-1 Receptor Associated Kinase

ITC . . . . . Isothermal Titration Calorimetry

LAMP . . . . . Loop-Mediated Isothermal Amplification

LB . . . . . Luria Broth

LBP . . . . . LPS Binding Protein

LFT . . . . . Lateral Flow Test

LMIC . . . . . Lower-Middle Income Country

LoD . . . . . Limit of Detection

LPS . . . . . Lipopolysaccharide

LTA . . . . . Lipoteichoic Acid

MALDI . . . . Matrix-assisted Laser Desorption Ionisation

MALDI-TOF Matrix-assisted Laser Desorption Ionisation Time-of-Flight

MAP . . . . . Mean Arterial Pressure

MBL . . . . . Mannose Binding Lectin

MCLB . . . . . Mammalian Cell Lysis Buffer

MDB . . . . . Methyl Binding Domain

MD2 . . . . . Myeloid Differentiation factor 2

MFI . . . . . Mean Fluorescence Intensity

MIC . . . . . Minimum Inhibitory Concentration

MS . . . . . Multiple Sclerosis

MST . . . . . Microscale Thremophoresis

MODS . . . . . Multiple Organ Dysfunction Syndrome

NEB . . . . . New England Biolabs

NFκB . . . . . Nuclear Factor Kappa-light-chain-enhancer of activated B cells

NGS . . . . . Next Generation Sequencing

NHS . . . . . National Health Service

NOD . . . . . Nucleotide Oligomerisation Domain

NTA . . . . . Nitrilotriacetic Acid

OD . . . . . Optical Density

PAMP . . . . . Pathogen-Associated Molecular Pattern

PBMC . . . . Peripheral Blood Mononuclear Cell

PBS . . . . . Phosphate-Buffered Saline

PCB . . . . . Printed Circuit Board

PCR . . . . . Polymerase Chain Reaction

PDB . . . . . Protein Database

PEG . . . . . Polyethylene Glycol

PICS . . . . . Persistent Inflammation, Immunosuppression and Catabolism Syndrome

PJI . . . . . Prosthetic Joint Infection

PoC . . . . . Point of Care

PRR . . . . . Pathogen Recognition Receptor

QD . . . . . Quantum Dots

QUALY . . . . Quality-Adjusted Life-Years

RA . . . . . Rheumatoid Autoimmune

RFU . . . . . Relative Fluorescent Units

RMS . . . . . Root Mean Square

RT . . . . . Room Temperature

SEAP . . . . . Secreted Embryonic Alkaline Phosphatase

SIRS . . . . . Systemic Inflammatory Response Syndrome

SL . . . . . Selective Lysis

SLE . . . . . Systemic Lupus Erythematosus

SOD . . . . . Superoxide Dismutase

SOFA . . . . . Sequential Organ Failure Assessment

SPR . . . . . Surface Plasmon Resonance

SSC . . . . . Side Scatter

SVR . . . . . Systemic Vascular Resistance

TAK . . . . . TGFβ-Activated protein Kinase

TIR . . . . . Toll/interleukin 1 (IL-1) Receptor

TLR . . . . . Toll-like Receptor

TNF . . . . . Tumour Necrosis Factor

TRIC . . . . . Temperature-Induced Fluorescence Change

ULVWF . . . . Unusually Large von Willebrand Factor Multimers

UDG . . . . . Uracil-DNA Glycosylases

WBC . . . . . White Blood Cell

WHO . . . . . World Health Organisation

WT . . . . . Wild-Type

1

Chapter 1 - Introduction

1.1 Part I: Sepsis

1.1.1 Sepsis and the link to antimicrobial resistance

Sepsis, under the 'Sepsis-3' diagnostic criteria, is currently defined not as a particular disease in itself, but a syndrome involving a constellation of different symptoms resulting in life-threatening organ dysfunction caused by a dysregulated host response to infection (Singer et al. 2016). The World Health Organisation (WHO) recently identified sepsis as a global health priority (World Health Organisation 2020). According to one study carried out in 2016, there are 5.3 million deaths caused by sepsis globally, each year. This equates to approximately one death every 4 hours in Scotland, a statistic which can be found advertised in hospital waiting rooms across the country (Scottish Government 2019). Frighteningly, after a more recent update, the true annual global death rate may be closer to double this previous estimate. By including multiple causes of death from 109 million records and broadening the study to include more data from lower-middle income countries (LMICs), there were a reported 48.9 million cases of sepsis and 11.0 million sepsis-related deaths in 2017, accounting for 19.7% of all global deaths (Rudd et al. 2020).

The lethality of sepsis is entangled with the urgency at which it progresses. Once sepsis has been diagnosed, finding the identity of the pathogen responsible for the underlying infection is the key to prescribing effective antibiotics. The time to effective antimicrobial treatment is the single biggest factor in the mortality of sepsis (Gao, Melody, et al. 2005; Mellor 2013; Seymour et al. 2017). In one study, it was found that 80% of patients survived if they received adequate antimicrobial therapy within one hour of documented hypotension. Each hour of subsequent delay for the following 6 hours was associated with an average decrease in survival of 7.6% (Kumar et al. 2006). At this rate, the chance of a patient surviving more than 10 hours without effective antimicrobial therapy is less than 50%, and the change of surviving more than 30 hours is less than 10%.

This reliance on rapid, broad spectrum antimicrobial therapy necessary to treat sepsis is one of the central drivers of antimicrobial resistance (AMR) (Niederman et al. 2021; Schultz et al. 2017). AMR is a naturally occurring phenomenon whereby microorganisms evolve to circumvent the methods used by antimicrobial therapies rendering them ineffective as treatment methods for infection. Although the WHO estimates that antimicrobial drugs have added on average 20 years to everyone's lives, AMR is now predicted to result in one person dying every 3 seconds due to a drug-resistant infection by 2050; this equates to 10 million people per year globally (O'neill 2016). Strikingly, 30-50% of all prescribed antimicrobials are not necessary according to the European Centre for Disease Prevention and Control (ECDC) (Llor et al. 2017), with this misuse of antimicrobials playing an active role in the growing and alarming threat of AMR. Although resistance exists in all microorganisms (bacteria, viruses, fungi and parasites), bacteria are of particular concern and a list of bacteria for which new antibiotics are urgently needed has been published in 2017 by the WHO (World Health Organization 2017).

1.1.1.1 The evolving definition of sepsis

The way medical professionals define sepsis has evolved over time as their understanding of the syndrome has improved, leading to regular reviews of diagnostic

criteria and treatment guidelines (Daniels et al. 2011; Cavaillon et al. 2020; Levy et al. 2003; Singer et al. 2016; Evans et al. 2021). There is sometimes confusion between sepsis and blood stream infections (BSIs). While sepsis refers to the symptoms of a dysregulated immune response to an infection, BSIs are characterised by the presence of a pathogen in the blood stream. One can have a BSI without reaching a septic state or have sepsis without detecting pathogens in the blood stream. Both conditions, however, require rapid and effective antimicrobial therapy although sepsis is considered to be more serious (Evans et al. 2021; Singer et al. 2016; Daniels et al. 2011; Levy et al. 2003). The term *septic shock* is used colloquially as a broad term to describe many aspects of the syndrome; however, it actually refers to an instance of severe sepsis specifically combined with persistent and dangerously low blood pressure (Evans et al. 2021). In this instance, vasopressors are required to sustain a mean arterial pressure >65 mmHg and when serum lactate remains > 2 mmol/l despite sufficient fluid challenge (Cavaillon et al. 2020; Singer et al. 2016).

The current criteria for sepsis diagnostics adhere to the sequential organ failure assessment (SOFA) mnemonic which factors in respiration, coagulation, liver-, cardiovascular-, renal- and central nervous system function. Each dysfunctional organ is given one point, and a SOFA score greater than 2 is associated with a mortality rate of >10% which is thus termed 'severe sepsis' (Singer et al. 2016). This update follows on from 'Sepsis-2,' which focused on onset of systemic inflammatory response syndrome (SIRS). SIRS is defined by a patient having two or more of the following: tachycardia (heart rate >90 beats/min), fever or hypothermia (temperature >38°C or <36°C), leukocytosis, tachypnoea (respiratory rate >20/min or PaCO2 <32 mm Hg (4.3 kPa)) or leukopoenia (white blood cell count >12,000/mm3 or <4,000/mm3 or >10% immature bands) (Evans et al. 2021; Singer et al. 2016). It presents a shift from what can be described as 'clinical signs' to a scoring system to assess the severity of 'organ dysfunction' with the aim to increase the specificity of diagnosis.

1.1.1.2 Limitations of the Sepsis 3 diagnostic criteria

In general, the absence of a lasting diagnostic consensus means that global, longitudinal surveillance remains a challenge and there is no consistent benchmark to which emerging technologies can be compared which creates a bottleneck at the interface between research and clinical adoption. Comparative studies have demonstrated diagnosis according to SOFA performs better, in terms of accuracy and sensitivity, at predicting patient mortality than SIRS (Bhattacharya et al. 2022; Chen, Shao, et al. 2019; Costa et al. 2018).

Some studies have suggested that the current definition and diagnostic criteria may lead to a decrease in the reported incidence of sepsis as an emphasis on organ dysfunction may preclude the early symptoms of sepsis, causing them to be missed (Cavaillon et al. 2020; Evans et al. 2021). This is particularly true in low-resource settings where, according to Rudd *et al.*, 85% of sepsis cases and sepsis-related deaths worldwide occurred in LMICs. The challenges of sepsis treatment in LMICs are numerous and varied: incorporating cost, accessibility, type and outright risk of infection (Rudd et al. 2020; Schultz et al. 2017).

For a patient to survive sepsis, hospital admission is a necessity and, as we have established, time to effective therapy plays a massive role in the chances of success (Kumar et al. 2006). Indeed, it is recommended that sepsis patients be treated in the ICU within 6 hours of diagnosis (Evans et al. 2021). The number of ICU beds in Europe/North America ranges between 5 and 30 per 100,000 people at a cost of 1% of total GDP in the USA (Halpern et al. 2004), whereas in Sub-Saharan Africa, this number is 0.1-0.2 beds per 100,000 inhabitants (Jochberger et al. 2008; Kwizera et al. 2016). Furthermore, the definition of what constitutes an ICU bed has also been brought into question (Schultz et al. 2017). Despite of this, there is evidence to suggest that the costs associated with ICU treatment in LMICs is around 5-10% those of high-resource countries (Kulkarni and Divatia 2013). Due to the significantly lower average age of a sepsis patient in LMICs, the number of quality-adjusted life-years (QUALYs) is much higher (Schultz et al.

2017). Taken together, prioritising ICU treatment during sepsis is still considered to be cost-effective overall (Schultz et al. 2017).

Early recognition of the symptoms, especially in the community remains crucial and, as such, alternative recommendations have been put forward for application in LMICs where there is a focus on physical examination, microscopy-based diagnostic assays by experienced staff are recommended as an alternative to rapid diagnostics, an initial quick-SOFA (qSOFA) assessment (blood pressure, respiratory rate and evidence of altered mental state) as opposed to more technical SOFA score, and an emphasis on identifying/ruling out some of the more common tropical diseases such as Ebola, malaria and dengue (Kwizera et al. 2016).

1.1.2 Sepsis symptoms

A *symptom* is defined as an individual's self-reported perception of an experience of disease or physical disturbance; it is therefore a subjective indication, and can include elements of fatigue, pain, and cognitive dysfunction (Dodd et al. 2001). Infections which result in sepsis are caused by pathogens such as viruses, bacteria, protozoa, parasites or fungi. These pathogens produce toxins as part of a survival and virulence strategy to infiltrate and colonise a host; these cause damage to tissues, organs and physiological processes. The body detects signs of the pathogens themselves as well as the damage they cause leading to an innate immune response. The immune response is incredibly powerful, but crucially, it is both localised to the site of infection and tightly regulated. The problem with sepsis is that when the immune response becomes dysregulated, it is no longer localised and instead becomes systemic.

A normal physiological immune response to an injury; for example, a small cut, is experienced as heat, swelling, pain and redness which is localised to the site of the injury. It is important to appreciate that inflammation is a good thing and a sign of a healthy, tightly regulated, protective response to an infection. The early warning signs of sepsis are characterised by a physiological manifestation of a delocalised, dysregulated inflammatory immune response:

- Fever (very high or very low temperature)
- Difficulty breathing
- Rapid heart rate
- Decreased urine production
- Confusion and/or slurred speech
- Cold and/or blotchy hands and feet (mottled skin) (Farthing et al. 2021)

Individually, these symptoms may appear insignificant and can be challenging to spot. The location of the infection may ultimately correlate with the most damaged organ, but not always, and initial symptoms are not necessarily related to the source of the infection (Minasyan 2019; Gao, Evans, et al. 2008). Collectively, however they may signify the beginning of a rapid and serious deterioration, and it is important to seek immediate medical attention. For this reason, efforts have been made over recent years to raise awareness of these early warning signs of sepsis in the form of government campaigns producing materials for traditional and social media, educational resources for schools and charities which fund research and conferences (Alliance 2017; Scotland 2023; Scottish Government 2019; *Sepsis Research FEAT | Sepsis Charity In UK And Awareness* 2023).

1.1.3 Causes and risk factors of sepsis

Common, communicable infections which can lead to sepsis include meningitis (inflammation of the linings of the brain) (Vergnano et al. 2005), pneumonia and lower respiratory tract infections (De Freitas Caires et al. 2018), urinary tract infections (infections of the urinary tract, bladder or kidneys) (Petrosillo et al. 2020), malaria, Dengue, HIV/AIDs and cellulitis (infection of the skin, often affecting the foot and leg) (Ladhani et al. 2021; Rudd et al. 2020); although virtually any tissue or organ has the potential to become the nidus of an infection that may result in sepsis. Pathogens can enter the body from the external environment, as

a result of injury or surgery, but also from our own commensal flora. Commensal microorganisms are non-communicable and do not usually cause harm, often existing as part of a symbiotic relationship on or in the body. Under rare circumstances however, commensal bacteria can become pathogenic; for instance, bacteria from the skin or gut enter the bloodstream through breaks in the skin (*e.g.* cuts, surgery such as joint replacement (Rutherford et al. 2016), catheterisation (Schmidt et al. 2012)) or damage to the gut lining (Sansonetti 2006). Up to 42% of sepsis cases are non-culturable, suggesting either that the causative pathogen is of viral origin (Lin, Harris, et al. 2018) or that these cases are caused by sterile inflammation.

Certain risk factors increase an individual's chance of getting an infection which may lead to sepsis or affect the immune response resulting in a worse outcome: age (neonates, infants, elderly), gender, microbiota, genetic diversity, lifestyle (smoking/alcohol consumption) *etc.* are all associated with an increased risk of sepsis (Cavaillon et al. 2020). Underlying causes can also be non-communicable *e.g.* stroke, cancer, diabetes, cirrhosis, COPD, Alzheimer's disease, chronic kidney disease, among others (Rudd et al. 2020).

1.1.4 Pathophysiology of sepsis

To gain a deeper understanding of what makes sepsis so challenging to diagnose and treat, we must explore what is happening both on a physiological level (organs and systems) and from an immunological perspective (cells and molecules).

It's only recently that sepsis has been characterised both as an immune response and an endothelial response (Chang 2019). During an innate immune response, white blood cells (leukocytes) are recruited to the site of an infection where, on recognition of a pathogen, they release pro-inflammatory cytokines and nitric oxide. Together, these cause vasodilation. It is crucial to appreciate that these processes are tightly regulated and serve a protective effect in healthy individuals. Widespread vasodilation leads to a decrease in systemic vascular resistance (SVR) which, in turn, results in a drop in blood pressure. The increased vascular diameter also causes blood vessels to become more permeable, causing fluid to leak out into the

tissues (oedema). This increases the distance oxygen must diffuse from red blood cells (RBCs) to get to cells in the tissues. A prolonged reduction in tissue perfusion in this way leads to hypoxia, a contributing factor in organ failure.

Another side effect of the systemic inflammatory response (SIRS) is the collateral damage caused to blood vessels by white blood cells (WBCs) destroying pathogens and damaging host cells. Damage to blood vessels induces the formation of microvascular thromboses (blood clots), however since this is happening systemically, the reserves of clotting factors are quickly depleted resulting in thrombocytopenia (characterised by a deficiency in platelets in 38% of sepsis patients; this correlated with increased mortality in a study by (Claushuis et al. 2016)). Naturally, the clots begin to break down and, as they cannot be repaired, blood begins to leak out of the blood vessels into the surrounding tissues. This is referred to as disseminated intravascular coagulation (DIC) or microthrombosis (DIT). Indeed, recent findings regarding the activation of the microthrombotic pathway, have shown unusually large von Willebrand factor multimers (ULVWFs) are exocytosed by endothelial cells and then become anchored to the cell surface. Here, ULVWFs recruit activated platelets and form microthromboses, in turn promoting DIC/DIT (Chang 2019).

Each of the physical symptoms experienced by the patient can be explained by the underlying combination of pathophysiological processes: namely DIC and microcirculatory dysfunction, as a result of a systemic immune response. For instance, DIC in the extremities can appear as mottled skin (Bourcier et al. 2017). In early-stage sepsis, a patient will experience a high temperature due to blood vessel dilation. As the sympathetic nervous system reacts to this decrease in SVR, it clamps the blood vessels shut (vasoconstriction) to try and increase SVR and in turn increase blood pressure. A transition from high temperature to low temperature may suggest that the patient has had sepsis for a long time. Cardiac output initially increases to compensate for decreased SVR (and decreased BP) which is characterised by a rapid heart rate (tachycardia). This does not last; eventually cardiac output drops as the heart becomes damaged due to systemic DIC and begins to fail. Likewise, the effects of dysregulated inflammation in the

brain and kidneys result in confusion and decreased urine production, respectively (Sonneville et al. 2013; Evans et al. 2021; Waterhouse et al. 2018). Vascular damage to the blood vessels in the lungs results in acute respiratory distress syndrome (ARDS), one of the common clinical signs of severe sepsis which results in the patients experiencing severe difficulties breathing (De Freitas Caires et al. 2018). Sepsis is the final common pathway to death for many diseases (Rudd et al. 2020; Paik et al. 2018). Indeed, there is significant overlap between severe COVID and viral sepsis, or sepsis caused by a respiratory infection (Li, Liu, et al. 2020; Rovas et al. 2022; Walsh et al. 2023) and with any late-stage disease there is a point at which the dying process becomes irreversible.

To summarise, the pathophysiology of sepsis is complex, involving multiple overlapping pathways. The systemic immune response causes rapid and widespread haemodynamic instability, DIC and endotheliopathy which in turn leads to decreased tissue perfusion and hypoxia; ultimately resulting in multiple organ dysfunction syndrome (MODS) and death.

1.2 Part II: The innate immune response to infection and the role of Toll-like receptors

To fully understand what goes wrong during sepsis and appreciate the disconnect between the importance of the pathogen and the lethal effects of a dysregulated immune system, it is crucial to first outline how the innate immune system works in healthy individuals.

1.2.1 A healthy immune response to infection

The main role of the innate immune system is to recognise signs of infection, in the form of *non-self* molecules, also known as pathogen-associated molecular patterns (PAMPs), whilst simultaneously ignoring the body's own *self-molecules*. On recognition of PAMPs, innate immune cells such as monocytes/macrophages, neutrophils and dendritic cells (DCs) produce pro-inflammatory cytokines (interferon-

gamma; IFNγ, tumour necrosis factor-alpha; TNFα, interleukin-1; IL-1, interleukin-6; IL6 and chemokine ligand-2; Cxcl2). These result in the common symptoms of inflammation: heat, pain, redness and swelling. In a healthy individual, the innate immune response is rapid, tightly regulated and localised to the site of infection. PAMPs are structurally-conserved molecules indicative of an infection and include molecules such as non-methylated CpG DNA in prokaryotes, ssDNA, dsRNA, ssRNA, flagellin of flagellated bacteria, lipopolysaccharide (LPS a.k.a. endotoxin) which is part of the outer membrane of Gram-negative bacteria, lipoteichoic acid (LTA) of Gram-positive bacteria cell walls, mannose, among others (Mogensen 2009).

PRRs are responsible for detecting PAMPs and can be classified into 5 main groups based on protein homology: Toll-like receptors (TLRs), nucleotide oligomerisation domain (NOD)-like receptors (NLRs), retinoic acid-inducible gene-I (RIG-I)-like receptors (RLRs), C-type lectin receptors (CLRs), and absent in melanoma-2 (AIM2)-like receptors (ALRs). All are broadly comprised of recognition domains which bind ligands (PAMPs), intermediate domains (often transmembrane) and effector domains which are involved in dimerisation and downstream signalling. TLRs, NLRs and CLRs are expressed on the surface of innate immune cells such as macrophages and DCs, in addition to eosinophils, mast cells and basophils, whereas some NLRs, RLRs and ALRs are expressed in the cytoplasm (Li and Wu 2021). This is with the exception of nucleic acid-binding TLRs (3, 7, 8 and 9) which are expressed on the endosome, lysosome or endolysosome (Duan et al. 2022; Mogensen 2009).

1.2.2 Immunology of sepsis

Upon detection of an infection, downstream signal activation results in the expression of pro-inflammatory cytokines (*e.g.* type I IFN, IL-1, IL-6, IL-12, TNF-α and IL-1ß); small ~40 kDa proteins which contribute to endocrine function and play a role in modulating the immune response (Mogensen 2009; Iwasaki and Medzhitov 2004). The key point is that, in addition to sensing PAMPs, PRRs are also able to detect certain damage-associate molecular patterns (DAMPs) which are released by apoptotic cells or damaged tissues (Federico et al. 2020; Goulopoulou et al. 2016).

DAMPs are produced in large quantities during infection due to the combined effects of direct pathogen toxicity and the collateral effects of pro-inflammatory cytokines on host cells. This initiates an autoamplification cascade which perpetuates rapidly and independently of the original pathogenic stimulus – resulting in the so-called cytokine storm (Chousterman et al. 2017).

In response to pro-inflammatory cytokines, endothelial cells increase expression of adhesion molecules (ICAM1/VCAM1) which allow immune cells to gain entry to tissues and excrete coagulatory factors (Chousterman et al. 2017). Platelets have many important immunological roles alongside clotting; they can sense infectious agents and release inflammatory mediators in response (Garraud and Cognasse 2015). They also bind to circulating neutrophils and aid in the formation of neutrophil extracellular traps (NETs) (GAWAZ et al. 1995; Clark et al. 2007). Depletion of platelets and clotting factors (throbocytopoenia) therefore represents further destabilisation of the immune response. Despite many recent advances, therapeutic strategies to mitigate the effects of the cytokine storm have been largely unsuccessful (Chousterman et al. 2017; Teijaro 2017; Cavaillon et al. 2020).

Sepsis-induced changes to red blood cells (RBCs; a.k.a. erythrocytes) promotes RBC clearance, eventually leading to haemolytic anaemia and increased mortality. Oxidative stress comes from activated neutrophils, endothelial cells, plasma and auto-oxidation of RBCs. During sepsis, erythrocytes become trapped in stopped-flow capillaries where they are in close proximity to oxo-active, pro-inflammatory neutrophils (Bateman et al. 2017).

Auto-oxidation of haemoglobin occurs under hypoxic conditions, at around 60% blood oxygen saturation (SO2) (Balagopalakrishna et al. 1996). Activated neutrophils release pro-inflammatory cytokines such as TNF, IL-1 and G-CSF. These cause NADPH oxidase to convert oxygen (O2) to the superoxide anion (O2-). This is converted to hydrogen peroxide, at which point oxidation of unliganded iron (Fe2+ to Fe3+) produces a hydroxyl radical (OH*) and hydroxide (HO). The hydroxyl radical causes DNA damage, amino acid oxidation and lipid peroxidation; the latter leading to membrane damage and decreased RBC deformability (Moutzouri et al. 2007; Lam

et al. 2021). Superoxide anion and nitric oxide becomes nitrate which is responsible for oxygen-dependent ATP efflux which plays a further role in coagulation. Bacterial virulence factors further promote oxidative stress, for example; Pyocyanin from *Pseudomonas* induces NADPH oxidase, inhibits superoxide dismutase (SOD) and inhibits catalase-mediated clearing of hydrogen peroxide (Bateman et al. 2017; Kell 2009; Joffre and Hellman 2021).

1.2.3 Toll-like receptors

TLRs, once of the five major classes of PRR introduced above, play a central role in both the innate and adaptive immune response (Duan et al. 2022; Tsujimoto et al. 2008; Akira and Takeda 2004). As a result of this, we believe that they may hold potential for pathogen identification and separation, and could help with sepsis diagnostics. TLRs for use in rapid diagnostics will be discussed at length in the introduction to Chapter 5.

1.2.3.1 Function, structure and expression of TLRs

The *Toll* gene was originally discovered in *Drosophila* (fruit flies) during the 1980s when it was found to control dorsoventral polarity during embryonic development (Anderson, Jürgens, et al. 1985). It was not until 1996 when its role in the innate immune response was hinted at as researchers demonstrated its anti-fungal function (Lemaitre et al. 1996). Around the same time, a mammalian homologue of Toll (later renamed TLR4) was shown to play a role in the inflammatory response where it induces the expression of inflammatory response-related genes via the NFκB pathway to control the expression of pro-inflammatory cytokines (IL-1, IL-6 and IL-8) (Medzhitov et al. 1997).

TLRs belong to a family of type I integral membrane glycoproteins and were initially described as IL-1 receptor-like proteins due to their conserved protein sequence (Rosetto et al. 1995). Over the past 40 years, there have been a total of 13 TLRs discovered, named TLR1 through 13, of which 1-10 are expressed in humans (Mogensen 2009). Their structure comprises of an extracellular (ecto-)domain;

each TLR with a variable number of leucine-rich-repeats (LRRs) according to the —L(X2)LXL(X2)NXL(X2)L(X7)L(X2)— motif, where X denotes any amino acid. Each TLR also has a cytoplasmic Toll/interleukin 1 (IL-1) receptor (TIR) domain responsible for downstream signalling (Mogensen 2009; Duan et al. 2022).

All innate immune cells (macrophages, DCs, NK cells, neutrophils, mast cells, eosinophils, basophils) and epithelial cells express TLRs (Chang 2019). DCs can be split into subsets based on their surface markers. These include myeloid DCs, plasmacytoid DCs (pDCs), CD8a+ DCs, and CD11b+ DCs. TLR7 is mainly expressed in pDCs (Iwasaki and Medzhitov 2004). According to Ishii and Akira, TLR1/6 are expressed constitutively on myeloid cells (Ishii and Akira 2004). Macrophages and myeloid DCs express TLRs 2, 3, 4 and 8. B-cells and plasmacytoid DCs both express TLR7 and 9 (Duan et al. 2022).

Until recently, RBCs were thought to be immunologically inert. However, Lam *et al.,* recently demonstrated how TLR9 is expressed on the surface of RBCs; contributing to a newly discovered role as 'immune sentinels' (Lam et al. 2021). In recent years there has been a number of studies showing how RBCs lack all genetic material, save for a small amount of mRNA to maintain their longevity and function, allowing them to take on a secondary role as modulators of the innate immune system (Doss et al. 2015; by Jennifer Doss et al. 2015; Anderson, Brodsky, et al. 2018). Human pDCs express TLR7 and 9, whereas blood monocytes express TLRs 1, 2, 4 and 5. As pDCs differentiate into mature DCs, they lose the expression of these TLRs and replace them with TLR3 (Visintin et al. 2001). Conversely, myeloid DCs express TLR1, TLR2, TLR3, TLR5, TLR6, and TLR8 (Vaure and Liu 2014; Duan et al. 2022). TLRs 1, 2, 4, 5 and 6 are expressed on the cell surface where they are suited to detect cell wall components of pathogens. TLRs 3, 7, 8 and 9 are expressed intracellularly, within the endosome, lysosome, endolysosome or endoplasmic reticulum.

All TLRs must dimerise to signal; TLRs 3, 4, 5, 7, 8 and 9 form homodimers. TLR2 is always found in combination with TLR1 or TLR6 in order to bind tri- or di-acylated peptides, respectively (Mogensen 2009; Duan et al. 2022; Akira and Takeda

2004; Ishii and Akira 2004). A full summary of TLR ligands can be found in Table 1.1 (Kawai and Akira 2011; Akira and Takeda 2004; Duan et al. 2022; Henrick et al. 2019). Intracellular TLRs are the nucleic acid binding receptors TLR3, 7, 8 and 9 which bind to dsRNA, ssRNA (7 and 8) and non-methylated CpG DNA, respectively. TLR4 is unique as it sits on the cell surface and recognises LPS on Gram-negative bacteria, but then can be internalised in an endosome (Vaure and Liu 2014). A possible explanation for this is that it allows the discrimination between replicable viral infiltration and non-replicable bacterial agents (Xagorari and Chlichlia 2008).

Table 1.1: Human Toll-like receptor ligands, targets, expression and cellular localisation (Lam et al. 2021; Akira and Takeda 2004; Mogensen 2009; Henrick et al. 2019; Duan et al. 2022)

TLR	Ligands	Pathogen Type	Cellular Expression	Cellular Localization
TLR-1 (with TLR-2)	Triacyl lipopeptides	Bacteria	Macrophages, Dendritic cells	Cell surface
TLR-2	Diacyl lipopeptides, Lipoteichoic acid, Peptidoglycan, Lipoarabinomannan, Porins, Envelope glycoproteins, GPI-mucin, Phospholipomannan, Zymosan, ß-Glycan	Gram-positive and Gram-negative Bacteria, Mycobacteria, *Neisseria,* Viruses (*e.g.,* measles virus, HSV, cytomegalovirus), Protozoa, *Candida*, Fungi	Macrophages, Dendritic cells	Cell surface
TLR-3	Double-stranded RNA (dsRNA)	Viruses	Dendritic cells, Epithelial cells	Endosomal
TLR-4	Lipopoly-saccharide (LPS), Envelope glycoproteins, Glycoinositolphospholipids, Mannan, HSP70	Gram-negative Bacteria, Viruses, Protozoa,	Macrophages, Dendritic cells	Cell surface (endocytosed on ligand binding)

TLR	Ligands	Pathogen Type	Cellular Expression	Cellular Localization
TLR-5	Flagellin	Flagellated Bacteria	Macrophages, Dendritic cells	Cell surface
TLR-6 (with TLR-2)	Diacyl lipopeptides, Lipoteichoic acid	Gram-positive Bacteria Mycoplasma	Macrophages, Dendritic cells	Cell surface
TLR-7	Single-stranded RNA (ssRNA)	RNA Viruses	Dendritic cells, Lymphoid tissue	Endosomal
TLR-8	Single-stranded RNA (ssRNA)	RNA Viruses	Dendritic cells, Lymphoid tissue	Endosomal
TLR-9	Unmethylated CpG DNA	Bacteria, Viruses, Protozoa	Dendritic cells, B cells, Lymphoid tissue, Erythrocytes	Endosomal, Cell surface of erythrocytes
TLR-10	Unknown (potentially diacyl lipopeptides, recent suggestion of sensing HIV	Unknown	Dendritic cells, B cells	Cell surface

1.2.3.2 TLR signalling in innate immunity

Ligand recognition by TLRs leads to dimerisation of the TIR domains which results in a signalling cascade/transduction, translocation of key transcription factors to the nucleus which regulate the expression of certain genes relating to inflammation. There are two main signalling pathways: MyD88-dependent signalling which activates the Nuclear factor kappa-light-chain-enhancer of activated B cells (NFκB) signalling pathway and leads to the production of pro-inflammatory

cytokines and the TRIF-dependent signalling pathway which leads to the production of both pro-inflammatory cytokines and type I interferons (IFNs) (Duan et al. 2022).

In the case of MyD88-dependent signalling, dimerised TIRs engage with MyD88 (sometimes *via* TIRAP) resulting in the formation of the myddosome. Recruitment of IL-1 receptor-associated kinases (IRAK) 1/2 and 4 activates tumour necrosis factor (TNF) receptor-associated factors 6 (TRAF6); an E3 ubiquitin ligase. This leads to the formation of the TGFβ-activated protein kinase (TAK)1:TAB2/3 complex which phosphorylates and activates the canonical IKK signalling pathway (NEMO (a.k.a. IKKγ, IKKα and IKKβ) leading to the translocation of transcription factor NFκB to the nucleus. Additionally, TAK1 activates mitogen-activated protein kinases (MAPKs). Specifically, MKK1/2, MKK4/7 and MKK3/6 which activate ERK/c-Fos, p38/CREB and JNK/c-Jun, respectively. CREB, c-Fos and c-Jun are also transcription factors which translocate to the nucleus to upregulate the expression of pro-inflammatory cytokines, in cooperation with NFκB.

Now, in the case of TRIF-dependent signalling, dimerised TIRs (for TLR3 and endosomal TLR4 in macrophages and conventional DCs) interact with TRIF and TRAM. The formation of the triffosome ensues with the involvement of TRAF3 and 6. TRAF3 activates TANK-binding kinase 1 (TBK1) and inhibitor of NF-kB kinase (IKKi) along with NEMO (a.k.a. IKK-gamma) and phosphorylates IFN regulatory factor 3 (IRF3), a transcription factor responsible for the upregulation of type I IFNs. Meanwhile TRAF6 interacts with receptor-interacting protein (RIP1) which recruits TAK1 complex and signals via IKK to NFKB to upregulate pro-inflammatory cytokines. A summary of TLR signalling is depicted in Figure 1.1 (Duan et al. 2022).

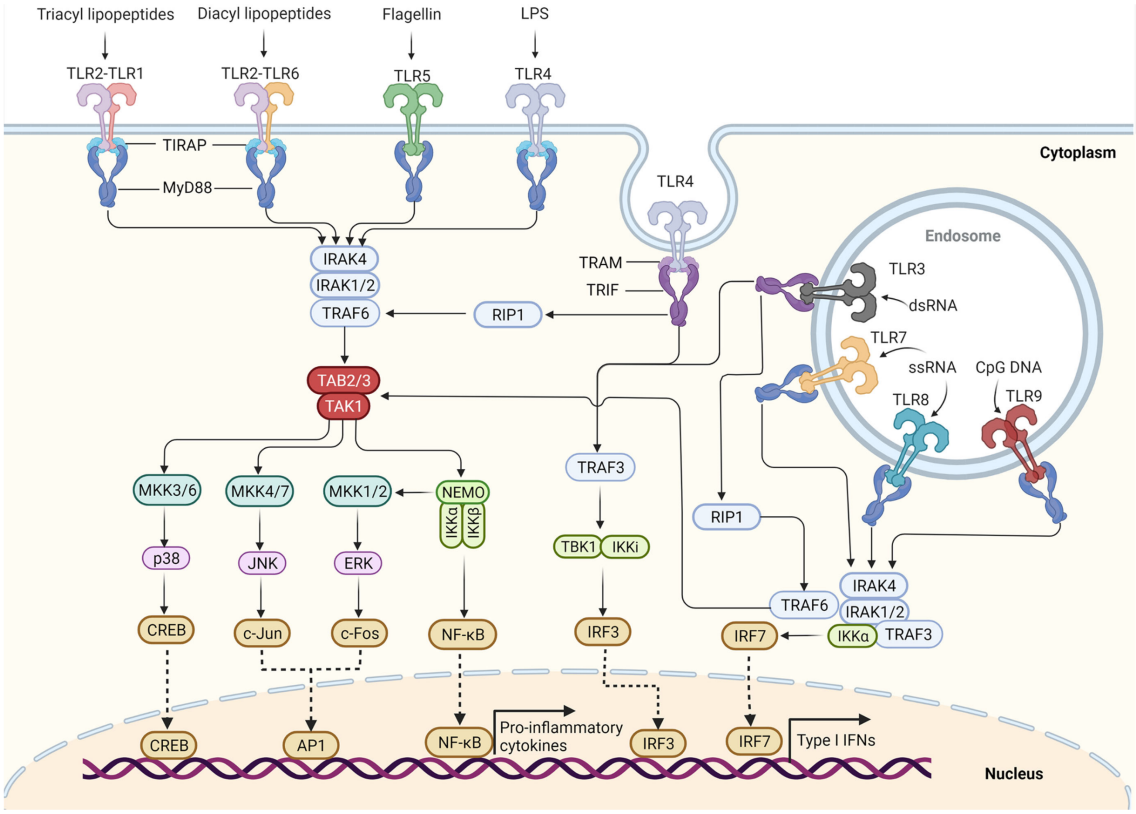

Figure 1.1: TLR signalling pathway in innate immune cells. TLR5, TLR4, and the heterodimers of TLR2–TLR1 or TLR2–TLR6 recognize the membrane components of pathogens at the cell surface, whereas TLR3, TLR7–TLR8, and TLR9 localize to the endosomes, where they recognize the nucleic acids from both the host and foreign microorganisms. TLR4 localizes at the plasma membrane, but it is endocytosed into endosomes upon activation. Upon binding to their respective ligands, TLR signalling is initiated by dimerization of receptors, leading to the engagement of TIR domains of TLRs with TIRAP and MyD88 (or directly interact with MyD88) or with TRAM and TRIF (or directly interact with TRIF). The TLR4 signalling switches from MyD88 to TRIF once TLR4 moves to the endosomes. Engagement of MyD88 recruits the downstream signalling molecules to form Myddosome, which is based on MyD88 and contains IRAK4 and IRAK1/2. IRAK1 further activates the E3 ubiquitin ligase-TRAF6 to synthesize the K63-linked polyubiquitin chains, leading to the recruitment and activation of the TAK1 complex. The activated TAK1 further phosphorylates and activates the canonical IKK complex, ultimately leading to the activation factor NF-kB. The activation of TAK1 also leads to the activation of MAPKs, including MKK4/7 and MKK3/6, which further activate JNK and p38, respectively. The activation of IKKb also leads to the activation of MKK1 and MKK2, which further activate ERK1/2. The activation of these MAPKs leads to some important transcription factor activations, such as CREB, AP1. These transcription factors cooperate with NF-kB to promote the induction of pro-inflammatory cytokines. Engagement of TRIF recruits the TRAF6 and TRAF3. Activated TRAF6 can recruit the kinase RIP1 and activate the TAK1 complex and IKK complex, leading to the activation of NF-kB and MAPKs. TRIF also promotes the TRAF3-dependent activation of the TBK1 and IKK-epsilon (originally IKKi), which further phosphorylates and activates IRF3. Among TLR7, TLR8, and TLR9 signalling in pDCs, IRF7 can bind to the Myddosome and is directly activated by IRAK1 and IKK-epsilon. Activation of IRF3 and IRF7 leads to the induction of Type I IFN. Reproduced from [@Duan2022], with permission

1.2.3.3 TLR signalling in adaptive immunity

The adaptive immune system is comprised of two branches; cell-mediated immunity (CMI; which involves T cells) and humoral immunity (antibody production by B cells).

To achieve activation of the adaptive immune system and clonal expansion, antigen presenting cells (APCs; including DCs, macrophages and B cells) must provide the antigen in addition to a costimulatory molecule (such as CD40, CD80, and CD86) to the T cell. Clonal expansion occurs when a B cell or a T cell recognises a specific antigen. The B cell rapidly divides to generate populations of both plasma cells and memory B cells that produce antibodies specific to that antigen, while the T cell proliferates into a clonal population of effector T cells that contribute to the cellular immune response. Crucially, TLRs are expressed on APCs and serve to link innate immunity to cell-mediated immunity by recognising PAMPs and enhancing antigen-presenting activity, cytokine production and expression of costimulatory molecules (Akira and Takeda 2004; Duan et al. 2022). This is actually not a new discovery; the role in adaptive immunity was reported back in 1997 by Medzhitov *et al.,* who showed how a constitutively active Toll mutant induced the expression of co-stimulatory molecule B7.1, which is needed to activate naive T cells (Medzhitov et al. 1997).

Different APC subsets express different combinations of TLRs and thus produce different kinds of inflammatory responses. IFNγ combined with ligand activation of TLRs 2, 4 and 9 promotes DC activation to enhance antigen-specific T cell responses (Sheng et al. 2013). LPS-induced TLR4 signalling can promote the redistribution of MHC Class I and II molecules to the surface of DCs (Turley et al. 2000). However, it was reported that activation of TLR2 on DCs induces increased effector and memory CD4+ T cell responses compared with TLR4 signalling activation (Guo et al. 2017). CD4+ T cells can also be driven to T-helper cells and promote accelerated polyclonal conversion to regulatory T cells (Tregs), which have an immunosuppressive function; for example, during Listeria infection, by activation of TLR9 and IL-12 (Dolina et al. 2020).

TLR signalling in innate immune cells (DCs/macrophages *etc.*) promotes DC differentiation and cytokine production to regulate T cell proliferation and maturation. There is a strict regulation of both innate and adaptive immune response in order to strike a balance between sensitivity to non-self signs of infection and tolerance to the body's own self-molecules. T cells (CD4+ and 8+) themselves also express TLRs. TLR2 and TLR4 are well-researched and are expressed on both CD4+ and CD8+ T cells. Indeed, CD8+ T cells were also shown to express TLR9. When challenged with CpG-ODNs they produced IL-8 (Hornung et al. 2002). MyD88-dependent signalling is necessary for CD4+ T cells to produce IFNg during intracellular bacterial infections (Zhang, Jones, et al. 2013) and activation of this pathway also promotes a Th17 response by both maintaining mTOR and linking IL-1 and IL-23 signalling (Hornung et al. 2002).

1.2.3.4 TLRs in disease

TLR-mediated innate immunity is tightly controlled (Akira and Takeda 2004; Tsujimoto et al. 2008): ligand activation, expression pattern, intracellular localisation, signalling pathway ensure TLRs play a key role in the mediation of systemic responses to invading pathogens during infection and sepsis. Logically, defective TLR sensing, either through host dysfunction or pathogen evasion, toxicity or subversion (Arpaia and Barton 2013; Jude et al. 2003), may promote infection of specific pathogens which leaves the host with a higher chance of colonisation.

1.2.3.5 TLRs in non-communicable disease

TLR signalling has both anti- and pro-tumour functions. For instance, mice lacking TLR2 expressed less pro-inflammatory cytokines (IFNg, TNFa, IL-1, IL6 and Cxcl2) which leads to increased tumour growth due to altered p21- and p16/pRb-dependent senescence (Lin, Yan, et al. 2013). Counterintuitively, an immunosuppressive cytokine response can be promoted by stimulation of TLR4 by LPS leading to lung tumour immune evasion (He et al. 2007) and upregulation of IL-6/-8 (Yang, Zhou, et al. 2010; Yang, Wang, et al. 2014). Furthermore, mutations

in MyD88 (L265P) can result in a higher constitutive pro-inflammatory response and thus increase the survival of malignant cells in certain types of lymphoma (Ngo et al. 2011), in turn resulting in increased mortality (Pham-Ledard et al. 2014).

1.2.3.6 TLRs in autoimmunity

Normally, the immune system is tolerant to the body's own cells and tissues. It is tightly regulated to accurately distinguish between self- and non-self antigens. A breakdown in these regulatory mechanisms leads to the loss of self-tolerance and studies have shown that improper activation of TLRs by self-antigens, coupled with the production of auto-antibodies and autoreactive T cells. Ultimately, this results in chronic, systemic inflammation: Autoimmunity. Examples of autoimmune diseases include rheumatoid arthritis (RA), systemic lupus erythematosus (SLE), multiple sclerosis (MS), Crohn's disease and diabetes. In RA, a correlation has been reported between TLR2/4 and the concentration of IL-12/-8 in synovial (joint) tissues (Radstake et al. 2004). TLR4 on CD4+ T cells correlates with disease severity, resulting in increased pro-inflammatory cytokines IFNγ and TNFα in response to LPS (Tripathy et al. 2017). In SLE, the body produces autoantibodies to its own CpG DNA and ssRNA. These self-antigens are detected by TLR7 and 9. TLR9 is protective in the context of SLE and limits stimulation of TLR7 (Fillatreau et al. 2021). Recent evidence also suggests TLR2 plays a role in diabetes (Sepehri et al. 2016).

1.2.3.7 TLRs in infection and sepsis

TLRs are central to the sepsis immune response (Tsujimoto et al. 2008; Kumar 2020; Akira and Takeda 2004; Lam et al. 2021) and multiple studies have suggested TLR2 and TLR4 be considered as biomarkers in sepsis diagnostics (Younis et al. 2018; Viemann et al. 2005). Mice lacking TLR2 and 4 are significantly more susceptible to *Salmonella* infection (Arpaia and Barton 2013) and children with TLR4 mutations are vulnerable to viral infection (Awomoyi et al. 2007). Mutations in TLR5 results in lower IL-10 and TNFa production in infections of the Gram-negative,

flagellated bacterium *Burkholderia pseudomallei* (Chaichana et al. 2017). TLR3 (Poly(I:C)) and TLR4 inhibition represents the main strategy to fight pathogen-associated inflammation and viral or bacterial sepsis. TLR7 recognises influenza A viral DNA and results in the production of pro-inflammatory cytokines and Type I IFN. Imiquimod is a TLR7 agonist shown to reduce airway and pulmonary inflammation in influenza A infection (To et al. 2019). TLR2 was shown to be constantly upregulated on blood monocytes but only transiently upregulated on granulocytes in neonates with sepsis (Viemann et al. 2005) and TLR2 expressed on bone-marrow-derived macrophages recognise envelope protein of SARS-CoV-2 (Zheng et al. 2021). TLR2 and 4 can also detect spike protein and signal via NFκB to produce IL-1ß (Zhao et al. 2021).

One particular SNP in TLR4 is involved in organ failure in sepsis (Mansur et al. 2014). Induction of sepsis in TLR-9 deficient mice via infection with *Neisseris meningitidis* showed increased levels of bacteraemia and increased mortality (Sjölinder et al. 2008). Sustained over expression of TLRs results in decreased expression of HLA-DR (a molecule involved in APC presentation) resulting in impaired adaptive immune response during sepsis (Younis et al. 2018; Monneret et al. 2019). Furthermore, the majority (65%) of known TLR modulators have been tested as potential vaccine adjuvants; compounds which enhance the antibody response to a vaccine (Luchner et al. 2021). Most candidates are represented by fragments of bacterial cell wall components, pathogenic nucleic acids, and other PAMPs or extracted from plants (Federico et al. 2020).

TLRs also sense DAMPs produced in high quantities due to the damage caused by the various pathologies in sepsis. DAMPs represent a broad class of molecules present in high amounts in disease, for example; fibrinogen (Chang 2019; Beltrán-García et al. 2020; Lopes-Pires et al. 2022; Kell 2009), HMGB1 (Tsujimoto et al. 2008; Pool et al. 2018; Sonneville et al. 2013; Siddiqui et al. 2021), mitochondrial DNA (Goulopoulou et al. 2016; Cavaillon et al. 2020), heat shock proteins (Duan et al. 2022) and CRP (Cavaillon et al. 2020; Steel et al. 2016), all of which are present in sepsis (Tsujimoto et al. 2008).

1.3 Part III: Diagnosing, treating and surviving sepsis

1.3.1 Sepsis diagnostics

The definition, symptoms, causes and risk factors of sepsis have been covered in detail in part I. In this section, the current clinical signs, diagnostic process, treatment options for patients in the UK, along with their limitations, will be described.

1.3.1.1 Clinical criteria for sepsis

Due to the urgency at which untreated sepsis can progress, any unexplained organs dysfunction raises the possibility of an underlying infection (Singer et al. 2016). In the past SIRS criteria focused predominantly on quantifying immune dysregulation (Bone et al. 1992), however over the past decade the current clinical criteria for diagnosis have evolved to include cardio-vascular, hormonal, neuronal, metabolic, and coagulation pathways (Singer et al. 2016; Shankar-Hari, Summers, et al. 2018; Evans et al. 2021). A patient who presents with a suspected infection (according to the symptoms outlined in part I) should initially be assessed according to the qSOFA criteria: respiratory rate <22/min, altered mentation or a systolic blood pressure <100 mmHg. If they satisfy 2 or more of these criteria, then the clinical practitioner should next look for evidence of organ dysfunction according to the more extensive SOFA criteria which measures each of the following:

- PaO_2/FiO_2 ratio
- Glasgow Coma Scale score
- Mean arterial pressure
- Administration of vasopressors with type and dose rate of infusion
- Serum creatinine or urine output Bilirubin
- Platelet count

The numerical results of each independent test are grouped according to severity and given a score from 0-4, meaning it is not the presence or absence of organ dysfunction, rather the severity. Once more, if the patient scored higher than 2 then they meet the criteria for sepsis. In addition, if vasopressors are required to maintain mean arterial pressure (MAP) (effectively blood pressure) >65 mm Hg and serum lactate is measured > 2 mmol/L then the patient is said to be in 'septic shock' (Singer et al. 2016).

1.3.1.2 Pathogen identification and antimicrobial susceptibility testing

According to the WHO latest guidelines on global sepsis management, '*a rapid, accurate diagnosis of sepsis improves clinical outcomes and represents a priority for both surveillance and clinical management, particularly in at-risk patients*' (World Health Organisation 2020). Survival is directly linked to effective antimicrobial therapy for which the causative pathogen must be isolated, identified and its susceptibility to a therapeutic agent confirmed. A major challenge associated with pathogen identification is that there is very little evidence of the pathogen found in the blood stream – only 1-10^3 colony forming units (CFU)/ml (Opota, Jaton, et al. 2015). In order to increase the number of viable pathogens to a concentration at which they can be detected, a blood sample is taken from the patient and split into separate aerobic and anaerobic culture bottles (6-10 ml) before being loaded onto a blood culture (BC) analyser (*e.g.* bioMérieux BacT/ALERT® Virtuo) for 12-72 hours. BC is the longest step in the entire process but is necessary, in the first instance, to rule out bacterial sepsis (viruses cannot be cultured) and to reach microbial concentrations in the order of 10^7-10^8 CFU/ml, which are needed for detection.

The BC analyser detects pathogen growth and flags samples as positive once their pathogen load passes a certain threshold. Samples are then removed and a Gram-stain is carried out; the Gram-status of the causative pathogen is the first opportunity to tailor antimicrobial therapy away from the initial empiric choice. Meanwhile, the positive BC sample is inoculated onto appropriate agar plates (*e.g.*,

blood, chocolate, heart-brain infusion, cystine–lactose–electrolyte-deficient agar) (informed by the result of a Gram-stain) and incubated at body temperature for 5~12 hours, at which point morphologically distinct, monomicrobial colonies can be picked from plates showing microbial growth (Ward et al. 2015; Weinbren et al. 2018). Identification from colonies is then carried out using matrix-assisted laser desorption ionisation time-of-flight (MALDI-TOF) mass spectrometry (MS). MALDI-TOF MS has the capacity to identify bacteria and yeasts to the species level in minutes by comparing the recorded spectrum to those in a database containing spectra of thousands of known organisms (Angeletti 2017). When necessary, traditional biochemical identification based on the visual appearance of the organism is also used in conjunction with MALDI.

It is not sufficient to simply find the identity of an organism; its susceptibility to a given antibiotic is also required to inform best treatment. An antimicrobial susceptibility test (AST), according to genotypic or phenotypic methods, is then performed for this purpose. *Genotypic* AST involves the detection of a resistance gene by sequencing, or PCR-based methods. It can be noted that the presence of a resistance gene might not correlate to bacterial growth in the presence of antibiotics (Goldenberg 2017). *Phenotypic* AST relies on determining the dosage of antibiotic required to meet the minimum inhibitory concentration (MIC) to visibly inhibit growth of an organism according to the European Committee on Antimicrobial Susceptibility Testing (EUCAST) breakpoints. Traditionally, phenotypic AST is done using a disk- or strip-diffusion test (Kuper et al. 2012). Traditional methods typically add 18-24 hours to the diagnostic process (Angeletti 2017), however, new technologies, such as the Alfred 60/AST, are able to provide MICs in accordance with the aforementioned EUCAST breakpoints in 5 hours (Lahanas et al. 2013).

Not all pathogens are amenable to BC, however; 41.5% of severe sepsis cases are culture-negative (Phua et al. 2013; Lin, McGinley, et al. 2018), suggesting a pathogenic aetiology may be of viral origin. Alternatively, despite enriched growth media, the detection of certain fastidious organisms relies solely on serology, antigen detection, and nucleic acid detection methods such as PCR (Fenollar and

Raoult 2007). In some cases, antibiotic treatment prior to identification inhibits microbial growth and leads to false negatives. For this reason, growth media is supplemented with antibiotic-binding beads to reduce this issue (Ward et al. 2015; Reddy et al. 2018). The pathogen identification and AST process will be discussed in more detail in Chapter 3.

Sepsis mortality decreased by 52.8% (47.7–57.5%) globally from 1990 to 2017 (Rudd et al. 2020). In the UK, there is an estimated 79.7% survival rate which yields approximately 200,000 new survivors each year (1 every ~3 minutes) (Rudd et al. 2020). It is widely accepted however, that sepsis survival is associated with increased long-term mortality and significant comorbidities. A recent study which followed over 94,000 sepsis survivors for up to 6 years reported a 15% mortality rate in the first year after discharge, followed by 6-8% for each subsequent year (Shankar-Hari, Harrison, et al. 2019a).

1.3.1.3 Mechanisms of AMR

In 1928, a common and naturally occurring genus of fungi *Penicillium* was observed to kill the bacteria *Staphylococcus aureus* by Alexander Fleming. After years of development, the isolation and purification of penicillin was achieved in the 1940s by Chain and Florey – leading to the massive use of the drug for wounded soldiers in 1944. Fleming, Chain and Florey received the Nobel Prize for their work in 1945. Many other antibiotics have been discovered since, all targeting either the bacteria wall/membrane, protein production or DNA replication/transcription (Kapoor et al. 2017).

However, the Golden Age of antibiotics is long since over and the new antimicrobial pipeline is stagnating. The use of antibiotics also imposes a selective pressure on bacterial population, as noted by Fleming on accepting the 1945 Nobel Prize. By driving AMR with a mis- and overuse of antimicrobials, not only in humans but also in animals (both pets but mainly agriculture), one of the main threats to our health is the emergence of “superbugs”; bacteria that are resistant to multiple - if

not all- existing drugs (also called multi-drug resistant pathogens). Carbapenem-resistant Enterobacteriaceae (CRE), for example, are a group of bacteria that have become resistant to "all or nearly all" available antibiotics, including carbapenems, which are typically reserved as the "treatment of last resort" against drug-resistant pathogens (Ventola 2015). *Enterobacteriaceae* are a family of Gram-negative bacteria which includes species within the subfamilies: *Salmonella, Escherichia, Klebsiella* and *Shigella*. These familiar pathogens cause a variety of severe infections, including bloodstream infections, community-acquired pneumonia, hospital-acquired pneumonia, ventilator-associated pneumonia, complicated urinary tract infections, and complicated intra-abdominal infections. Therefore, antibiotic resistance in these bacteria has significant clinical and socioeconomic impacts (Sheu et al. 2019). CRE are already spreading in Europe (and worldwide), with an estimated 15,947 number of infections with carbapenem-resistant *K. pneumoniae*, and 2619 with carbapenem-resistant *E. coli* for the EU/EEA in 2015 (Cassini et al. 2019).

Randomly occurring point mutations in the genome which confer a survival advantage, are evolutionarily conserved and passed on to other bacteria. Bacteria with plasmids that contain the genetic code for resistance may be exchanged "vertically" (mother-daughter) and/or "horizontally" through bacterial transformation, transduction, or conjugation. If an antibiotic is prescribed to a patient but turns out to be ineffective or is administered at a concentration too low to kill or prevent the growth of the bacteria, then the bacteria will keep growing. This creates a selective pressure for the mutation; the resistance gene will then be shared to other microorganisms (Kapoor et al. 2017). Beyond human patients, the misuse/overuse of antibiotics in animals or as growth promoters in agriculture can also lead to resistance than can then be passed on to bacteria which are infectious to humans. In the UK, the majority of methicillin-resistant *S. aureus* (MRSA) strains identified in cats and dogs are commonly associated with human infections (Davies, S. C; Grant 2013).

There are five broad types of mechanisms to make bacteria resistant to antibiotics/antimicrobial drugs (Yeaman and Yount 2003):

1. inactivation of the drug before it reaches its target
2. outer layers of the cell are impermeable to the drug
3. the drug can enter the cell but is then pumped out
4. the target of the drug is changed so that it can no longer be recognised
5. the metabolic pathway is changed to render the antibacterial target redundant

Despite the significant risk posed by AMR, large pharmaceutical companies are inherently discouraged from investing in the development of new antimicrobial drugs. Drug development is costly and the threat of resistance is typically mitigated by prescribing novel antibiotics sparingly, using them as a last resort for as long as possible. In addition to this, patients take antibiotics for much shorter durations compared to other medications to treat chronic diseases, such as hypotension or arthritis (Gould and Bal 2013). These factors act together to limit the return on this investment. In recent years, alternative strategies to incentivise investment into the development of novel antimicrobial therapeutics have been investigated; these include insurance frameworks to mitigate risk (Towse et al. 2017) or voucher schemes to extend patent exclusivity (Outterson and McDonnell 2016).

1.3.2 Rapid pathogen identification in blood

There exist several emerging approaches to identify a pathogen from blood samples without the need to carry out a BC (Table 1.2); these have been reviewed extensively in Chapters 4 and 5. One method is based on the principle of selective lysis to first remove contaminating human DNA from the sample. MolYsis (MolZym) is a commercially available kit which uses chaotropic buffers to selectively lyse blood cells. The exposed human DNA is immediately degraded by DNases. Intact pathogens are removed from the lysate and subsequently lysed by muralytic enzymes to expose their DNA which can then be purified using a column (Wiesinger-Mayr et al. 2011). Evidence suggests that at high bacterial concentrations of spiked blood (>1000 CFU/ml) conventional PCR is not inhibited by the presence of human DNA, however

at clinically relevant concentrations (<100 CFU/ml) it is not possible to reliably carry out PCR. The use of mild polar detergents with an elevated basic pH (2M Na_2CO_2 pH 9.8, 1% Triton-X100) is sufficient to lyse human blood cells and degrade the released DNA. Such detergents have been reported to remove 98% of human DNA, in turn increasing the limit of detection of RT-PCR to 10 CFU/ml (Trung, Hien, et al. 2016). In spite of this success, selective lysis is difficult to generalise for all pathogens as they are liable to lyse pathogens with a weak membrane, all cfDNA is removed alongside the human DNA by design and the technique therefore cannot be used in cases where the patient has already been treated with antibiotics.

Blauwkamp *et al.,* have recently developed an infrastructure which employs next-generation sequencing (NGS) to identify and quantify microbial cell-free DNA (cfDNA). On receipt, samples (4 ml blood plasma sent in the post at room temperature) are spiked with a known concentration of control DNA which is later used for signal calibration and contamination control. cfDNA is extracted from blood using a magnetic bead-based DNA enrichment kit before automated library preparation takes place. Samples are then subjected to single-end 75-base sequencing on the Illumina NextSeq500. This method is highly sensitive, with a limit of detection of 33-74 molecules of DNA/µl sample and specific with results showing a 93.7% agreement with BC (Blauwkamp et al. 2019). Up to 85% of results were returned the day after sample receipt. A 53 hr turnaround time to obtain a species-level identification is significantly shorter than the 92 hrs achieved by conventional methods. However, this test does not include an AST, which typically takes ~12 hr in a UK hospital (Ward et al. 2015). Due to the high abundance of host DNA relative to a very small proportion of microbial DNA in the sample, effectively constituting a high amount of noise in the sample, whole blood plasma sequencing of cfDNA takes 29 hrs. If pathogen cfDNA could be enriched from total cfDNA then sequencing would take only a small fraction of this time.

The aim of this thesis is to engineer new approaches for pathogen separation and detection to tackle antimicrobial resistance. The untapped potential of recombinantly expressed and fluorescently labelled TLRs 2, 4 and 9 will be

investigated to detect Gram-positive bacteria, Gram-negative bacteria, and microbial DNA, respectively.

Table 1.2: A comparison of the novel approaches to enrich low concentrations of pathogens (whole cells/DNA from whole blood without the need to culture

Method	Target	Examples	Principle	Limitation
Selective lysis	Pathogen DNA via removal of human cells	MolYsis (MolZym GmbH, Bremen, Germany)	1) Lyse blood cells to expose human DNA 2) Degrade human DNA using DNases 3) Lyse remaining bacterial cells then purify pathogen DNA for detection	Pathogens with weak membrane lysed along with human cells cfDNA is removed Cannot be used on patients after antibiotic treatment
		Mammalian cell lysis buffer (Trung *et al.,* 2016)	1) Lyse blood cells to expose human DNA 2) Pellet intact bacteria and discard human material in supernatant 3) Purify/amplify pathogen DNA for detection *via* PCR	”
Non-specific binding	Pathogen DNA (non-methylated CpG motif)	Looxster DNA enrichment kit (SIRS-lab GmbH, Jena, Germany)	Magnetic bead separation using human CXXC finger protein 1 (CFP1)	Reports of poor performance (Wiesinger-Mayr *et al.,* 2011) Kit discontinued by manufacturer in 2019

Method/Target	Examples	Principle	Limitation
	HpaII + McrB (Liu *et al.,* 2016)	Magnetic bead separation using methyl-sensitive restriction enzymes	Not tested with whole blood Not commercially available
6x Gram-positive and 2x Gram-negative bacteria including MRSA and MSSA	LysE35A (Lopes *et al.,* 2016)	Magnetic bead separation using mutated lysozyme	Not commercially available
Anionic phospholipids on surface of bacteria	*bis*-Zn-DPA (Lee *et al.,* 2014	Magnetic bead separation. Ligand forms covalent bonds with cell surface lipids	Not commercially available
LPS of Gram-negative bacteria and LTA of Gram-positive bacteria	Septiflo (Jagtap *et al.,* 2018)	LPS/LTP captured on membrane (no receptor). AuNPs used as signal amplification probes to detect Gram-status of organism	
Cell surface carbohydrates of bacteria	Mannose binding lectin (MBL) (Kang *et al.,* 2014)	Magnetic bead separation using modified MBL	Highly modified receptor Used primarily for blood purification, not diagnostics

1.4 Part IV: Summary, hypothesis and aims of the thesis

1.4.1 Summary

In the UK sepsis kills more people than bowel, breast and prostate cancer, combined (CRUK 2020) and is responsible for one fifth of global deaths annually (Rudd et al.

2020). The definition of sepsis has evolved over time (Bone et al. 1992; Daniels et al. 2011; Singer et al. 2016), current diagnostic criteria focus on characterising the organ dysfunction caused by a dysregulated immune response to infection (Singer et al. 2016; Shankar-Hari, Summers, et al. 2018). Symptoms of sepsis include fever, difficulty breathing, rapid heart rate, decreased urine production, confusion, and cold hands and feet (Farthing et al. 2021). The underlying pathophysiology of sepsis involves a systemic immune response, endothelial dysfunction, and coagulopathy, leading to organ failure and death (Minasyan 2019; Cavaillon et al. 2020).

Though there have been many recent advances, there are limitations to the diagnostic criteria, and there is an urgent need for improved rapid sepsis diagnostics (Reddy et al. 2018). Sepsis is a complex and heterogeneous condition and there are many challenges associated with stratifying a treatment response (Scicluna et al. 2018; Leligdowicz and Matthay 2019; Cavaillon et al. 2020). Prompt and effective antimicrobial treatment is crucial to eliminate the underlying infection and ultimately survival, with each hour of delay being associated with a decrease in survival rate (Kumar et al. 2006; Seymour et al. 2017; Daniels et al. 2011). Many advances in sepsis treatment have not translated into effective new treatments and sepsis survivors often face significant comorbidities (Cavaillon et al. 2020; Shankar-Hari, Summers, et al. 2018).

Pathogen identification and antimicrobial susceptibility testing are necessary for a patient to transition from broad spectrum antibiotics onto an antibiotic targeted treatment against the causative pathogen (Goldenberg 2017; Reddy et al. 2018; Weinbren et al. 2018). The gold standard of pathogen identification has relied on blood culture for over 30 years (Holliman 1986). Blood cultures are taken to amplify and isolate the causative pathogen, a process which takes between 1 and 5 days (Opota, Croxatto, et al. 2015). The culture isolate is then quickly identified using and MALDI-TOF MS (Angeletti 2017). Antimicrobial susceptibility testing is performed to determine the most appropriate antibiotic treatment however, by the time the results come back (1-5 days), the patient will have been on broad

spectrum antibiotics for the duration of this time. Common causes of sepsis include both communicable infections and non-communicable diseases.

An indirect and somewhat unavoidable consequence of immediate administration of broad-spectrum antibiotics is AMR. Of note, unsuccessful antimicrobial therapy may not have any consequence to the patient as long as a suitable treatment is found and they make a full recovery. However the misuse and overuse of antimicrobials contribute to the emergence of drug-resistant infections and the consequences of promoting AMR are serious (O'neill 2016; Blaskovich et al. 2017; Ventola 2015).

Overall, this extensive summary of the literature covers the diagnosis, treatment, and survival of sepsis, importantly highlighting the limitations and the need for innovative approaches to improve patient outcomes.

1.4.2 Motivation for the thesis

We have established that the main factor in survival chance is time to effective treatment and that one of the fundamental limitations for rapid diagnostics is the requirement for a blood culture step to increase the concentration of hard-to-find pathogens (Ward et al. 2015; Reddy et al. 2018). Considering the current state of BSI management in UK hospitals, in addition to the aforementioned limitations to alternative methods of separating pathogens from blood (Table 1.2), we have identified the need for a novel strategy to rapidly and non-specifically enrich pathogens from blood samples in order to circumvent the need for blood culture in hospitals, thus significantly reducing the time to effective antimicrobial therapy for treatment. The goal of this project is to develop these strategies to be compatible with existing detection assays such as MALDI-TOF, flow cytometry and next-generation sequencing.

1.4.3 Structure of the thesis

The structure of the thesis will be as follows: **Chapter 2** presents a detailed methodology for the experiments carried out in Chapters 3 through 6, focusing on methods of bacterial culture and quantification, DNA extraction and quantification,

protein labelling strategies and flow cytometry. **Chapter 3** describes an evaluation of the current state of clinical diagnostics, with works carried out in the microbiology laboratory of Glasgow Royal Infirmary (GRI) to ascertain key parameters to which a rapid pathogen separation test should be aimed. In **Chapter 4,** multiple novel assays were developed in order to accurately quantify the binding performance of PRRs to bacteria *in vitro.* This was done using a species-specific antibody against *E. coli.* **Chapter 5** investigates how well the labelling strategy and pathogen detection assay developed in Chapter 4 translates to recombinant TLR2 and TLR4 with *E. coli* and *S. aureus.* Due to high proportion of non-culturable sepsis cases, in addition to the effects of antimicrobial therapy prior to blood samples being taken, in **Chapter 6**, TLR9 is tested as a means of separating pathogen DNA for downstream applications in PCR/DNA sequencing. Finally, **Chapter 7** provides a general summary of the presented work, a discussion of its implication in the wider literature and exploration of possible future directions.

2

Chapter 2: Materials and Methods

The goal of this work is to evaluate the potential of new sample processing strategies to enrich bacteria from clinical samples for more rapid diagnostics. This chapter focuses on the experimental procedures required to create a framework whereby bacteria can be accurately cultured, detected and quantified. The fundamentals of accurately quantifying bacteria are presented in section 2.5, then examples of such techniques will be compared in terms of their performance and applicability to a clinical setting in Chapters 3-6.

2.1 Sample preparation of bacteria

E. coli and *S. aureus* were chosen as model strains representing Gram-negative and Gram-positive bacteria. Care was taken to select minimally infectious examples of each species according to their biological safety level (BSL). Strains expressing GFP were required to compare the proportion of bound to unbound receptor for methods which rely on fluorescence for detection. Unless otherwise specified, *E. coli* and *S. aureus* will henceforth refer to the two strains in **bold** in table 2.1.

Bacterial cultures were grown from 5 µl glycerol stock overnight at 37°C in 10 ml Luria broth (LB) containing appropriate antibiotic see Table 2.1. The following morning, 200 µl of the overnight culture was added to 10 ml of fresh LB media

and incubated at 37°C for ~2 hrs until OD^{600} reached ~0.66; this was equivalent to ~1x10^8 CFU/ml (see section 2.3.2). Glycerol stocks were replenished from a 1:1 ratio of culture mixed with glycerol containing 20% v/v peptone and stored at -80°C until required. Cultures of 10^8 CFU/ml could then be serially diluted 10-fold to prepare lower concentrations of bacteria.

Table 2.1: A summary of the different strains of bacteria used in this project.

Species	Strain	Antibiotic resistance	Plasmid	Biological safety level (BSL)
Escherichia coli	K-12 JM109	Ampicillin 100 mM (Amp100)	-	1
Escherichia coli	BL21 DE3 expressing GFP	Ampicillin 100 mM (Amp100)	pET28A (inducible with 1mM IPTG)	1
Escherichia coli	LF82 wild type	-	-	2
Escherichia coli	**LF82 expressing GFP**	**Chloramphenicol 20 mM (Chl20)**	**PJAR70: (pA-CYC184)**	**2**
Escherichia coli	ATCC	-	-	2
Staphylococcus aureus	**RN4220 expressing GFP**	**Erythromycin 10mM (Ery10)**	**pCN57**	**2**

2.2 Sample preparation and handling of whole blood

Whole blood was donated by healthy volunteers in accordance with health and safety and ethics approval at the Institute of Infection, Immunity and Inflammation, University of Glasgow. Informed consent was acquired prior to donation and donor information was treated anonymously. Depending on the experimental requirements, blood was taken in either sodium heparin or EDTA vacutainers.

Red blood cells (RBCs) were lysed using ACK lysing buffer (ThermoFisher Scientific) or EasySep Red Blood Cell lysis buffer (StemCell). Equal volumes

of blood and a 1x solution of buffer made up in distilled water were incubated at room temperature (RT) for 5 min. White blood cells (WBCs) were pelleted using centrifugation (1000 g, 5 min) at which point the supernatant containing the lysed RBCs was discarded and the sample washed in ~10 ml sterile PBS. If the pellet still appeared red, then the lysis was repeated with a shorter 2-3 min incubation. All tips and tubes were soaked in 10% Chemgene lab disinfectant (HLD4H) for >16 hrs before being disposed of according to the waste disposal stream for clinical samples used in the laboratory.

Positive blood culture samples were identified through routine work by collaborators in the Glasgow Royal Infirmary. A register was kept of routine micro sample ID alongside the results achieved in the routine lab analysis (pathogen ID, time to flag positive in blood culture analyser), against an anonymised sample ID attributed for the purpose of this study.

2.2.1 Peripheral blood mononuclear cell (PBMC) isolation

Blood was diluted 1:1 v/v with sterile dPBS then carefully layered onto Ficoll (Ficoll-Paque™ PREMIUM, 1.078 g/ml, Cytiva) in a falcon tube (3/15 ml Ficoll to 10/20 ml diluted blood in a 15/50 ml falcon tube, respectively) using a Pasteur pipette. Samples were centrifuged at 400 g for 30 min at RT (brake off; ~40 min) to fractionate the major components of blood based on density. A Pasteur pipette was used to carefully transfer the Buffy layer containing PBMCs from the interface between the plasma and the Ficoll to a clean tube. To wash, the tube was topped up to 15/50 ml with sterile dPBS and centrifuged at 30 g for 10 min (brake on). Supernatant was discarded and the pellet was resuspended by gently flicking the base of the tube. The was repeated twice more at 300 g and 200 g, respectively. The pellet was then resuspended in 12/25 ml dPBS and stored on ice while an aliquot (2x10 µl) of dead cells were stained using Trypan blue. Live cells were counted using a haematocytometer/light microscope. PBMCs were pelleted at 600 g for 10 min then resuspended at $5x10^6$ cells/ml. If PMBCs were not required that day, 1 ml aliquots were added drop-wise to freezing buffer [foetal bovine serum

(FBS) containing 20% v/v dimethylsulfoxide (DMSO)] were stored at -80°C until required. Alternatively, cells were frozen in Cell Banker cell freezing media (11910, AMSBIO) according to the manufacturer's instructions.

2.3 Detection of whole bacteria

2.3.1 Culture-based approaches

In accordance with hospital practice, the Miles-Misra method was used to quantify the number of viable bacteria in a sample (Miles et al. 1938). The method involves plating 20 µl of culture onto a nutrient agar (LB or cystine lactose electrolyte deficient (CLED) (PO0120A, ThermoFisher Scientific)) plate and incubating overnight. Once dry, the 20 µl drops formed a ~2 cm spot and were placed in a 37°C incubator overnight. Each bacterium will form an individual colony and since there is an upper limit to how many colonies can be counted in a single ~2 cm spot, the sample must be serially diluted to a concentration below ~200 CFU/spot. The error associated with such high dilution factors is discussed in section 2.5.1. The following day, the number of colonies are counted and used to calculate the number of CFU/ml according to their respective dilution factor.

2.3.2 Optical density

2.3.2.1 Absorbance spectrometry

A UV-visible spectrophotometer (Biophotometer, Eppendorf) was used to estimate the concentration of highly concentrated cultures of bacteria. UV-vis spectrometry gives a measured optical density (OD), *i.e.* amount of light absorbed by the sample at 600 nm (OD_{600}). Samples were loaded into an optically clear cuvette with a 1 cm path length (Fisherbrand™ Polystyrene Semi Micro Cuvettes for Visible Wavelengths). The spectrophotometer was first blanked using 1 ml of medium/buffer (*e.g.* LB or PBS) before comparing the change in absorbance in samples of bacterial suspension.

2.3.2.2 McFarland standards

A similar approach employed in clinical laboratories involves using a densiometer/nephelometer (e.g. densiCHECK plus, bioMérieux) to relate the turbidity of a bacterial suspension to its concentration (CFU/ml). A McFarland standard is a solution of barium chloride and sulfuric acid which, when mixed, produces precipitate of barium sulfate. A McFarland standard of 0.5 is equal to approximately $1.5x10^8$ CFU/ml and OD_{600} of 0.08 ~ 0.1 (Mcfarland 1907). The machines are typically pre-calibrated and ~3 ml of sample is required for each measurement, loaded into a FACS tube (*e.g.* Fisherbrand, FB59525).

2.3.3 MALDI-TOF MS

The pathogen identity of samples was ascertained via Matrix-Assisted Laser Desorption Ionisation Time-of-Flight Mass Spectroscopy (MALDI-TOF MS) at the Glasgow Royal Infirmary clinical microbiology laboratory using a VITEK®MS MALDI-TOF (bioMérieux).

A small volume (2 µl) of sample was added onto a measurement spot to which 0.5 µl of the matrix solution is added and the slide allowed to dry before being placed in the MS machine and run. The matrix solution is comprised of a mixture of volatile phenolic solvents such as α-cyano-4-hydroxycinnamic acid (CHCA) (Figure 2.1A) which penetrate the cell wall and co-crystallise with the proteins on evaporation. CHCA appears on the spectrum as a sharp peak and is used as an internal standard.

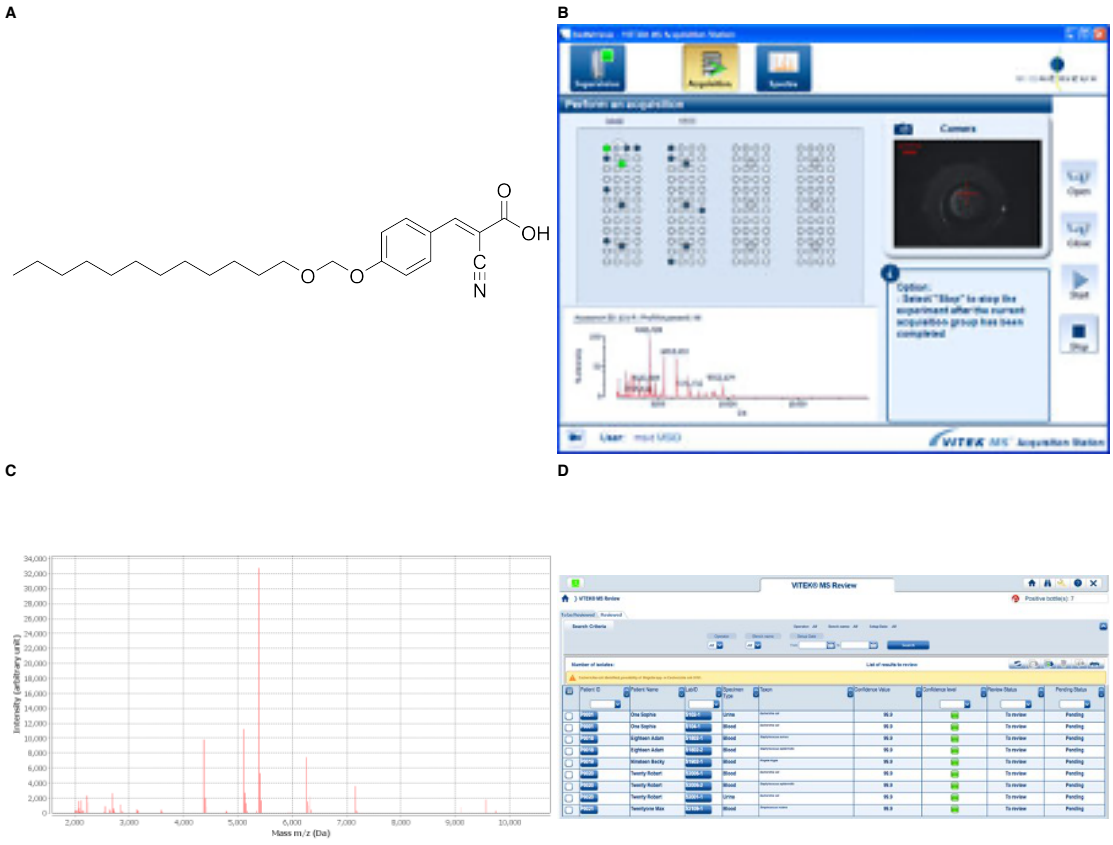

Figure 2.1: MYLA® software for pathogen identification using the VITEK®MS MALDI-TOF (bioMerieux). **A)** Chemical structure of matrix solution alpha-cyano-4-hydroxycinnamic acid (CHCA). **B)** Data acquisition shows the slide layout with blue circles indicating loaded samples not yet run, green circles represent positive IDs with high confidence, amber and red circles indicate IDs with low confidence and negative IDs, respectively. The dark square shows a live feed of the spot; the laser can be seen repeatedly firing at the biological material deposited on the slide. Below, a thumbnail of the m/z spectrum is shown and an enlargement **(C)**. **D)** shows a screenshot of the results, particular attention should be drawn to the 'taxon' column of the table, which gives the pathogen identity.

Each slide contains 51 spots, including three controls to which the *E. coli* (ATCC) control strain was tested. The slide is split into 3 equal sections, each one with its own positive control. First, the control spot is read, if this fails then the whole section is abandoned and the machine moves on to the next. The slide is rapidly processed by the MS machine (within minutes). Figure 2.1 B-D gives an overview of data acquisition and results software. Although low (~100 CFU/ml) limits of

detection are reported in the literature (Zhu et al. 2016) for pathogen identification using MALDI, a successful identification strongly relies on the associated database.

2.3.3.1 Limit of detection of MALDI-TOF MS

E. coli concentrations ranging from 10^2 to 10^9 CFU/ml were prepared according to section 2.1. 1 ml of each concentration was centrifuged for 3 min at 5000 g and the supernatant discarded before the pellet resuspended in 20 µl PBS. To prepare lysed samples, 1 ml aliquots were centrifuged at 5000 g for 3 min before the supernatant was discarded. Bacterial pellets were resuspended in 20 µl total lysis buffer [25 mM tris-HCl, 10 mM EDTA, 1% SDS, 100 nM NaCl, pH 8.0] and 2 µl was then loaded onto the MALDI slide as outlined in above in section 2.3.3. The ID of each method of sample prep method (neat, centrifuged or lysed) was recorded as positive or negative and compared in order to find the limit of detection. To validate the efficacy of the lysis buffer; a serial dilution of *E. coli* was made from 10^8 - 10^1 CFU and quantified using the Miles-Misra method (Section 2.3.1). Except for the highest concentration, no growth was seen on any of the plates indicating that all cells were lysed.

2.3.3.2 Effect of culture medium on time to positive detection of bacteria using blood culture

Under aseptic technique, a pre-seeded culti-loop (Thermo Scientific) was used to inoculate blood agar (BA) with *E. coli* (ATCC 5922) and *S. aureus* (ATCC 25923). Plates were incubated for 24 hrs at 37°C then single colonies were re-sub-cultured onto fresh BA plates and grown for another 2 hrs to get single-isolate colonies. 3-5 colonies were picked with an inoculating loop and emulsified in sterile saline to achieve a 0.5 McFarland standard equivalent to ~1.5x10^8 CFU/ml. The suspensions were then serially diluted to a concentration of ~250 CFU/ml.

Excess patient blood in EDTA from healthy controls (>70 ml) was pooled for this experiment. Universal tubes (30 ml) 10 ml of the medium (*i.e.* blood, PBS or LB) was added using a stripette in a lamina flow hood. Each medium was spiked with 125 CFU (500 µl) of either *E. coli* or *S. aureus* (n=3), leaving 3 tubes left sterile as a negative control for medium contamination.

The mock sepsis samples (10 ml) were then inoculated into labelled SN Virtuo™ blood culture bottles using a MediMop (a BC vial adapter which avoids the use of sharps). The tops of each bottle were cleaned before and after each inoculation using an alcohol wipe. Seeded BC bottles were then incubated in a BACT/ALERT® VIRTUO® (biomerieux) blood culture analyser until they flagged positive, at which point they were removed and sub-cultured onto fresh BA plates and incubated for 18-24 hrs. To facilitate recovery on terminal subculture, the bottle was plated as soon as possible after flagging positive. Any colonies which grew were identified using MALDI (see section 2.3.3) to confirm purity. All bottles still negative after 5 days in the BC analyser were also sub-cultured to confirm an absence of growth to check for false negatives.

A Dummy Patient (chi number 1402650000) and first name (LABS ONE) are used to indicate the sample/study. The blue barcode sticker (e.g. SAWPRTTV) is removed from the blood culture bottle. A 'lab number' (e.g. 21.1419421.C) is associated with each sample and used to search for the BC result using the MYRA computer system once they have been processed. See Chapter 3 for full results.

2.4 Detection of DNA

2.4.1 Preparation of DNA

Short (20 ~ 24 nt) strands of microbial DNA typically used for stimulation of a TLR9-mediated immune response *in vivo* can be purchased. These CpG oligodinucleotides (ODNs) come in many flavours depending on the host reactivity and type of response they can elicit. In our case, we were only interested in demonstrating physical binding between recombinant TLR9 and microbial DNA. ODN 2216 (InvivoGen) reportedly binds to human TLR9 and was used for section 2.8.1 experiments.

2.4.1.1 DNA extraction

The Wizard® Genomic DNA Purification Kit (Promega) was used according to the manufacturer's instructions with the following exceptions/alternations: RNase

solution was left to incubate for the maximum amount of time recommended in the protocol (60 min), care was taken to allow the ethanol to fully dry (often taking <1 hr) before resuspension of the DNA pellet overnight at 4°C in 25 µl rather than the recommended 100 µl.

In the PureLink™ Genomic DNA Mini Kit (Invitrogen), DNA extraction was carried out according to the manufacturer's instructions, with careful attention paid to completely dry the column prior to addition of the elution buffer so that the elution volume remained the same between samples. In order to maximise the concentration of DNA which could be used for the subsequent qPCR reaction, the smallest recommended volume of elution buffer was used (26 µl). Once eluted, gDNA samples were kept on ice then stored at -80°C until needed.

2.4.1.2 DNA fragmentation by sonication

gDNA intended for use with TLR9 was fragmented into shorter, uniform fragments to better mimic what could likely be found in a clinical sample. Samples of extracted and purified gDNA were thawed on ice then pooled and adjusted into 100 µl aliquots of 100 ng/µl in 0.65 ml Bioruptor Pico microtubes (Diagenode).

gDNA samples were sonicated using a Bioruptor® Pico (Diagenode) for 25 cycles of 30 s on / 30 s off, pausing to vortex halfway through with water temperature set at 4°C. The optimum number of cycles required to obtain the desired average fragment length of ~500 bp varied between sample types was optimised empirically (data not shown). The concentration of gDNA was compared pre- and post-sonication using NanoDrop and fragment length was verified by gel electrophoresis (data not shown). In brief, 10 µg per sample was added to loading dye (BioRad) and mixed by gently pipetting. Samples were loaded into a 1% agarose gel containing 3 µl ethidium bromide (EtBr). A 1 kb DNA ladder (NEB) was used to compare fragment lengths and the gel was run at 100 V for 40 ~ 60 min, taking care not to let the DNA run off the end of the gel.

2.4.2 Optical approaches to DNA quantification

2.4.2.1 NanoDrop

In this work, NanoDrop measurements were performed using a NanoDrop 2000 spectrophotometer (ThermoFisher Scientific). A sample (1.2 µl) was placed in the measuring spot and the optical density measured according to the manufacturer's instructions.

2.4.2.2 Qubit

Qubit™ HS dsDNA Assay Kit (ThermoFisher) is an alternative method for nucleic acid quantification. It involves incubating an intercalating fluorescent dye which binds between strands of double stranded DNA (dsDNA) according to the manufacturer's instructions. The samples are then measured using a proprietary fluorimeter.

2.4.2.3 Quantitative real-time polymerase chain reaction (qRT-PCR)

2.4.2.3.1 SYBRgreen qRT-PCR PowerUp™ SYBR™ Green Master Mix (Applied Biosystems) was used with primers (Forward: 5'-TGGTAATTACCGACGAAAACCGC-3' and Reverse: 5'- ACGCGTGGTTACAGTCTTGCG-3') designed to amplify a 147 bp fragments of the *UidA* gene from *E. coli* (K-12; JM109) as demonstrated by Mcomber (2013). gDNA was extracted and purified from *E. coli* using a commercialised (PureLink) kits introduced in section 2.4.1.1, according to manufacturer's instructions. The DNA concentration was measured using NanoDrop and Qubit™ and purity was checked using NanoDrop.

Standards were made by adjusting the DNA stock to 100 ng/µl and serially diluting 1:10 to give samples of 10^{-15} to 10^{-7} g. Each standard (1 µl), plus a negative control, was used in triplicate for each qPCR assay. Based on the estimate that each cell contains 4.5×10^{-15} g of DNA and, bearing in mind there is one copy of *UidA* per cell Mcomber (2013), we calculate that the standards represent a range of approximately 0 – 10^8 genome copies.

The qPCR assay mixtures consisted of 5 µl 2x PowerUp™ SYBR™ Green Master Mix (Applied Biosystems), 50 nM of each primer and 1-5 µl DNA template. The reaction was made up to 10 µl with nuclease-free water. Amplification was carried out on the StepOnePlus Real-Time PCR System (Applied Biosystems) according to the manufacturer's instructions; 2 minutes at 50°C to activate Uracil-DNA glycosylases (UDG) followed by 95°C for 2 minutes to activate the Dual-Lock™ DNA polymerase. 40 cycles of 95°C for 15 seconds (denaturation) plus 60°C for 1 min (annealing/extension). Melt curve analysis was also conducted to check for non-specific primer annealing.

It is important to check that cycle threshold (CT) threshold *i.e.* the relative fluorescence intensity of the sample at which the CT value is reported, was standardised between the standards and samples. This threshold is assigned by the software and should be in the exponential region where all CT values were either exported and used to calculate DNA concentration manually using R or calculated using the proprietary StepOne™ software.

2.4.2.3.2 TaqMan qRT-PCR Primers specific to the 16S rRNA gene in *E. coli* (forward: 5'-TAC GGG AGG CAG CAG T-3' and reverse: 5'-TAT TAC CGC GGC TGC T-3') were taken from a paper by (Trung, Hien, et al. 2016), in addition to generic bacterial 16S rRNA primers (forward: 5'-TCC TAC GGG AGG CAG CAG T-3' and reverse: 5'- GGA CTA CCA GGG TAT CTA ATC CTG TT-3') from a paper by (Nadkarni et al. 2002). There are 7 copies of 16S rRNA per *E. coli* cell (Coenye and Vandamme 2003; Mcomber 2013), we calculate that the standards represent a range of approximately 0 to $3x10^6$ genome copies. gDNA extracted from *E. coli* was used to make standards for absolute quantification as reported above. Primers were optimised according to the procedure outlined in the kit. The qPCR assay mixtures were made up of 10 µl TaqMan™ Fast Advanced Master Mix (Applied Biosciences), 300 nM of each primer, 175 nM probe, 1-5 µl DNA (optimised experimentally; data not shown) and made up to a total reaction volume of 20 µl with nuclease-free water. As with before, the amplification assay was carried out

using the StepOnePlus Real-Time PCR System (Applied Biosystems) using the fast programme recommended by the kit; 2 minutes at 50°C to activate UDG followed by 95°C for 2 minutes to activate the polymerase. 40 cycles of 95°C for 1 second (denaturation) plus 60°C for 20 seconds (annealing/extension).

2.5 Comparing methods of quantifying bacteria

Thorough characterisation of the detection/enrichment methods developed in this project relied on the accurate quantification of dilute concentrations of bacteria (10^1-10^8 CFU/ml). In the literature quantification can be overlooked – studies often only provide an estimated starting concentration or the minimum starting concentration for which method worked. For this project, it is crucial to be able to reliably create mock sepsis samples of a known bacterial concentration and, once a detection/enrichment method has been tested, to know how many bacteria have been captured (as a proportion of the input CFU). Several different methods are at our disposal which can be split into two categories: detection of whole pathogens and detection of pathogen DNA. Both have their respective advantages depending on the experimental context; an ideal method in a research laboratory may not be suitable for a clinical microbiology laboratory.

2.5.1 Relating optical density to concentration

The simplest means of calculating the concentration of viable microorganisms is by counting them according to the Miles-Misra method (see section 2.3.1). However, highly concentrated cultures must be diluted several times to be able to distinguish individual colonies on the plate which are one source of significant error.

$$colony\ number\ in\ 20\mu l\ \times\ adjustment\ to\ 1\ ml\ \times\ dilution\ factor$$

Each measurement was done for N replicas, with $N > 3$. If we define $n_{CFU}(i)$ the number of colony-forming units (CFU) counted for the ith replica, we can define the sample mean number of colony-forming units as:

(Eqn. 1)

$$\overline{n_{CFU}} = \frac{1}{N}\sum_{i=1}^{N} n_{CFU}(i)$$

And the corresponding sample standard deviation as:

(Eqn. 2)

$$\sigma_{\overline{n_{CFU}}} = \sqrt{\frac{1}{N-1}}\sum_{N}^{i=1}(n_{CFU}(i) - \overline{n_{CFU}})$$

If we assume that the relationship between the number of bacteria $\overline{n_B}$ in the plate and the number of colony-forming units $\overline{n_{CFU}}$ is linear:

(Eqn. 3)

$$\overline{n_B} = \alpha.\overline{n_{CFU,}}$$

If DF is the dilution factor, $\overline{N_B}$ the average number of bacteria in the starting volume (pre-dilution) and $\overline{N_{CFU}}$ the average number of CFU in the starting volume, then:

(Eqn. 4)

$$\overline{N_B} = DF.\overline{n_B} = \alpha.\overline{N_{CFU,}}$$

By combining equations 3 and 4:

(Eqn. 5)

$$\overline{N_B} = DF.\overline{n_{CFU}}$$

If u now denotes the uncertainty of measurements:

(Eqn. 6)

$$\frac{u_{\overline{N_{CFU}}}}{\overline{N_{CFU}}} = \sqrt{(\frac{u_{DF}}{DF})^2 + (\frac{u_{\overline{n_{CFU}}}}{\overline{n_{CFU}}})^2}$$

If we assume that there is no uncertainty on the dilution factor ($u_{DF} = 0$) , then:

(Eqn. 7)

$$u_{\overline{N_{CFU}}} = \overline{N_{CFU}}.\frac{u_{\overline{n_{CFU}}}}{\overline{n_{CFU}}} = DF.u_{\overline{n_{CFU}}}$$

The uncertainty is defined here as the sample standard deviation, consequently:

(Eqn. 8)

$$\sigma_{\overline{N_{CFU}}} = DF.\sigma_{\overline{n_{CFU}}}$$

Equation (8) highlights one of the main limitations of the culture method; if one sample is diluted 1000 times and leads to a counting of 10±2 CFU/ml, then results for the raw sample will be $1x10^4 \pm 2x10^3$ CFU/ml. At the other end of the spectrum, sampling 20 µl from extremely dilute cultures ($<10^2$ CFU/ml) may result in an underestimate of the number of bacteria present. The dilution required to count CFU might consequently lead to significant standard deviations.

UV-vis spectrophotometry can be used to quantify the optical density (OD; a.k.a turbidity) of bacterial cultures as a measure of absorbance at $OD_{600.}$ To determine its range of sensitivity, an overnight culture of 5 ml *E. coli* (K12 JM109; Amp100) was centrifuged (4000 g for 5 min at RT), the supernatant discarded and the pellet resuspended in 5 ml sterile PBS. The absorbance at OD_{600} was empirically adjusted to ~1.0 which is the real-world upper limit of the linear range of detection for the spectrophotometer. The sample was diluted to produce samples ranging from 1000, 800, 600, 400, 200, 100 and 50 µl of the starting suspension. Each sample was made up to 1 ml in sterile PBS and absorbance at OD_{600} was measured and recorded. The samples were then plated in triplicate according to the Miles-Misra method (see section 2.3.1). Colonies were counted and the starting concentration (CFU/ml) of each sample was calculated. Based on these results, an OD_{600} of 0.65 was used to adjust cultures of bacteria to a working concentration of ~$1x10^8$ CFU/ml which could then be then further serially diluted (Figure 2.2A).

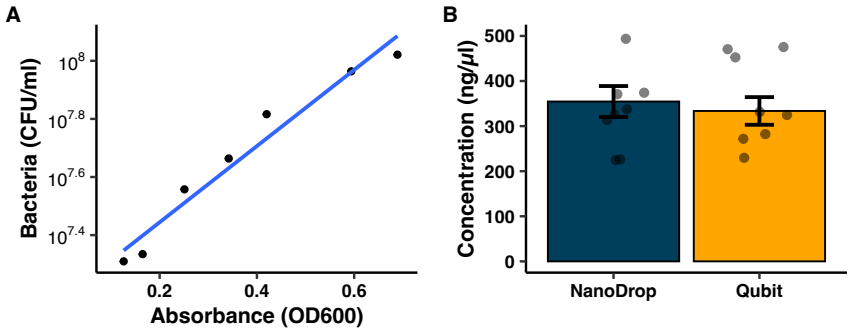

Figure 2.2: Optical approaches to pathogen quantification. **A)** Standard curve relating optical density OD600 to concentration of bacteria (CFU/ml). Equation of the linear regression (blue): $y = 157050119.4x - 2798379.8$, $R^2 = 0.992$. **B)** Comparison between Nanodrop and Qubit. Genomic DNA was extracted from 1 ml aliquots of *E. coli* (overnight culture, grown up to exponential phase) and the concentration measured using Nanodrop and Qubit. Error bars show standard error of the mean (n=8). Shapiro-Wilk's test demonstrated a normal distribution (p=0.162 and 0.439 for Qubit and NanoDrop data, respectively) and an independent t-test indicated the measurements from each method were not statistically significant (p=0.657).

2.5.2 Quantification of DNA is necessary at low microbial concentrations

Lower concentrations of bacteria need something more sensitive than optical density. The basic principle of DNA extraction involves cell lysis, wash, precipitation/column binding, wash (purification) and finally elution/resuspension (Figure 2.3).

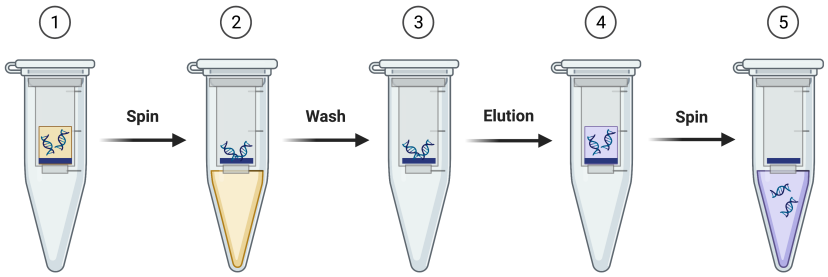

Figure 2.3: DNA extraction protocol using Purelink™ Genomic DNA Mini Kit (Invitrogen). 1. cell lysis, 2. wash to remove cell debris, 3. DNA bound to column, 4. elution of DNA, 5. pure, concentrated gDNA.

One of the fastest and easiest ways to quantify the total amount of DNA in a sample is to use NanoDrop (ThermoFisher Scientific) or Qubit (ThermoFisher Scientific). NanoDrop is a form of UV-vis spectrophotometry used for nucleic acid quantification. It relies on the principle that DNA and RNA absorb light at 260 nm; the amount of light that passes through the sample is measured by a photodetector. Optical density is then converted to concentration according to the Beer-Lambert law. Proteins absorb at 280 nm, so the fraction A260 nm/A280 nm provides an indication of purity (Desjardins and Conklin 2010). NanoDrop 2000 has a limit of detection of 2 to 15,000 ng/µl (*NanoDrop 2000/2000c Spectrophotometers - User Manual*, 2009) which gives it a theoretical lower limit of ~10^6 CFU. Qubit™ HS dsDNA Assay Kit (ThermoFisher) is an alternative method for nucleic acid quantification. It involves incubating an intercalating fluorescent dye which binds between strands of double stranded DNA (dsDNA). The samples are then measured using a fluorimeter. Qubit has the advantage that only dsDNA is measured so in theory the measurement is not skewed by the presence of impurities, however there

is no readout on this. The limit of detection is 0.2 to 100 ng, depending on the volume of sample added (1-20 µl) (Qubit™ dsDNA HS Assay Kit; (Nakayama et al. 2016)); which equates to a lower limit of ~10^5 CFU.

A comparison of the accuracy and reliability of NanoDrop and Qubit is shown in Figure 2.2B). Genomic DNA (1 ml aliquots of bacteria in exponential-phase (~10^8 CFU/ml), n=8) was extracted using the Wizard® Genomic DNA Purification Kit (Promega). These results showed there was no significant difference between NanoDrop or Qubit at the concentration tested. Importantly, these results highlighted the considerable variability between replicates (standard error of ±34.4 and ±30.7 ng/µl, respectively) for both techniques.

DNA extraction kit accuracy, sensitivity and reliability is an important factor to consider. Based on the estimate that each cell contains 4.5 fg of DNA (x10^{-15} g), we calculated 7.9 x10^7 ± 7.6x10^6 and 7.4 x10^7 ± 6.8x10^6 CFU/ml in the original samples for NanoDrop and Qubit, respectively. This suggests that the recovery of the gDNA extraction kit was only approximately 10%.

To determine if the variability of Nanodrop and Qubit were in fact due to the DNA extraction process, we compared two similar, commercially available kits. The Wizard® Genomic DNA Purification Kit (Promega) works by precipitating protein using a high salt buffer to leave the high-molecular weight gDNA in solution before it is purified and concentrated using isopropanol. Alternatively, in the PureLink™ Genomic DNA Mini Kit (Invitrogen), the cells are lysed and DNA is bound to a column, washed and finally eluted. DNA extraction kits are typically designed to be used with 1 ml of an overnight culture (~10^9 CFU), however much lower concentrations were required to simulate clinical samples or test the enrichment efficiency of a particular method of sample preparation. It was important to use the most sensitive kit available to try to minimise the loss of sample caused by the DNA extraction kit itself.

The suitability of the DNA extraction kits (section 2.4) for quantification using qPCR was determined using serially diluted of *E. coli* ranging from 10^7 to 10^2 CFU/ml followed by qPCR amplification (section 2.4.2.3.1). Figure 2.4A shows the

Wizard kit does not maintain a linear relationship between input bacteria and Ct value. Indeed, in this assay, a Ct value over 32 may be indicative of non-specific amplification, a common limitation to SYBRgreen qPCR. Contrasting this with the PureLink kit, the results show it can successfully extract DNA down to 10^2 CFU/ml. The negative control (no DNA) is still amplified, but there is sufficient separation from the sample at 10^2 CFU. Not only this but the linear range extends through all concentrations of DNA tested with a good separation of Ct values between each 10-fold dilution (Figure 2.4B).

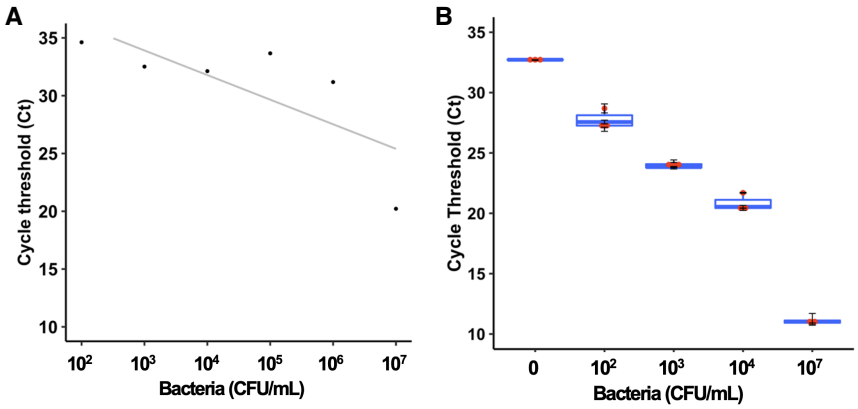

Figure 2.4: Comparison between **(A)** Wizard® Genomic DNA Purification Kit (Promega) and **(B)** PureLink^{TM} Genomic DNA Mini Kit (Invitrogen). *E. coli* was serially diluted from 10^7 – 10^2 CFU and subjected to gDNA extraction according to the two kits. Fragments of the UidA gene were amplified using qPCR with the PowerUP^{TM} SYBRgreen master mix (Applied Biosciences).

2.5.3 Probe-based qPCR is more sensitive than intercalating dyes

Higher sensitivity qPCR would enable better quantification of the percentage recovery of bacterial material and more confidently track the improvement/optimisation of new pathogen processing methods, particularly at the low concentrations ($<10^3$ CFU / 10^{-12} g DNA) seen in patient blood samples. SYBRgreen qPCR uses an intercalating dye which binds dsDNA; the more amplified DNA, the greater the fluorescence. Taq-man qPCR, on the other hand, relies on a fluorescent probe which hybridises with the target DNA sequence; the probe consists of a reporter dye at

one end and a quencher dye at the other. During PCR, the Taq polymerase cleaves the probe if it is bound to the amplified target sequence, separating the reporter dye from the quencher and generating fluorescence. An additional advantage of Taq-man qPCR is that it runs in ~40 minutes as opposed to 2.5 hours for SYBRgreen, however, it is more expensive.

Raw Ct values (*i.e.* the number of PCR cycles required to pass the Ct fluorescence threshold) were exported from StepOne^{TM} software (Applied Biosystems) and processed using a script in R. Each qPCR plate contained a standard curve containing a known concentration of DNA ranging from 10^{-7} - 10^{-15} g DNA, in triplicate technical replicates. SYBRgreen qPCR gave a limit of detection 10^{-12} g DNA (~10^{3} CFU) (Figure 2.5A). Notably, using Taq-Man PCR achieved a limit of detection of ~1 fg which is 3 orders of magnitude more sensitive than SYBRgreen and representative of a single *E. coli* bacterium (Figure 2.5B). In later experiments (data not shown), a linear regression model was fit to this and the equation of the line of best fit ($y = mx + c$) was used to convert the Ct value of each sample to the concentration of DNA (g). This was then used to extimate the number of bacteria (CFU/ml).

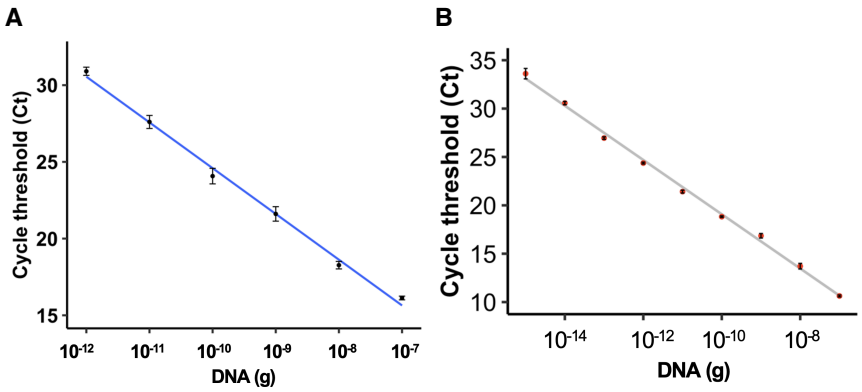

Figure 2.5: Comparison between limits of detection achieved by different qPCR master mixes. **(A)** qPCR amplification standard curve using PowerUP^{TM} SYBRgreen qPCR Master Mix (Applied Biosystems). DNA was extracted and purified from *E. coli* using the Wizard^{TM} genomic DNA extraction kit (Invitrogen), adjusted to 100 ng, then serially diluted to 1 pg. *E. coli* specific UidA primers were used at 50 nM each. **(B)** qPCR amplification standard curve using TaqMan Fast Advanced qPCR Master Mix (Applied Biosystems). DNA was extracted and purified from *E. coli* using the PureLink^{TM} genomic DNA extraction kit (Invitrogen), adjusted to 100 ng, then serially diluted to 1 fg. Generic 16S primers (blue) and *E. coli* specific 16S primers (red) were used at 300 nM each. This figure illustrates the limit of detection for TaqMan qPCR master mix to be 1 fg DNA. Error bars represent standard deviation, n=4. Negative controls were undetectable.

In summary, we opted to use OD_{600} ~0.65 to adjust the concentration of exponential-phase cultures to 10^8 CFU/ml which were then diluted further. DNA extraction kit efficiency was found to be one of the largest sources of error due to poor sensitivity and high variability. It was shown that the PureLink^{TM} Genomic DNA Mini Kit (Invitrogen) offered significant improvement in terms of accuracy and reliability for DNA extraction. qPCR was a reliable method for absolute quantification of pathogen DNA, both SYBRgreen and Taq-Man produced a linear standard curve which could be used to convert Ct value to DNA concentration. For more dilute cultures of bacteria (*i.e.* 10^3 CFU/ml), Taq-man qPCR was the most sensitive method. Finally, the Miles-Misra should be used for experiments which concern microbial viability, despite error caused by sampling low microbial concentrations and the effect of dilution factors at high concentrations.

2.6 Selective lysis of host cells

The selective lysis (SL) method was adapted from (Trung, Hien, et al. 2016; Trung, Thau, et al. 2019). Equal volumes (1 ml) of the mammalian cell lysis buffer (MCLB1) [1% Triton X-100, 2 M Na_2CO_3, pH 9.8] are mixed with a 1 ml sample of blood/PBS containing bacteria and incubated at RT for 3 minutes with gentle inversion. An equal volume (2 ml) of neutralisation buffer [Tris-HCl, pH 4.5] is then added to prevent further lysis of the bacteria. The sample is then immediately centrifuged (4500 g; RT) for 5 minutes to pellet the bacteria. The number of bacteria remaining in the pellet was then measured to determine the enrichment efficiency of SL. Care was taken not to leave the samples in MCLB1 for any longer than the recommended 3 min since lysis is very much time dependent and over-exposure would result in loss of bacteria as well as host cells. Intact bacteria remain in the pellet while the lysed mammalian cells, which are in the supernatant, can now be discarded. For control samples, PBS is added instead of MCLB1 or neutralisation buffer in order to distinguish the pathogen loss by the handling procedure from the effect of the lysis/neutralisation buffer. Remaining bacteria are quantified either by Miles-Misra (section 2.3.1), qPCR (section 2.4.2.3).

2.7 Protein biochemistry

2.7.1 Molecular tagging of recombinant receptors

Recombinant PRRs (see Table 2.2) were purchased from RD (Novus/BioTechne) in 50 µg aliquots. Proteins arrived lyophilised and were either resuspended in sterile PBS at a concentration of 200 µg/ml (according to the manufacturer's instructions) or 1 mg/ml for fluorescent labelling. Concentrations of resuspended protein were confirmed using NanoDrop and stored at -20°C until required.

Table 2.2: Recombinant PRRs used in this project

Receptor name	Tag	BioTechne catalogue number
TLR2	His	2616-TR

Receptor name	Tag	BioTechne catalogue number
TLR2	Fc	1530-TR
TLR4	His	1478-TR
TLR4	Fc	9149-TR
TLR9	Fc	7960-TR
MD2	His	1787-TR
TLR4:MD2 complex	His	3146-TM

2.7.2 Fluorescent labelling

For assay development tests, rabbit anti-*E. coli* (4329-4906, Bio-Rad Laboratories) was stained for using an AF647-labelled secondary donkey anit-rabbit IgG antibody (406414, BioLegend) at 1.25 ng/µl.

Recombinant receptors (see Table 2.2) were fluorescently labelled with AlexaFluor^{TM} 647 (AF647) according to the manufacturer's instructions (A30009, ThermoFisher Scientific). This technique labels free primary amine groups on lysine residues and is therefore amenable to any protein containing this free functional group.

His-tagged receptors could be conjugated to quantum dots (QDs) functionalised with nitrilotriacetic acid (NTA). Commercial CdSe/ZnS core-shell QDs were transferred from toluene to water via surface ligand exchange. His-tagged recombinant TLRs 2 and 4 were self-assembled at a molecular ratio of 5:1 TLRs:QD on the nanoparticle surface via their his-tag ligating metal ions at the QD interface. Successful conjugation and the optimal ratio of QD to receptor was confirmed by electromobility shift assay (EMSA).

2.8 Assays to characterise receptor binding

2.8.1 Microscale thermophoresis

NanoDrop measurements of AF647-labelled FcTLR9 gave a total yield of 0.388 µM or 0.269 µM (TLR9 alone *i.e.* corrected for the absorbance of the fluorophore at A650); the latter was used to calculate the concentrations for this experiment. Based on a reported K_D of 10-200 nM (Latz et al. 2004; Rutz et al. 2004), it was decided

that 20 nM of FcTLR9:AF647 should be used for the maximum concentration per experiment. According to the manufacturer's instructions, the suggested working concentration of CpG 2216 (sequence: 5'-ggGGGACGA:TCGTCgggggg-3'; Invitrogen) is 1-5 µM, however it is not clear if this is for *in vivo* experiments. Taking this and the maximum solubility of CpG ODN of 5 mg/ml into account, we resuspended the ODNs in 40 µl PBS to give a concentration of 4 mg/ml (606 µM).

A pre-test was first carried out to ensure FcTLR9 was suitable to proceed with the test. 40 nM stock of FcTLR9:AF647 was mixed with an equal volume of PBS (final concentration is therefore 20 nM), loaded into a capillary (~4 µl; n=4) and measured using the NanoTemper Monolith. There was no adsorption of the fluorescently labelled protein to the walls of the capillary, signified by a smooth bell curve with no dips (Figure 2.6A). Protein aggregation was also tested by looking at the MST trace; the resulting smooth curve shows no protein aggregation and fluorescence intensity is >300 RFU (Figure 2.6B).

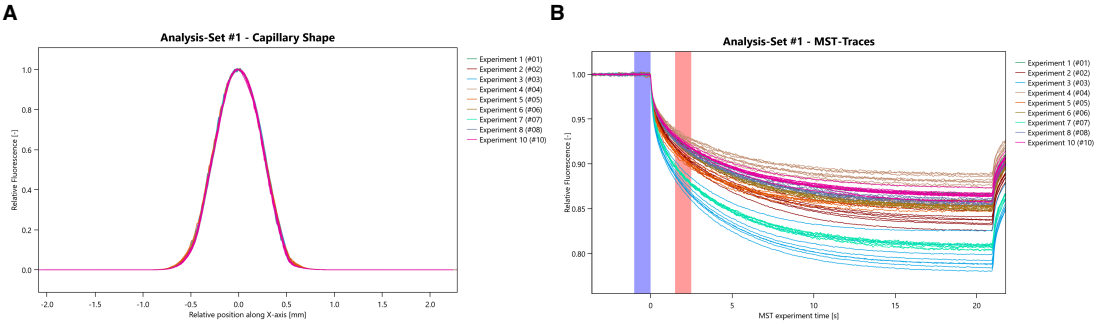

Figure 2.6: MST pre-test to check for **(A)** protein adsorption to the capillary walls and **(B)** protein aggregation.

A binding check was carried out to compare two samples, both with a fixed concentration of TLR9, but with one containing minimal CpG DNA and the other with a high concentration. The signal:noise ratio (high DNA : low DNA) was used to indicate if the sample binds. The signal:noise ratio can be improved by changing buffer or spinning down the target protein to pellet any protein aggregates and transferring the protein to another tube. The following buffers were tested:

- PBS (pH 7.4)
- PBST (0.05% Tween20, pH 7.4)
- MST Buffer containing magnesium (50 mM tris, 150 mM NaCl, 10 mM $MgCl_2$, 0.05% Tween 20, pH 7.4)
- Acidified MST buffer (pH 6.0, 1 mM $MgCl_2$) to mimic native endosome conditions (Rutz et al. 2004)

2.8.2 TLR2 capture assay

Assay development and optimisation is covered in detail in Chapter 4. TLR2 (1 µg/well in PBS) was immobilised on a 96-well plate overnight at 4°C. Bacteria were prepared according to section 2.1 then added to the plate at a concentration of 10^7 CFU/well (10^8 CFU/ml). Plates were incubated at RT for 30 min, then unbound bacteria was washed off the plate using PBS. Bound bacteria should remain immobilised to the bottom of the plate so there was no need to centrifuge. Before measuring the concentration of bacteria on the plate, a serial dilution of bacteria from 10^8-10^0 CFU/ml (in addition to a negative control) was made in triplicate in order to generate a standard curve.

Bacteria were quantified using a fluorescent plate reader (PHERAstar, BMG Labtech); laser power was set to the maximum (4095 units) and a high gain setting was selected. In later versions of the assay, captured bacteria were lysed prior to measuring fluorescence to liberate their GFP into solution and improve the fluorescent signal. To do this, 20 µl of lysis buffer [25 mM tris-HCl, 10 mM EDTA, 100 mM NaCl, 1 % SDS, pH 8.0] was added and the plate incubated for 30 min at 50°C.

Bacteria were later quantified using the BacTiter-Glo™ Microbial Cell Viability Assay (Promega) which is a colorimetric assay to quantify to amount of ATP in each cell. Samples were prepared according to the manufacturer's instructions. This method was chosen due to its increased sensitivity at lower concentrations of

bacteria. With this assay, there was no need for a separate lysis step and the same BMG plate reader was used to measure luminosity rather than fluorescence.

Raw fluorescence values were exported from the plate reader in the form of a .csv file and processed using R. A script was written, similar to with qPCR analysis (section 2.4.2.3), to fit a linear regression model to the standard curve data and use the equation of the line of best fit ($y - mx + c$) to convert fluorescence intensity / luminosity to cell concentration (CFU/ml).

2.8.3 Pathogen staining for flow cytometry analysis

Bacteria (10^7 CFU/sample) were blocked with 3% bovine serum albumin (BSA) for 15 min on ice temperature and washed once before addition of the appropriate receptor for 30 min on ice. Unbound receptor was washed off and stained cells were resuspended in 100 µl PBS for imaging flow cytometry (IFC) analysis. For samples tested with anti-*E.coli*, the secondary antibody was then added for 30 min at RT, washed as per the other samples. To wash, samples were centrifuged (1000 g for 5 min) before supernatant was discarded and the pellet resuspended in 500 µl sterile PBS; washes were repeated 3 times.

2.8.4 Imaging flow cytometry

Imaging flow cytometry (IFC) data was used to characterise binding of fluorescently labelled receptors to fluorescent bacteria expressing GFP. Samples in solution are run on an Amnis® ImageStream® X Mk II imaging flow cytometer (CYTEK) which records side-scatter, fluorescence and brightfield (BF) image data via the INSPIRE control software (CYTEK). Cell feature data is processed in a similar manner to conventional flow cytometry (CFC) data, by plotting features which in this case have been extracted from the images in the form of histograms and scatter plots saved in a raw image file (.rif). Data is extracted from these images during post-processing using the IDEAS software.

2.8.4.1 IFC detection of bacteria

During data acquisition, magnification was always set 60x and fluidics speed was set to 'low' to achieve the highest sensitivity. 10,000 events were acquired for each sample with the 488 and 642 nm lasers set to 20 and 150 mW, respectively (set using a raw max. pixel saturation; 98% of events below the saturation point ($4x10^3$ RFU) for each channel). Compensation controls were acquired with BF and SSC off and all lasers on. Single-stained controls *i.e.* GFP-bacteria alone and UltraComp eBeads™ Plus (01-3333-42, Invitrogen™) bound to each of the receptors individually were used for compensation. Data was pre-processed in the IDEAS(R) software (CYTEK). Compensation controls were used to generate a compensation matrix which, once batch-applied to all samples, corrected for spectral overlap between different channels. At this point, raw feature values for gradient root mean square (RMS) bright field (BF), area BF, aspect ratio BF, mean fluorescence intensity Ch02, Ch05 and Ch06 were exported as .csv files to be processed in R. A detailed explanation regarding optimisation of the analysis workflow can be found in Chapter 4.

2.8.4.2 IFC detection of DNA

FcTLR9 (1 µg/sample, not fluorescent) was mixed with protein A-coated magnetic beads (1 µm DynaBeads, 10 µl/sample; ThermoFisher Scientific) and incubated for 15 min at RT. Microcentrifuge tubes were placed on a magnet and any unbound receptor was removed. Samples were washed once with PBSTM buffer [PBS, pH 6.0, 1 mM $MgCl_2$, 0.05% Tween20]. DNA (1 ng/sample equated to approximately 10^7 CFU) was added to each sample and incubated at RT for 15 min. Unbound DNA was removed by washing once using the magnet. Bound DNA was then stained using DAPI (4',6-diamidino-2-phenylindole) or PI (propidium iodide) (1 µg/sample).

To ensure results captured the variability in capture efficiency of the FcTLR9-functionalised magnetic beads to DNA, rather than preceding conjugation steps. A stock of functionalised beads was therefore made fresh for each experiment and then

split between replicates before DNA was added. Conjugation/washes were carried out in PBSTM buffer to limit non-specific binding, until the final step where samples were resuspended in 100 µl PBSM (no Tween20) to prevent detachment. Samples were left on ice and protected from light until they could be analysed using IFC.

IFC analysis of DNA followed broadly the same steps as with bacteria with the following exceptions: Only the 405 nm laser was needed (set to 120 mW) to excite the fluorescent DNA dye and, since there was only one marker being detected there was no need to perform compensation. Samples were processed in IDEAS$^{(R)}$ software (CYTEK) to manually gate on single, DNA-positive DynaBeads. A full explanation of the experimental and analytical optimisation we undertook can be found in Chapter 6.

2.8.4.3 IFC analysis of blood

Due to its viscosity, whole blood (section 2.1) needed to be diluted to avoid the introduction of air bubbles in the sample line. A 32-fold dilution was experimentally determined as optimal (data not shown), which is supported by (Headland et al. 2014)) who recommend a 1:40 dilution. Dilutions were done in FACS buffer [2% FBS, 5mM EDTA, 0.05% Tween20] in order to optimise cell viability. RBC-lysed blood (section 2.2) required no such dilution however FACS buffer was used wherever possible. Samples containing human blood also required the laminar flow hood housing the ImageStream flow cytometer to be switched on and care was taken to dispose of all human samples according to the clinical waste disposal protocol in our laboratory.

To determine the binding target of recombinant TLR2 and 4 in blood, we stained whole and RBC-lysed blood for monocytes (PE-CD14; BioLegend) and neutrophils (PE-CD15; BioLegend). Blood was first prepared in PBS for live/dead staining using eFluor450 (eBioscience^{TM}). Then, due to the fact both markers were labelled with the same fluorophore, separate samples were stained for CD14/15 in FACS buffer. Stained samples were washed once more with FACS buffer and then submitted for analysis using IFC.

Data acquisition followed the same procedure as section 2.8.4.1 with a number of exceptions: 405 nm and 561 nm lasers were set at 120 mW and 200 mW, respectively (max. for both), having made sure raw max pixel intensity at $4x10^3$ was below 2% of the total number of cells in each channel. Single-stained controls were acquired for compensation (1000 events). Samples were processed in IDEAS$^{(R)}$ software (CYTEK) to manually gate on live, single cells in focus which were double positive for TLR and PE. More detail can be found in Chapter 5.

2.9 Markdown, data analysis graph plotting

Data analysis, graph plotting and statistical analysis were all carried out using R (Version 4.1.2+). Typesetting of the thesis document was done in R Studio / R Markdown adapted from the oxforddown thesis template (Lyngs 2019). Where possible, raw data in the form of an Excel or .csv file from each experiment was imported and tidied in an R script. This was saved as a .csv file and then imported into the relevant thesis R markdown file (.Rmd) wherein it could be plotted according to a common theme and colour scheme. This way, all data reported in the thesis is accessible directly from the working directory which contains all code used to plot the results. Schematics were created using Biorender.com unless stated otherwise. Statistics were carried out using R when biological replicates were available according to the schematic in Figure 2.7). For experiments where only technical replicates were available, these were averaged and error bars representing standard deviation of the mean were plotted where applicable.

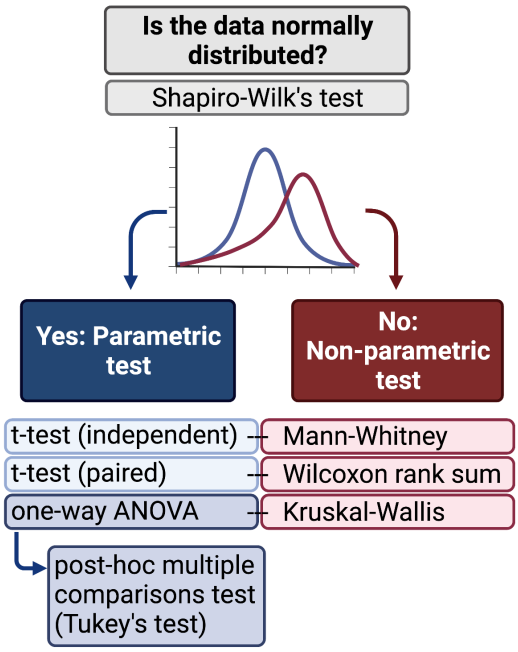

Figure 2.7: Statistical tests. Created with BioRender.com

3

Chapter 3: Understanding the clinical significance

3.1 Introduction to the clinical diagnostics workflow for the detection of bloodstream infections

Blood culture is the current gold standard for microbial bloodstream infection (BSI) diagnostics (Lamy et al. 2016). One of the challenges associated with pathogen identification is that there is very little evidence of the pathogen to be found in the blood stream – only 1-1000 colony forming units (CFU)/ml (Opota, Jaton, et al. 2015). Contrast this with the 10^9 red-blood cells/ml and 10^7 white blood cells/ml and the challenge becomes evident: finding pathogens in blood is like finding a needle in a haystack. To increase the number of viable pathogens to a concentration at which they can be detected, two blood samples (6~10 ml each) are taken directly from the patient into pressurised blood culture vacutainers; one designed for aerobic growth and one for anaerobic. Samples are loaded onto an automated blood culture analyser (*e.g.,* bioMérieux BacT/ALERT® Virtuo) which incubates them at 37°C and monitors for signs of microbial growth such as changes in pH or CO_2 production. Eventually, if there is sufficient microbial growth, a

colorimetric reaction takes place and the sample is flagged as positive, ready to be removed for downstream processing. Blood culture is the longest step in the entire diagnostic process (1-5 days (Opota, Jaton, et al. 2015)) and is only applicable to microbial infection. In 42% of samples no growth is detected, suggesting a non-culturable, viral or sterile cause of the patient's symptoms (Lin, Harris, et al. 2018). Importantly, and especially for rapidly deteriorating conditions like sepsis, this delay in diagnostics can provoke over-prescribing of broad-spectrum antimicrobials, in turn further fuelling antimicrobial resistance (Niederman et al. 2021).

Some products have been commercialised to perform diagnosis directly from whole blood (*i.e.* without blood culture), such as PlexID, MagicPlex, SepsiTest, SeptiFast and VYOO. Most are based on nucleic acid amplification, which is sensitive enough to detect generic material at the concentrations typically measured in whole blood ($10^{3\text{-}4}$ genome copies/ml (Opota, Jaton, et al. 2015)). However, this reliance on genetic material precludes the measurement of minimum inhibitory concentrations necessary to determine the susceptibility of a pathogen to antimicrobials. Current techniques are also probe-dependent, and thus only the gene fragments selected for amplification for can be found. New approaches are emerging using techniques such as next generation sequencing, but many of these techniques are still incompatible with raw, unprocessed patient blood samples and are still comparatively expensive compared to the gold standard of blood culture ($560 (Cao et al. 2022) *vs.* $178 for blood culture (Pliakos et al. 2018)).

Developing a diagnostic method suitable for clinical translation can be challenging and deployment can be hindered by a range of limitations such as scalability, cost or practicality. Getting a clinical perspective from very early on in the development process is therefore imperative. In the context of this work, access was granted to the microbiology department of the Glasgow Royal Infirmary (GRI). The goal was to better understand the current detection process and identify the best avenues to explore for integrating TLRs into the clinical workflow. The overall workflow for BSI detection at the GRI is presented in Figure 3.1.

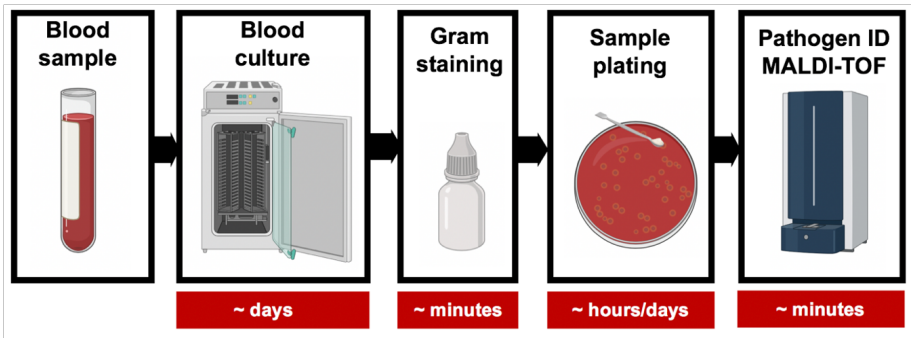

Figure 3.1: Workflow for detection of BSIs using MALDI-TOF MS at the Glasgow Royal Infirmary. Red rectangles indicate an estimation of the time required for each step of the process.

Similarly to ~80% of UK hospitals (Angeletti 2017), microbial pathogen detection at the GRI is based on matrix-assisted laser desorption/ionisation time-of-flight mass spectrometry (MALDI-TOF MS). MALDI-TOF MS has indeed been recognised as one of the most cost-effective diagnostic tools for bloodstream infections ($45.99 per test) compared to molecular-based techniques such as PCR ($67.90 per test) or peptide nucleic acid fluorescence *in situ* hybridisation (PNA-FISH; $139.05 per test), among others. Although efforts have been made to use MALDI-TOF MS directly from clinical samples such as urine (Pinault et al. 2019) or to reach lower limits of detection by improving the hardware/database (*e.g.*, reported limit of detection of 100 CFU/ml for bacteria (Zhu et al. 2016)), the National Health Service (NHS) still relies on a culture-based protocol and a proprietary database for pathogen ID.

To better appreciate the time scale associated with this step, the GRI provided data associated with their equipment. As presented in Figure 3.2, time to detection by the automated blood culture analyser was always greater than 8 hours and highly variable depending on bacterial species.

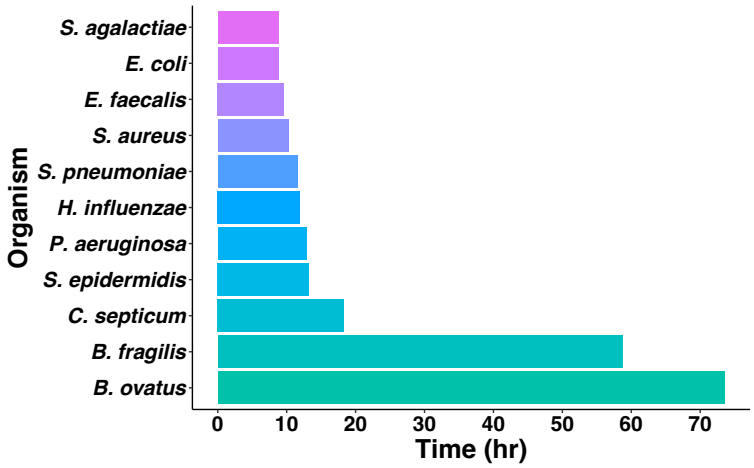

Figure 3.2: Mean time to detection as a function of bacterial species in blood using BioMerieux 'Virtuo' automated blood culture analyser. Data was provided by collaborators at the GRI.

After a blood culture sample flags positive, a small volume of the sample is collected for Gram-staining. Determining the Gram-status of the causative pathogen is a significant milestone in the BSI diagnostic process for this is the first point at which the specificity of antimicrobial therapy can be narrowed (Niederman et al. 2021). The positive sample is sub-cultured (plated onto fresh agar), informed by the result of the Gram-stain, and incubated once more to yield so-called mono-microbial colonies. This stage also adds significant delays to pathogen identification since some bacteria can be slow to grow but also because this step does not rely on automated equipment. A staff member must check regularly, and manually, for growth onto the plate. Depending on the frequencies of check-ups and opening hours of the laboratory, this second culture step can also add hours/days to diagnostic.

Once pure, mono-microbial colonies have been observed visually on the plate, a small portion is taken for identification using MALDI-TOF MS. Once the identity of the pathogen is known, a second portion is taken for antimicrobial susceptibility testing (AST). Phenotypic AST relies on determining the dosage of antibiotic required to meet the minimum inhibitory concentration (MIC) to visibly inhibit growth of an organism according to the European Committee on Antimicrobial Susceptibility Testing (EUCAST) breakpoints. Traditionally, phenotypic AST was

done using disk- or strip-diffusion tests (Kuper et al. 2012), which would typically add 18-24 hours to the diagnostic process (Angeletti 2017). New technologies, such as the Alfred 60/AST, are now able to provide results in 5 hours (Hatanaka 1993). A summary of clinically available molecular diagnostics tools can be found in Table 3.1

Table 3.1: Summary of current methods of clinically available molecular diagnostics tools for pathogen ID and AST of BSIs in the UK. Average time of 27.91 hours (Ward et al. 2015)

	Required prior blood culture	Identification	Antimicrobial susceptibility test	Time (+28 hr if requires blood culture)	Relative cost/sample
MALDI-TOF MS (Florio *et al,* 2018)	Yes	Species level	Certain metabolites (*e.g.* β-lactam ring)	15 min (28 hr)	+
FilmArray (Ward *et al.,* 2015)	Yes	24 pathogens	3 genes	1 hr (29 hr)	++
Verigene (Ward *et al,.* 2015)	Yes	Gram-positive assay (9 species, 4 genera) Gram-negative assay (5 species, 4 genera)	Gram-positive assay (3 genes) Gram-negative assay (6 genes)	2.5 hr (30.5 hr)	++
Alfred 60/AST (Lahanas *et al.,* 2013)	Yes	No	Yes (empirical MIC)	5 hr (33 hr)	++

	Required prior blood culture	Identification	Antimicrobial susceptibility test	Time (+28 hr if requires blood culture)	Relative cost/sample
Accelerate PhenoTest BC kit (Starr *et al.,* 2019, Marschal *et al.,* 2017)	No	Gram-positive assay (4 species, 2 genera) Gram-negative assay (4 species, 4 genera) Yeasts (2 species)	Same as ID	ID 27.5 hr AST 40 hr	+++
T2Dx (Beyda *et al.,* 2013)	No	*Candida* panel (5 species) Bacteria panel (5 species)	No	*Candida* 3 hr Bacteria 5 hr	+++

We acknowledge that not all clinical laboratories process blood samples in the same way, however we evaluated the process in the GRI to provide clinically relevant targets for the optimisation of the proposed technology. More specifically, I focused on the quantification of key missing parameters, such as the sample type supported by MALDI-TOF MS and its limit of detection (LoD). The process of scooping colonies from a plate with a plastic loop is crude and implies a high concentration of bacteria is loaded onto each MALDI slide and suggests a high variability between samples. Selective lysis (SL) is a pre-existing method of sample preparation of bacteria from whole blood which aims to lyse and remove host cells from a sample to leave intact bacteria (Machen et al. 2014; Trung, Hien, et al. 2016). Here, it is tested for its compatibility with subsequent pathogen ID using MALDI-TOF MS.

3.2 Results

3.2.1 Limit of detection of the GRI MALDI-TOF MS

While the GRI MALDI-TOF MS is typically used with pure bacterial colonies, the first objective was to determine if the equipment worked with a liquid sample (mimicking the sample type that we would obtain if we were to enrich bacteria using TLRs). For that, the limit of detection of MALDI-TOF MS was determined at the GRI with PBS samples, spiked with *E. coli* concentrations ranging from 10^2 to 10^9 CFU/ml. For samples that were loaded directly, none of the identifications worked (Table 3.2; "suspension"). The concentration was increased by centrifuging the samples and resuspending the pellet in as small a volume as could be loaded onto the MALDI slide (2 µl). A positive detection was recorded for slides containing more than $1.2x10^6$ colonies in the 2 µl sample, corresponding to *circa* $1.2x10^7$ CFU/ml (Table 3.2; "concentration"). Interestingly, there appears to also be an upper limit of detection, as slides containing more than $1.3x10^8$ colonies could not be identified by the equipment. It has been reported in the literature that the LoD of MALDI-TOF MS could be improved by lysing bacteria, to increase the probability of detecting bacterial material onto the slide (Pinault et al. 2019). In these tests however, total lysis prevented positive bacterial identification (Table 3.2; "total lysis").

The MALDI detects proteins in the size range of 2-20 kDa (Angeletti 2017); if some, or all, are denatured or degraded by the lysis buffer, then the spectrum obtained will be different. This suggests that intact bacteria are required for MALDI-TOF MS, if we intend to use the database provided in the clinic. For these results, it seems clear that the current LoD of MALDI-TOF MS at the GRI is too high to work directly with patients' samples (containing typically 1-10^3 CFU/ml *vs.* a LoD of 10^7 CFU/ml). However, blood culture might be enough to reach those concentrations, in which case, all the subsequent steps (Gram staining, plating) could be avoided (potentially reducing hours/days to the diagnostics).

Table 3.2: Results of detection of spiked *E. coli* samples in PBS using MALDI-TOF MS (VITEK MS; Biomerieux). For each dilution of *E. coli* ranging from 10^9 down to 10^2 CFU/ml, three sample preparation methods were tested; n=3 technical replicates (Rep.): Direct *suspension* (1 ml), *concentration* by centrifugation followed by resuspension in a volume of 2 µl, and *total lysis* of the direct suspension culture. A total of 2 µl of each sample was added to the MALDI slide with HCCA matrix solution. The method of sample preparation is indicated by an asterisk (*). Plus (+) and minus (-) symbols indicate positive and negative identification, respectively.

Starting concentration (CFU/ml)	**Suspension (1 ml)**	**Concentration (2 µl)**	**Total Lysis (2 µl)**	**Rep. 1**	**Rep. 2**	**Rep. 3**
$1.28x10^9$	*			-	-	-
	*	*		-	-	-
	*		*	-	-	-
$1.28x10^8$	*			-	-	-
	*	*		+	+	+
	*		*	-	-	-
$1.20x10^7$	*			-	-	-
	*	*		+	+	+
	*		*	-	-	-
$1.30x10^6$	*			-	-	-
	*	*		-	-	-
	*		*	-	-	-
$1.20x10^5$	*			-	-	-
	*	*		-	-	-
	*		*	-	-	-
$1.38x10^4$	*			-	-	-
	*	*		-	-	-
	*		*	-	-	-
$1.20x10^3$	*			-	-	-
	*	*		-	-	-
	*		*	-	-	-
$2.00x10^2$	*			-	-	-
	*	*		-	-	-
	*		*	-	-	-

3.2.2 Limit of detection of the GRI blood culture analyser

In order to experimentally determine bacterial concentration post-blood culture, the bacterial load of four positive blood culture samples was determined using the Miles-Misra method. Except for one patient (16A), the three other samples revealed concentrations that are higher than the MALDI LoD (Figure 3.3). More samples

were in the process of being tested prior to 2020, however this was cut short due to restricted access to the clinical lab during the COVID-19 pandemic. The average concentration for patients 19A, 20A and 28A is 9.0 $\pm 4.6 \times 10^7$ CFU/ml, which is in accordance with the literature (Opota, Jaton, et al. 2015). Assuming blood culture leads to concentrations greater than 10^7 CFU/ml, it would consequently be possible to directly detect bacteria after blood culture.

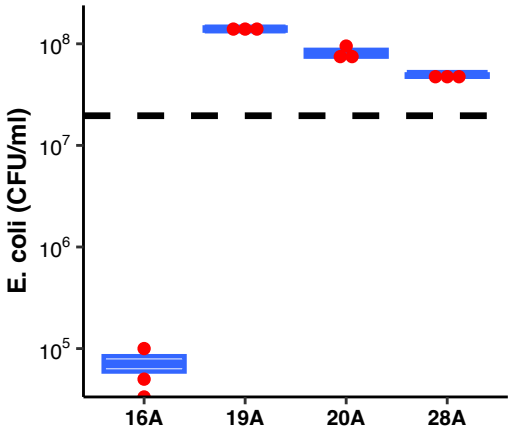

Figure 3.3: Estimated concentration of bacteria (expressed as CFU/ml) measured using the Miles-Misra method in four patient blood samples which flagged positive on blood culture analyser BacT/ALERT Virtuo (bioMerieux). MALDI-TOF MS confirmed the pathogen identity to be *E. coli*. The black horizontal dashed line indicates the LoD of MALDI (1.2×10^7 CFU/ml). On each box the central mark indicates the median, and the bottom and top edges of the box indicate the 25th and 75th percentiles, respectively. The whiskers extend to the most extreme data point (n=3 technical replicates).

3.2.3 Seeded study to determine the potential benefit for pre-enrichment of bacteria from patient blood prior to blood culture analysis

Since the goal of this PhD thesis is to investigate new sample processing approaches, the next step was to test whether pre-enrichment of bacteria from a patient blood sample would result in a faster time-to-positive (T_{pos}) result on the blood culture analyser, by isolating bacteria from growth inhibitors present in blood.

A reduced T_{pos} would provide crucial justification for the pre-enrichment of bacteria from patient blood samples by novel methods which will be discussed in later chapters. These methods seek to reduce the time a patient spends on broad

spectrum antibiotics by speeding up the pathogen identification and AST process. The goal is to use pre-enrichment to 'piggy-back' off the high-throughput AST methods currently used by the NHS which rely on high (10^7 CFU/ml) concentrations of bacteria which are only attainable by blood culture. In the absence of any growth contaminants found in blood, the culture time should in theory be significantly shorter after pre-enrichment.

Overnight cultures of bacteria (*E. coli* and *S. aureus*) were adjusted to a McFarland standard of 0.5, signifying approximately ~10^8 CFU/ml. Stocks were then serially diluted down to 125 CFU/ml in horse blood, PBS or LB. At this point, 100 µl was plated on blood agar and incubated overnight to order to confirm the actual concentration of bacteria. Colony counts indicated 300 CFU/ml and 180 CFU/ml for *E. coli* and *S. aureus*, respectively, which was within an acceptable margin of error associated with this method of serial dilution and the Miles-Misra plating technique. A similar approach was taken for each of the media stocks to find out if there was any contamination and no growth was observed in any of the control plates.

Each sample was then placed in a blood culture bottle in the GRI blood analyser (BACT/ALERT Virtuo, Biomerieux). Once the blood culture bottles flagged positive, they were sub-cultured and grown overnight before a MALDI isolate was taken to confirm the identity of the positive growth (and rule out any contamination). Bottles which were negative after 5 days were also sub-cultured to check for false negative growth in the BC analyser.

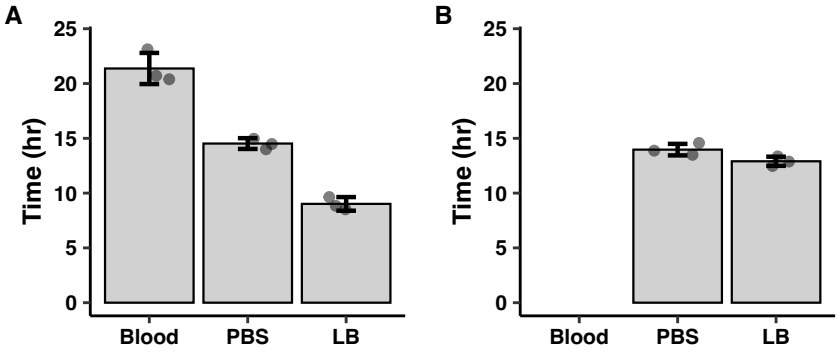

Figure 3.4: Time to flag positive for blood, PBS and LB media spiked with 300CFU/bottle **A)** *E. coli* and **B)** 180 CFU/bottle *S. aureus*. One-way ANOVA indicated incubation media had a significant impact on time to flag positive (p=1.14e-5) for *E. coli*, however not for *S. aureus* (p= 0.0518). n=3 technical replicates.

The effect of culture medium (blood, PBS or LB) on time to flag positive for *E. coli* and *S. aureus* in the BACTEC Virtuo blood culture analyser is shown in Figure 3.4. *E. coli* flags positive after 21.4 (±1.4), 14.5 (±0.5), 9.0 (±0.6) hrs for blood, PBS and LB, respectively. For *S. aureus*, cultures spiked into blood did not grow at all, PBS flagged positive after 14 (±0.5) hrs and LB after 12.9 (±0.4) hrs. None of the control bottles (sterile) flagged positive in 5 days and sub-culture/MALDI results confirmed there was no contamination. Further, sub-culture/MALDI isolates of all positive samples identified only *S. aureus* or *E. coli,* as expected. This data suggests the presence of inhibitory factors in whole blood significantly delays the time to flag positive for *E. coli* and completely prevents growth in *S. aureus*. The use of a nutrient rich broth such as LB appears to promote rapid growth, particularly for *E. coli*. The growth rate of *E. coli* and *S. aureus* is comparable, in spite of the difference in starting concentration. The choice of culture medium clearly has a significant effect on the growth time suggesting that pre-enrichment of bacteria from whole blood could speed up diagnostics.

3.2.4 Selective lysis: a surrogate approach to rapid, indirect pathogen enrichment

While my goal is to investigate if TLRs can be used to enrich bacteria, I had the opportunity to join an international project focusing on a point-of-care (PoC) system for *E. coli* detection where pathogen isolation was done using selective lysis. Here, the findings related to the point-of-care system and then an investigation into whether selective lysis could be used to further test the GRI MALDI-TOF MS will be presented.

3.2.4.1 Paper-based LAMP device for the detection of *E. coli* in blood

PoC devices capable of rapidly detecting pathogens, out of a clinical setting, with minimal cost and training, are reported as being the future of sepsis diagnostics (Steel et al. 2016; Oeschger et al. 2019; Reddy et al. 2018). Colleagues at the University of Glasgow recently developed a device of this nature to detect malaria in 98% of infected individuals in a double-blind study (Reboud et al. 2019). The device combines three novel methods to yield accurate results within 1 hr:

- paper-based sample preparation of whole blood to extract DNA (~15 min)
- loop-mediated isothermal amplification (LAMP) of species-specific fragments of DNA (~1 hr)
- lateral-flow test (LFT) detection of amplified DNA (<5 min)

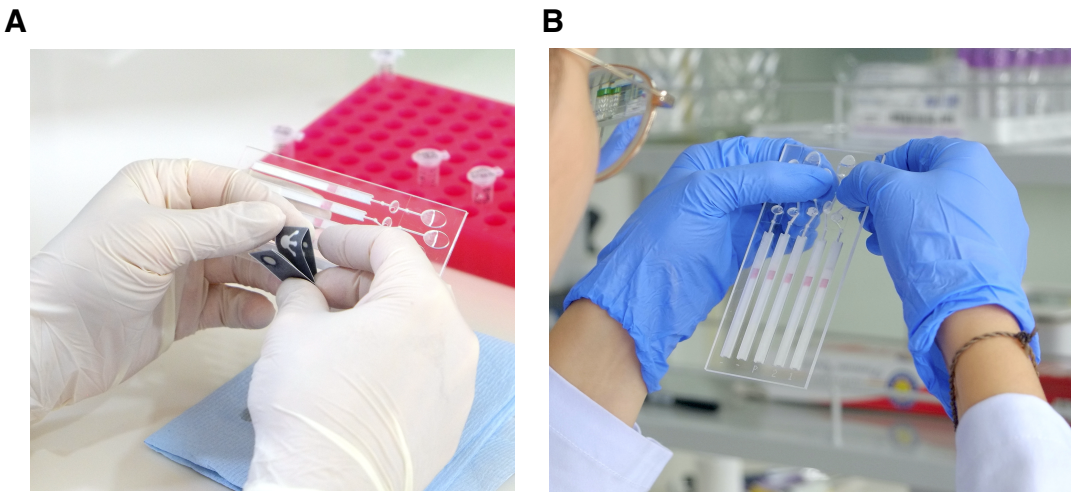

Figure 3.5: Point-of-care devices for the rapid extraction, amplification and detection of pathogen DNA from whole blood. **(A)** DNA is extracted from a finger-prick of whole blood using a paper-based microfluidic device. **(B)** Amplified pathogen DNA is manually flushed from the LAMP reaction chamber on to the LFT for detection.

Paper-based DNA extraction is carried out from a finger-prick of whole blood (~10 µl) on a Whatman paper strip measuring ~10 cm x 2 cm. The paper is printed with hydrophobic wax ink which keeps the sample liquid contained within specific regions of blank paper and thus allows the creation of chambers and channels. Each time the device is folded, capillary flow results in liquid transfer and each fold represents a different reaction step: lysis, distribution, washing and elution (Figure 3.5A). The eluted sample containing extracted DNA is hole-punched and inserted into the plastic amplification/detection device (Figure 3.5B). LAMP is a rapid alternative to PCR which does not require temperature cycling (Crippa et al. 2012) (Figure 3.6). Mastermix containing FITC-/biotin- tagged primers is added and the sample incubated at 65°C for 45 min. The amplified DNA is then flushed from the reaction chamber onto the LFT strip where it binds red nanobeads and is carried laterally, once more *via* capillary flow (Reboud et al. 2019). If the target DNA fragment has been amplified, two bands can be observed on the LFT strip. If no amplification occurs, then only the upper band can be seen; this also serves as a positive control for the LFT assay (similar to LFT COVID tests).

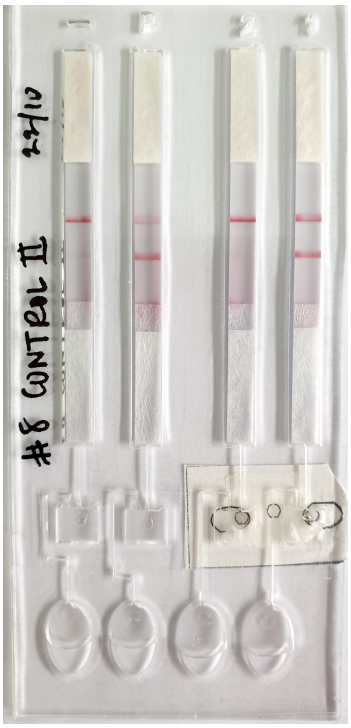

Figure 3.6: Example of point-of-care LFT device control. Reading from left to right on the control device , the first two LFT strips (- and P) are a negative and positive controls for the LAMP reaction, respectively. The negative control ensures tests for contamination with E. coli DNA in the device/reagents. The positive control contained Plasmodium pan DNA (a mix of DNA from 4 different species) spiked in at 1.1 ng/sample. The third LFT strip from the left (2) is for amplification of the human breast cancer gene (BRCA1) which acts as a positive or negative control depending on the sample type. In control samples carried out in PBS, it's a negative control for contamination with human genetic material from the environment. With blood samples, it's a combined positive control for both DNA extraction and amplification of human material in blood. For samples subjected to selective lysis using mammalian cell lysis buffer (MCLB), it is a positive control for the total removal of human material. Finally, the furthest right test strip (1) to confirm the presence or absence of E. coli is on the far right-hand-side. The assay is not designed to be quantitative, however in some instances amplification of trace quantities of the pathogen can result in a faint red band in a clean sample. In this case it is important to compare the test strip result to the positive and negative controls; if the test strip is fainter than the negative control (far-left hand strip), then the sample can be classed as free of infection.

Here, the device was adapted by other members of the group to amplify and detect *E. coli* DNA, as opposed to the work previously done for malaria. My contribution was to investigate whether SL could be combined with the device for blood analysis. I joined the Vietnamese-German Centre for Medical Research, which is part of 108 Military Central Hospital in Hanoi, to determine 1) how well

the device performed in a clinical laboratory and 2) if sensitivity could be improved with the inclusion of a selective lysis pre-treatment step, namely mammalian cell lysis buffer (MCLB), developed by the Vietnamese team.

Samples consisted first and foremost of a mixture of positive and negative controls spiked in PBS and whole blood. A total of 53 samples were run. Of these 45 (84.9%) showed successful extraction, amplification and detection of their positive (*P.* pan) and negative (*E. coli*) controls, and were therefore referred to as working devices (Appendix Figure A.1). Whole blood was spiked with either 10^6 CFU/ml (n=9) or 10^3 CFU/ml (n=3) *E. coli,* to represent a sample from a sepsis patient (Figure 3.7A). Performance was below 30% for both concentrations of bacteria tested. For the healthy controls, 100% of the working devices gave a true negative result.

A blind study of 20 whole blood samples from patients was carried out, half positive for *E. coli* infection and half healthy controls (HC). Five of each were prepared for LAMP/LFT analysis using selective lysis and paper-based DNA extraction, respectively, and the number of 'correct' samples was recorded (Figure 3.7B). Both methods of sample preparation performed poorly; 25.0 % and 33.3% yielded successful results for paper extraction and selective lysis, respectively.

It must be noted that the devices used for this part of the investigation were of an older design, leftover from a previous field study abroad. This means they could have been out of date by the time they were used for this experiment. LFTs contain lyophilised antibodies which would likely degrade over time and with repeated fluctuations in air pressure during long haul flights that the older devices were subjected to. Using newer devices would be expected to have a noticeable improvement on the success of the experiment. From this data, the use of SL to improve the LoD of the PoC devices tested here did not yield the expected results. In the next section I investigate the recovery of viable pathogens and pathogen DNA after SL treatment to confirm the problem came mostly from the PoC devices.

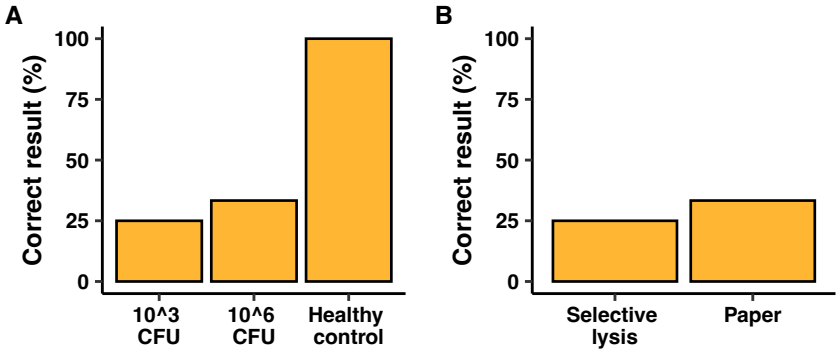

Figure 3.7: Point-of-care device performance. **(A)** Healthy blood spiked with *E. coli* at 10^3 and 10^6 CFU/ml copared to health control (no bacteria). **(B)** Double-blind study with clinical samples comparing sample preparation using selective lysis and paper-based DNA extraction. Results are expressed as a percentage of workding devices - those with correct *E. coli* and *P.* pan controls (yellow).

3.2.4.2 Recovery of pathogen DNA after selective lysis treatment

The recovery of *E. coli* DNA after SL was quantified using qPCR amplification of the 16S rRNA gene. A standard curve of serially diluted *E. coli* DNA was used to convert Ct value to concentration of DNA (g). Controls were incubated with PBS instead of MCLB1 but otherwise treated identically in order to measure the amount of loss due to the handling process rather than the buffer itself. DNA recovery is linearly proportional to the concentration of input bacteria for most of the range of samples tested (Figure 3.8). The limit of detection (LoD) is said to be reached when this linearity plateaus *i.e.* when there is no longer a change in DNA yield as the starting concentration of bacteria continues to decrease, ~10^3 CFU/ml in this case. It was found that this limit was mostly imposed by the DNA extraction kit used. Nevertheless, DNA recovery using selective lysis is effective and DNA should have been found in the PoC devices (especially for the high concentrations (~10^6 CFU/ml) tested).

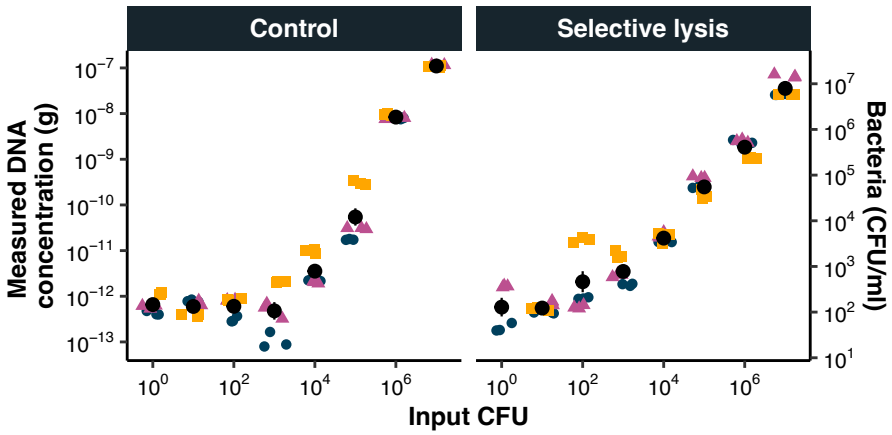

Figure 3.8: Recovery of *E. coli* DNA after selective lysis treatment. **A)** gDNA was extracted from a serially diluted of bacteria ranging from 1x10^7 to 0 CFU/ml and quantified using qPCR. **B)** Samples were treated with selective lysis buffer prior to DNA extraction. Samples of the same colour/shape represent qPCR technical replicates, each colour/shape represents a technical replicate for gDNA extraction. Black points represent mean and error bars represent standard deviation (n=3).

3.2.4.3 Bacterial viability is affected by selective lysis treatment

For coupling with MALDI-TOF MS, it is not sufficient to rely solely on gDNA quantification for characterisation of SL. Although it is much more sensitive, yield seems to be affected by the inherent variability of the gDNA extraction kit, and the majority of the methods used in the clinical microbiology lab for pathogen ID/AST need viable (culturable) bacteria. Reliance of the literature on amplification-based techniques can therefore be misleading.

Selective lysis was performed once more on a 10-fold serial dilution of *E. coli* ranging from 1x10^1 ~ 1x10^7 CFU/ml in 1 ml PBS. The number of viable bacteria remaining after SL was quantified using the Miles-Misra method, and used to calculate the number of CFU/ml Figure 3.9. As with before, in order to compare the loss of bacteria caused by SL and the loss associated with the method in general, an identical dilution of samples was subjected to the same method, except PBS was used instead of MCLB1 and neutralisation buffer.

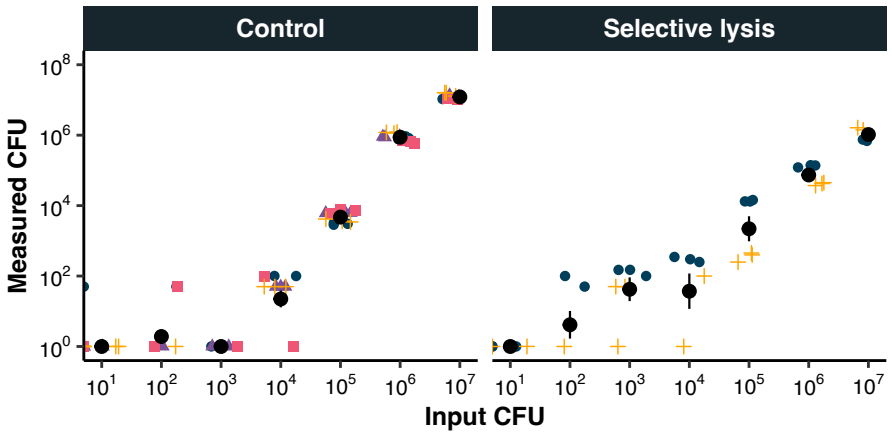

Figure 3.9: Recovery of viable *E. coli* (CFU) after selective lysis treatment. Samples of the same colour/shape represent qPCR technical replicates, each colour/shape represents a technical replicate for gDNA extraction. Black points represent mean and error bars represent standard error (n=3).

If the Miles-Misra method were 100% efficient, we would expect a 1:1 ratio of input CFU to measured CFU and a linear relationship when plotted on a logarithmic scale. Looking first at the control in Figure 3.9, we see that at high concentrations of bacteria ($10^6 \sim 10^7$ CFU/ml) we are able to recover a high proportion of the input bacteria. At 10^5 CFU/ml, we are only able to detect 10% of the input bacteria and at 10^4 CFU/ml the number further decreases to 1%. For the SL samples, if we focus on high bacterial loads ($<10^5$ CFU/ml), treatment using MCLB stops ~90% of the cells from growing. At lower input CFU, however, we see a good separation from the negative control. Below 10^4 CFU/ml, the curve is expected to plateau due to the sampling error of the Miles-Misra method and this may likely just be noise (section 2.5). The loss of viable bacteria is a severe limitation for MALDI-TOF MS analysis or AST; ultimately, these results suggest that this SL is not suitable for sample preparation of viable bacteria from positive blood culture.

3.3 Discussion

In this chapter, the clinical diagnostics workflow for bloodstream infections was evaluated in order to highlight potential points at which a novel sample preparation method could be introduced to speed up pathogen identification. By all accounts,

blood culture causes a significant delay to patient treatment (Mellor 2013; Seymour et al. 2017), however our investigation showed that it is nevertheless essential. A reliance on pathogen identification using MALDI-TOF MS means the bacterial load of a patient sample must be increased from 1-1000 CFU/ml in whole blood (Opota, Croxatto, et al. 2015) to 1.2 x 10^7 CFU/ml (Figure 3.3). Although it has recently been demonstrated that MALDI-TOF MS can be used to detect pathogens directly from blood using a bespoke database of spectra (Pinault et al. 2019), it is not possible with the workflow currently employed in the NHS. Blood culture has therefore been the gold standard of reaching this limit of detection (LoD) for several decades.

3.3.1 Pre-enrichment could reduce time to positivity of blood culture

Motivated by the restrictions imposed by the sensitivity of MALDI-TOF MS, the decision was taken to test methods of pre-enrichment of bacteria from blood. I tested if a method developed to remove bacteria from whole blood could reduce the time to flag positive using a blood culture analyser in the hospital and, in turn highlight the extent to which whole blood negatively impacts microbial growth.

Results showed that the time to flag positive for *E. coli* (and *S. aureus*) in blood was improved by the removal of bacteria from blood (Figure 3.4), suggesting pre-enrichment of bacteria direct from whole blood would be beneficial to the overall diagnostic process. The incubation times measured here were much longer than validation data shared by the GRI (Figure 3.2) wherein an identical concentration of *E. coli* and *S. aureus* would take ~8 and ~ 11 hours, respectively. This is comparable to the times recorded for the bacteria in LB media (Figure 3.4).

For experiments on time to positivity, blood from healthy donors was collected in EDTA vacutainers. EDTA is a chelator of metal ions (such as calcium and magnesium) used by enzymes to carry out essential biological processes. By chelating calcium, EDTA inhibits the coagulation cascade, in turn preventing blood from clotting (Banfi et al. 2007). It is therefore added to blood vials to slow the metabolism of host cells and prevent clotting (Kell 2009). This begs the question

whether EDTA was inhibiting microbial growth in blood. Typically, if a synovial fluid sample is accidentally provided in EDTA then it cannot be cultured. Bearing in mind that *S. aureus* is responsible for a high proportion of prosthetic joint infections and septic arthritis (Rutherford et al. 2016), then this may explain why we saw no growth in our tests. More specifically, researchers have shown a mixture of EDTA and desferroxamine B can inhibit biofilm formation by methicillin-susceptible *S. aureus* (Al-Azemi et al. 2011). The presence of EDTA in the vacutainers used in this experiment has likely led to an under-representation of the microbial growth time in blood culture analyser bottles. It is important to try to limit coagulation, however a better alternative would be sodium citrate or heparin vacutainers which are less inhibitory to microbial growth than EDTA.

Automated blood culture analysers run 24 hrs a day. Consequently, many more replicates would be needed to clearly define the bacterial load of positive blood culture samples as these will not be processed for several hours if they flag as positive outside of standard working hours (Monday-Sunday; 8:00-20:00). The additional time spent in the incubator could significantly increase the bacterial load they carry by the time they are processed by staff. Indeed, hospital logistics play a powerful role in the overall duration of the diagnostic process. In a paper by Weinbren *et al.*, they reduced the overall time to detect blood culture isolates from 16-26 hr to less than 12 hrs simply by physically moving the blood culture analyser into the same room as the equipment for downstream processing (*e.g.* MALDI). (Weinbren et al. 2018). This goes to show that a thorough appreciation of the entire clinical diagnostic process is crucial in order to have a measurable impact on patient outcomes, not just an understanding of the science on a molecular scale.

3.3.2 Selective lysis does not improve the limit of detection of MALDI-TOF MS in a clinical microbiology setting

Positive blood culture samples are plated (sub-cultured) and grown overnight to isolate pure, monomicrobial colonies. To identify the species of pathogen, these colonies are transferred onto a MALDI slide using a small plastic scoop. We

demonstrated that successful pathogen ID is also compatible with samples in liquid suspension (Table 3.2), which allowed us to load specific concentrations of bacteria and determine the LoD of MALDI-TOF MS. At ~10^7 CFU/ml, blood culture, despite the delay it causes to patient treatment, remains a necessary preparatory step to reach such a high concentration of bacteria. Using current methods available in the GRI, detecting pathogens in whole blood directly is not possible.

Selective lysis is a method of removing host cells from a sample of whole blood. Collaborators have demonstrated that their method of selective lysis (using mammalian cell lysis buffer (MCLB)) is able to remove 98% of human genetic material and has a LoD of ~100 CFU/ml using qPCR to detect pathogen DNA (Trung, Hien, et al. 2016). Here, we quantified the impact of this buffer on bacterial viability (as opposed to DNA recovery). It was found that at high bacterial concentrations, a significant proportion (94%) of viable bacteria are lysed, meaning the LoD of the MALDI could not be met with viable clinical samples (Figure 3.9). The importance of viability cannot be stressed enough, since phenotypic AST relies on measuring growth of an organism in the presence of increasing concentrations of an antibiotic. A fundamental caveat of using chemical rather than enzymatic lysis to remove human cells is its time-dependent nature: too much time spent in the buffer (*i.e.* longer than the recommended 3 minutes in the protocol) and the bacteria will be discarded in the supernatant. Selective lysis also inherently depletes all bacterial circulating free DNA (cfDNA). This could be seen as a significant disadvantage since cfDNA is an interesting source of information for detecting sepsis as highlighted by the recent work of (Blauwkamp et al. 2019).

3.3.3 Point-of-care devices are not yet sensitive enough for the direct detection of *E. coli* in whole blood

One potential way around the limitations of MALDI would be to employ a PoC device capable of rapidly and directly detecting trace quantities of pathogen DNA in a sample of whole blood (Reboud et al. 2019). To this end, a device developed to detect Malaria DNA was adapted and evaluated to see if it could detect *E. coli* DNA

in a clinical setting. In an endemic/pandemic use case; for example, the detection of malaria (Reboud et al. 2019) or SARS-COV19 (Song et al. 2021), there is only one causative pathogen which must be identified. For sepsis, there are hundreds of potential culprits. In addition to this, the bacterial load in a sample of sepsis blood is 1-1000 CFU/ml (Opota, Jaton, et al. 2015), compared to 10^5 cells/ml for malaria. In a 10 µl drop of blood, there would consequently be a maximum of 10 CFU/assay, making the required sensitivity of the device much more stringent. As we have shown in Figure 3.7, this was not possible with the tested devices.

Selective lysis was employed as a pre-treatment to remove host cells to improve the sensitivity of the device. (Trung, Hien, et al. 2016) have reported removal of 98% of human DNA when measured using PCR. Human blood contains 4.0-6.0x10^5 cells/ml. If just 2% of these remain after lysis, this still equates to 8.0x10^3 ~ 1.2x10^4 cells/ml which may likely present as additional peaks in the MS spectrum and in turn contribute to the negative MALDI results. Any remaining human genetic material suggests incomplete lysis by MCLB, this may in turn hinder successful qPCR amplification of pathogen DNA and thus impair the limit of detection, indicated in Figure 3.6 by the presence of two bands of *BRCA* control. An important follow up experiment would be to quantify how much human "contamination" is required to prevent MALDI from yielding a positive result.

3.3.4 Conclusion

Selective lysis is a method of indirect pathogen enrichment whereby human blood cells are lysed using a buffer containing a mild detergent. Fundamental structural differences in the bacterial cell wall mean that they are left intact ready for subsequent detection in a less complex solution. Collaborators successfully demonstrated the SL can speed up pathogen identification using PCR (Trung, Hien, et al. 2016; Trung, Thau, et al. 2019). Our results showed that although this is true, selective lysis significantly impacts pathogen viability yielding a lower concentration of culturable pathogens and slower subsequent growth times. This ultimately makes pathogen detection using methods reliant on culture, such as

MALDI-TOF MS or phenotypic AST, take longer. An ideal sample processing approach would consequently include both whole pathogen and pathogen DNA separation to maximise the amount of material available for diagnostics.

Toll-like receptors (TLRs) are a class of pathogen recognition receptor (PRR) which can bind to pathogen/damage associated molecular patterns (PAMPS/DAMPS). They target broad characteristics of pathogens such as non-methylated CpG DNA, ssRNA viruses, cell surface components like lipopolysaccharide (LPS) of Gram-negative bacteria or lipoteichoic acid (LTA) on Gram-positives, flagella *etc.* TLRs are employed by the innate immune system to raise a standardised inflammatory response upon detection of a pathogen. The range of possible targets which TLRs can detect presents an interesting opportunity to design a pathogen enrichment system based on the selection of PAMS/DAMPS to which they can bind. Consider a multiplexed assay able to determine the Gram-status of bacteria to rapidly inform antimicrobial therapy pre-blood culture, or to extract pathogen DNA ready for qPCR or sequencing for a patient who has already received antimicrobial therapy. The next chapters will focus on better understanding if TLRs can help towards that goal. Of particular interest are TLR2, TLR4 and TLR9. TLRs 2 and 4 bind to Gram-positive, Gram-negative bacteria, respectively, and these will be the focus of chapters 4 and 5. TLR9 binds to the non-methylated CpG motif of prokaryotic DNA and will be investigated in Chapter 6.

4

Chapter 4: Method development for the binding characterisation of pathogen recognition receptors

4.1 Introduction

In this chapter, direct methods of pathogen enrichment, *e.g.* using an antibody to directly bind to and enrich a pathogen, are investigated. While antibodies are limited when it comes to sepsis diagnostics by their specificity to one particular target, pathogen recognition receptors (PRRs) have the potential to overcome such limitations (Sorgenfrei et al. 2022).

Before testing samples in a clinical context, the first challenge, as highlighted in the introduction, is to determine if the receptors can successfully bind bacteria *in vitro*. From a biochemical perspective, these questions are discussed in terms of *ligands, analytes* and *substrates.* Approaches such as atomic force microscopy (AFM), surface plasmon resonance (SPR), microscale thermophoresis (MST) or isothermal titration calorimetry (ITC), which require pure samples of the ligand and target in question, should be ruled out. Measuring the binding affinity of TLR2 to a synthetic ligand Pam3CSK4, for instance, has been done before (Vasselon et al. 2004) but the strength of the interaction on a molecular scale does not provide sufficient

information to infer how well TLR2 could bind to whole bacteria in a culture. Indeed, Mogensen *et al.,* credit TLR2 with the capacity to bind 10 distinct ligands found on the cell surface. If complexed with either TLR1 or TLR6, the number increases to 13, and these molecular patterns can be found on bacteria, protozoa, fungi and viruses (but crucially, not eukaryotes) (Mogensen 2009). The real-world binding capacity will be altered further by other properties such as surface charge, competitive- or non-specific binding. In reality, the number of available ligands per cell is not yet known. For this problem, we need to focus on cell-binding assays which can quantify the proportion of the initial sample which is bound by the receptor.

As a starting point, inspiration was taken from two typical techniques accessible to most biologists in research laboratories: enzyme-linked immunosorbent assay (ELISA) and (imaging) flow cytometry (IFC). The common denominator of these techniques lies in the exploitation of antibodies' propensity to bind specific molecular motifs on cells. Effectively, both are examples of immunoassays where the techniques differ in their method of detection: colorimetric (*e.g.* horseradish peroxidase and tetramethylbenzidine), fluorescence or chemiluminescent. The approach we will take here is to first establish whether the techniques can be adapted to detect bacteria using an anti-*E. coli* antibody, which binds to somatic and capsular antigens which form part of the cell wall, as a positive control. The antibody will then be swapped out for a recombinantly expressed TLR which will subsequently be evaluated for its potential as an *in vitro* pathogen enrichment candidate in Chapter 5.

4.1.1 Flow cytometry

Flow cytometry is a fluidic-based, multiparametric, single-cell approach used to identify and quantify cells within a heterogeneous population. Developed in the late 1960's, the first flow cytometer was described in 1972 (Bonner et al. 1972; Fulwyler 1965) and has since developed into an integral discipline within both research and clinical immunology and cellular biology.

In conventional flow cytometry, cells in suspension are pumped through a narrow tube and focused to its centre using sheath flow. As single-cells pass through a

laser, they scatter light forwards (FSC; forward scatter) and to the side (SSC; side scatter). This scattered light is detected by photomultiplier tubes (PMTs), the intensity of which is then analysed computationally. This information alone can provide meaningful insights into the size and granularity (a measure of the internal complexity) of cells and thus allows a cell identification within a mixed sample. The power of flow cytometry to subtype cells increases exponentially when they are fluorescently labelled with either a dye or fluorescent antibody. DNA dyes, for instance, allow cells to be identified based on the relative quantity of genetic material which provides valuable insights into cell cycle analysis (Jayat and Ratinaud 1993). Antibody labelling makes it possible to classify cells based on molecular epitopes both on the surface or inside of a cell. Fluorophores are excited by light of a particular wavelength and emit light at another. By selecting fluorophores with excitation wavelengths that correspond to lasers available in the machine and emission wavelengths which both correspond to specific band-pass filters and have minimal overlap with one another, a multiplexed panel can be designed to identify several phenotypic markers simultaneously.

Starting with one colour, technological advances over the last 50 years have resulted in improvements which saw an increase from 4-8 colours (limited by the choice of available fluorochromes) to 10-20 becoming the norm in a research setting (Robinson et al. 2023; Steen 2000). The fundamental principles have remained very much the same since its inception and, in many aspects, miniaturisation of technology has not resulted in improved performance (Steen 2000). Enhancements in dyes in terms of stability, longevity, colours, and an ever-expanding selection of antibodies on offer for the detection of a wider variety of cell types. The replacement of high-pressure Hg/Xe lamps with solid-state diode light sources has complemented this wider selection of dyes and fluorophores. In recent years, the advent of full spectrum flow cytometry (or spectral flow cytometry) has increased the maximum panel size to 40-50 markers (Park, Lannigan, et al. 2020; Konecny et al. 2023; Ferrer-Font et al. 2021). By replacing single detectors, which have a band-pass filter to measure a portion of the spectrum corresponding to one fluorophore, with multiple

detectors designed to measure the entire visible spectrum, more fluorophores can be resolved and used in tandem. There is a variation of the technique called mass cytometry, commercially known as CyTOF (Fluidigm/Standard BioTools), which uses antibodies conjugated to isotopically pure metals instead of fluorophores. Detection is done using time-of-flight mass spectrometry to acquire a spectrum of the mass/charge ratios of each marker, of which ~50 can typically be used in a single panel (Doerr 2011).

Another major area of progress is data analysis; in the early years of flow cytometry the advent of personal computers with enough memory to store data in a list and perform linear/logarithmic transformations made a significant improvement to gating strategies (Steen 2000). More recently, the arrival of datasets with increasing numbers of markers has called for analysis strategies able to tease out meaningful conclusions from highly complex datasets. High-dimensional analysis has become the norm in single-cell RNA sequencing analysis and is now being introduced into flow cytometry for larger panels (Robinson et al. 2023; Marsh-Wakefield et al. 2021).

The minimisation of spectral overlap is an art unto itself, helped by improved fluorophores with narrower excitation and emission spectra and experience in selecting the best combination for a particular cytometer/assay. Total eradication of spectral overlap is often unavoidable and results in the fluorescence of more than one fluorophore being detected in a single channel. To correct for this, samples can be *compensated* so that the fluorescence measured in each channel (by each detector) comes from the specific marker in question, minimising the probability of detecting false positives. This is done by acquiring data with single-stained compensation controls; the magnitude of spectral overlap in undesirable channels is stored in a compensation matrix which is subsequently used to correct for this overlap in each sample, providing laser power is kept the same (Roederer 2002).

Once samples have been run, they are typically processed using proprietary software such as FlowJo by BD Biosciences or IDEAS by CYTEK/Amnis/Luminex/Merck. Gating is a process which involves selecting feature values (*e.g.* fluorescence

intensity or SSC) to be plotted either as one-dimensional histograms or two-dimensional scatter plots then manually selecting regions of the plot which indicate a particular phenotypic characteristic to be grouped, or gated. The process is performed sequentially to separate out cells which have multiple mutual or divergent characteristics and is called a *gating strategy.* Gating strategies can be saved as templates and applied to multiple sample files in batches, however biological replicates can vary slightly depending on numerous factors, such as time of day, laboratory temperature or pipetting error. This slight variation in the mean fluorescence intensity can have significant impact on the percentage of cells which ultimately fall outside of the gate. Indeed, there is an acceptance of inherent subjectivity when it comes to manual gating which, in the past, has even led to experts to advise researchers to invest in better computer screens (Herzenberg et al. 2006). It's this subjectivity which will be challenged in this chapter.

4.1.1.1 Flow cytometry for the detection of bacteria

Flow cytometry is very popular in the fields of cell biology and immunology; however it has never been considered to be at the forefront of microbiology. This is somewhat surprising since flow cytometry was shown to be able to detect bacteria decades ago (Steen et al. 1982). Indeed, some important discoveries have been made by using flow cytometry to investigate bacterial growth; for example, a number of studies in the late 1970's and early 1980's all noticed a steady decrease in cell size and DNA content as cells enter the stationary phase (Bailey Jila Fazel-madjlessi et al. 1977; Paau et al. 1977; Hutter and Eipel 1978; Skarstad et al. 1983). Comparison with optical density (OD) highlighted that the 'gold standard' actually leads to an underestimate in cell concentration – a doubling time of 23 and 18 min for OD and flow cytometry, respectively. Researchers made the observation that the decrease begins in early log phase when nutrients are still in abundance. Remarkably, this finding never caught on and OD is still the primary means of quantifying bulk cultures of bacteria at high concentrations ($>10^8$ CFU/ml). Flow cytometry has also been used to perform antimicrobial susceptibility testing. Initially, cells had

to be fixed and permeabilised to enable dye to infiltrate the cells and bind to DNA. Live cells were stained on ice but when they were removed and run in the machine, the dye was found to be actively removed *via* an efflux pump. This led researchers to try metabolic inhibitors, however ultimately the success of the assays was reliant on dye uptake (Walberg and Steen 2001). The fact bacterial genomes are approximately 1000-fold smaller than mammalian cells makes the process even trickier with dimmer fluorescent signals.

More recently, Moor *et al.,* have written a protocol for the quantification of bacterial surface binding antibodies in different bodily fluids (Moor et al. 2016). TLR2 has been shown to directly bind bacteria *in vivo* (Dziarski and Gupta 2000; Vasselon et al. 2004) and employed in a biosensor to detect bacteria at the point of care (McLeod et al. 2020). However, TLRs have, to our knowledge, never been used as a means of fluorescently labelling bacteria for flow cytometry.

4.1.1.2 Imaging flow cytometry

Imaging flow cytometry (IFC) is a hybrid technique between conventional flow cytometry, described above, and fluorescence microscopy. Sample preparation and data analysis follows a standard flow cytometry approach, however for each cell, an image is also recorded. Images open up the possibility of much more complex analyses, such as:

1. Visual confirmation of a sub-population. What you see is more likely to be what you get.

2. Significantly more features extracted from images than from fluorescence intensity alone. More image features opens the door to high-dimensional analysis, even when the panel size is limited.

3. Fluorescence and scatter intensity is no longer an individual numerical value per cell but rather can be provided as a spatial representation per pixel.

4. Full-scale, high throughput image analysis pipelines using software such as CellProfiler/ImageJ can now be used with flow data to investigate morphological changes, colocalisation and translocation.

IFC was considered here for two reasons: 1) to map binding patterns on bacteria, and 2) for the potential to explore binding of other cell types, such as immune cells, without antibodies. By no means does IFC replace conventional flow cytometry (CFC), however it does allow the researcher to look at things from a different perspective and this can yield more relevant conclusions in certain cases. IFC has been used to probe interactions between methicillin-resistant *S. aureus* (MRSA) and osteoclasts (Bongiorno et al. 2020), *Aerormonas veronii* and macrophages (Havixbeck et al. 2015), and *Pseudomonas aeruginaosa* and *Acanthamoeba polyphaga* (Dey et al. 2019). These studies rely on specific antibodies for the pathogens in question and tend to focus on the interaction between microbial pathogens and much larger eukaryotic cells.

One of the challenges associated with analysing bacteria with IFC is image resolution. Due to their small size, correctly identifying the boundary between one cell and the next can be challenging and can lead to instances where multiple cells are classed as one, a problem sometimes referred to as coincident, or swarm detection (Van Der Pol et al. 2012). In this work, it could mean an overestimate in the true percentage of stained cells when; for example, if one cell is bound to an antibody/TLR but the rest are not. The detection of free bacteria, *i.e.* those which aren't bound to or associated with the much larger host cells, is significantly more complex and appears to be lacking in the literature.

Importantly, sensors used in IFC have specific features that can also help improve the detection of small particles such as bacteria. CCD sensors have higher dynamic range and lower noise than the PMTs found in conventional flow cytometers. IFC lasers range from 70-300mW in power compared to ~7-20mW in a conventional flow cytometer - more powerful lasers allow smaller, dimmer particles to scatter more light (Botha et al. 2021). Combined with a slower sample flow rate, the application

of time-delay integration of the intensities of each pixel as they flow across the sensor effectively allows for longer exposure times for each cell. Finally, triggering of an event occurs for both SSC and fluorescence. In a recent study which compared the performance of 3 flow cytometers: a BD FACS Aria III (conventional flow cytometer), an Apogee A60 Micro-PLUS (high resolution flow cytometer) and an ImageStream X Mark II (which is used in this work). Results showed IFC was able to detect beads ranging from 110-1300 nm and came out on top when detecting single-labelled extracellular vesicles in blood plasma (Botha et al. 2021).

4.2 Results

4.2.1 Designing an ELISA-style TLR2 capture assay

Before exploring IFC, a simpler approach to characterise receptor binding was taken to develop a 96-well capture assay. Capture assays, in their simplest form, involve three main steps: molecular recognition, signal transduction and signal generation (Banala et al. 2013). A typical example is an enzyme-linked immunosorbent assay (ELISA), which makes use of the molecular specificity of an antibody to detect and quantify the amount of a protein of interest in a heterogeneous solution, for example a cell lysate. It is common in basic immunology research and allows you to answer questions like *how much analyte is produced in response to a stimulus?* or in diagnostics for the detection of a biomarker indicative of a particular disease such as the presence of anti-citrullinated protein antibodies (ACPA) in rheumatoid arthritis. Establishing whether a patient is ACPA positive opens the clinical gateway to treatment pathways for the disease (Suwannalai et al. 2012).

There are multiple ways to set up an ELISA (Verma et al. 2013); in a common variant called a sandwich ELISA, an antibody is coated onto the surface of the wells in a 96-well plate. As each element is layered on top of the last, excess or non-specifically bound material must be thoroughly washed off using PBS containing a small amount (0.01-0.05% v/v) of detergent. Free space on the surface of the well must then be blocked using, for example, bovine serum albumin (BSA) or powdered

milk, in order to minimise non-specific binding and increase the specificity of the assay. The analyte is then added, followed by a secondary reporter antibody which is either bound directly to the detection enzyme HRP, or requires the addition of a tertiary antibody. On addition of the substrate (*e.g.* tetramethylbenzidine; TMB) the enzyme catalyses a colorimetric reaction, the intensity of which is proportional to the amount of ligand bound to the antibody (Figure 4.1).

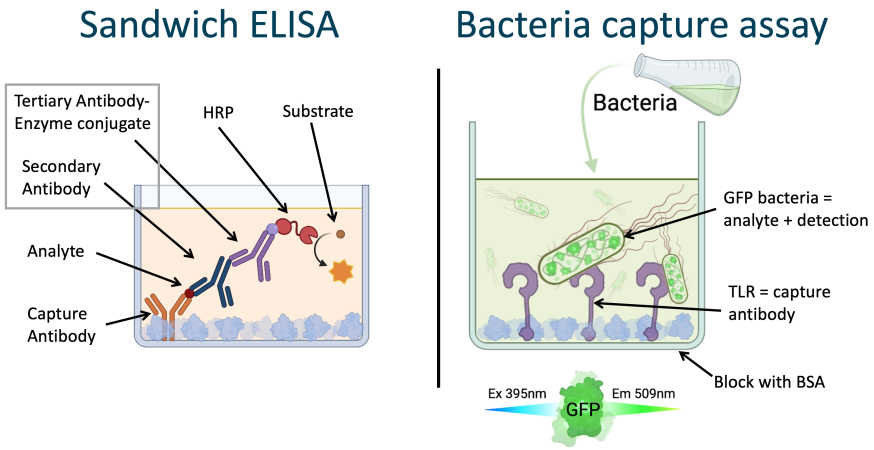

Figure 4.1: Principle of the proposed bacterial capture assay in comparison to a conventional sandwich ELISA. A standard ELISA has been adapted to detect bacteria using toll-like receptors immobilised on the surface of the plate rather than an antibody. Instead of a secondary or tertiary antibody conjugated to an enzyme for detection, bacteria expressing green fluorescent protein are used. This is effectively the analyte, secondary and tertiary antibodies, enzyme and substrate, all in one. ELISA; enzyme-linked immunosorbent assay, HRP; horse radish peroxidase, GFP; green fluorescent protein, TLR; toll–like receptor, BSA; bovine serum albumin, Ex; excitation wavelength, Em; emission wavelength.

Often, ELISA-style capture assays are used to detect bacterial antigens by heating the samples to promote antigen shedding or lysis (Verma et al. 2013), for example; pertussis (whooping cough) (Ibsen et al. 1993) and *Bacillus cereus* (Chen, Ding, et al. 2001). Paladines *et al.,* on the other hand, have recently developed an ELISA-based approach to detect whole, live *Legionella pneumophila* cells *via* lipopolysaccharide (LPS) expressed on the cell surface using polyclonal and recombinant antibodies. Rather than the colorimetric detection method described above, they extracted the DNA and performed quantitative real-time polymerase chain reaction (qPCR) to determine the recovery of the assay (Paladines et al.

2022). To our knowledge, an ELISA-style capture assay for the detection of whole pathogens using TLRs has never been published before.

The assay principle is described in Figure 4.1 (right), whereby binding of GFP expressing *E. coli* is characterised with a fluorescent plate reader. Due to the limited sensitivity of the plate reader, initial tests showed no difference in green fluorescence signal between wells containing bacteria and those left without (Appendix B.1). The decision was therefore taken to introduce a lysis step prior to measuring the fluorescence of the bacteria in order to liberate the GFP contained within the layer of bound bacteria on the surface of the well. Having the fluorophore in solution should, like in the standard protocol using HRP/TMB, increase the sensitivity of the assay. The lysis method needed to be detergent-based so that it could be carried out in a 96-well plate, a requirement which ruled out alternative approaches such as sonication or bead-beating. Bacteria (10^7 CFU) were incubated in 20 µl lysis buffer [25 mM tris-HCl, 10 mM EDTA, 100 mM NaCl, 1 % SDS, pH 8.0] for 30 min at 50°C. Figure 4.2A shows GFP fluorescence intensity of the samples containing lysis buffer remained the same pre- and post-lysis (t=0 min and t=30 min, respectively), indicating that growth of the culture has been stopped. This was confirmed by the lack of any growth observed on plates streaked with the lysed samples which were grown overnight (data not shown). The fluorescence intensity of the control, on the other hand, doubled. This is because bacteria in the control continued growing during the 30 min incubation (doubling time of *E. coli* in growth media is 22.5 min under optimal conditions (Liang, Ehrenberg, et al. 1999)). GFP fluorescence intensity of samples containing lysis buffer did not decrease, also indicating there is no degradation of GFP by the detergent or the heating step. Although Figure 4.2A shows that growth is stopped by the lysis buffer, it does not prove that lysis was complete and GFP is not still locked up inside non-viable cells. To test this, the experiment was repeated in a 1.5 ml microcentrifuge tube so samples could be pelleted by centrifugation. Figure 4.2B shows minimal GFP in the pellet of lysed samples in contrast to an abundance in the pellet of the control.

Likewise, all the GFP from the lysed samples is contained within the supernatant. Taken together these results demonstrate successful chemical lysis of *E. coli*.

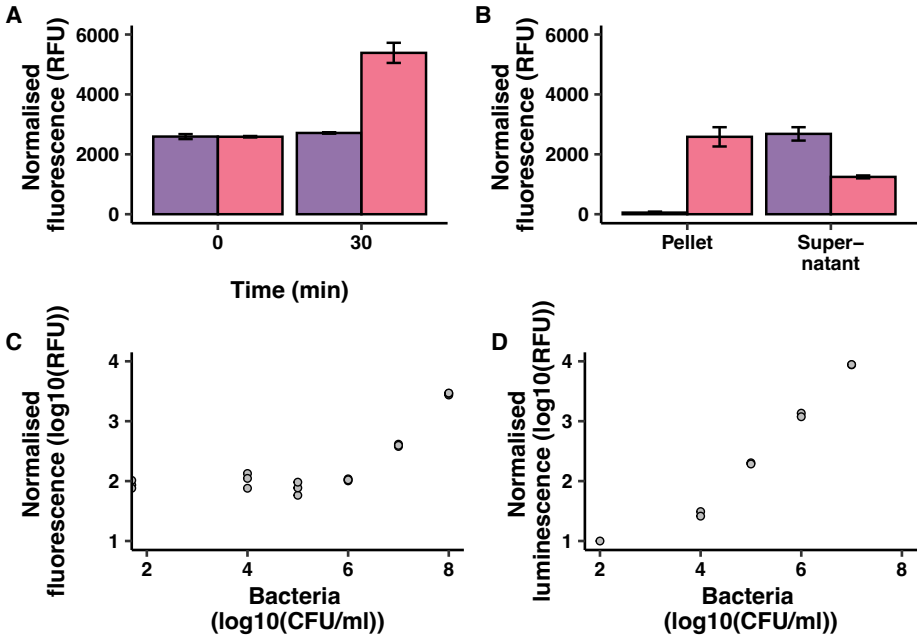

Figure 4.2: A) Bacterial lysis and plate reader sensitivity to GFP bacteria. Fluorescence intensity of GFP bacteria was compared pre- and post-lysis. 10^7 CFU *E. coli* in each well of a 96-well plate were incubated in the presence (purple bars) and absence (pink bars) of 20 μl lysis buffer [25 mM tris-HCl, 10 mM EDTA, 100 mM NaCl, 1 % SDS, pH 8.0] for 30 min at 50°C (n=2). **B)** Lysis was repeated in a 1.5 ml microcenrifuge tube and pelleted by centrifugation (5 min, 1000 xg) (n=3). **C)** Fluorescence intensity of GFP *E. coli* serially diluted from 10^8 down to 10^4 CFU/ml presented on a logarithmic scale. 100 μl per sample was added to each well and the fluorescence measured (n=2). **D)** ATP, produced by live bacteria, catalyses the conversion of luciferin to oxyluciferim, in the presence of magnesium and oxygen, to produce light. Luminescence is measured to quantify bacterial 'activity'. *E. coli* serially diluted from 10^8 down to 10^2 CFU/ml. 100 μl per sample was added to each well and the luminescence measured according to the BacTiter-Glo microbial viability assay kit (Promega) (n=3 technical reps.).

The limit of detection (LoD) of lysed bacteria was measured to be ~10^6-10^7 CFU/ml (Figure 4.2C); even taking the best-case scenario, measuring GFP fluorescence would only enable the detection of 1-10% of cells with a starting concentration of 10^8 CFU/ml. Instead of measuring GFP content, an alternative approach was found in a paper by (Ngamsom et al. 2017), who developed a point-of-care device for rapid screening of *E. coli* based on the bioluminescent

reaction between luciferin/luciferase catalysed by ATP from live bacteria (Figure 4.3). This group achieved a limit of detection of ~2x10^3 CFU/ml. The technology is available from a kit (BacTiter-Glo from PROMEGA) and using this we were able to achieve a LoD of 10^4 CFU/ml (Figure 4.2D), 1000-fold more sensitive than measuring GFP fluorescence. The lysis/luminescence reaction is carried out in a single step at room temperature, which only takes 10 minutes, and the bacteria do not need to be modified to express the GFP gene, opening up the possibility to test more strains of bacteria.

Once the reading of bacterial load was optimised, and taking inspiration from the sandwich ELISA, receptors were immobilised on a plate at a concentration of 1 µg/ml (Figure 4.3). The approach was to first test how well the assay worked using an anti-*E.coli* antibody before moving on to test TLRs 2 and 4.

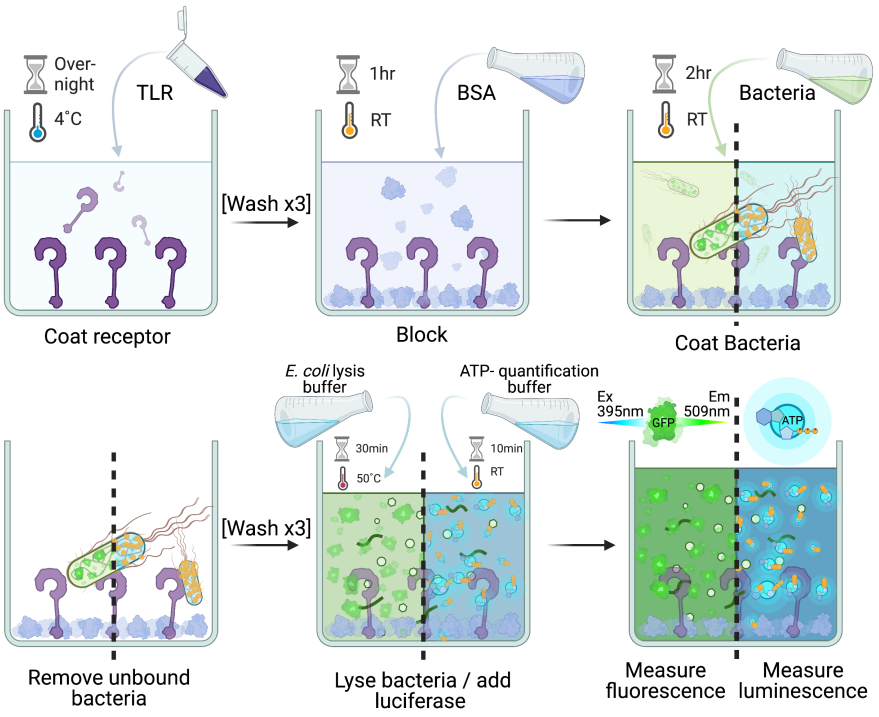

Figure 4.3: An overview of the bacterial capture assay method. Receptors/antibodies are coated onto wells overnight at 4°C before the excess is removed and quantified, then washed 3 times using PBS or an alternative buffer containing detergent. Free space in the wells is blocked with bovine serum albumin to reduce non-specific binding of bacteria to the hydrophobic surfae of the plate. Bacteria are added for 2 hrs before excess, unbound cells are washed off 3 times. To liberate GFP from a single layer on the surface of each well, bacteria are incubated for 30 min in 20 μl lysis buffer [25 mM tris-HCl, 10 mM EDTA, 100 mM NaCl, 1 % SDS v/v, pH 8.0] at 50°C. GFP fluorescence intensity is measured using a 488 nm laser. RT; room temperature. Alternatively, bacteria are lysed and quantified using an ATP luminescence assay (BacTiter-Glo, PROMEGA).

Initial tests with the anti-*E.coli* antibody suggested that the assay was working well, with increasing concentrations of antibody leading to higher ATP luminescence (Figure 4.4A). However, on inclusion of a proper negative control it became clear that bacteria bind to the plate non-specifically at similar concentrations to when a receptor is present, making any conclusions on the binding capabilities of TLRs hard to make. Furthermore, when anti-E.coli was included as a positive control for comparison with TLRs, minimal binding was observed (Figure 4.4B). We tried to exploit the presence of the Fc fusion tag on the recombinant TLRs. Plates coated with protein A should enable the orientation-specific attachment of the receptors

with a much higher affinity than regular plates which rely on passive adsorption. None of these techniques were able to provide any discernible improvement to the assay (Appendix B.1).

To summarise, several strategies have been tested to limit this binding in negative controls (*e.g.* surface chemistry of the plate, buffers *etc.*), but none led to an improvement of assay signal:noise ratio of the assay (Appendix B.1) and reproducibility remained a challenge despiteinitially promising results and a significant amount of time spent trying to optimise the assay. Ultimately, binding in the absence of receptors presents the biggest limitation to this method and the decision was taken to move on with alternative strategies to investigate protein:bacteria interactions. In the next section, receptors will be fluorescently labelled to enable detection of bacteria *via* flow cytometry.

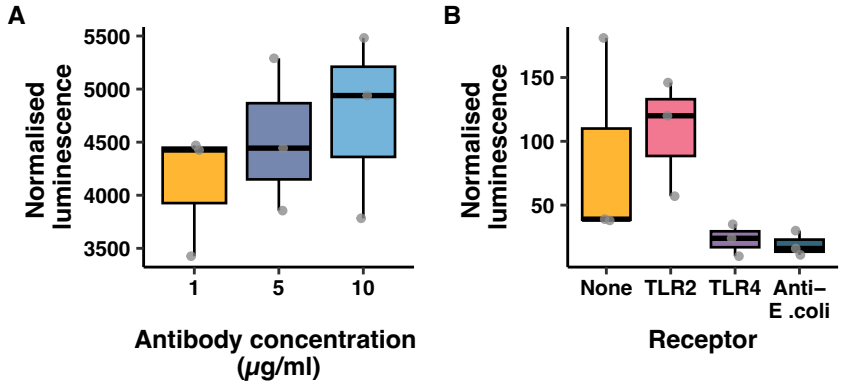

Figure 4.4: Capture performance of ELISA-style assay. **A)** Anti-*E.coli* antibody was coated onto the plate at concentrations ranging from 0-10 μg/ml and bacteria (10^7 CFU per well) were quantified by measuring ATP luminescence using the BactTiter-Glo kit (Promega). **B)** Comparison between plates coated with TLR2, 4 and anti-Ecoli at a concentration of 1 μg per well and compared to wells without any receptor (n=3 technical replicates). The magnitude of the scale on the y-axis is relative to the optimum settings chosen for each assay.

4.2.2 Flow cytometry assay design

To establish whether bacteria could be detected using IFC, *E. coli* expressing green fluorescent protein (GFP) were harvested during exponential growth and their concentration adjusted to 10^8 CFU/ml using UV-vis spectrophotometry. As a

model system to develop a suitable assay to characterise receptor:pathogen binding, 100 µl samples of bacteria were stained with 1 µg/ml anti-E. coli antibody (Bio-Rad). After washing, the primary antibody was stained with 1.25 ng/µl AF647-labelled secondary antibody (Figure 4.5A). Samples were run on an ImageStream Mark II imaging flow cytometer (currently CYTEK) where 10,000 cells were acquired. Example images can be seen in Figure 4.5B where the top row shows a sample stained with antibody and the bottom shows the control. Interestingly, non-fluorescent bacteria (*i.e.* the wild-type (WT)) could not be detected with the standard settings. This was thought to be because they are too small to sufficiently perturb the laser and produce an SSC signal large enough to be distinguished from background noise. However, in later experiments, I found that WT-*E. coli* (dimensions: ~1 µm x ~1 µm x 2 µm) were being automatically gated out alongside the SpeedBeads (1 µm x 1 µm) automatically by IDEAS. WT-*E. coli* likely lost their plasmids and make up 5~10% of the population.

Single-stained controls were used to compensate for spectral overlap between channels before feature values, such as fluorescence intensity of GFP (green) and AF647 (red) channels, were exported from the proprietary IDEAS software as text files and analysed further in R. Green fluorescence intensity distribution is broadly similar in the control and the antibody sample with the exception of a small peak close to zero (Figure 4.5C). This small peak of GFP-negative (probably dead) *E. coli* are only fluorescent, and therefore detectable with the current default settings, due to fact they are bound to the antibody.

The distribution of red fluorescence sees a notable increase upon the addition of the antibody (Figure 4.5D) indicating that binding between antibody and bacteria can successfully be detected using IFC. The fact we see overlapping peaks between sample and control means that only a portion of the bacteria are bound at this concentration of antibody. Quantification of the percentage of positive cells is therefore challenging and a reliance on manual gating would result in inaccurate estimates of the percentage of bacteria which have been stained. We therefore need a mathematically robust, automated method of setting a fluorescence

threshold, above which cells can be classified as positive to allow comparison between independent samples.

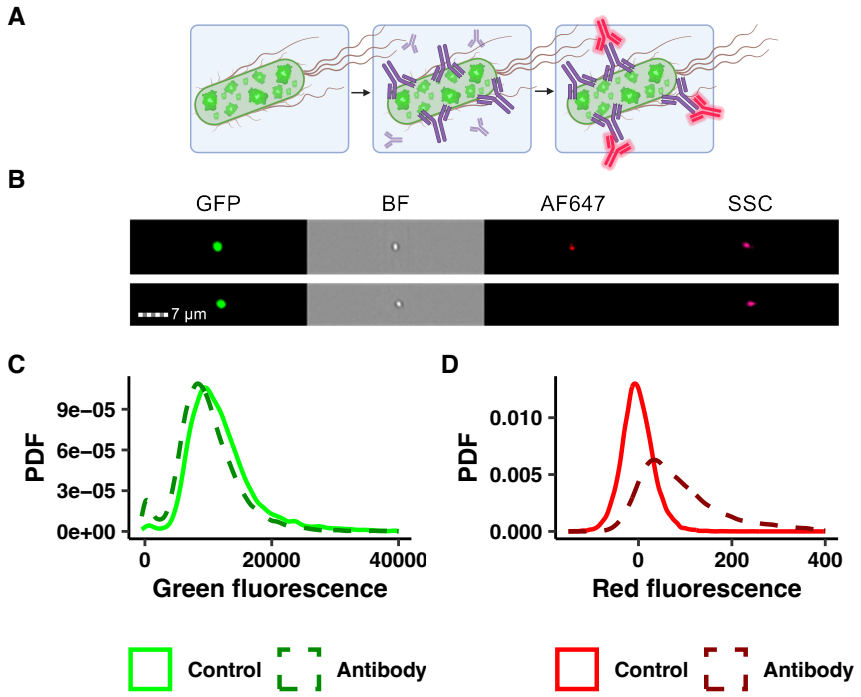

Figure 4.5: Assay design. **A)** GFP bacteria were first stained with a primary antibody against components of the cell wall structure for 30 min at room temperature. Samples were washed by centrifugation 3 times in sterile PBS to remove excess, unbound antibody. A fluorescent secondary antibody conjugated to AlexaFluor 647 (AF647), was then added to facilitate detection of the bound primary antibody and washed 3 times before samples were analysed using imaging flow cytometry (IFC). Created using Biorender.com. **B)** IFC images of GFP *E. coli* stained with secondary antibody (top) and without (bottom). **C-D)** Density plots of the green (GFP) **(C)** and red (AF647) **(D)** fluorescence intensity. Control (GFP *E. coli* only) and the sample incubated with the antibody are represented by full and dashed lines, respectively. GFP; green fluorescent protein, BF; bright field, AF647; Alexa-Fluor 647 fluorescent antibody, SSC; side-scatter, PDF; probability density function.

4.2.2.1 Bivariate normal distribution analysis

From a control sample of GFP *E. coli*, red and green fluorescence intensities for each bacterium are exported from the IDEAS software and first fit to a bivariate normal distribution in R. An automated gating strategy was then applied by defining an ellipse (show in yellow, Figure 4.6) encompassing the high-density region of the distribution with a probability of false positive of 99.73% (to represent the

proportion of points falling within 3x standard deviations from the mean). The ellipse is then applied to the sample stained with antibody and the percentage of cells outside of the ellipse is calculated.

If the data were normally distributed, 99.73% of points would fall within the ellipse and 0.27% would be classed as false positives. However, we see from Figure 4.6C and D that in some cases, the distribution of green fluorescence is clearly skewed and in Figure 4.6D, 2.40% of cells are falsely recorded as positive in the control (leading to an overestimate in the percentage of positive cells in the sample). An alternative processing approach was consequently developed to address this.

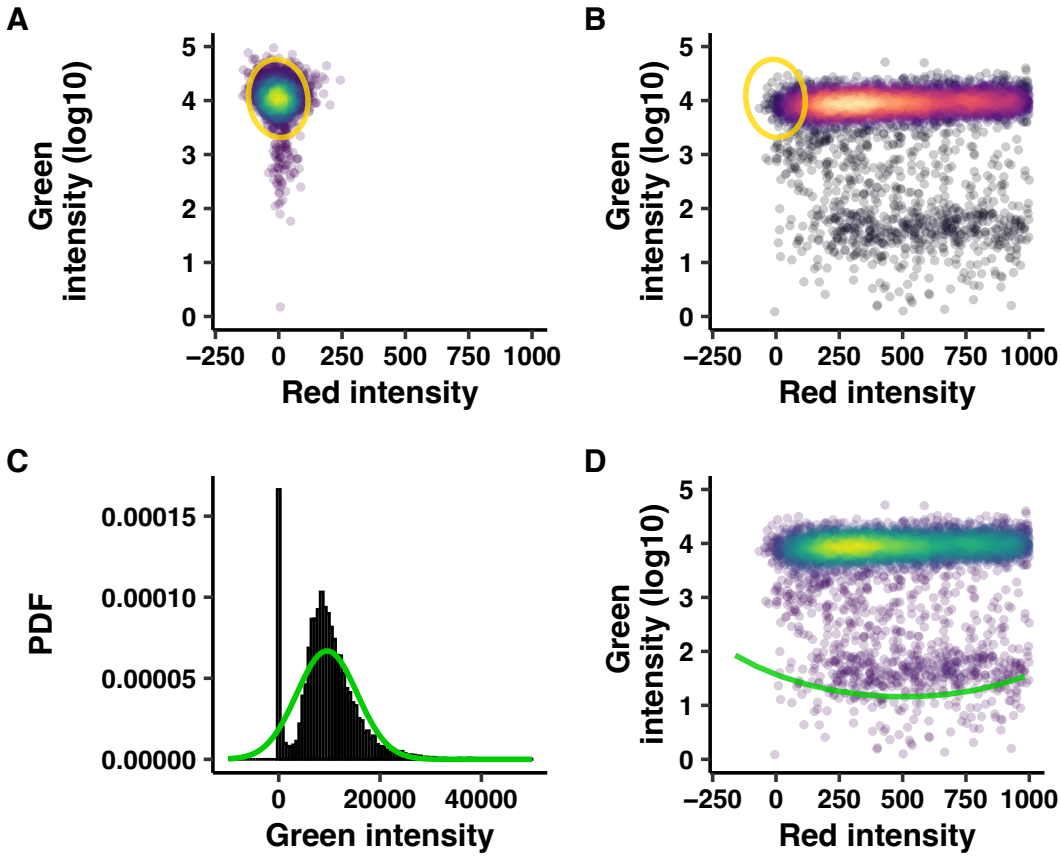

Figure 4.6: An automated gating strategy based on the bivariate normal distribution. Scatter plots showing red and green fluorescence intensity (n=10000) comparing **(A)** GFP *E. coli* control and **(B)** a sample of bacteria stained with the antibody. The ellipse (yellow) is defined by fitting fluorescence intensities of the control to a bivariate normal distribution. The percentage of cells outside of the ellipse can then be compared between samples. **C)** A density plot showing green fluorescence intensity distribution of a poor control. The normal distribution is plotted in as a green line. **D)** Scatter plot of the same control showing an example of a poorly fitting ellipse (green).

4.2.2.2 Simplified automated gating strategy

The proportion of points from a normally distributed dataset which lie within 3 standard deviations (s.d.) of the mean is 99.73%. If we consider the red fluorescence signal (assuming red intensities are indeed normally distributed), 99.865% of bacteria in a control group (*i.e.* without red receptors) would have a red intensity below the mean red intensity+3s.d. value. Similarly, 0.135% (100%-99.865%) of GFP-expressing cells would have a green fluorescence intensity below mean green intensity-

3s.d. value. This is the statistical margin of error for a normally distributed sample and could represent debris or dead bacteria. As opposed to assuming a specific distribution for the red/green intensity profiles, here, bacteria signals are first classed by intensities and a threshold is automatically set when 99.865% of the total number of bacteria without receptors is reached in the red channel (Figure 4.7A), and 0.135% for the green channel (Figure 4.7B). Upon the addition of receptors, the number of bacteria above these two thresholds is used to define a percentage of red or green fluorescent cells as seen in Figures 4.7C and D (defined hereafter as percentage of positive cells).

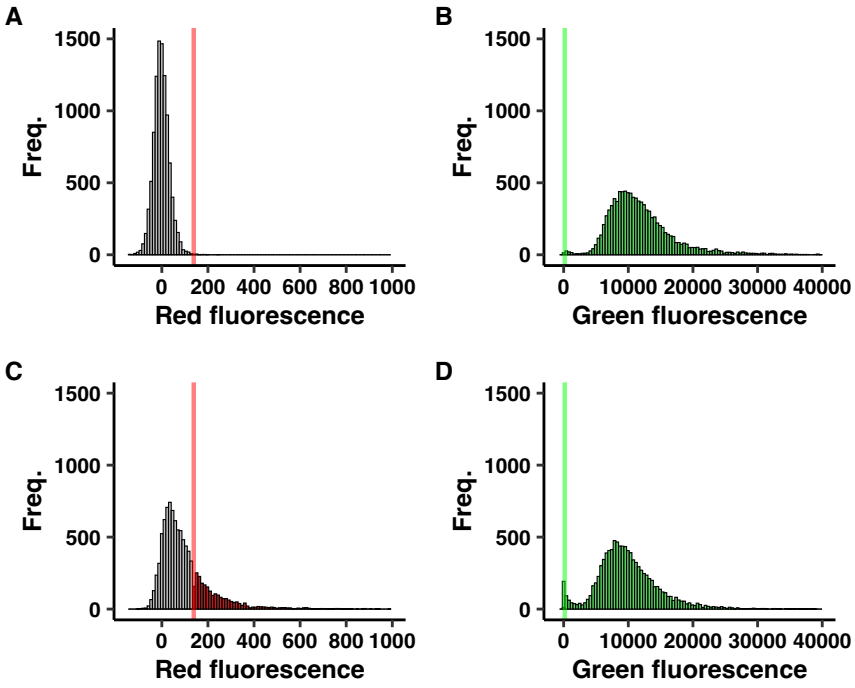

Figure 4.7: A simplified automatic gating strategy. Histograms summarising the frequency of fluorescence intensity of red **(A, C)** and green **(B, D)** fluorescence distribution, respectively. Thresholds were defined using the control datasets **(A, B)** at 99.865% of datapoints for red and 0.135% green, highlighted with vertical lines. The samples **(C, D)** are labelled with 1 μg/ml primary anti-*E. coli* antibody and 1.25 ng/μl, fluorescent secondary antibody. Positive cells are coloured in red/green whereas negative cells are gray (n=10,000).

Notably, the threshold to define GFP-positivity in Figure 4.7B seems lower than the gating threshold that would be chosen manually. As presented in the

previous section, some samples led to a bimodal distribution for the green-intensity profiles. Although this was not observed in most case, bimodality can skew the threshold toward low green intensities, thus leading to a potential over estimation of the number of GFP expressing bacteria. It is not critical in this work since the analysis is done with bacteria only as opposed to a mixture of cells, but if this bimodality were to become an issue the mode could be used instead of the mean for threshold estimation.

4.2.2.3 A gating strategy for image quality

The accuracy of feature extraction relies on the quality of the images captured. A histogram of gradient root mean squared (RMS) of bright-field (BF) images depicts the average gradient of pixel intensities across each image which is effectively an indication of its sharpness. Images in focus have a relatively high gradient whereas those which are blurry have a low gradient (Figure 4.8A).

Selection of cells in focus is usually done manually in the IDEAS software package; however here, each of the features were exported into R to apply an automated gating strategy with a threshold of 1 s.d. below the mode gradient RMS in the brightfield channel to define cells in focus. Similarly, area and aspect ratio were also gated independently to identify images with single cells. A threshold of ± 1 s.d. of the mode was used for area and -1 s.d. of the mode for aspect ratio.

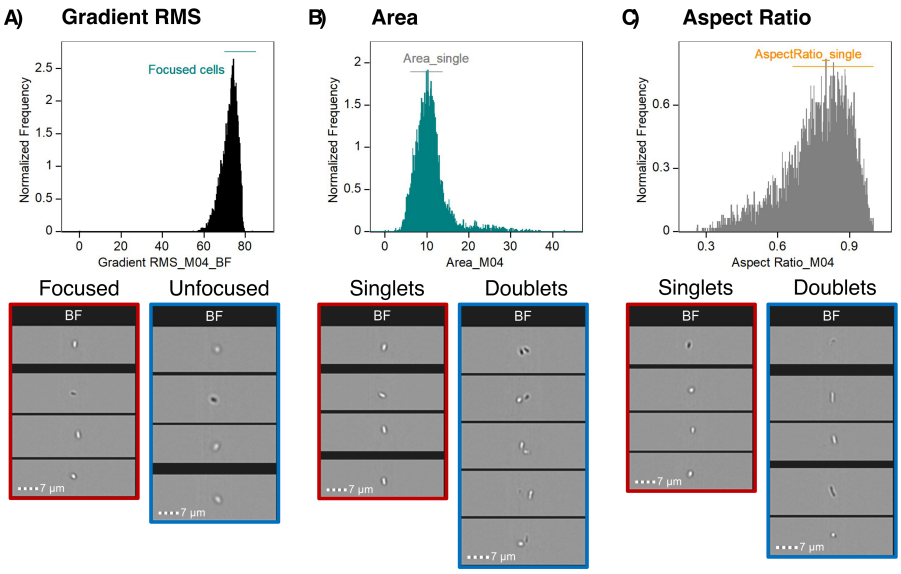

Figure 4.8: An automated gating strategy to optimise image quality. **A)** Histogram showing the normalised frequency of gradient RMS for BF images. The teal gate highlights cells in focus with a threshold set at the mode - 1 s.d. **B)**. Doublets, aggregates and debris we removed by setting a threshold of ±1 s.d. at the mode cell area. Singlets are highlighted within the grey gate. **C)** The remaining doublets, aggregates and debris were selected according to a threshold at the mode aspect ratio -1 s.d. (singlets are highlighted with the orange gate). Cells were gated sequentially, meaning cells in focus were then gated based on their area to remove doublets/aggregates which were themselves gated on their aspect ratio. Example BF images of cells within each gate are indicated with a red box and examples of cells outside of the corresponding gate are in a blue box.

For each population, including *all cells* prior to any gating, a threshold of 99.865% was set on red fluorescence intensity according to section 4.2.2.2. A comparison between each of the controls and a sample stained with 1 µg/ml antibody can be seen in Figure 4.9.

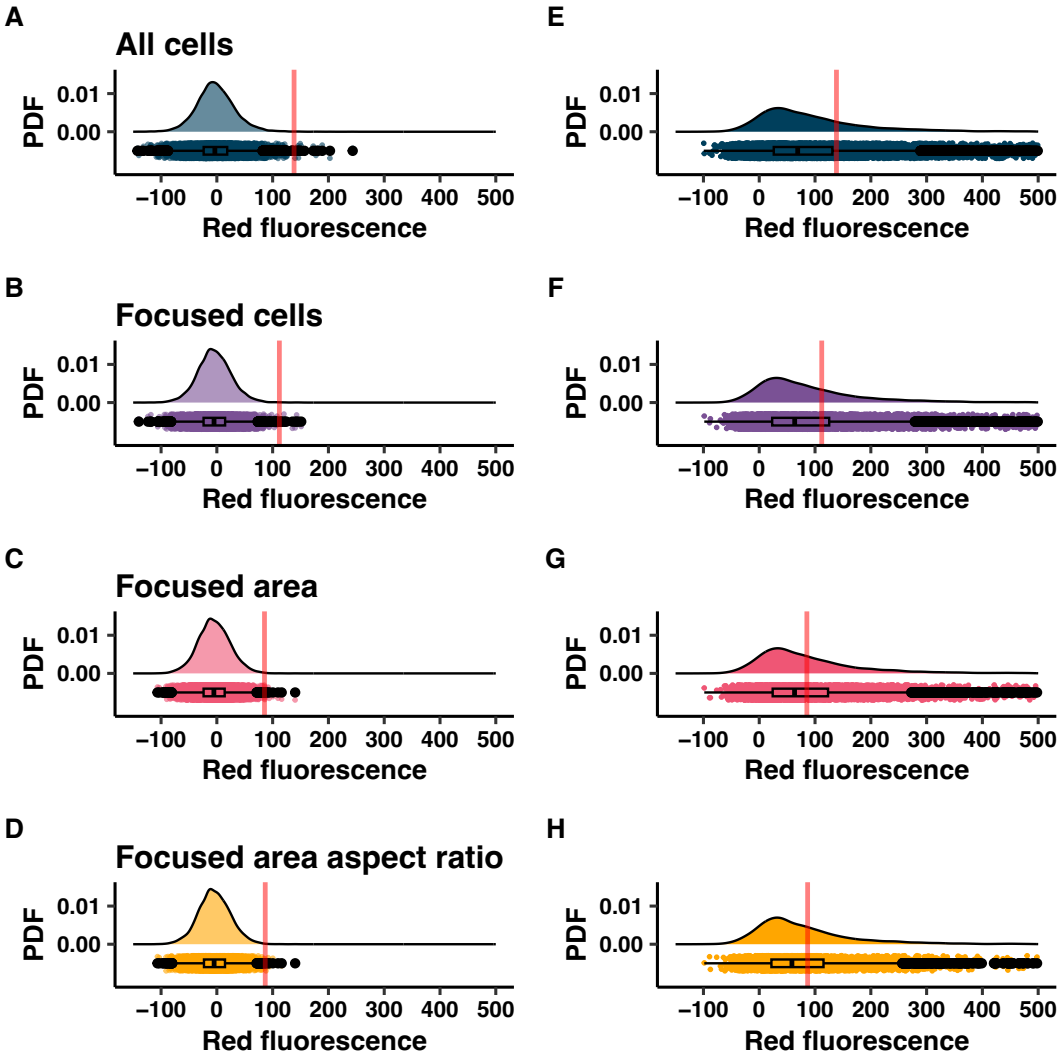

Figure 4.9: Raincloud plots comparing the red fluorescence intensity between different populations of bacteria gated on image quality. Left column **(A-D)** shows the control which is used to calculate the threshold (99.865 of points) above which cells are classified as red-positive and bound to the receptor (shown as vertical red lines). Right column **(E-H)** shows a sample with 1 μg/ml antibody for each population. Raincloud plots are essentially density plots (clouds) presented on the same axes as a horizontal box plot to summarise the median (middle line), 25th and 75th percentiles (outer lines), minimum and maximum points (whiskers) and outliers (black points). A jitterplot is also included behind the boxplot (rain) as an alternative representation of density. Raincloud colours indicate the different population: all (n=10,000), focused cells (n=7864), focused single cells gated on area (n=5975) or focused single cells gated on both are and aspect ratio (n=3815).

Gating for cells in focus has a significant effect on the red threshold, decreasing from 140.4 RFU (relative fluorescence units) for all cells, to 112.0 RFU for cells in

focus. Similarly, gating based on cell area further decreases the threshold to 85.37 RFU. Gating on aspect ratio however did not have much of an effect (86.71 RFU) and was not included in the final gating strategy. Depending on gating, variation in the number of all cells detected as red- and green-positive can consequently be observed; in the example depicted in Figure 4.10, the number of antibody-positive cells (red-positive) ranged from ~20% to ~30% depending on the gates applied.

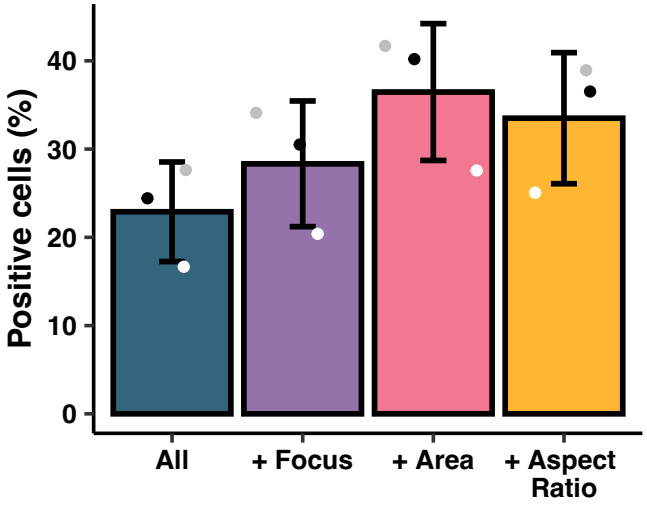

Figure 4.10: Mean percentage of red- and green-positive cells stained with 1 μg/ml antibody for each differentially gated population. Points represent individual technical replicates (n=3) and errorbars show standard deviation of the mean.

4.2.3 An optimised, automated workflow for the detection of bacteria using IFC

An overview of the optimised workflow which has been outlined over the course of the previous pages is depicted in Figure 4.11. Data are acquired using an Amnis ImageStream Mark II imaging flow cytometer using the INSPIRE software which produces a raw image file (.rif). The number of cells recorded depends on the expected size of the sub-population of interest. Ideally, more than 5000 cells are required after gating for single cells in focus; in these experiments 10,000-100,000 cells were typically acquired.

The .rif file is loaded into the IDEAS software package and a compensation matrix is generated from the fluorescence information of single-stained control samples in order to correct for spectral overlap between different channels. The same compensation matrix can be applied to all samples in a batch and saved as a compensated image file (.cif). Features extracted from BF, SSC and fluorescence information can then be plotted and analysed and the session saved as a data analysis file (.daf). Gating is usually then carried out manually using IDEAS, however, at this point we choose to export the raw feature values of gradient RMS, and area of BF images along with the mean fluorescence intensity of the green (bacteria) and red (antibody/receptor) channels for processing in R.

Text files (one per sample) are imported as a list and gated using an automated thresholds derived from 1 s.d. below the mode gradient RMS value and 1 s.d. either side of the mode area of BF images to ultimately leave single cells in focus. Next, the calibration control containing GFP bacteria alone is used to set red and green fluorescence intensity thresholds at 99.865% and 0.135%, respectively, as previously described. Finally, the percentages of cells which pass the threshold are calculated for each sample and presented as results.

This standardised workflow can be applied to data from each experiment quickly and reproducibly, with the assurance that an accurate and mathematically robust threshold has been used to calculate the percentage of cells successfully bound by the antibody or receptor of interest. This method inspires greater confidence in comparisons between experiments carried out independently, especially with samples producing faint fluorescence signals which would undoubtedly be miscalculated using traditional manual gating approaches.

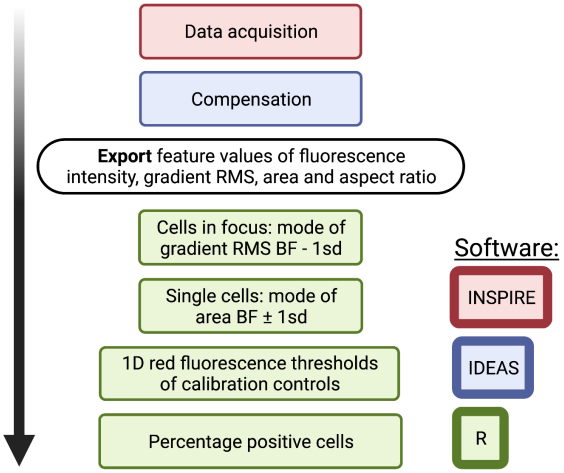

Figure 4.11: An optimised workflow for quantifying the percentage of bacteria cells bound to receptor using IFC. The software used at each stage is indicated in red, blue and green for INSPIRE, IDEAS and R, respectively. BF; brightfield images, RMS; root mean squared, sd; standard deviation.

4.2.3.1 IFC-based detection of *E. coli* using anti-*E.coli*

As a proof of principle of the proposed processing pipeline, samples containing 10^8 CFU/ml *E. coli* were labelled with concentrations of anti-*E. coli* antibody ranging from 1 – 8 µg/ml. Samples were analysed according to the workflow in Appendix Figure 4.11 and raincloud plots were made to evaluate the distribution of fluorescence intensities. To probe the reproducibility of the experimental procedure for detection, triplicate technical replicates were compared. Examples of 0, 1 and 8 µg/ml can be seen in appendix **??**. Subtle differences in the median fluorescence intensity are apparent in the median values of the boxplots, however the distributions are consistent between replicates.

As shown in Figure 4.12, an increase in antibody concentration leads to an increase in average red fluorescence intensity; however, both the mean and the standard deviation of the distribution increases as a function of antibody concentration as opposed to the entire distribution shifting to higher intensity values. The percentage of red-positive cells increases from 36.5±7.8% to 97.0±0.2% for primary anti-*E.coli* antibody concentrations ranging from 1 - 8 µg/ml. The sample with 0 µg/ml antibody was a negative control to which only the fluorescent

secondary antibody has been added. This shows minimal (0.89±0.53%) background binding of the secondary antibody (Figure 4.13). It can also be noted that the average green fluorescence does not change much as a function of antibody concentration (Figure 4.12 right column). As previously detailed, green fluorescence follows a bimodal distribution with one peak close to zero and another at approximately 10,000 RFU when antibodies are present. The red portions of each bar in Figure 4.13 show cells which do not express GFP but are bound by antibodies and accounts for less than 10% of all positive cells.

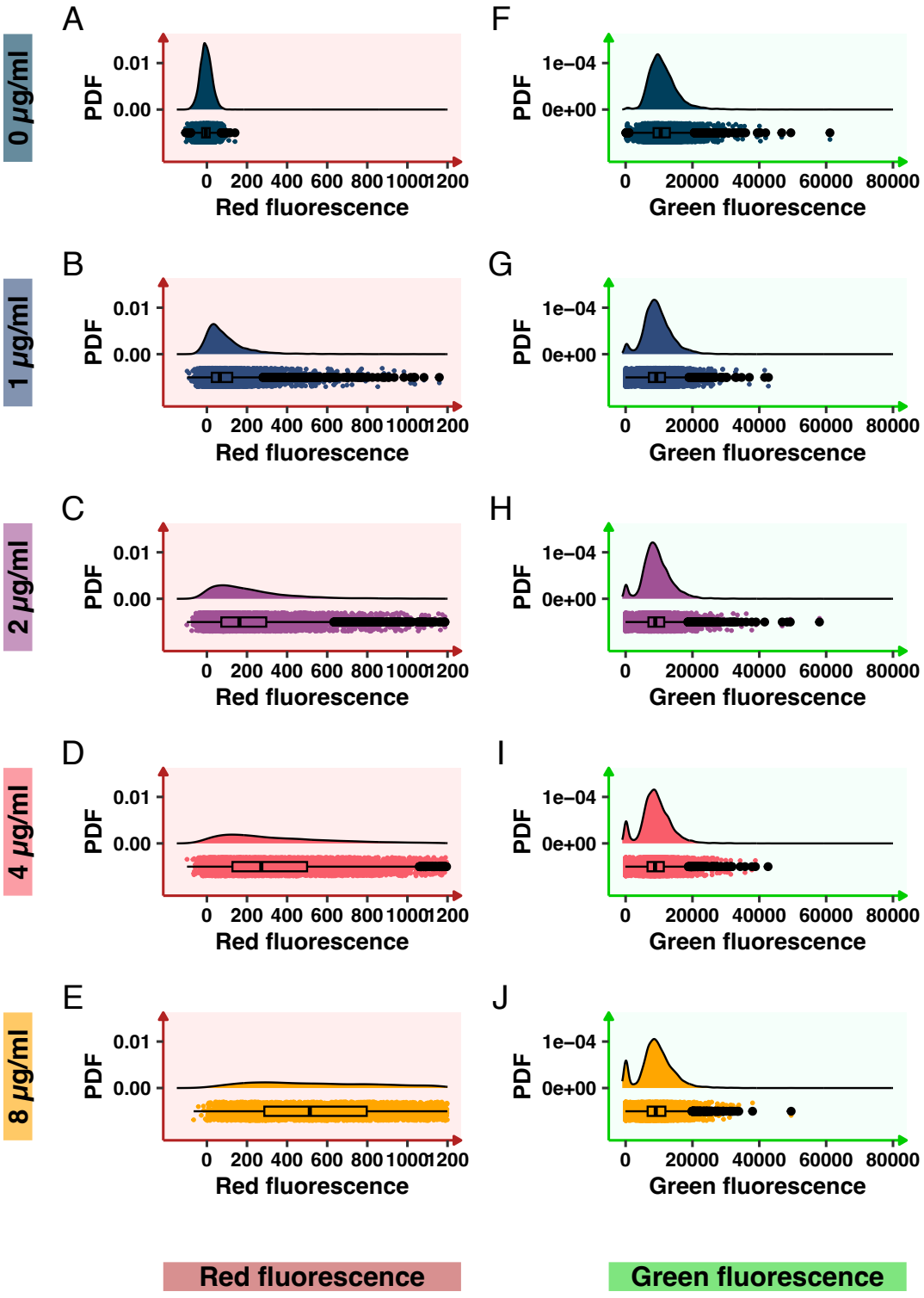

Figure 4.12: Comparison of red (left column) and green (right column) fluorescence intensity between technical replicates carried out at the same time. Raincloud plots show concentrations ranging from 0-0.8 μg/μl antibody. The concentration of AF647 secondary antibody was kept constant at 1.25 ng/μl.

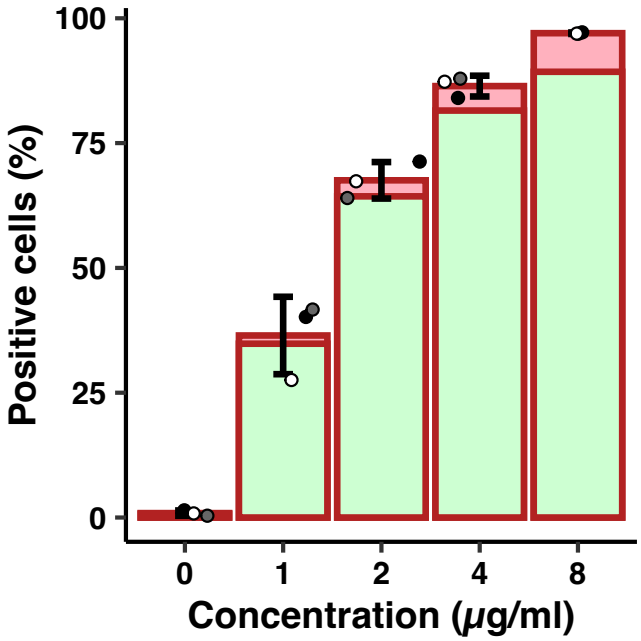

Figure 4.13: Mean percentage of positive cells for different concentrations of anti-E. coli antibody used to label *E. coli*. The green portions of each bar indicate the percentage of green and red positive cells whereas red portions indicate the percentage of cells which are only red positive. Points represent individual technicnal replicates ($n = 3$) and errorbars show standard deviation of the mean.

4.3 Discussion

After establishing the clinical criteria for pathogen identification in Chapter 3, the focus of the project turned towards developing an assay to characterise the binding performance of TLRs to bacteria *in vitro*. Significant limitations were placed on labwork during the COVID-19 pandemic: access to the GRI clinical lab was stopped, as was a 2-3-month mobility to The University of Bath to characterise TLR:bacteria binding capacity in PoC biosensors. When access to the University lab was allowed again, the challenge became optimising an assay from scratch, in isolation. Coming from a biochemistry background, it seemed logical to begin with the types of assays typically available in a biology research laboratory.

4.3.1 Binding in the absence of any antibody is a significant limitation of immobilisation-based assays

A standard sandwich ELISA protocol was adapted to immobilise a receptor/antibody on the surface of a 96-well plate and the detection antibody, enzyme and substrate were replaced with bacteria expressing GFP. Measuring GFP fluorescence using a plate reader proved unreliable in detecting less than 10^7 CFU/ml, so an ATP quantification kit was tried instead. This proved much more sensitive and enabled 10^4 CFU/ml bacteria to be detected. Initial tests with an anti-*E.coli* antibody looked very promising and appeared to demonstrate a concentration-dependent response. However, on inclusion of more thorough controls, we observed significant issues with binding of bacteria to the plate in the absence of any receptor. Several optimisation steps were tried but none were able to overcome this issue. Paladines *et al.,* similarly observed significant background binding of bacteria to their plates, however not to the same degree as what has been measured here – they were still able to measure a 100-fold difference between the negative control and the samples (Paladines et al. 2022).

If this assay were to be continued, one option could be to try and leverage the inherent stickiness of the bacteria and flip the assay on its head. By intentionally coating the bacteria to the plate then using a fluorescently labelled antibody for detection. Again, the assay could be limited by the sensitivity of the fluorescent plate reader. In this instance, alternative detection methods such as the IN Cell analyser (GE Healthcare), a fluorescent microscope which images well-by-well, could be tested. These results consequently highlight the importance of adequate negative controls; without the inclusion of a sample containing no receptor, limitations of binding would have been missed. In summary, the ELISA-style capture assay was not successful and attention was next turned to a technique which does not rely on the immobilisation of a receptor to a plate.

4.3.2 Imaging flow cytometry proves to be an accurate method for detection of single bacteria

The ImageStream has been shown to reliably detect microparticles down to 20 nm in size (Headland et al. 2014) and was used here to demonstrate its accuracy for characterisation of a microbial cell binding assay. IFC was superior at quantifying receptor-bound bacteria compared to a capture assay as it allows cells to be measured in suspension, thus circumventing the issue of binding in the absence of a receptor introduced by immobilising bacteria on a plate. Preliminary tests showed a measurable increase in red fluorescence in samples stained with AF647-labelled anti-*E.coli*. Signals were, however, relatively faint and manual gating based on two clear populations (bacteria with and without receptor) was not possible. Typically, in this situation, the concentration of antibody would simply be increased until a distinct population of labelled cells could be distinguished from those which are unbound, however this would not be feasible due to the cost of recombinant TLRs which must be purchased and then labelled using a kit with especially poor yield. From a diagnostic perspective, total saturation of receptor binding sites is not important. It does not matter how many molecules are bound to each bacterium, so long as there are enough to be able to distinguish it from the calibration control and overcome the threshold. For this reason, a more robust method of automated gating was needed. Rather than relying on the proprietary IDEAS software package, I exported the raw fluorescence data per cell for further analysis in the open-source programming language, R. At this point, the fluorescence distribution could be analysed statistically in order to assign a threshold at which cells can be classified as positive. The original plan was to fit red and green fluorescence to a bivariate normal distribution, as had been done by (Malek et al. 2015; Davey and Kell 1996). This worked very well for some datasets, however in some instances, an imperfect fit led to a significant overestimate in the percentage of positive cells. For this reason, a simplified strategy was developed instead.

The same approach was also applied to gate out poor-quality images which can lead to misrepresentations of cell fluorescence and the application of masks.

ImageStream is not recommended for size estimation based on area since, at 60x magnification, each pixel represents an area of 0.3 µm^2 which is a significant proportion of a 1 µm^2 bacterium. Additionally, considerable haloing of the default mask can be seen which leads to an overestimation in particle size (Headland et al. 2014). Despite the limited resolution, it was found to be beneficial to gate for focused cells using gradient RMS and singlets using area. Gating on aspect ratio had little additional effect on the results while decreasing the overall sample size significantly (in the example in Figure 4.9, the number of cells decreased from 10,000 to 7864 after gating cells in focus, to 5975 after gating for singlets based on area and finally to 3815 by gating single cells on area and aspect ratio). Care should consequently be taken when deciding on the optimum gating strategy as it can result in loss of sample without any improvement to the results. Here, the decision was taken to use 'single cells in focus gated on area' for the analysis of all subsequent experiments.

Event detection in the ImageStream is triggered based either on fluorescence or scatter in all channels of the CCD. Our results showed that wild-type, non-fluorescent bacteria do not typically produce sufficient scatter to be recorded as an event. A small population of GFP-negative bacteria is evidenced by the secondary peak at zero (RFU) in Figure 4.12 which, on average, accounts for 5.70±1.68% of the total red-positive population, regardless of the concentration of antibody used (Figure 4.13C). The GFP gene is located on a plasmid which confers antimicrobial resistance to chloramphenicol. Once the bacteria have grown to exponential phase, they are washed and resuspended in PBS ready for staining, and no longer cultured in the presence of any antibiotic. Without this selective pressure the plasmid will eventually be lost, since those bacteria no longer have selective advantage and, if anything, are burdened with a fitness cost by continuing to express the metabolically expensive and unnecessary resistance gene (Alexander and MacLean 2020). Once the efficacy of the detection method has been fully optimised to work at high enough efficiencies, the next step would be to then start working with non-fluorescent, wild-type pathogens, something which was not achieved during this project. This would have to be done on a strain-by-strain basis and would be very time consuming if

each pathogen needed to be transformed with a plasmid expressing GFP. One way to bypass this would be to make use of a bacterial stain such as SYTO 9 (Duquenoy et al. 2020; Holm and Jespersen 2003) which labels both Gram-positive and Gram-negative bacteria with a green fluorophore and can be purchased as a kit from ThermoFisher Scientific. Alternatively, researchers have reported that by removing the notch filter on the 405nm laser, which contains a 435nm longpass filter, SSC can be acquired in a second channel enabling the reliable detection of much smaller particles than would otherwise be possible relying on the default, 785nm laser alone (Botha et al. 2021). This would be worth confirming in the future to enable the detection of non-fluorescent bacteria, thus broadening the choice of strains available.

4.3.3 Conclusion

Manual gating, in general, is can be time-consuming, unreliable and difficult to standardise between both operators and laboratories (Saeys et al. 2016; Finak et al. 2016; Aghaeepour et al. 2013; Herzenberg et al. 2006). The simplicity of the proposed model is its main strength, offering notable improvements to accuracy, reliability and time. The proposed workflow, summarised in Figure 4.11, enabled up to 97.01±0.15% of *E. coli* to be identified as positive in a solution of PBS. The standardised workflow can be applied to data from each experiment quickly and reproducibly, with the assurance that an accurate and mathematically robust threshold has been used to calculate the percentage of cells successfully bound by the antibody or receptor of interest. The method inspires greater confidence in comparisons between experiments carried out independently, especially with samples producing faint fluorescence signals. Moving forward, in the next chapter the automated gating strategy will be applied to characterise the binding of TLRs to bacteria in PBS and in whole blood.

5

Chapter 5: Detection of bacteria in blood using imaging flow cytometry

5.1 Introduction

In the previous chapter, a method of characterising receptor binding to bacteria using imaging flow cytometry was developed to stain *E. coli in vitro*. A typical immunostaining procedure was followed whereby bacteria were stained with a species-specific primary antibody, then detected using a fluorescent secondary antibody raised against the isotype of the primary anti-*E. coli* antibody. I found that at the concentrations tested, binding of the antibody only resulted in a subtle increase in fluorescence intensity of the bound/positive cells and this made traditional manual gating techniques challenging. An automated gating strategy was therefore developed to quantify the percentage of bacteria bound to the antibody based on a threshold set according to the red/green fluorescence signal of the negative control (GFP bacteria). As previously discussed, a single antibody is diagnostically limited for the detection of the broad range of causative pathogens implicated in sepsis. In this chapter, we leverage the capabilities of PRRs to detect a range of PAMPs, which are common across different species, in order to overcome the limitations of species-specific antibodies and detect whole bacteria using IFC. The aims of this chapter are

as follows: 1) to determine if TLR2 and 4 can be used to detect Gram-positive (*S. aureus*) and Gram-negative (*E. coli*) bacteria, respectively, and 2) to determine if the performance of the assay measured in Chapter 4 translates from PBS to whole blood.

5.1.1 Recombinant PRRs for *in vitro* pathogen detection and separation

5.1.1.1 Mannose-binding lectin

PRRs have previously been used to detect and separate bacteria *in vitro.* The most extensively characterised example is mannose-binding lectin (MBL). Originally discovered in 1975, MBL has since been reported to bind to a wide range of molecular targets including lipoteichoic acid, mannan, peptidoglycan, lipoarabinomannan and lipophosphoglycan *via* its carbohydrate recognition domain (Turner 1996; Townsend et al. 2001). These are present on fungi, protozoa, Gram-positive and Gram-negative bacteria and, over the years, MBL has been shown to bind both obligate (Townsend et al. 2001) and pathogenic bacteria and fungi (Neth et al. 2000; Wong et al. 2013; Kang, Super, et al. 2014). Interestingly, (Neth et al. 2000) observed heterogeneous binding between different isolates (both clinical and control) of the same strain.

More recently, after being modified to remove the native collagen-helix domain and add an Fc-tag, the ability of recombinant FcMBL to detect, separate and purify pathogens and toxins from whole blood has been extensively characterised. From an engineering perspective, the modes by which FcMBL has been employed are particularly interesting. Indeed, many centre around the exploitation of the Fc-Protein A interaction which is routinely used to immobilise or purify recombinant proteins. (Kang, Super, et al. 2014) attached FcMBL to magnetic beads and used them to purify pathogens from whole blood using an 'extracorporeal blood cleansing device'; effectively a magnet used to dialyse bacteria from a sample under continuous flow at a rate of ~1 L/hr (comparable to traditional kidney dialysis). The group demonstrated removal of >90% of *E. coli* and *S. aureus* using this method (Kang, Super, et al. 2014). The separation efficiency increased to >99% and flow rate to ~12 L/hr by using a process of haemofiltration/haemoadsorption instead of magnetic

separation. This means, instead of relying on magnetic beads, FcMBL is covalently bound to the inside of a series of hollow fibre tubes, through which the sample of whole blood is run. Treatment resulted in a marked decrease in the concentration of pathogens detected in spleen, lung, liver and kidney in rats injected with 10^6 CFU/ml *E. coli* or *S. aureus* (Didar et al. 2015). The binding capabilities and applications of FcMBL are not limited to pathogens and bloodstream infections. Circulating tumour cells (CTCs) are implicated in metastasis and are comparably elusive to pathogens in a sepsis patient. FcMBL-mediated magnetic separation results in >90% capture efficiency against seven types of cancer cells *in vitro* and >90% CTCs in mice bearing advanced 4T1 breast tumours (Kang, Driscoll, et al. 2017). A clinical study following on from this devised an ELISA-style assay to quantify the concentration of PAMPs enriched from whole blood using FcMBL-magnetic beads. By incubating MBL conjugated to horse radish peroxidase (HRP), they were able to detect PAMPs released by/present on 47/55 (85%) of clinical isolates from different species, regardless of whether the pathogen was still viable or intact (Cartwright et al. 2016). This is particularly useful if the patient has received bacteriolytic antimicrobial therapy prior to having blood taken. Finally, in the PoC research space, an electrochemical biosensor has been developed to detect CRP, PCT (both *via* an antibody) and molecular mannan (using FcMBL), in whole blood, in parallel (Zupančič et al. 2021).

The primary objective of each of these studies was to separate FcMBL-bound pathogens from the sample before returning the blood to the patient, with little demonstrable evidence of how to identify the causative pathogen in a clinical context. The importance of rapid pathogen ID and subsequent AST with relation to the effective treatment of sepsis cannot be understated and has been discussed extensively in Chapter 3. Didar *et al.,* acknowledge that separation alone would not be sufficient to fully clear the *nidus* of an infection and recommend the coadministration of their haemofiltration therapy with antibiotic treatment. Furthermore, they suggest that pathogens could be eluted from the hollow fibre tubes using calcium-free media (Didar et al. 2015). In another study, FcMBL-mediated magnetic separation was

used to prepare positive blood culture samples for identification using MALDI-TOF MS in order to save the subsequent 24~72 hr secondary incubation to isolate single colonies. The results resulted in the successful identification of 94.7 and 93.2% of Gram-negative and Gram-positive bacteria, respectively, exhibiting a notable improvement in the enrichment of gram positive bacteria and fungal bloodstream infections over existing methods (Kite et al. 2022).

5.1.1.2 Toll-like receptors

Toll-like receptors (TLRs) are a family of PRRs employed by the innate immune system to detect a broad range of PAMPs in order to mount an immune response. TLRs have not yet been subjected to the same rigour of characterisation as FcMBL and, we believe, present an untapped resource waiting to be exploited for *in vitro* pathogen detection and separation. Although not quite as extensive as MBL, TLR2 binds the widest selection of PAMPs of all the TLRs, and through multiplexing with other members of the TLR superfamily, has the potential to be extended further, whilst retaining the ability to make broad, important distinctions between diagnostically relevant pathogen characteristics (Mogensen 2009; Akira and Takeda 2004). The PAMPs and their corresponding targets of TLRs are outlined in Table 5.1.

Mayall *et al.,* presented the first application of TLRs for diagnostic detection. His-tagged, recombinant TLR4:MD2 complex was immobilised on an NTA-coated gold electrode and demonstrated that it could detect molecular LPS down to a concentration of 1 ng/ml. They then went on to show dose-dependent binding of heat-killed *Salmonella typhimurium* from 10^5 to 10^0 cells/ml whilst remaining insensitive to Gram-positive *S. aureus* (10^5 cells/ml or *Rhabdovirus* (10^5 viruses/ml)) (Mayall, Renaud-Young, Chan, et al. 2017; Mayall, Renaud-Young, Gawron, et al. 2019). A similarly poised group also working towards the design of a TLR-based PoC device have demonstrated the ability of a TLR2/6 biosensor to preferentially bind Pam2CSK4, a diacylated molecular ligand of Gram-positive bacteria, over LPS. Tests then showed that the device could detect two Gram-negative strains, *Enterococcus*

hirae and *Bacillus licheniformis* down to 10^4 and 10^2 CFU/ml, respectively (McLeod et al. 2020). More recently, the group followed this up with the capture of flagellated, Gram-negative *E. coli* at a concentration of 10^2 CFU/ml using TLR5 (Singh et al. 2021). Other groups have demonstrated the use of recombinant TLRs for detecting pathogen genetic material and this will be discussed extensively in Chapter 6 (Amini et al. 2014).

Such studies have proven that it is indeed possible to detect whole pathogens, at clinically relevant concentrations, using recombinantly expressed TLRs. However, to our knowledge, their efficacy has not yet been validated in whole blood samples, nor have TLRs been shown to detect bacteria *via* flow cytometry. Gram-negative pathogens are known to shed LPS (Hanzelmann et al. 2016). Distinguishing between the respective signals of molecular/free LPS and pathogen-bound LPS could be difficult, potentially leading to an overestimation in the concentration of bound pathogens. Finally, biosensors are subject to steric limitations caused by immobilisation of the protein which could abrogate binding.

5.1.1.3 Additional examples

There are also other examples of recombinant receptors which have been exploited for their ability to bind PAMPs. (Lopes et al. 2016) demonstrated that a mutated lysozyme (LysE35A) was capable of enriching 90% of 10^3 CFU/ml *S. aureus* in PBS *via* immunomagnetic separation (IMS). The separation efficiency decreased substantially when applied to whole blood, as is typically the case with complex solutions, to 4-30%, however receptor maintained a LoD of 10 CFU. Apolipoprotein H (*ApoH*; a.k.a. ß2-glycoprotein I) was shown to bind *E. coli, Enterococcus gallinarum* (Gram-positive microorganism) and *Candida tropicalis* (fungus) at a LoD as low as 1 CFU/ml from 5 ml whole blood (Vutukuru et al. 2016). An alternative approach used Bis-Zn-DPA, a synthetic ligand capable of binding both Gram-positive and Gram-negative bacteria. This method was able to functionalise magnetic beads and enrich >99% of bacteria from a starting concentration of 10^5 *E. coli* spiked into diluted whole blood. A polyethylene-glycol (PEG) linker was shown to add space

between the ligand and the bead, in turn reducing steric hindrance and increasing binding efficiency (Lee et al. 2014). Table 5.1 provides a summary of many the different PRRs and antibodies used for pathogen detection *in vitro*.

Key considerations for this chapter include whether or not the labelling strategy developed in Chapter 4 continues to work with TLRs (not antibodies). In addition to this, we will test whether the assay and analysis will continue to yield reliable results in a challenging, complex sample of blood wherein there are significantly more host cells than bacteria. Unforeseen interactions between TLRs and host cells must be distinguished from 'desirable' interactions with bacteria, and accurately quantified.

Table 5.1: Summary of receptors used for *in vitro* pathogen detection and separation. 'Capture efficiency' refers to the number of bacteria spiked into a sample presented as a percentage of the total unless marked with an asterisk (*). An * indicates the percentage refers to the proportion of tested samples which were flagged positive. LoD; limit of detection, IMS; immunomagnetic separation.

Receptor	Molecular target	Pathogen tested	Method	LoD Buffer	LoD Whole blood	Reference
		E. coli		-	10^4 CFU/ml (>90%)	Kang *et al.*, 2014
		S. aureus	IMS microfluidic device	-	10^4 CFU/ml (>95%)	Kang *et al.*, 2014
	Various			10^4 CFU/ml (85%)	10^4 CFU/ml (76%)	Bicart-See *et al.*, 2016
FcMBL		*Candida albicans*		-	10^4 CFU/ml (>95%)	Kang *et al.*, 2014
		Various clinical isolates	Modified IMS ELISA	-	*(85% positive)	Cartwright *et al.*, 2016
		E. coli, S. aureus, C. albicans, LPS	Hollow fibre tubes	-	10^8 CFU/ml (90-99%)	Didar *et al.*, 2015

Receptor	Molecular target	Pathogen tested	Method	LoD Buffer	LoD Whole blood	Reference
	Mannan	-	Bio-sensor	-	31.25 ng/ml (relative peak area)	Zupančič *et al.*, 2020
TLR2/1	Tri-acylated lipopeptide (Gram-negative bacteria)	(Pam3CSK4)	Bio-sensor	7.5 µg/mL	-	She *et al.*, 2017
TLR2/6	Di-acylated lipopeptide (Gram-positive bacteria)	*Bacillus licheniformis, Enterococcus hirae*	Bio-sensor	10^2 CFU/ml	-	McLeod *et al.*, 2020
TLR3	Viral dsRNA	poly(I:C) (dsRNA mimic)	Bio-sensor	0.06 µg/ml	-	Amini *et al.*, 2014
TLR4/ MD2	LPS on Gram-negative bacteria	*S. typhimurium*	Bio-sensor	$<10^1$ heat-killed cells/ml	-	Mayall *et al.*, 2017, 2019
TLR5	Flagellin	*E. coli*	Bio-sensor	10^2 CFU/ml	-	Singh *et al.*, 2021
Mutated lysozyme (LysE35A)	-	*S. aureus*	IMS	(~90%) 10^3 CFU/ml	10 CFU (4-30% at 103)	Lopes *et al.*, 2016
Bis-Zn-DPA	Gram-negative bacteria	*E. coli*	IMS micro-fluidic device	-	$5x10^6$ CFU/ml (>99%)	Lee *et al.*, 2014
HpaII	Non-methylated CpG	*Yersinia pestis*	IMS	1pg pathogen DNA:1µg human DNA (>80%)	-	Liu *et al.*, 2016

Receptor	Molecular target	Pathogen tested	Method	LoD Buffer	LoD Whole blood	Reference
ApoH (ß2-glyco-protein I)	Various	*E. coli, Enterococcus gallinarum, Candida tropicalis*	IMS	-	1 CFU/ml (mixed reliabil-ity)	Vutukuru *et al.*, 2016
Anti-LPS	Gram-negative bacteria	LPS	IMS	100 fg/ml	*(80% positive)	Jagtap *et al.*, 2018
Anti-LTA	Gram-positive bacteria	LTA		1 pg/ml	*(80% positive)	
Anti-*E. coli*	-	*E. coli*	IMS micro-fluidic device	6 CFU	-	Ngamsom et *al.*, 2017

5.2 Results

As outlined in the previous chapter, the primary goal here was to adapt the assay we developed in Chapter 4 to determine whether recombinantly expressed TLRs 2 and 4 could be used to detect whole bacteria. TLR2 binds a selection of different PAMPs, mostly specific to Gram-positive bacteria such as *S. aureus*, while TLR4 binds to lipopolysaccharide (LPS) which is found exclusively on the surface of Gram-negative bacteria like *E. coli*. (Mogensen 2009). These two TLRs were chosen to cover the broadest selection of pathogens with the added ability to distinguish between the Gram-status of bacteria by combining them.

We presented a method of quantifying the percentage of bacteria bound to an anti-*E.coli* antibody using IFC where a primary anti-*E.coli* antibody was detected using a fluorescent secondary antibody raised against the isotype of the Fc-region of the primary (Figure 5.1A). Over the course of the following pages, I will describe the iterative process of how the labelling method was revised several times before success could be demonstrated with TLRs. A summary of the different labelling variations can be seen in Figure 5.1.

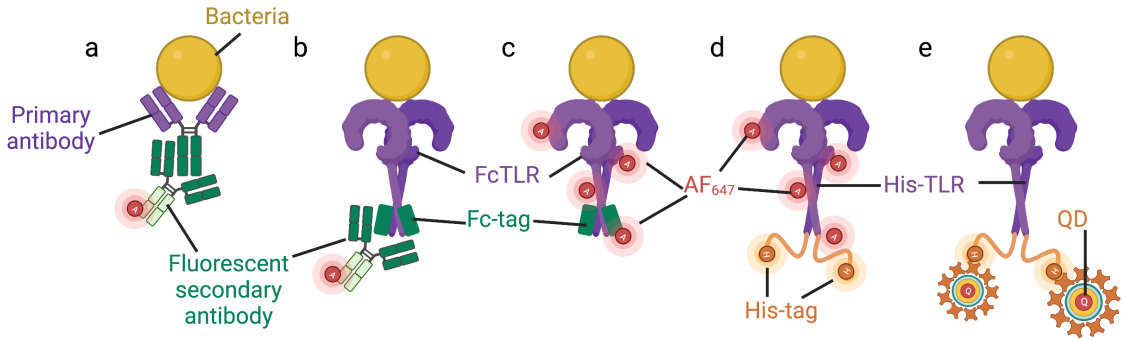

Figure 5.1: Summary of TLR labelling strategies. **(A)** Species-specific primary anti-E.coli antibody is detected using a fluorescently labelled (AF647) secondary antibody raised to the isotype of the primary antibody (discussed in detail in Chapter 4). **(B)** Fc-tagged TLR2 binds to Gram-positive *S. aureus* and is detected by fluorescently-labelled secondary antibody raised to the isotype of the Fc-tag. **(C)** Fc-TLR2 is directly fluorescently labelled using an NHS-EDC kit to covalently attach the fluorophore (AF647) to free primary amine groups of lysine residues. **(D)** TLRs can be purchased with a his-tag instead of an Fc-tag. In this instance, the his-tag is not used. **(E)** The his-tag is used to bind alternative fluorophores such as quantum dots (QD) functionalised with nitrilotriacetic acid (NTA).

5.2.1 Adaptation of the assay to work with recombinant Toll-like receptors

Initially, anti-E.coli was simply swapped out for recombinantly expressed TLR2 which could be purchased with an Fc-tag (Bio-techne/RandD systems; Cat. 1530-TR). Fc-tags, referring to the Fc-portion of an IgG antibody, are typically used to immobilise proteins by exploiting their high affinity interaction with protein A, for example, recombinantly expressed, Fc-tagged proteins are purified from their supernatant using protein A columns. Fc-tags have worked especially well for groups working with MBL (Kang, Super, et al. 2014; Bicart-See et al. 2016; Cartwright et al. 2016; Didar et al. 2015). In our case, the presence of the Fc-tag was particularly useful since it meant that bound receptor could be detected as before, using a fluorescent secondary antibody against the FcIgG isotype (Figure 5.1B). Different TLRs could be used to target different PAMPs and so long as the isotype of the Fc-tag was unique, they could be detected using secondary antibodies conjugated

to different coloured fluorophores, thus creating a modular, multiplexed panel.

The approach was first tested with FcTLR2 and Gram-positive *S. aureus* expressing GFP. Samples were analysed on the ImageStream and analysed according to the process outlined in Chapter 4. The binding looked promising, with 37.5, 46.9 and 52.2% of bacteria measured as double positive for GFP and FcTLR2 at 0.5, 1.0 and 2.0 µg/ml receptor, respectively (Figure 5.2A). However, comparing this to a sample stained with only the secondary antibody, we see a higher degree of binding detected: 72.8, 57.2 and 73.5% double positive cells for 0.5, 1.0 and 2.0 µg/ml fluorescent secondary antibody, respectively (Figure 5.2B). Increasing the number and stringency of the wash steps, in addition to the inclusion of a blocking step using 3% bovine serum albumin (BSA) offered no reduction in detecting the binding between the secondary antibody and *S. aureus* (data not shown).

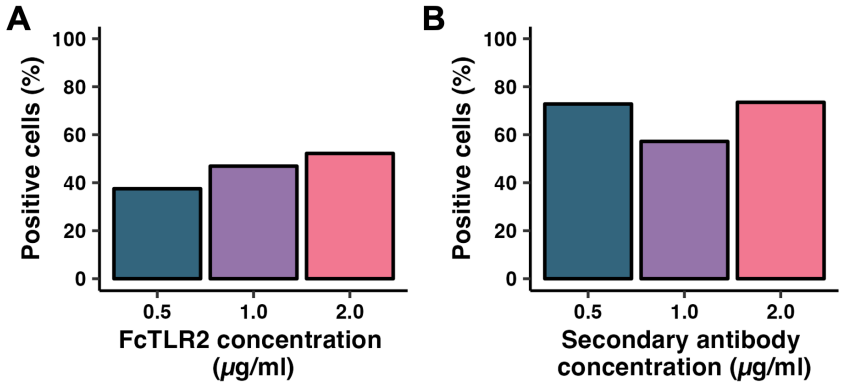

Figure 5.2: Detection of FcTLR2 binding to GFP-expressing *S. aureus* using fluorescently labelled secondary antibody. **(A)** FcTLR2 (0.5, 1.0 or 2.0 μg/ml) was incubated with 10^7 CFU/ml *S. aureus*. Bound receptors were detected by incubating fluorescently labelled secondary antibody (1.25 μg/ml) for 20 min on ice. Samples were run on ImageStream (Amnis) and analysed in R studio as outlined in chapter 4. **(B)** Shows the percentage of positive cells stained with only the fluorescent secondary antibody as a negative control for binding in the absence of any FcTLR2 (n=1 technical replicates, 10^7 CFU bacteria).

5.2.2 Complications with Fc-tags

In order to try and ameliorate the suspected non-specific binding caused by the fluorescent secondary antibody, FcTLR was directly labelled using a different

approach with Alexa Fluor™ 647 (Microscale Protein Labelling Kit; Cat. A30009; Invitrogen™) (Figure 5.1C). The kit was selected for use with small quantities of protein (<100 µg). AF647 is the same fluorophore attached to the secondary antibody so direct comparison was possible to experiments in Chapter 4. This fluorophore has a succinimidyl (NHS ester) moiety which reacts with any exposed primary amine groups on lysine residues. The process consists of a 15 min incubation followed by purification using size exclusion beads to trap any unbound NHS-fluorophore. For the labelling method to work, there must not be any exposed lysine residues in, or close to, the active site which could abrogate binding between the TLR and the bacteria due to steric hindrance (see Chapter 6).

Binding of FcTLR2 and FcTLR4 to *E. coli* and *S. aureus* was compared to a new negative control: the Fc portion of human IgG (FcIgG). Direct fluorescent labelling of Fc-tagged TLRs revealed a high degree of binding (68.47 - 89.07%) to *S. aureus*, irrespective of receptor and concentration (Figure 5.3; yellow bars) which suggested that all available binding sites were saturated by the Fc-tag rather than the receptor itself. *E. coli*, on the other hand, exhibits a dose-dependent response, however, little difference can be seen between the different receptors (Figure 5.3; blue bars). From this experiment, the presence of an Fc-tag is problematic for the assay.

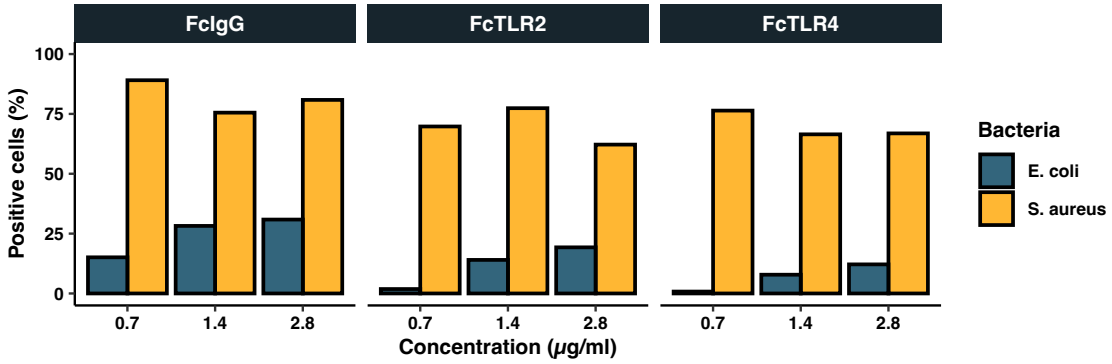

Figure 5.3: Direct fluorescent labelling of Fc-tagged TLRs using an NHC-EDC labelling kit. 50 μg aliquots of lyophilised recombinant TLR were resuspended in PBS at 1 mg/ml and fluorescently labelled with AF647 using the Microscale Protein Labelling Kit (ThermoFisher Scientific) according to the manufacturer's instructions. Labelled receptors at a 2-fold serial dilution ranging from 0.7-2.8 μg/ml were incubated with 10^7 CFU/ml *S. aureus* (yellow bars) and *E. coli* (blue bars). FcTLR2 and FcTLR4 were compared to the Fc-portion of a human IgG antibody (n=1).

5.2.3 Removal of Fc-tag facilitates specific binding of TLR2 to *S. aureus*

Recombinant TLRs can alternatively be purchased with his-tags; short, 6-10 amino acid long histidine repeats which are purified using nickel-affinity columns. His-tagged TLRs were labelled with AF647 (Figure 5.1D) and the percentage of positive *S. aureus* and *E. coli* was once again compared. Focusing first on *S. aureus*, without the Fc-tag, TLR2 binds in a concentration-dependent manner: 8.7, 33.4 and 58.2% of bacteria are bound to TLR2 for 0.7, 1.4 and 2.8 µg/ml, respectively, which is roughly in line with the log2 serial dilution of receptor added. TLR4 behaves as expected and binds significantly less due to the lack of LPS present on the surface of *S. aureus*. Changing our perspective on FcIgG, it can now be used as a positive control for *S. aureus* (Figure 5.4; yellow bars). Comparatively, significantly less binding was observed between *E. coli* and all of the receptors compared to *S. aureus*. Minimal binding (<3%) could be seen with TLR4 with more binding observed with FcIgG (3.6 to 9.3%), a negative control for *E. coli*. Binding of TLR2 to *E. coli* appeared to be dose-dependent. We measured 5.8, 10.0 and 10.4% of positive cells at 0.7, 1.4 and 2.8 µg/ml which was greater than TLR4 but not significantly different from the IgG negative control (Figure 5.4; blue bars). Further investigation into TLR4 was therefore necessary.

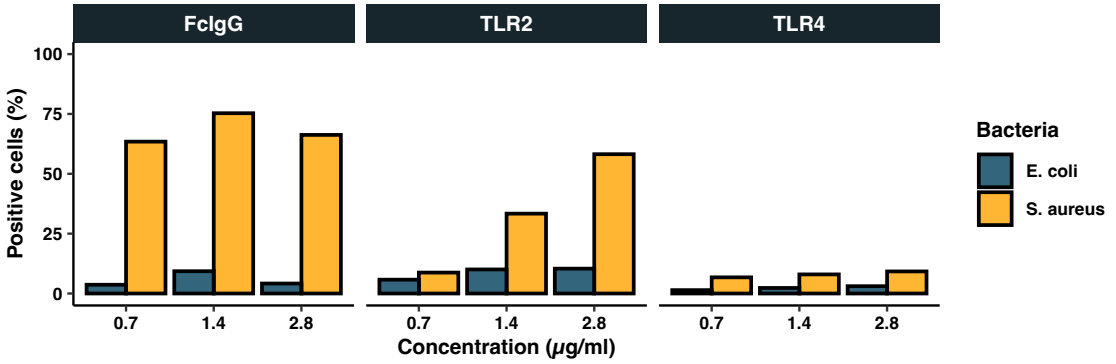

Figure 5.4: Binding of fluorescently labelled his-tagged PRRs. Alternative receptors, without an Fc-tag, were purchased and fluorescently labelled with AF647 as described above. Labelled receptors at a 2-fold serial dilution ranging from 0.7-2.8 μg/ml were incubated with 10^7 *S. aureus* (yellow bars) and *E. coli*. TLR2 and TLR4 were compared to the Fc-portion of a human IgG antibody (n=1).

5.2.4 MD2 does not improve TLR4 binding to *E. coli*

Bacterial LPS is highly variable between species and as such, sensing *in vivo* is carried out, not only by TLR4, but by 3 other proteins: LPS binding protein (LBP), CD14 and Myeloid differentiation factor 2 (MD2). TLR4 and MD2 form a complex whereas LBP and CD14 are referred to as accessory proteins. The picture built up in the literature is that LBP first binds LPS, transfers it to CD14 which in turn transfers it to the TLR4-MD2 complex (Park and Lee 2013; Kim et al. 2007). MD2 is reported to be the component of the complex which interacts directly with LPS and is therefore essential for its recognition (Viriyakosol et al. 2001). (Christiansen et al. 2012) compared the response of whole blood stimulation with synthetic LPS to *E. coli* culture and showed that while LPS-induced cytokine response was equally reduced by neutralisation of either CD14 or MD2, CD14 neutralisation was significantly more effective for reduction of an *E. coli*-induced cytokine response. This goes to show how the strength and the sensitivity of the *in vivo* immune response can be altered by the concerted effort of multiple proteins involved in the complex. *In vivo* sensitivity/activity is measured by production of downstream signalling products, however it does not tell us which proteins could be used to bind Gram-negative bacteria with a high enough affinity to be detected using our flow cytometry assay. On a molecular scale, x-ray co-crystallisation of the protein with (synthetic) molecular ligands is used to demonstrate the ability to physically bind and used to infer *in vivo* interactions. Indeed, work by (Kang, Nan, et al. 2009) suggests LPS induces the dimerisation of MD2 and TLR4.

Mayall *et al.,* demonstrated human TLR4/MD2 was able to successfully detect LPS using an electrochemical biosensor. The TLR4/MD2 complex was immobilised on an electrode and cyclic voltammetry was used to measure the change in resistance of addition of the ligand; this was shown to be logarithmically proportional to the concentration of LPS (Mayall, Renaud-Young, Chan, et al. 2017; Mayall, Renaud-Young, Gawron, et al. 2019). Based on the literature, we combined a fixed concentration of TLR4 (2 µg/ml) with MD2 (0-1.5 µg/ml) to see if an improvement

in *E. coli* binding could be achieved. There was little difference observed for MD2 concentrations below 1.5 µl/mg (Figure 5.5A). Increasing the MD2 concentration to 1.5 µg/ml led to a significant increase in the proportion of *E. coli* detected (~17.5%). The test was then repeated using an equal ratio of TLR4:MD2 to replicate *in vivo* dimerisation, but the trend could not be confirmed (Figure 5.5B). In the interest of time, it was decided to focus on the characterisation of TLR2.

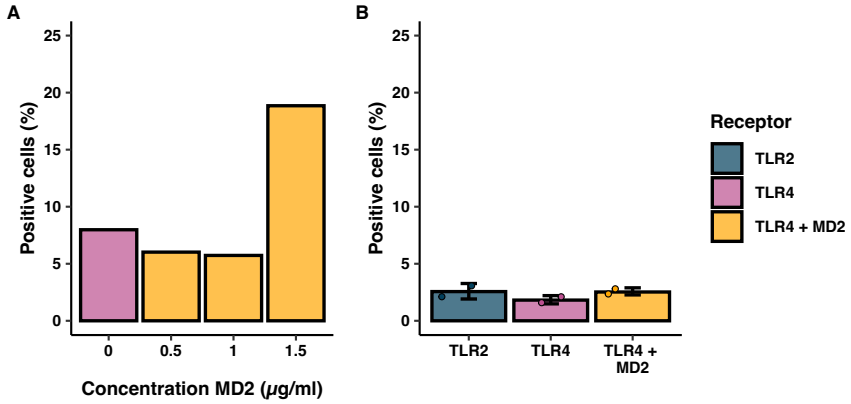

Figure 5.5: The effect of MD2 cofactor on the capacity of TLR4 to bind Gram-negative *E. coli*. **(A)** A fixed concentration of AF647-labelled TLR4 (2 μg/ml) was mixed with MD2 ranging from 0.5-2.5 μg/ml and 10^7 CFU GFP-expressing *E. coli* and incubated on ice for 30 min (n=1). The percentage of bacteria bound to receptor was measure using ImageStream. **(B)** A 1:1 ratio of TLR4:MD2 (2 μg/ml of each protein) was compared to TLR2 and TLR4 independently for *E. coli* binding (n=2).

5.2.5 TLR2 binds on its own to *S. aureus* in PBS

As opposed to *E. coli*, a high percentage of *S. aureus* was consistently found to bind TLR2 (up to 90.6 ± 4.5%) (Figure 5.6; pink bars and density plots in Appendix Figure C.1). Recent evidence has shown TLR4 binding *S. aureus* (Chu et al. 2018; Hanzelmann et al. 2016). Here, the percentage of positive cells for TLR4 binding range from 7.8 ± 2.5% - 22.6 ± 7.0%. The response to TLR4 appeared to be dose-dependent up to a concentration of 1 µg/ml, but that trend seemed to be lost as the concentration of TLR4 was increased further (Figure 5.6; yellow bars).

MD2 was also included in the analysis and showed a level of binding comparable to TLR4 (18.6 ± 1.4%; Figure 5.6; purple bars). Although there is evidence of

MD2 playing a role in the TLR2 immune response (Dziarski and Gupta 2000; Dziarski, Wang, et al. 2001), the level of binding of *S. aureus* to TLR2 on its own is significantly higher than that observed with MD2 and TLR4. TLR2 not only binds more cells than a species-specific antibody, but has a much broader variety of ligands to which it can bind. TLR2 remains to be tested with other strains of bacteria, however results here suggest it would make an ideal candidate for detection of Gram-positive bacteria for the detection of pathogens in blood samples.

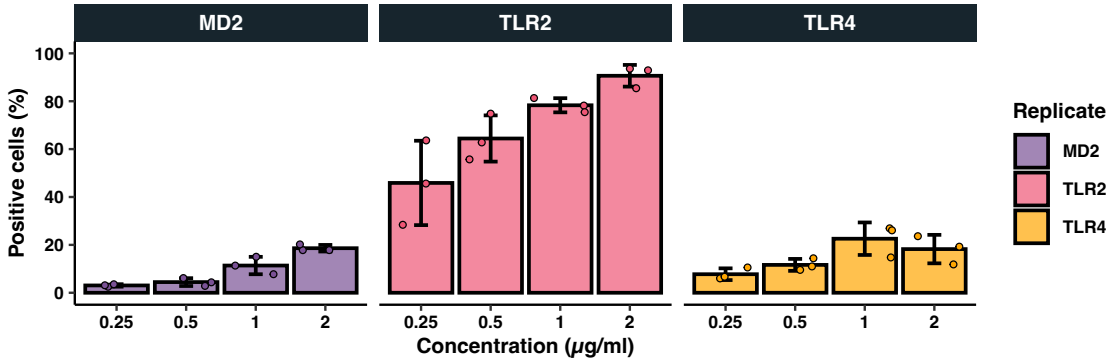

Figure 5.6: Dose response of MD2 and TLR binding in PBS. *S. aureus* (10^7 CFU) expressing GFP was stained with PPR ranging from 0.25-2.0 μg/ml. MD2 (negative control; purple), TLR2 (pink) and TLR4 (yellow). Error bars show standard deviation of the mean (n=3 technical replicates).

The aim of this chapter was to determine how well fluorescently labelled TLRs bind to bacteria. Thus far, we have described the evolution of labelling strategy/assay development (Figure 5.1) which saw the reduction of binding of the negative controls relative to that of TLR. A particular challenge was the strain-specific problems we encountered with *S. aureus* binding to Fc-tags which was overcome by labelling the TLRs directly with AF647 and using receptors without Fc-tags. The application of the gating strategy developed in Chapter 4 allowed us to confirm that TLR2 on its own can bind with high affinity to *S. aureus* in PBS, while little to no binding has been observed for *E. coli*. On the other hand, the experiments have also demonstrated that TLR4 on its own does not bind to *E. coli* or *S. aureus*. Replacement of AF647 with QD_{630}, whilst providing an improvement in yield, resulted in a lower percentage of bound bacteria in spite of their improved photoluminescent properties.

5.2.6 TLRs bind *S. aureus* in whole blood

While more strains of bacteria would need to be tested to confirm the trend, it can be hypothesised from the previous section that TLR2 is a relevant marker for Gram-positive bacteria detection. Blood is significantly more complex than PBS; it is composed of 4-6x10^9 cells/ml erythrocytes (RBCs), up to 1.6x10^7 leukocytes and 1.3x10^5 thrombocytes (Opota, Jaton, et al. 2015) and therefore presents additional challenges when it comes to quantifying how well the TLRs work. Interestingly, however, none of the work aiming to employ recombinant TLRs in a diagnostic device have been tested with whole blood (McLeod et al. 2020). Tests were therefore done to compare the binding capacity of TLRs to bacteria in whole- and RBC-lysed blood in order to assess their interaction with WBCs.

The complexity of blood samples necessitated a change of image processing to analyse the data from IFC. The gating strategy used in this section can be divided into three steps:

1. Select single cells in focus.
2. Distinguish host cells from bacteria using SpeedBeads (an internal control used to calibrate the machine fluidics).
3. Quantify the percentage of GFP bacteria bound to AF647-labelled TLRs.

Due to the presence of all the blood cells, it is no longer suitable to gate for image quality using thresholds set by deviations from the average. Therefore, steps 1 and 2 must now be completed manually in the IDEAS software platform (Figure 5.7).

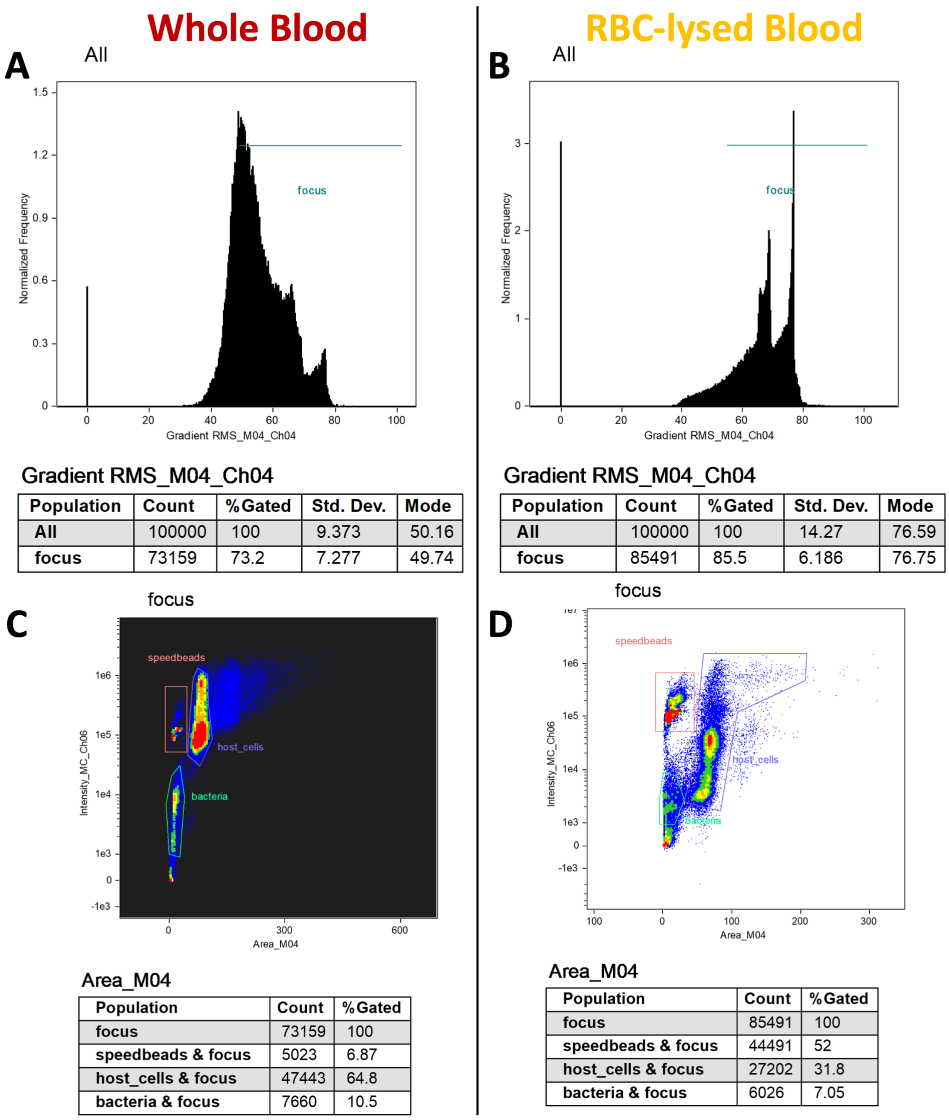

Figure 5.7: Revised IFC gating strategy for preliminary processing blood samples using IDEAS software. Example plots are taken from a sample of whole- (left column) and RBC-lysed blood (right column) spiked with 10^8 CFU/ml and stained with AF647-labelled recombinant TLR2. The gating strategy was applied to all samples before feature values were exported for populations of host cells (purple) and bacteria (turquoise) for further processing in R. **A, C)** Cells in focus were gated by taking everything with a gradient RMS value greater than 55 for BF images. **B, D)** Host cells (purple), bacteria (turquoise) and SpeedBeads (salmon pink) were gated based on SSC intensity *vs.* Area BF images.

Cells in focus were selected by taking all objects with a gradient RMS greater than 55 for BF images (Figure 5.7 A, C). Area *vs.* SSC (intensity_MC_Ch06) was used to gate out debris and distinguish between bacteria, host cells and SpeedBeads (Figure 5.7 B, D). Typically, singlets are selected using area *vs.* aspect ratio, however

this does not allow bacteria to be separated from SpeedBeads. Due to the limited resolution of the BF images, *S. aureus* and SpeedBeads appear to have an almost identical morphology and therefore cannot be distinguished based on shape or size. They do however have very different refractive indices (Appendix Figure C.2) and so can be gated and removed based on SSC intensity. SpeedBeads are, by default, removed automatically by the IDEAS software prior to acquisition based on their size and SSC. In the lysed blood samples, however, they all appear to be bound to fluorescent TLR (Figure 5.8B). No TLR can be detected bound to SpeedBeads in whole blood samples, nor has it been seen with any previous tests in PBS. It is imperative the TLR-bound SpeedBeads are gated out so as not to lead to an overestimate in the percentage of TLR-positive cells. Single, host cells in focus are shown in Figure 5.8 C and D. The biconcave shape of erythrocytes is distinctly recognisable. A faint, red haloing can be seen in Ch05 (AF647 channel) of the leukocyte images suggesting an interaction with TLR (Figure 5.8 D).

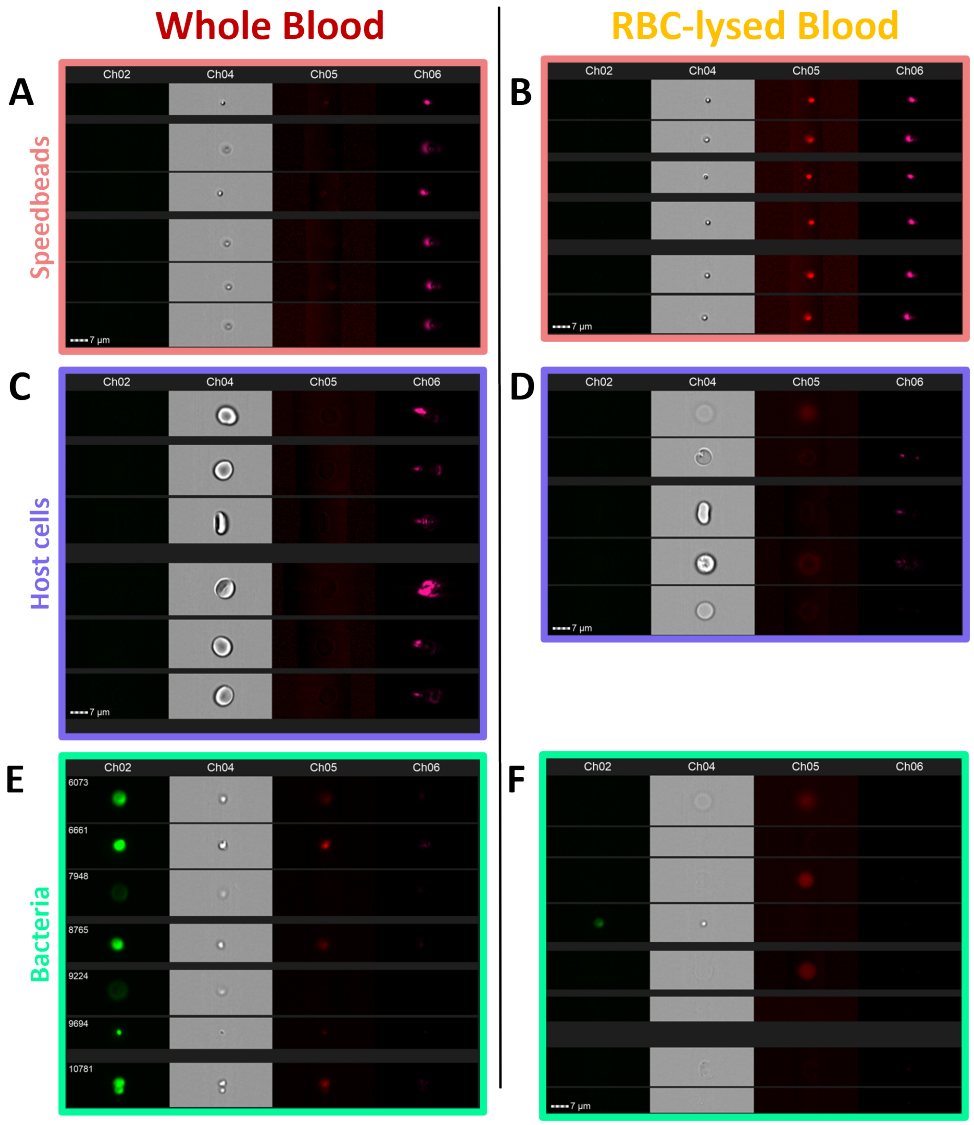

Figure 5.8: Example images of whole- (left column) and RBC-lysed blood (right column) spiked with 10^8 CFU/ml and stained with AF647-labelled recombinant TLR2. The gating strategy was applied to all samples before feature values were exported for populations of host cells (purple) and bacteria (turquoise) for further processing in R. Host cells (purple), bacteria (turquoise) and SpeedBeads (salmon pink) were gated based on SSC intensity *vs.* Area BF images. **A, B)** Images of SpeedBeads gated on area *vs.* SSC intensity showing a red signal from TLR2 for RBC-lysed cells. **C, D)** Images of host cells gated on area *vs.* SSC intensity. **E, F)** Images of bacteria gated on area vs. SSC intensity. Ch02; GFP fluorescence images, Ch04; brightfield (BF) images, Ch05; AF647 fluorescence images, Ch06; side-scatter (SSC) images.

Bacteria are most recognisable by their GFP fluorescence in channel 2 (Ch02), however Figure 5.8E illustrates how they can be detected using area and SSC alone in whole blood. This is not the case in the RBC-lysed sample where we see a mix of

bacteria and a high number of cells with low granularity; potentially representative of dead or dying leukocytes caused by the high concentration of bacteria (Figure 5.8F). This phenomenon may also be explained by poor-quality masks applied to the BF images which would result in an underestimation of the area of host cells, in turn causing them to appear in the same region of the plot as bacteria (Figure C.3). For this reason, GFP-bacteria are distinguished from blood cells based on fluorescence intensity using a gate set at 5000 RFU (Appendix Figure C.4). There were only 623 ± 93 GFP bacteria, across samples stained with TLR2 or TLR4.

Fluorescent TLRs were able to detect bacteria successfully in blood samples. In a total of six whole blood samples, 6121 ± 625 free bacteria were stained with TLR2 and TLR4. Of these, it was found that 3.4 ± 0.6% and 6.7 ± 0.7% were bound to TLR2 and TLR4 respectively - which is significantly lower than results obtained in PBS. In the same samples, populations of host cells associated with bacteria were found to have 1.4 ± 0.1% and 1.8 ± 0.4% bound by TLR2 and TLR4 (*i.e.* red, green double positive), respectively (Figure 5.9). This suggests that the fluorescent TLRs were able to detect both free bacteria and those associated with host cells. From these results, it is unclear if the binding affinity of TLR4 is higher than that of TLR2 in whole blood; the opposite of what was shown in PBS and the general perception of the literature. Since the populations are so small, the difference could be attributed to variation in concentration of the respective TLRs. If TLRs were not added in excess of bacteria then a lower concentration may result in a higher average fluorescence intensity.

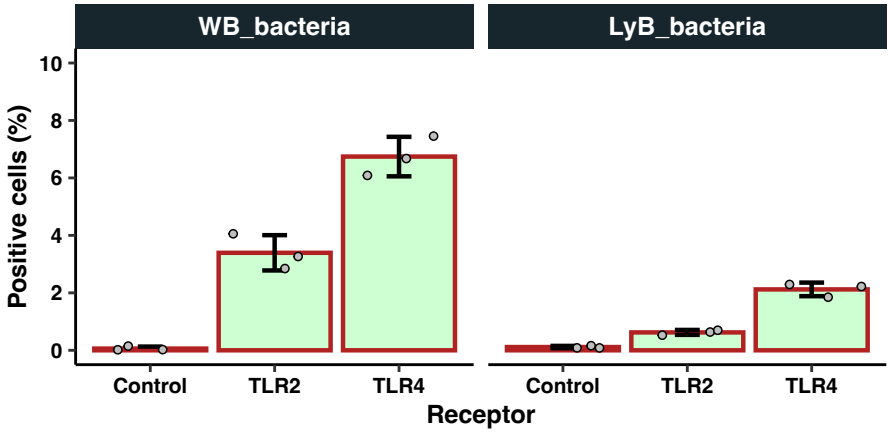

Figure 5.9: Recombinant TLRs 2 and 4 have the capacity to detect *S. aureus* in blood. Comparison between the percentage of GFP-positive bacteria bound to fluorescently labelled TLRs.

5.2.7 TLRs appear to bind neutrophils and dead leukocytes

There is a significant amount of TLR bound to host cells in the absence of any bacteria on the image. Figure 5.10 and Figure 5.11 show the red fluorescence intensity of TLR positive populations of whole and RBC-lysed blood samples, respectively. TLR2 binds 24.6 ± 0.8 % of cells in the whole blood and TLR4, on the other hand binds 47.9 ± 16.2 % (Figure 5.10E). Indeed, 88.5 ± 7.7 % of cells in the RBC-lysed samples were positive for TLR2 and 24.5 ± 0.5 % for TLR4, respectively (Figure 5.11E). However, by inspecting the images of each of the samples, it is clear that the intensity of the TLR signal in Ch05, although surpassing the threshold of positivity, is barely visible by eye (Figure 5.10D). Furthermore, plotting mean fluorescence intensity (MFI) gave a profoundly different impression of the interaction between the TLRs and RBCs, with only $8.3x10^4 \pm 8.4x10^3$ RFU for TLR2 and $1.8x10^5 \pm 1.1x10^5$ RFU for TLR4 in whole blood (Figure 5.10F) compared to $2.3x10^6 \pm 8.5x10^4$ RFU for TLR2 and $1.2x10^6 \pm 8.5x10^4$ RFU for TLR4 in lysed blood (Figure 5.11F).

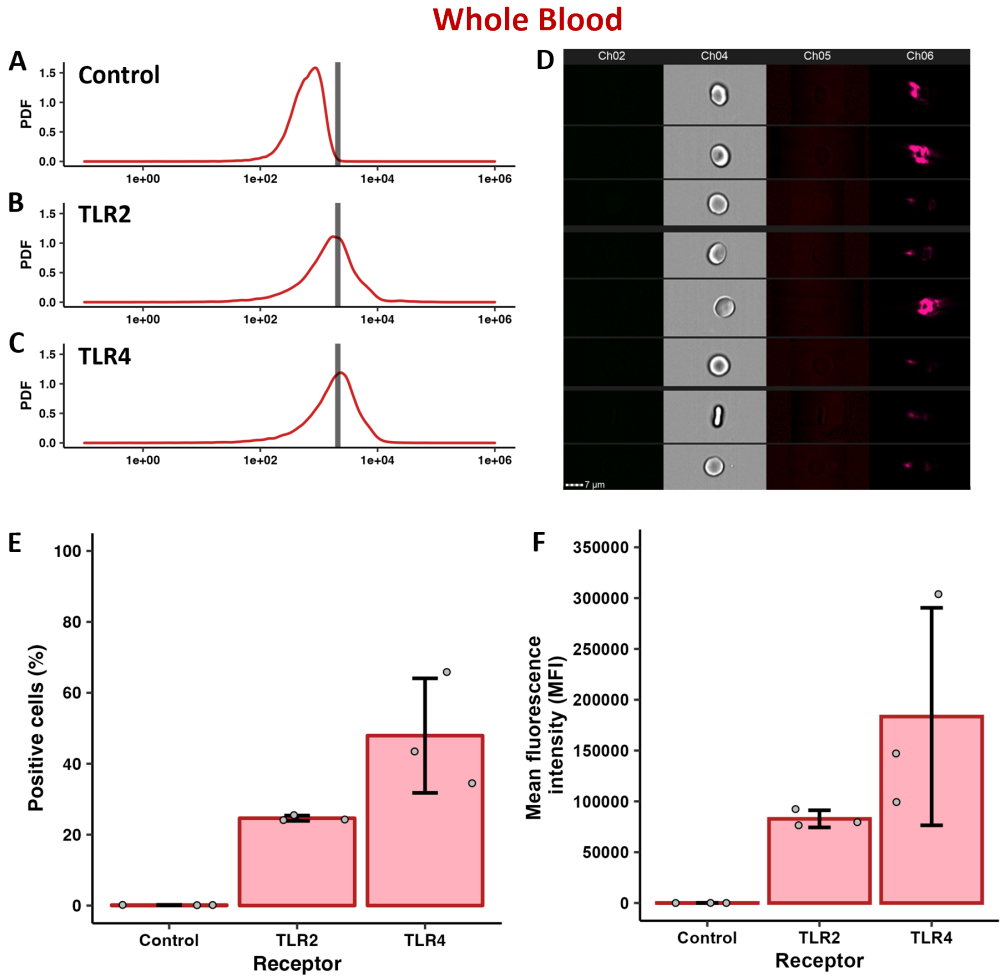

Figure 5.10: Investigation into the interaction between TLR and host cells in whole blood. **A-C)** Density plots showing the distribution of AF647 (red) fluorescence signal in samples of blood spiked with 10^7 CFU/ml *S. aureus* for control (no receptor), TLR2 and TLR4, respectively. Host cells in focus were manually gated in IDEAS before feature values were exported for subsequent analysis in R. A threshold (vertical gray line) was set based on 99.865% of points in the negative control (Blood + bacteria). **D)** IFC images of red-positive host cells (RBCs) showing a minimal visible red signal in spite of being classified positive for TLRs (Ch05). **E)** The percentage of host blood cells fluorescently labelled with TLR2 and TLR4. **F)** Bar plots showing mean fluorescence intensity (MFI) of TLR-positive host cells in whole blood. (error bars show standard deviation of the mean, n=3 technical replicates).

TLRs 2 and 4 are expressed on monocytes and neutrophils (Marsik et al. 2003). For successful signal transduction, TLR2 either forms a homodimer, or a heterodimer

with TLR6 or TLR1; TLR3 forms a homodimer (Mogensen 2009; Koymans et al. 2015). Results here may indicate that the source of the red fluorescent signal on host cells could be coming from dimerisation between the fluorescent, recombinant TLRs and native TLRs expressed on the surface of monocytes and neutrophils. This may account for the significant binding observed in the RBC-lysed blood sample, however it must be noted that even if this is true, the proportion of RBCs seen to be interacting with TLR is nevertheless higher than expected. WBCs only account for ~1% of cells in whole blood, which is significantly lower than the percentage of positive cells we have observed.

These results suggest that the interaction between recombinant TLRs and host WBCs is more than just non-specific binding. It could be indicative of a specific molecular interaction which may have diagnostic relevance as TLR expression has been shown to change in sepsis (Viemann et al. 2005; Tsujimoto et al. 2008). Furthermore, the comparison between MFI shows a limitation of relying solely on the percentage of positive cells as we fail to account for the overall fluorescence population intensity of the positive population and subsequently overestimate the interaction between the TLRs and RBCs (Figure 5.10F).

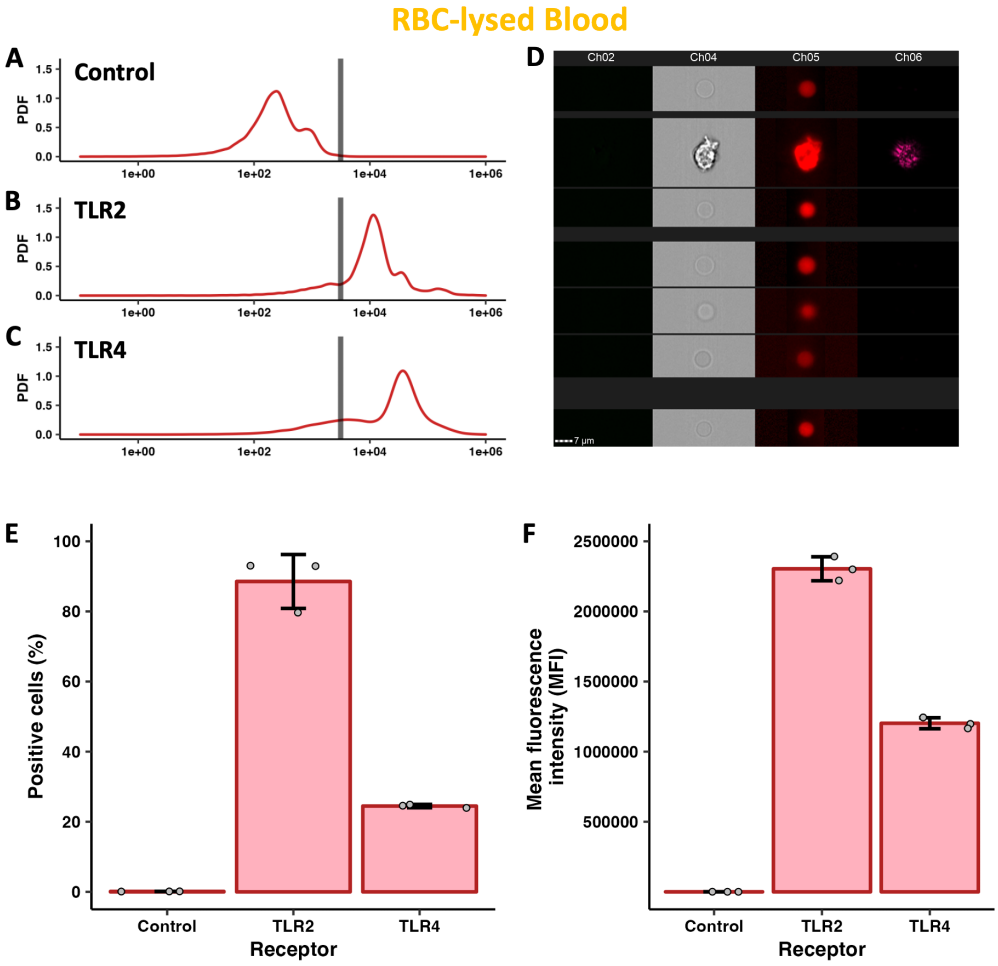

Figure 5.11: Investigation into the interaction between TLR and host cells in RBC-lysed blood. **A-C)** Density plots showing the distribution of AF647 (red) fluorescence signal in samples of blood spiked with 10^7 CFU/ml *S. aureus* for control (no receptor), TLR2 and TLR4, respectively. Host cells in focus were manually gated in IDEAS before feature values were exported for subsequent analysis in R. A threshold (vertical gray line) was set based on 99.865% of points in the negative control (Blood + bacteria). **D)** IFC images of red-positive host cells (WBCs) showing a minimal visible red signal in spite of being classified positive for TLRs (Ch05). **E)** The percentage of host blood cells fluorescently labelled with TLR2 and TLR4. **F)** Bar plots showing mean fluorescence intensity (MFI) of TLR-positive host cells in RBC-lysed blood. (error bars show standard deviation of the mean, n=3 technical replicates).

Next, we asked which WBCs the TLRs are binding to in the lysed blood sample. Plots of SSC *vs.* TLR fluorescence intensity (Ch05) reveal populations of TLR-

bound cells which can be distinguished based on their granularity. In the lysed blood sample, highly granular cells scatter the most light and include, as their name suggests, granulocytes (basophils and neutrophils). Lymphocytes have mid-level granularity and as cells die, they tend to shrink and decrease in granularity. Figure 5.12A exposes two populations of TLR2-bound WBCs with very high and very low SSC accounting for 0.68 and 13% of the total number of cells in this sample of TLR2-stained WBCs, respectively. By reviewing the images of these two populations we see that the more numerous, low-SSC subtype is barely visible in the BF images and appear to have a red-haloing of TLR. Supporting this, nothing is visible in the SSC image (Ch06, pink, Figure 5.12B). The highly granular population, on the other hand, reveals images of what are most likely to be neutrophils as basophils and eosinophils are significantly more rare (Figure 5.12C). Bacteria can be seen in some of the images of the putative neutrophils suggesting that the TLR could be introduced when the bacteria are engulfed, however further investigation would be required to determine if this is happening with any certainty.

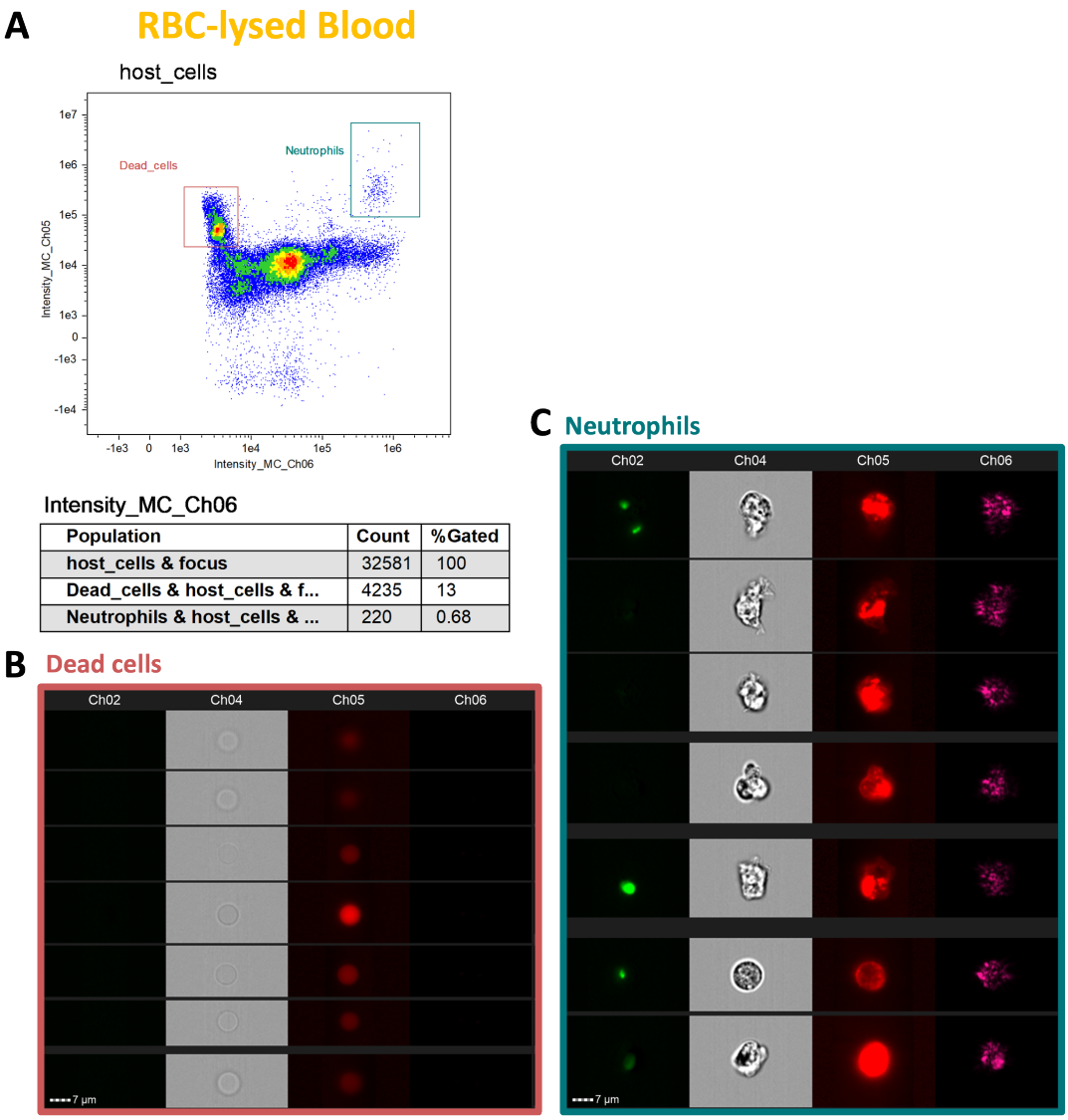

Figure 5.12: Host cells in focus in samples of RBC-lysed blood spiked with *S. aureus* are gated based on SSC intensity ($Intensity_MC_Ch06$) *vs.* TLR fluorescence intensity ($Intensity_MC_Ch05$). TLRs bind two populations of leukocytes **A)** Scatter plots of AF647 fluorescence intensity (Ch05) *vs.* fluorescence intensity of SSC reveal a single population of high-TLR cells in whole blood and two populations of high-TLR in RBC-lysed blood which can be distinguished based on SSC. **B)** IFC images of putative dead cells bound to fluorescent TLR in RBC-lysed blood. **C)** IFC images of putative neutrophils bound to fluorescent TLR in RBC-lysed blood. Example plots and images are taken from a samples of RBC-lysed blood spiked with 10^8 CFU/ml and stained with AF647-labelled recombinant TLR2.

The same approach was applied to a sample of whole blood where there is just one population of RBCs with high TLR signal (Figure 5.13A) representing 1.13% of the total number of cells. On closer inspection of these images, all RBCs

with visibly high TLR signal are bound to bacteria expressing GFP. Indeed, in the BF images even individual *S. aureus* can be seen and the green/red signals are colocalised to the same point in the image, suggesting the TLR is not bound to the erythrocyte at all (Figure 5.13B).

Two subsequent experiments were carried out to determine 1) if the high level of TLR binding to host cells was caused by the bacteria and 2) the true identity of the TLR-bound WBCs using specific neutrophil and monocyte markers. Unfortunately, for reasons out of our control, the ImageStream was out of order for a number of months towards the end of the project and these experiments did not produce any meaningful data.

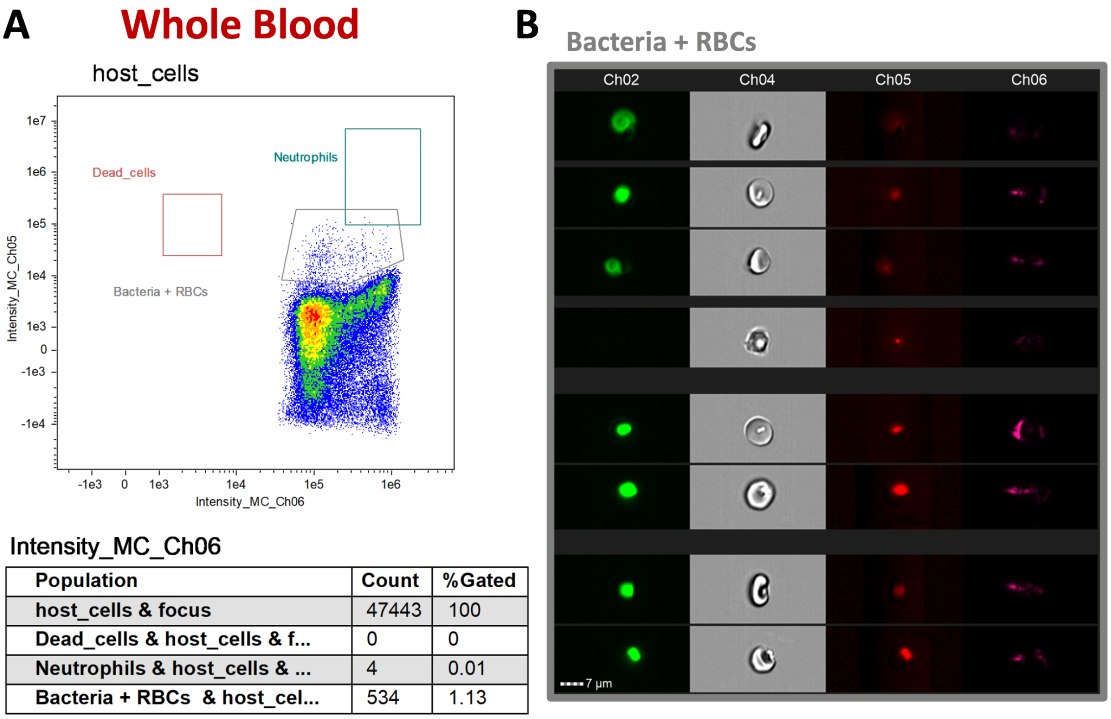

Population	Count	%Gated
host_cells & focus	47443	100
Dead_cells & host_cells & f...	0	0
Neutrophils & host_cells & ...	4	0.01
Bacteria + RBCs & host_cel...	534	1.13

Figure 5.13: Host cells in focus in samples of whole blood spiked with *S. aureus* are gated based on SSC intensity ($Intensity_MCCh06$) *vs.* TLR fluorescence intensity ($Intensity_MCCh05$). TLRs bind a single population of leukocytes **A)** Scatter plots of AF647 fluorescence intensity (Ch05) *vs.* fluorescence intensity of SSC reveal a single population of high-TLR cells in whole blood and two populations of high-TLR in RBC-lysed blood which can be distinguished based on SSC. **B)** IFC Images of erythrocytes bound to TLR-labelled *S. aureus* expressing GFP. Example plots and images are taken from a samples of whole blood spiked with 10^8 CFU/ml and stained with AF647-labelled recombinant TLR2.

5.3 Discussion

After optimising an assay to accurately detect and quantify the percentage of bacteria bound by an antibody in Chapter 4, the next step was to determine the binding capacity of recombinantly expressed TLRs. The first challenge was to adapt the assay to work with the new receptors.

5.3.1 Fc-tags present significant challenges when working with *S. aureus*

Based on the success of FcMBL (Kang, Super, et al. 2014; Bicart-See et al. 2016; Cartwright et al. 2016; Zupančič et al. 2021; Kang, Um, et al. 2015; Kang, Driscoll, et al. 2017), recombinantly expressed FcTLRs 2 and 4 were purchased as a starting point. An Fc-tag is a fairly substantial (~50 kDa) amino acid sequence derived from the Fc-domain of the immunoglobulin G (IgG) antibody. The gene sequence is ligated to the N-/C-terminus of a protein of interest during the cloning process and, once expressed, produces an Fc-chimeric fusion protein. There are a great many examples of how exploiting the high-affinity, reversible interaction between the heavy chain of the Fc-domain and protein A is used in biological research. For instance, protein A is used to fill a purification column, the protein of interest can be purified from the supernatant of the expression system.

Initial results looked promising and showed a dose-depending response toward the percentage of bound bacteria on increasing the concentration of receptor however, we observed higher binding to the secondary antibody alone which suggested the TLRs were not doing anything (Figure 5.2). Direct labelling of FcTLRs to avoid the need for the secondary antibody did not help, suggesting the problem lay in the Fc-tag (Figure 5.3). Interestingly, *E. coli* and *S. aureus* behaved very differently, measurements suggested any receptor with an Fc-tag bound *S. aureus* with an affinity >70% whereas *E. coli* only bound a maximum of 30% of bacteria.

The high affinity interaction we observed between *S. aureus* and the Fc-tag is almost certainly due to the presence of Staphylococcal protein A (SpA) on the surface of the pathogen (Bouvet 1994). Francois *et al.,* demonstrated the intentional use of anti-SpA-coated magnetic beads for the separation of methicillin-resistant *S. aureus* (MRSA) from clinical samples (Francois et al. 2003). However, in other contexts, SpA is reported to present significant challenges when developing flow cytometry assay for the detection of bacteria (Moor et al. 2016). One way to circumvent the issues with Fc-tags would be to try an alternative Gram-positive pathogen which

does not express SpA; *e.g. Pseudomonas aeruginosa.* In these preliminary assays, we have however been limited to testing strains of bacteria expressing GFP.

The Fc-tag has not been an issue for Ingber *et al.*, when trying to capture *S. aureus* (Kang, Um, et al. 2015). One possible explanation for this is in these studies, the Fc-tag was used for immobilising the protein on to magnetic beads or in hollow fibres and the protein would therefore contribute to blocking of the Fc region. In our tests however, blocking with BSA was not sufficient to abrogate Fc-binding. In one study, an additional boost in capture efficiency caused by an Fc:SpA was described as a bonus (Bicart-See et al. 2016).

5.3.2 TLR2 holds promise for detecting *S. aureus* in PBS and whole blood

We found that if receptors lacking an Fc-tag were used, a true dose-dependent interaction could be seen for TLR2 binding to *S. aureus,* resulting in a capture efficiency of up to 90%. Notably, the negative control (MD2) bound less than 20% of bacteria (Figure 5.4). Moving on to *S. aureus*-spiked whole blood, several changes to the gating strategy were required due to the complexity of the sample, in order to gate populations of bacteria and host cells (Figure 5.7. Under the same conditions as the tests done in PBS (10^7 CFU/ml bacteria, 2 µg/ml receptor), the percentage of bound bacteria decreased significantly (4-7% for TLR2 and 4, respectively) Figure 5.9).

One possible explanation for this may be down to the simple reason that if a 1 ml sample of whole blood is spiked with $1x10^7$ CFU bacteria (in line with previous experiments to mimic a positive blood culture sample), only 0.17% of the cells in the sample will be bacteria. In addition, approximately 25% of acquired events are discarded as debris or poor-quality images. This means that when acquiring a sample of 100,000 events on the ImageStream, the theoretical maximum number of bacteria which could be detected would only be ~13,000 (we detected just over 6000 which is approximately half of the theoretical maximum number of detectable bacteria present in the sample). Removal of the Fc-tag means that detection using a fluorescent secondary antibody was no longer possible and an alternative labelling

strategy was needed. A method to label free primary amine groups on lysine residues facilitated direct conjugation of the fluorophore (AF647) to the TLRs. This method produced good results, however presented one major limitation: the exceptionally poor yield of protein produced by the NHS-EDC fluorophore labelling kit. Indeed, with a 50 µg vial of lyophilised protein resuspended at 1 mg/ml, less than 8% of the starting concentration could be retained which presents a considerable time and cost limitation on the method (Appendix Figure C.5).

There is therefore a need for increased sensitivity. To address this, we briefly explored an alternative labelling strategy. Quantum Dots (QDs) are nanocrystalline semiconductors which display ~100-fold brighter photoluminescence than conventional fluorophores, making them ideal for the fluorescent detection of rare cells. Irrespective of their emission, QDs have a broad excitation band ranging from <300-450 nm and a narrow, intense emission band specific to their respective size (typically 30-100 nm in diameter) which lends them well to multiplexing applications (Algar 2020). Commercial CdSe/ZnS core-shell QDs were prepared by colleagues in the School of Chemistry. They were modified with glutathione (GSH) for aqueous solubility and facilitated direct self-assembly of his-tagged recombinant proteins onto ZnS (Zn^{2+}) shells (Figure 5.1E). TLRs 2 and 4, in addition to LPS-binding protein (LBP), were self-assembled on the nanoparticle surface *via* his-tag ligating metal ions at the QD interface. Successful conjugation and the optimal ratio of QD to receptor was confirmed by electromobility shift assay (EMSA) (data not shown). Unlike AF647, free-QDs are bright enough to be detected on the ImageStream even if they are not bound to bacteria. On a density plot of SSC, these free-QDs produce a second peak at zero, and therefore needed to be gated out so as not to skew the distribution. Singlets in focus are gated according to automated thresholds set on ±1 standard deviation of the mode of the Gradient RMS and Area values from brightfield images (Appendix Figure C.6), as in the previous experiments. Once more, intensity profiles of bacteria without QD:TLRs are then used to set a threshold based on 99.865% of data points (Appendix Figure **??**C.7). QDs were

tested using IFC and GFP-expressing bacteria. QD_{630}-labelled TLR2 (2 µg/ml) was used to stain 100 µl of *S. aureus* (10^8 CFU/ml).

Results showed that the percentage of positive cells was in fact lower than previous tests with AF647-labelled TLR2 (67.7 ± 12.7%), however the advantage of using QDs is that during the conjugation process, unbound QD is not washed away and no TLR is lost in the process. Once conjugated, the TLR:QD (His10:NTA) interaction should remain stable during storage. In spite of the lower percentage of bound bacteria, QDs therefore offer an indirect advantage over the AF647-labelling kit. Furthermore, binding of free-QDs and QDs conjugated to LPS-binding protein (QD:LBP) was found to be comparable; 22.3 ± 1.7% and 24.5 ± 2.4 %, respectively (Appendix Figure C.8). Taken together, this indicates an increase of 45% of bound bacteria was down solely to QD:TLR2. Further optimisation with QDs is clearly necessary, however the tests carried out here were done right at the very end of the project and so there was not enough time to do more experiments.

5.3.3 TLR4 remains challenging

Clues to successfully recapitulating the function of TLR4 in vitro may lie in the assembly of the LPS binding complex. TLR4 has proven challenging and the addition of MD2, a cofactor which is reported to be essential for TLR4-mediated LPS detection *in vivo* (Viriyakosol et al. 2001), offers no improvement in the context of this assay to detect *E. coli*. The Birss group were able to demonstrate successful detection of Gram-negative bacteria using a combination of TLR4 and MD2 using an ESI-based biosensor (Mayall, Renaud-Young, Chan, et al. 2017; Mayall, Renaud-Young, Gawron, et al. 2019).

The TLR4-MD2 complex used in both studies appears to be a simple mix of the two proteins, and so the dimerisation process is likely to take place on interaction with LPS. This is supported by (Mayall, Renaud-Young, Chan, et al. 2017) who reported a logarithmically proportional resistance to charge transfer which provides evidence for ligand-induced homodimerisation by the TLR4-MD2 complex. They stress the importance of controlling the orientation of the receptors by immobilising

them on the electrode which is not something we can control for with free receptor in solution. From the data presented, it is not clear if the device is capable of detecting LPS which has been shed by the pathogen. This could explain the signal for samples at a concentration of $<10^0$ cells/ml. Additionally, in our experience, the concentration of heat-killed pathogens, often purchased to circumvent the need for access to a Cat2 laboratory, quoted by the manufacturer is not particularly reliable and differs substantially between different strains (data not shown).

5.3.4 TLRs may bind to neutrophils and monocytes

Initially, the decision to pursue the pathogen:receptor characterisation with the ImageStream was motivated by practical reasons: namely the availability of the machine during COVID lockdowns. The properties of the CCD sensor made the ImageStream suitable for detecting small particles, and while the goal was to quantify TLR:pathogen binding in PBS, the gating strategy developed in Chapter 4 was sufficient to accomplish this. However, when we began to test the binding capacity of TLRs to bacteria in blood, the limitation to my method became clear: setting a 1-dimensional threshold on AF647 fluorescence intensity could not reliably distinguish between bacteria which were bound to morphologically complex eukaryotic cells. Our data showed TLRs 2 and 4 are expressed *in vivo* on the surface of granulocytes (99% neutrophils) and monocytes (Akira and Takeda 2004). Data presented here tentatively suggests that the recombinant TLRs we are incubating with samples of RBC-lysed blood (containing WBCs) are binding to neutrophils and dead cells (Figure 5.12) with high affinity (Figure 5.11f). At this stage however, it is still not possible to say with certainty that this is the case as the ImageStream stopped working during the final months of the project.

Although the initial aim was to export pre-selected feature data into R for processing, the IDEAS software package has many useful features for image analysis. Masking/segmentation is the process of defining a region of interest based on image properties. Information (*i.e.* "features") are then extracted from the pixels within the mask. The default mask in IDEAS simply defines the outline of the

cell, however this needs to be fine-tuned (dilated or eroded) to more accurately define the region of interest. Multiple masks can be combinatorially applied to each image to increase the complexity of the gate.

The pixels within the mask are then translated' into 'features:' quantitative measures of morphological parameters such as area, aspect ration, focus (gradient RMS intensity) which were explored in Chapter 4. These features can be used to define subsequent masks or then can be extracted to describe, distinguish, or analyse different elements within the population. In total, 84 features can be extracted per channel and these are split into 5 main categories:

- Intensity features (mean intensity, total intensity, max/min pixel intensity, standard deviation, range, spot intensity, threshold features *etc.*)
- Shape features (area, perimeter, aspect ratio, circularity/eccentricity, major/minor axis length, elongation *etc.*)
- Texture features (contrast, correlation, entropy (randomness of pixel distribution), homogeneity (measure of closeness in pixel distribution), energy (sum of squared pixel intensities)
- Positional features (centroid X and Y coordinates, distance to centroid, radial distance, angle (between different masks/features))
- Colocalisation features (bright detail colocalisation, Pearson's correlation between two channels, Manders' coefficient (proportion of signal overlap), spot count)

Single bacteria can be gated on using SSC and Area, as showing in Figure 5.7C, however in RBC-lysed blood it was not possible to isolate the same population of free bacteria. There appear to be two reasons for this: a significant proportion of bacteria seem to be interacting with leukocytes (Figure 5.8F) and the default masks applied to images underestimates the area of dead leukocytes leading them to appear in the bacteria gate (Appendix Figure C.3). By including a gate on

GFP (Appendix Figure C.4) we highlighted the small number of free bacteria remaining in the sample of leukocytes. It is entirely likely that the interaction between recombinant TLRs and host cells is quenching the pool of TLRs and limiting how many are available to the bacteria which are smaller and therefore have fewer binding sites. This prompts the following question: Is TLR interacting directly with the neutrophils or with bacteria which are then being phagocytosed? Figure 5.12C shows highly granular cells with a strong TLR2 signal (red), some of which appear to have engulfed GFP *S. aureus*.

By improving our gating strategy, masking and feature extraction, ImageStream may be able to shed light on these outstanding questions. Many of the neutrophils in Figure 5.12C appear very aspherical which may be a sign of apoptosis. By including a live/dead stain and setting a threshold on the eccentricity (circularity), we could exclude unhealthy cells from the analysis. Multiple groups have demonstrated how to quantify the proportion of pathogens which have been internalised by a cell (Ploppa et al. 2011; Phanse et al. 2012; Haridas et al. 2017; Botha et al. 2021). In brief, an internal mask can be created based on an eroded default BF area mask. The spot mask can then be used within the internal mask to define bacteria based on the following criteria: any particles with a green signal less than 3 pixels square, a spot to background intensity of 7.5 or greater and an area greater than 2 pixels. The spot count feature can then be used to define the number of bacteria per cell (Adapted from (Ploppa et al. 2011)). Furthermore, it would be interesting to determine the correlation between eccentricity (a marker of apoptosis) and number of internalised GFP bacteria and to calculate the number of healthy neutrophils which are TLR+ but GPF-. Alternatively, colocalisation of the GFP and TLR signals may shed light onto the interaction between recombinant TLRs and host cells. A sample of PBMCs could also be stained for common leukocyte markers (CD14, CD15, CD19, CD3 and CD45) followed by staining with anti-TLRs and then AF647-labelled recombinant TLRs in order to fully illuminate the identity of the WBC subtype, the expression level of each TLR and whether there is colocalised binding with recombinant TLR.

5.3.5 Conclusion

TLRs have the potential to bind a great many PAMPs, like MBL, however have the potential to confer diagnostically relevant information such as Gram-status through multiplexing. Optimisation of the assay developed in Chapter 4 through a series of different labelling strategies and ultimately showed that TLR2 could bind over 90% of *S. aureus* in PBS. The binding performance dropped substantially in whole blood which may be due to recombinant TLRs dimerising with host receptors on neutrophils and monocytes, or DAMPs on cells undergoing apoptosis. This remains to be confirmed, however, and requires further investigation to determine the diagnostic relevance of such interactions.

Receptors which bind whole cells, such as TLR2 and 4, reach their limitation if a patient has been treated with bacteriolytic antibiotics, since in this case there will be no sign of the whole, intact pathogen. TLR9, an endosomal receptor from the same family, binds to non-methylated CpG DNA – a motif which is much more common in prokaryotes, will be investigated in the final results chapter for its ability to detect and distinguish pathogen DNA from host.

6

Chapter 6: Detection of pathogen DNA using TLR9

6.1 Introduction

TLRs are a family of PRRs which play a vital role in detecting various molecular components of pathogens. In chapters 4, and 5, we developed an assay to measure how well recombinantly expressed TLR2 and 4 detect whole bacteria in blood. In this chapter, we will investigate TLR9's ability to detect pathogen DNA.

6.1.1 Clinical importance of DNA detection in sepsis diagnostics

Although different approaches are available in clinical settings for pathogen identification and antibiotic susceptibility testing, the reliance on blood culture clearly impedes rapid diagnostics (Reddy et al. 2018; Seymour et al. 2017). Many antibiotics work by disrupting the integrity or synthesis of the bacterial cell wall, resulting in lysis (Zhang, Yan, et al. 2021; Yeaman and Yount 2003; Blaskovich et al. 2017). Lysed pathogens can no longer be cultured and so in many cases, early treatment with broad spectrum antibiotics prior to a blood sample being taken for culture can significantly inhibit pathogen identification and prevent the patient being moved on

to specific antimicrobial therapy with less severe side effects (Kapoor et al. 2017). Under these circumstances, detection of pathogen genetic material may be the key to overcoming such diagnostic limitations.

Indeed, some products have been commercialised to perform diagnosis directly from whole blood, such as PlexID, MagicPlex, SepsiTest, SeptiFast and VYOO. Most of these are based on polymerase chain reaction (PCR) to amplify pathogen specific fragments of DNA and are shown to be sensitive enough to detect genetic material at the concentrations typically measured in whole blood ($10^{3\text{-}4}$ genome copies/ml(Opota, Jaton, et al. 2015). The BioFire Film Array is a commercially available system for multiplexed PCR made by Biomerieux. The proprietary cartridge-based sepsis panel has the capacity to detect 43 targets; including Gram-positive and Gram-negative bacteria, fungi and 10 AMR genes (Messacar et al. 2017; Banerjee et al. 2015). PCR unlocks the diagnostic potential of cell-free DNA (cfDNA) found in blood plasma; however it is ultimately reliant on designing primers specific to known targets. If the pathogen is rare or unknown, then it will be missed.

The sequencing of blood stream infection causing pathogens has emerged as a diagnostic tool that avoids the need of blood culture. As an example, a US-based company called KARIUS has recently developed an infrastructure which employs next-generation sequencing (NGS) to identify and quantify microbial cfDNA. On receipt, samples (4ml blood plasma sent in the post at room temperature) are spiked with a known concentration of control DNA which is later used for signal calibration and contamination control. cfDNA is extracted from blood using a magnetic bead-based DNA enrichment kit before automated library preparation takes place. Samples are then subjected to single-end 75-base sequencing on the Illumina NextSeq500. This method is highly sensitive, with a limit of detection of 33-74 molecules of DNA/µl and specific with results showing a 93.7% agreement with blood culture. It was shown that 85% of results were returned the day after sample receipt. A 53 hour turnaround time to obtain a species-level identification is significantly shorter than the 92 hours achieved by conventional methods (Blauwkamp et al. 2019). Although promising, time to diagnostics for patients with sepsis is still

too long. The sample preparation for such approaches is based on bulk cfDNA separation. This means, due to the very high concentration of human DNA measured in plasma (0.1-10 µg/ml (Blauwkamp et al. 2019)), there is a lot of "noise" also causing further delays in diagnostics. Moreover, any pathogen DNA not found in the plasma will be missed. Although clinical sequencing on this sort of scale has come down in price significantly over the past few years, it is not yet cost-effective on a global scale and not widely available outside of the USA. One possibility to improve this technology would be to offer an alternative method of sample preparation to first remove the abundance of host genetic material, either by selective lysis or direct selection of pathogen DNA.

6.1.2 Novel approaches to sample preparation for pathogen DNA detection in blood

As we have discussed in Chapter 3, selective lysis (SL) is a method used to lyse and remove host cells from a sample to leave intact bacteria for downstream identification using PCR. We demonstrated that SL causes significant damage to the viability of the bacteria and it was disregarded for pathogen ID using MALDI-TOF MS. In this chapter we will focus on alternative methods for DNA enrichment.

6.1.2.1 Indirect pathogen enrichment through selective lysis of host cells

MolYsis (MolZym) is a commercially available kit which uses chaotropic buffers to selectively lyse blood cells. The exposed human DNA is then immediately degraded by DNases. Intact pathogens are removed from the lysate and subsequently lysed by muralytic enzymes to expose their DNA which can then be purified using a column (Wiesinger-Mayr et al. 2011). A recent study investigated pathogen recovery of sonicated fluids from prosthetic joint infection (PJI) samples with a bacterial load of >10 CFU/ml (n=4). Enrichment was measured using metagenomic sequencing (Illumina HiSeq) with and without treatment with the MolYsis kit. Results show that MolYsis treatment resulted in 7.0-59.4% of reads mapping to the known pathogen, representing a 481- to 9580-fold increase compared to an

unenriched sample. Importantly, this is sufficient to carry out genotypic AST analysis, virulence prediction or strain-typing (Thoendel et al. 2016). This success was recapitulated in spiked whole blood samples by (Wiesinger-Mayr et al. 2011), where a LoD of 10-10^3 CFU/ml as measured by PCR and gel electrophoresis followed by microarray hybridisation. However, the process takes 3 hours before access to enriched pathogens, which in some cases might still be too long (McCann and Jordan 2014). Several new, "in-house" methods are proposed in the literature to reduce time and cost.

In a preliminary study conducted on sputum samples from patients suffering from lower respiratory infections, 2.2% v/v saponin was used for selective lysis of human cells before bacterial DNA was extracted according to an automated protocol and enriched samples are sequenced using MINion (Oxford Nanopore Technologies). Enrichment offered 96.6% sensitivity and 41.7% specificity for pathogen detection compared with culture and, once combined with qPCR, both increased to 100% (n=40) (Charalampous et al. 2019). The key advantage to this procedure is the 6 hour turnaround time from sample to result and, although hospitals in the UK are not equipped with MINion, an alternative, available sequencing approach could be substituted (*e.g.* HiSeq). However, while the LoD of $10^{3\text{-}5}$ CFU/ml is within the clinical range of culture-based respiratory samples, it is $10^{2\text{-}3}$-fold too high for whole blood samples and so culture step would also be necessary.

In the work of (Machen et al. 2014), a mild, non-ionic detergent at an alkaline pH is used on a positive blood culture sample to selectively lyse human cells. The sample is syringed through a 0.45 µm filter to capture intact pathogens, which are then washed. A scraping is taken and loaded directly onto a slide for identification using VITEK MALDI-TOF MS and AST using the VITEK 2 achieving 94% (n=100) identity and 93.5% (n=1012) category agreement with conventional clinical methods, respectively. Critically, this was achieved in 11.4 hours compared to 56.3 hours using traditional methods. One limitation to this study could be the syringe filtration step which is particularly labour intensive and low throughput in terms of sample

number; this is not the case in the MCLB method of selective lysis which relies on centrifugation to pellet un-lysed cells and DNA.

Although the methods outlined above are promising, there are multiple limitations to the removal of human material to concentrate pathogens. Most notably is the simultaneous disposal of cfDNA which is discarded along with the human lysate, and upon which tests like KARIUS are based. For the same reason, patients who have received antibiotic therapy would be ruled out as candidates for selective lysis as only viable, intact pathogen cells are retained. Finally, the stringency with which human DNA is removed is a delicate balance: too harsh and the buffers will also lyse the cell walls of weaker bacteria, too mild and the remaining human material may serve as a contaminant in subsequent downstream processing steps. Moreover, the efficacy of the lysis buffer is time-dependent, which may create problems in terms limits batch size and scalability.

6.1.2.2 Direct enrichment of pathogen DNA using novel recombinant receptors

Several approaches take advantage of the differences between pathogen and human DNA methylation. Indeed, approximately 75% of CpG motifs are methylated in bacteria (Tost 2010), a characteristic which has been exploited for separation purposes.

The Looxster DNA enrichment kit (SIRS-lab GmbH, Jena, Germany) is a magnetic bead separation kit. Complete cell lysis is followed by DNA extraction and purification. Pathogen DNA is then bound to a column functionalised with the methyl-sensitive human CXXC finger protein 1 (CFP1). The column is washed and finally the pathogen DNA is eluted. In a study comparing several commercially available pathogen isolation kits, Looxster was shown to contain the highest amount of contaminating human DNA attributed to its large initial sample volume (5 ml) and required time to result (7 hours). Nevertheless, it was one of the most sensitive with a LOD of 100 CFU/ml for *Pseudomonas aeruginosa* and the most reproducible

(Wiesinger-Mayr et al. 2011). Despite its strong performance the kit was discontinued by the manufacturer in 2019.

The methyl-binding domain (MDB) receptor binds methylated CpG motifs characteristic of human DNA. This can be fused to an Fc tag which allows the receptor to be coated onto Protein A magnetic beads to enrich human DNA. Sequencing analysis of mock Malaria samples resulted in an 8-fold increase in human reads (Feehery et al. 2013). The receptor is used in a commercialised kit called the NEBNext Microbiome Enrichment Kit (New England Biolabs). However, <1% of bacterial DNA was recovered from clinical PJI samples (n=4) assessed by NGS (Thoendel et al. 2016). To our knowledge, this kit has not yet been tested for the enrichment of bacterial DNA from patient blood samples. Magnetic bead separation using a methyl-sensitive restriction enzyme *HpaII* has successfully been used for sequencing, offering a 100-fold enrichment. However, it has not been used with whole blood samples and nor is it available commercially (Liu et al. 2016).

6.1.3 TLRs for detection of pathogen DNA

There are four TLRs which detect pathogen genetic material in humans: TLR3 senses viral dsRNA, TLRs 7 and 8 both bind viral ssRNA but differ in their ligand specificities, cellular expression profiles and signalling pathways in order to confer individual roles in the immune response. Lastly, TLR9 binds to non-methylated CpG DNA (Mogensen 2009). From a diagnostic perspective, the nucleic acid-sensing TLRs remain under-explored. Only TLR3 has been tested as a biosensor using poly(I:C); a molecular mimic for viral dsRNA (Amini et al. 2014).

TLRs 3, 7, 8, and 9 are all endosomal receptors, meaning unlike cell surface receptors (*e.g.* TLR2/4) which encounter whole cells, they are typically exposed to short nucleic acid fragments from pathogens which have been endo-/phagocytosed. Nucleic acid sensing TLRs are translated in the endoplasmic reticulum (ER) and trafficked to the endosome. TLR9 is then endocytosed and trafficked from the plasma membrane to the endosome where it meets ssDNA which has been internalised and fragmented during phagocytosis (Latz et al. 2004; Wagner 2004). Some studies

have reported that DNaseII treatment is required to generate TLR9 ligands which result in downstream signalling (Pawaria, Moody, Busto, Nündel, Choi, et al. 2015; Pawaria, Moody, Busto, Nündel, Baum, et al. 2015; Chan et al. 2015a). The distinction between self and non-self nucleic acids is crucial as misrecognition of the host's own nucleic acids can result in autoimmune diseases such as psoriasis or systemic lupus erythematosus (SLE) (Fillatreau et al. 2021). This distinction does not rely solely on the recognition of specific foreign molecular characteristics by the TLRs themselves, but several regulatory mechanisms which make a concerted effort to reduce the likelihood of a TLR encountering a self nucleic acid. This 'regulatory redundancy' is conferred by receptor compartmentalisation, expression, ligand availability and signal transduction (Lind et al. 2022).

TLR9 was first reported to produce a Th1-mediated immune response to non-methylated CpG DNA over 20 years ago (Hemmi et al. 2000). Its structure, conserved across the whole family of TLRs, resembles a question mark. The outer horseshoe comprises of a series of 25 leucine-rich repeats (LRRs) which are responsible for the interaction with CpG DNA (Pan et al. 2012). The first crystal structure of the C-terminal domain (CTD) was produced by Collins and Wilson who suggested the TLR9-CTD was capable of binding and signalling by itself and that the dimer is not physiologically relevant (Collins and Wilson 2014). Later evidence was presented to the contrary when TLR9, co-crystallised with stimulatory CpG DNA, formed a symmetric TLR9–CpG-DNA dimer with the DNA bound vertically at the interface between the two subunits. When co-crystallised with non-stimulatory CpG DNA, TLR9 remained as a monomer (Ohto, Shibata, et al. 2015). More recently, crystal structure data has identified a second DNA binding site which interacts with cytosine *via* a 5'-xCx motif. It was reported that cooperative binding of DNA to both sites promotes dimerisation and activation (Ohto, Ishida, et al. 2018). Pohar *et al.,* determined the minimal sequence requirements of CpG DNA comprised of two cytidine-guanosine (CG) dinucleotide motifs separated by 6-10 nt (Pohar et al. 2015). The first CG motif is directly preceded by a 5'-thymidine and there is an elongated poly-thymidine tail at the 3' end of the molecule. Sensitivity

was lost if ODNs were shorter than 21 nt with an adenosine immediately adjacent to the CG motif. In order to elicit a controlled immune response in vivo, synthetic CpG oligodinucleotides (ODNs) are used and, depending on the type of response required, different classes of ODN can be used. Class A CpG ODNs have a phosphodiester central CpG-containing motif and a phosphorothioate 3'-poly-guanosine tail in order to induce production of IFN-α in the absence of TLR9-dependent NFκB signalling (Krug et al. 2001). Surface plasmon resonance (SPR) of an Fc-TLR9 fusion protein revealed pH-dependent, direct CpG-sequence-dependent binding. Methylation of cytosine resulted in a weaker interaction and increased dissociation whereas non-methylated CpG DNA bound much more strongly and dissociated much less, with a binding affinity K_D of 200 nm (Rutz et al. 2004).

The aim of this chapter is to obtain proof of principle data that shows whether or not recombinant TLR9 can distinguish between bacterial DNA and human DNA based solely on the methylation status of CpG *in vitro*, and to ultimately determine whether the receptor has the potential to be used to detect pathogen DNA in the sepsis diagnostic workflow we have investigated in Chapter 3.

6.2 Results

6.2.1 Analysis of the crystal structure of TLR9 suggests AF647 may block its interaction with CpG DNA

Microscale thermophoresis (MST) is a biophysical technique used for measuring protein:protein or protein:DNA interactions to determine their binding affinity and stoichiometry. Fluorescently labelled proteins are excited using two lasers: one fluorescent laser and another infra-red laser to induce a small temperature change within the capillary. The equipment measures the temperature induced fluorescence change (TRIC), an inherent property of fluorophores, and the movement of particles in response to changes in temperature *i.e. thermophoresis.* The MST signal is a combination of these two quantifiable properties which change as a function of the protein microenvironment; this is determined by the amount of bound *vs.* unbound

ligand, in addition to the hydration shell. The MST signal is compared across a concentration gradient of the unlabelled ligand and used to plot a Langmuir binding isotherm (1/MST *vs.* concentration), the gradient of which can used to determine the binding affinity (K_D) (Kastritis and Bonvin 2013; Müller and Westerlund 2017).

The signal:noise ratio of high DNA:low DNA in this sample is used to indicate if the is any measurable binding between the protein of interest and ligand.

Preliminary controls indicated that labelled TLR9 did not aggregate or over-adsorb to the walls of the glass capillary, and the measured fluorescence was within a detectable range. Next, a test was carried out which involves comparing two samples; both contained fixed concentrations of TLR9, one measured the MST signal from trace amounts of CpG DNA to get a baseline for non-specific binding. The other one measures MST signal when a much higher concentration of CpG DNA (20 nM) is added. Several different buffer conditions were tested in order to improve the signal:noise ratio (high DNA:low DNA). The concentration of detergent (Tween20) was increased to try to lower non-specific binding in the 'trace DNA control'. The pH was lowered from pH 7.2 (PBS) to pH 6.0 to mimic the acidic conditions of the endosome (Rutz et al. 2004). This decision was supported by Amini *et al.*, who concluded that any signal detected by TLR3 at pH 7.0 could be attributed to non-specific binding (Amini et al. 2014). Only when they increased the acidity of their binding conditions did they observe a linear signal with their dsRNA biosensor. In spite of these adjustments there was no measurable difference between the samples, the signal:noise ratio was significantly different enough to confirm successful binding between TLR9 and CpG DNA (data not shown).

MST may have been unsuccessful due to the labelling strategy used. NHS-EDC chemistry conjugates a fluorophore, in this case AF647, to the free primary amine groups of lysine residues *via* its succinimidyl NHS ester moiety. Labelling efficiency, and more importantly, retention of the function of the protein, is therefore dependent on the number, steric exposure and location of these free primary amine groups. To probe this further, the crystal structure of TLR9 was downloaded from the Protein Database (PDB) and examined using PyMOL, a piece of 3D modelling software

which allows proteins to be coloured by monomer, chain, amino acid, functional group or atom. Proteins are often co-crystallised bound to their ligand (either natural or synthetic). Physical distances between atoms can then be measured in Angstroms (1 Å= 10^{-10} m = 0.1 nm) to determine whether the addition of a fluorophore would be possible and if so, whether it would sterically inhibit the interaction with a ligand, cofactor or another monomer.

The crystal structure of TLR9 homodimer (Ohto, Ishida, et al. 2018) can be seen in Figure 6.1 wherein each of the ring-/horseshoe-shaped TLR9 monomers were coloured in green and teal with the single-stranded CpG DNA ligand depicted as an orange surface. Figure 6.1 A and B show a top-down and side-view of the complex, respectively, and illustrate how two fragments of single-stranded CpG DNA bind at the interface between the two TLR9 monomers. Figure 6.1 C-F show examples of active site lysine residues (pink) and their proximity to CpG motifs on the fragment of DNA (dark red). Taken together, these images show there are indeed several lysine residues found within the active site of TLR9 and their distances to CpG DNA range from 5-7 Å. The helical width of double-stranded DNA is ~20 Å(Ussery 2002), meaning the width of the single-stranded CpG ligand is ~10 Å. AF647 is estimated to be ~30 Å(~1.5 Åper C-C double bond, ~21 atoms across at its widest point) and is therefore likely to sterically hinder the binding of CpG DNA and the subsequent dimerisation of a second TLR9 monomer.

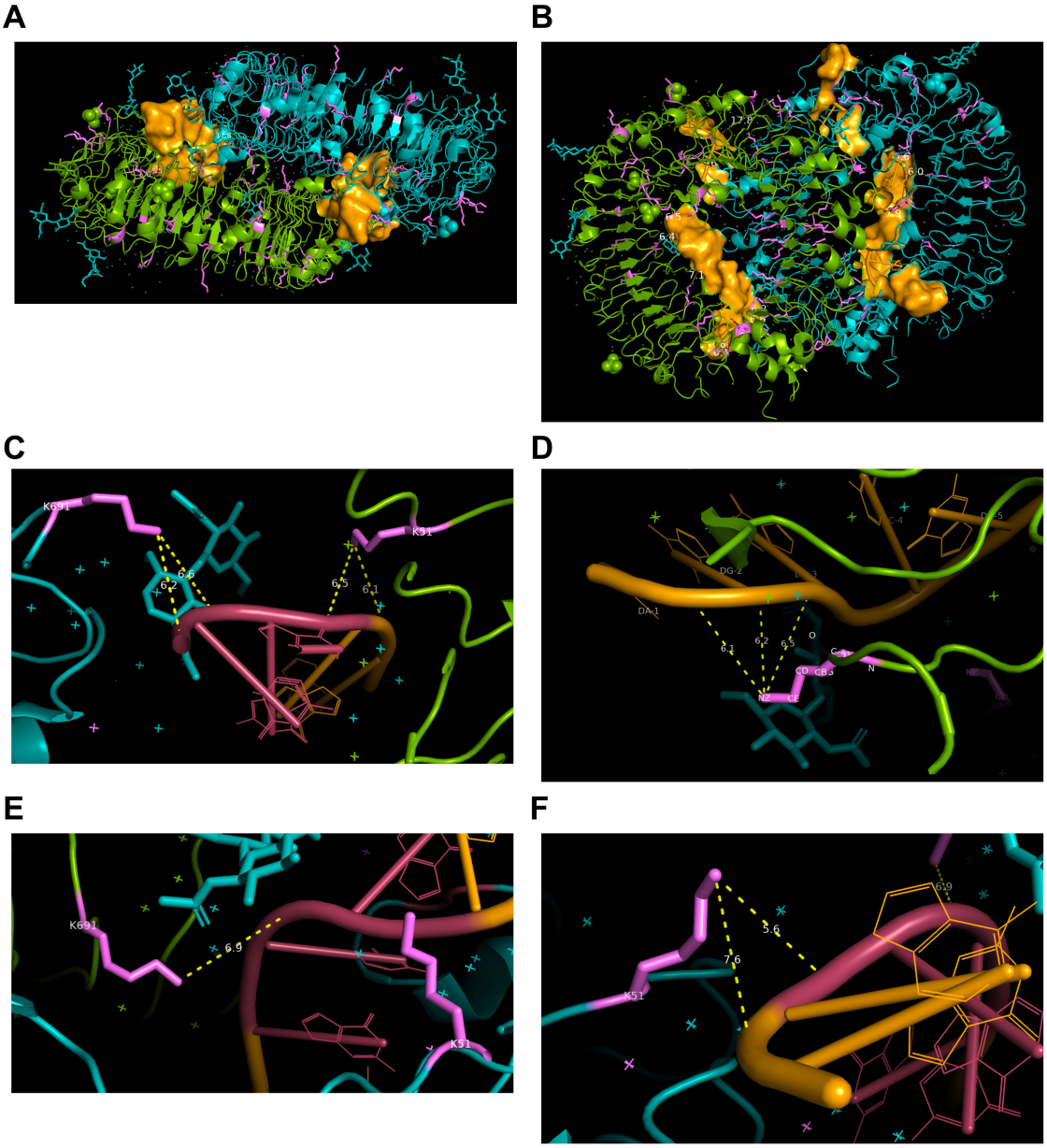

Figure 6.1: Crystal structure of TLR9 reveals multiple lysine residues in the active site. Top **(a)** and side-view **(b)** of mouse TLR9 homodimer TLR9 monomer A; green, TLR9 monomer B; teal) bound to single-stranded CpG DNA (orange surface). Multiple lysine residues (pink) can be seen within 7 Åof the CpG DNA ligand (dark red). Dashed yellow lines represent distances between lysine residues, annotated in white. **(c-f)**. PDB: 5zln, images generated using The PyMOL Molecular Graphics System, version 2.5.2, Schrodinger, LLC.

For comparison, the same process was carried out for TLR2 (Appendix Figure D.1), for which we have been able to demonstrate successful binding to *S. aureus* after labelling with the same strategy in Chapter 5. In contrast to TLR9, TLR2 (teal or green) can also form a heterodimer with TLR1 (Appendix Figure D.1A, B) or TLR6 (Appendix Figure D.1C, D) in order to bind tri-acylated lipopeptides (Gram-negative bacteria) or di-acylated lipopeptides (Gram-positive bacteria), respectively (Mogensen 2009; Koymans et al. 2015). Where two fragments of CpG DNA run through the entire TLR9 dimer, a single molecule (Pam3CSK4, Pam2CSK3 or lipoteichoic acid (LTA); orange) sits at the top where the two horseshoe-shaped monomers of the TLR2 binding complex overlap (Appendix Figure D.1 A, C). This is likely because TLR2 is expressed on the cell surface (Koymans et al. 2015) and its natural ligands are comparatively short, and are presented on the surface of bacteria. In fact, according to the three examples shown in Appendix Figure D.1, AF647 only comes within close proximity (5-9 Å) to a single lysine residue (Lys347). We can therefore conclude that while conjugation with AF647 may still affect dimerisation of TLR2, it is much less likely to affect ligand binding.

6.2.2 Immunomagnetic separation using FcTLR9-functionalised beads

Moving forward, an alternative detection strategy for TLR9-bound DNA was clearly needed. The initial plan was to continue a project to produce TLR9 in house. When I joined the group, the construct had been designed, cloned into *E. coli* and sequence-verified. Efforts were made to transfect the plasmid into mammalian HEK293T cells, then express and purify the protein. A small amount (20 µg) of pure protein was successfully purified and verified to be TLR9 using Western blot (data not shown). Cloning and expression is costly and time-consuming; in lieu of the COVID-19 pandemic, the decision was therefore taken to purchase recombinant TLRs from BioTechne which also opened up the possibility of working with TLRs 2 and 4.

Taking inspiration from the IFC assay developed for TLR2 and 4 (Chapters 4 and 5), FcTLR9 was attached to magnetic beads. Unlike in Chapter 5, there is

no issue using Fc-tagged proteins with DNA and this enables orientation-specific conjugation to protein A magnetic beads (2.8 µm, DynaBeads, Thermofisher). This would simultaneously give TLR9 enough mass to be detected in a cytometer while removing the need to directly label it with a fluorophore. The magnetic property of the beads facilitates easy wash steps and bound DNA can easily be detected using a commonly available fluorescent dye (*e.g.* DAPI (4',6-diamidino-2-phenylindole) or PI (propidium iodide)) (Figure 6.2).

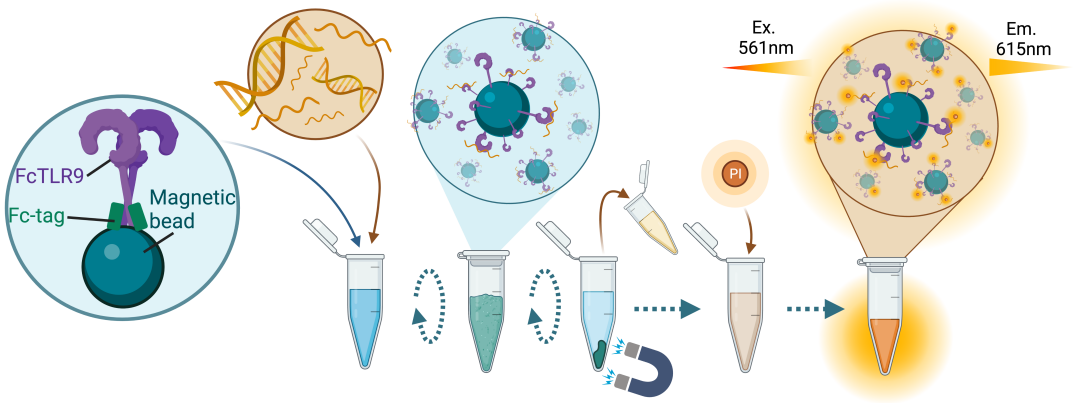

Figure 6.2: TLR9 labelling strategy and assay for detecting DNA using IFC. FcTLR9 (1 μg/sample) was conjugated to 10 μl Dynabeads (ThermoFisher Scientific) then mixed with DNA (CpG ODN, *E. coli, S. aureus* or human) in PBS (100 ng/sample) for 30 min on ice. Unbound DNA was washed off before bound DNA could be stained (with either DAPI or PI; 10 μl/sample). After 30 min incubation on ice, DNA fluorescence was measured using IFC.

6.2.2.1 TLR9-functionalised magnetic beads successfully bind CpG DNA

As a proof of principle, TLR9-functionalised magnetic beads were tested with CpG ODNs; short (24 nt), single-stranded sequences of non-methylated CpG DNA used to stimulate a TLR9-mediated immune response in *in vivo* experiments. To be sure that the fluorescent signal was coming from the TLR9-bound DNA, baseline fluorescence of a sample of unfunctionalised DynaBeads was measured first, then each element of the assay was added in succession and the mean fluorescence intensity of the bead population was measured using imaging flow cytometry.

Beads were selected based on side-scatter and the change in DNA (DAPI or PI) fluorescence intensity was measured.

Interestingly, DynaBeads have a much higher amount of native fluorescence than was expected when excited using the 405 nm laser (for DAPI excitation), this increases substantially if the 561 nm laser is used (for PI excitation) (Figure 6.3. The decision was taken to normalise mean fluorescence of each sample against that of the DynaBead control. Small changes in fluorescence intensity can then be seen on addition of the DNA, DNA and dye (DAPI), or TLR9 and dye, respectively. Results showed there was little change to the autofluorescence of the beads until they are functionalised with TLR9, incubated with DNA and stained, at which point the normalised mean fluorescence increases by approximately 2-fold (Figure 6.3A). The experiment was repeated using PI to stain the DNA which led to a substantial increase in overall fluorescence and a much greater difference between the test sample and controls (Figure 6.3B). PI was then used for all subsequent tests.

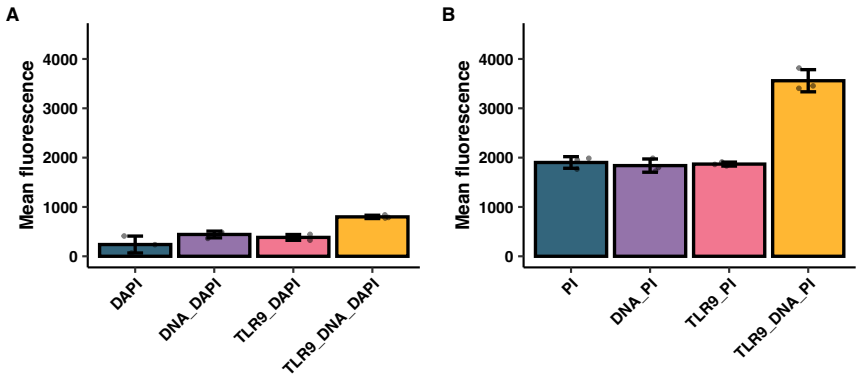

Figure 6.3: TLR9 successfully binds non-methylated CpG DNA. FcTLR9-functionalised protein A magnetic beads were mixed with 100 ng CpG DNA for 30 min. A comparison between DNA dyes; **(A)** DAPI and **(B)** PI. Fluorescence was measured using Imaging Flow Cytometry. Error bars represent standard error of the mean, n=3 technical replicates.

TLR9 is expressed intracellularly (Mogensen 2009; Akira and Takeda 2004). Therefore, it is likely to be exposed to short fragments of single-stranded DNA from engulfed bacteria, rather than long strands which are obtained directly after DNA extraction (Koymans et al. 2015). There is some amount of confusion in the

literature regarding whether TLR9 can physically bind to double stranded DNA as well. Total genomic DNA was extracted from overnight cultures of *E. coli* and *S. aureus* and sonicated to yield double stranded fragments of DNA <400 base pairs long; longer than the CpG ODN control DNA (24 nt) but shorter than whole genomic DNA (gDNA). The test was repeated with 100 ng double-stranded gDNA and stained with PI, which showed that it is possible to bind double-stranded *E. coli* DNA using TLR9-coated beads (Figure 6.4A). It was not possible, however, to detect double-stranded *S. aureus* DNA (Figure 6.4B); a possible explanation for this could be the variability between the GC content of the pathogen (Nishida 2013; Ngoi et al. 2021; Piovesan et al. 2019).

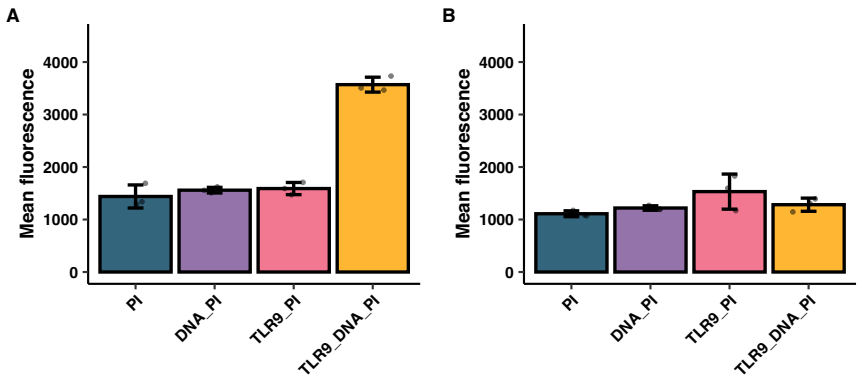

Figure 6.4: TLR9 successfully binds double-stranded pathogen DNA. FcTLR9-functionalised protein A magnetic beads were mixed with 100 ng DNA extracted from **(A)** *E. coli* and **(B)** *S. aureus* for 30 min. Fluorescence was measured using Imaging Flow Cytometry. Error bars represent standard error of the mean, n=3 technical replicates.

6.2.2.2 Recombinant TLR9 is not able to distinguish between pathogen and human DNA

Human DNA has a GC content of around 40.9%, however this is known to be highly variable (Piovesan et al. 2019; Kudla et al. 2006). To further probe the impact of GC content has on binding affinity, a control experiment was carried out to compare the measured fluorescence of human vs. pathogen DNA. Once more, 100 ng/sample DNA was tested with TLR9-coated magnetic beads. Results revealed increased binding to human DNA (Figure 6.5), comparable to *E. coli* and the CpG

ODN control, suggesting that GC content plays a greater role in binding capacity than expected and that the external portion of TLR9 alone is unable to distinguish between human and pathogen DNA based methylation status alone.

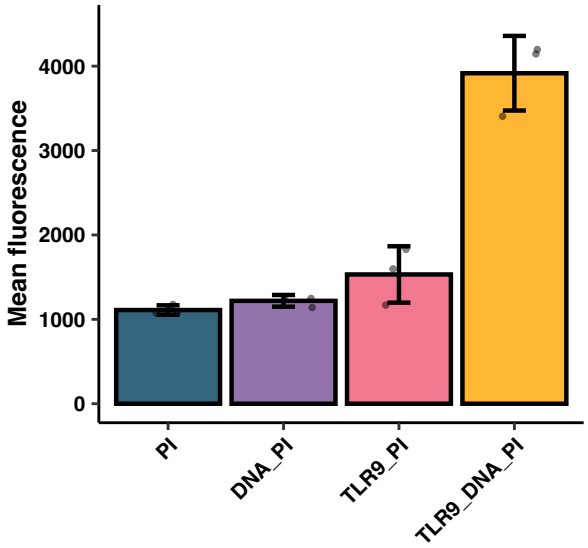

Figure 6.5: TLR9 appears to bind human DNA with a similar affinity to pathogen DNA. FcTLR9-functionalised protein A magnetic beads were mixed with 100 ng human DNA for 30 min. Fluorescence was measured using Imaging Flow Cytometry. Error bars represent standard error of the mean, n=3 technical replicates.

Finally, tests were carried out in whole blood, which was spiked with CpG ODN, *S. aureus* and *E. coli* DNA (100 ng/sample of each). Protein A is notoriously sticky and may bind a variety of undesirable substrates such as host antibodies which naturally have an Fc-region. To try to account for this, we included a blocking step with 3% BSA to coat any unbound Protein A on the surface of the beads followed by a single wash step to remove any non-specifically bound proteins. Here, there was no detectable increase in CpG ODN fluorescence on TLR9-functionalised beads compared to any of the controls (Figure 6.6A). Interestingly, TLR9-functionalised beads incubated in blood samples spiked with *E. coli* or *S. aureus* DNA showed a decrease in fluorescence signal compared to controls without the addition of pathogen DNA (Figure 6.6B). Based on the previous results, we would expect a high fluorescent signal from TLR9-functionalised beads stained with PI (*i.e.* no

additional pathogen DNA) if TLR9 could bind circulating-free host DNA present in the blood sample. Since we don't see any binding to this control, we can hypothesise that the beads may be binding non-specifically to something other than CpG DNA target in spite of the efforts to block.

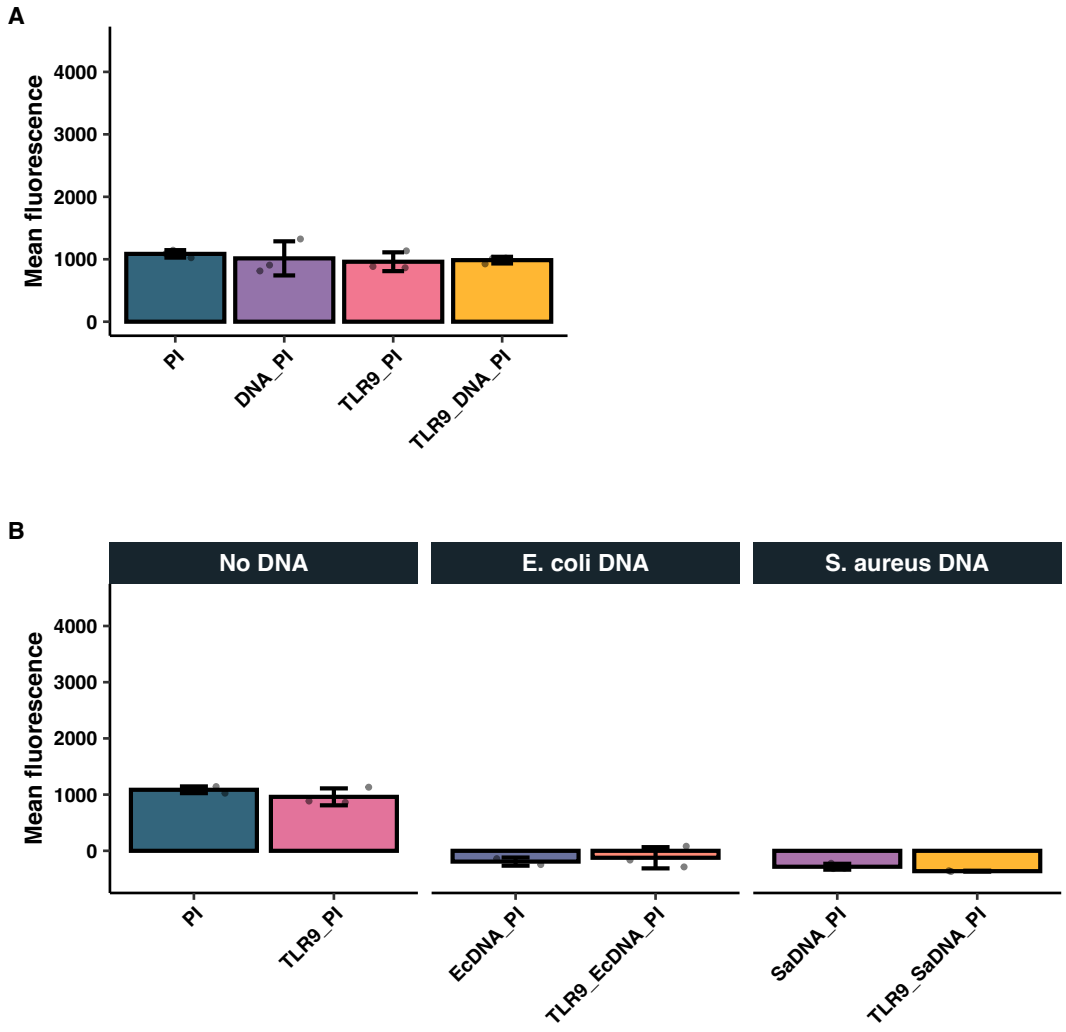

Figure 6.6: TLR9-functinalised beads do not bind microbial DNA in blood. (DNA 100 ng) was spiked in to 100 μl blood, FcTLR9-functionalised protein A magnetic beads were added and mixed for 30 min. **(A)** CpG ODN and **(B)** A comparison between *E. coli* and *S. aureus* DNA. Fluorescence was measured using Imaging Flow Cytometry. Error bars represent standard error of the mean, n=3 technical replicates.

6.3 Discussion

The clinical importance of DNA detection in sepsis diagnostics is significant because traditional methods, such as blood culture, have limitations in providing rapid and accurate results. Importantly, early treatment with muralytic antibiotics can prevent pathogen identification through blood culture (Kapoor et al. 2017). Up to 42% of sepsis cases are culture-negative; an unknown proportion of these could be of non-bacterial, possibly viral, origin (Lin, McGinley, et al. 2018). DNA detection methods, such as PCR (Wiesinger-Mayr et al. 2011; Machen et al. 2014) and sequencing (Charalampous et al. 2019; Feehery et al. 2013; Liu et al. 2016; Blauwkamp et al. 2019; Thoendel et al. 2016), offer faster and more sensitive detection of pathogens in sepsis (Goldenberg 2017), however not without their own limitations.

PCR-based methods amplify pathogen-specific DNA fragments. In spite of the clear advantages in specificity and speed, and recent advantages in panel size, PCR remains limited by the number of targets available per assay. Wilson *et al.,* reported that approximately 80% of culturable sepsis cases were caused by only 14 pathogens (Wilson et al. 2011) – well within the limit of a modern, commercially available PCR panel for sepsis diagnostics (*e.g.* <43 targets (Messacar et al. 2017; Banerjee et al. 2015)). However, the remaining 20% with unknown origin could be caused by an infeasibly high number of pathogen species. Successful pathogen ID through sequencing is not limited in such a way, however, it does face constraints in terms of cost and scalability of sequencing all DNA contained within a blood sample, including that belonging to the host which is in significant excess (~10^6-fold (Opota, Jaton, et al. 2015)). Sample preparation techniques, such as selective lysis (discussed extensively in Chapter 3) and direct enrichment of pathogen DNA, aim to improve the efficiency and sensitivity of DNA detection by separating the pathogens/pathogen genetic material from that of the host. TLR9 is a PRR which recognises non-methylated CpG DNA and plays a role in detecting pathogen genetic material as part of the innate immune response (Mogensen 2009; Akira and Takeda 2004). In this chapter, the suitability of recombinant TLR9

for direct enrichment of pathogen DNA was investigated using immunomagnetic separation and imaging flow cytometry.

6.3.1 Immunomagnetic separation of DNA by TLR9 was successfully quantified using IFC

Characterisation of a protein-DNA interaction such as TLR9-CpG DNA lends itself to many biochemical techniques. We used MST, a highly sensitive method of determining the K_D of an interaction using small quantities of protein (data not shown). A high degree of noise prevented MST from yielding any meaningful results and investigations into the 3D crystal structure of TLR9 in complex with CpG DNA revealed several free lysine residues in the TLR9 active site/dimerisation interface (figure 6.1). This led us to conclude that conjugation to the fluorophore, reliant on NHS/EDC chemistry to bind to the primary amine group of free lysine residues, likely blocked DNA from accessing the active site of TLR9. Taking inspiration from Chapters 3 and 4, an assay was designed to capture and enrich DNA using FcTLR9-coated magnetic beads and use IFC to compare the mean fluorescence intensity of a stained DNA (figure 6.2). For the first time, flow cytometry showed the successful immunomagnetic enrichment of CpG DNA by recombinant TLR9 at concentrations resembling a positive blood culture (100 ng = ~10^8 CFU; figure 6.3).

6.3.2 The ability of TLR9 to bind to DNA is influenced by GC content and methylation status

Previous studies reported CpG DNA must be processed by DNaseII to produce short, single-stranded fragments in order to raise a TLR9-mediated immune response (Chan et al. 2015b). To test whether this selectivity was conferred through binding and/or signalling, FcTLR9-beads were used to separate dsDNA from *E. coli* and *S. aureus*. Figure 6.4 shows an increase in DNA fluorescence when TLR9-beads were exposed to *E. coli* but not *S. aureus* DNA.

In order to be considered for a diagnostic test, TLR9 must distinguish between self and non-self DNA on a molecular level. There are two factors defining the affinity

of the TLR9-DNA interaction: GC content and methylation status. Percentage GC content differs between species with microbial GC content ranging from 28 ~ 68% (Liu et al. 2016), specifically *E. coli* has ~53% (Nishida 2013) and *S. aureus* 32.7% (Ngoi et al. 2021) genomic GC content. Human genomic GC content sits in the middle of this range, at 40.9% (Piovesan et al. 2019). (Liu et al. 2016) reported that enrichment efficiency of microbial DNA using a modified restriction endonuclease was broadly correlated to microbial GC content, however by no means directly proportional. In combination with the findings presented in this Chapter, this suggests that GC content alone does not confer binding to TLR9.

CpG methylation is a method of epigenetic regulation of gene expression. Human CpG dinucleotides are methylated at a frequency of 70-80% (Jabbari and Bernardi 2004; Tost 2010)) across the genome on average, with some coding sequences exhibiting almost 100% CpG methylation (Barbitoff et al. 2020). By contrast, most bacterial genomes, including *E. coli* and *S. aureus*, have very low levels of CpG methylation or lack it altogether. It has been suggested that TLR9 binds both self and non-self DNA, however only non-methylated CpG DNA results in sufficient allosteric changes in the ectodomain (which is missing in the FcTLRs used here). Recognition of the specific motif, *in vivo,* results in close apposition of the cytoplasmic signalling domains and thus downstream signalling (Latz et al. 2004).

Mammalian CpG methylation is involved in development and diseases, particularly in cancer. Tumourigenesis has been linked to hypermethylation of CpG motifs (Locke et al. 2019). Methylome profiling is a new method of targeted next generation sequencing done by magnetic enrichment of DNA using an anti-5mC antibody conjugated to magnetic beads (Lizardi et al. 2017). Indeed, (Liang, Zhang, et al. 2022) developed an assay for the rapid, assessment of global DNA methylation as a cancer biomarker with a sensitivity of 15 pg DNA. Adapting this assay for a sepsis sample in order to take the unbound fraction of DNA forward may be a suitable method of pre-treatment for pathogen ID. Interestingly, a recent study has reported 5mC hypomethylation in late-onset neonatal sepsis (Sankar et al. 2022).

Since downstream signalling appears to be so integral to the distinction between self and non-self DNA, a TLR9-mediated reporter system to couple TLR9 signal activation to the downstream expression of a colorimetric reporter gene, may be better suited for sepsis diagnostics. Indeed, Invivogen^{TM} manufacture HEK293 reporter cell lines for each of the members of the TLR superfamily. Secreted embryonic alkaline phosphatase (SEAP) was placed under the control of NFκB promoters. SEAP produces a colorimetric change on addition of a substrate added to the supernatant which can be detected by spectrophotometry in a similar way to an ELISA. In a similar fashion, (Huang et al. 2009) created a series of TLR(2-9)-HEK293 reporter cell lines in order to determine the source of contamination in a microbial product produced in *E. coli*. They detected the presence of LPS in one sample *via* activation of the *HEK*-TLR4 line. Another contaminated sample activated multiple cell lines, including the native HEK293 negative control. Native HEK293 cells reportedly express TLR5 constitutively, and so the source of this contamination was confirmed as flagellin. Furthermore, to our knowledge, none of these lines have been tested in a diagnostic context.

6.3.3 Challenges associated with magnetic separation in whole blood

Optimising a bead system in blood is challenging. Immunoglobulin G (IgG) is the primary isotype found in blood plasma and extracellular fluid (Murphy 2014); incidentally, it is the Fc region of IgG which is relied upon for attaching the receptor to the protein A. The beads are at risk of being overwhelmed by host antibodies when used with whole blood samples. This however, was not a problem for Fc-MBL (Kang, Super, et al. 2014; Cartwright et al. 2016; Kang, Driscoll, et al. 2017; Bicart-See et al. 2016). It is reported that the major factor affecting non-specific binding is surface charge (Scheepers et al. 2019), this has been reduced by blocking with zwitterionic anti-fouling polymer brushes by (Van Andel et al. 2019; Rodriguez-Emmenegger et al. 2011). When not used as a blocking agent, it has been reported polyethylene glycol (PEG) spacers placed between the receptor and the bead can

improve the separation efficiency of magnetic bead systems by improving the steric freedom of the receptor and reducing surface charge of the bead (Lee et al. 2014). PEG has been demonstrated as an effective blocking agent for magnetic beads to reduce non-specific binding (Kang, Super, et al. 2014; Lee et al. 2014). According to a mathematical model developed by (Kang, Um, et al. 2015), smaller magnetic beads perform better down to a diameter of ~300nm where the reduction in size sees diminishing returns. These are significantly smaller than the 1 µm beads used in this study. Improved signal-noise ratio would significantly benefit the detection of small quantities of DNA and could be achieved by using brighter dyes such as quantum dots (Tao et al. 2015; Liu et al. 2016).

6.3.4 Conclusion

In this chapter, we have developed a method of quantifying PI-stained DNA bound to TLR9-functionalised magnetic beads using IFC. Results showed that TLR9 was capable of detecting ssCpG DNA and dsDNA from *E. coli*, but not from *S. aureus*, suggesting the genomic GC content played a greater role in the capture efficiency than methylation status. TLR9 was able to bind human DNA exceedingly well. The current landscape of the literature, in conjunction with the results obtained here, suggest that the recombinantly expressed ectodomain of TLR9 is not capable of distinguishing between self and non-self DNA *in vitro*. Further optimisation of the magnetic bead system for use in whole blood in combination with a pre-treatment to remove some of the host material prior to TLR9-mediated enrichment may help to improve separation efficacy using this method.

7

Chapter 7 - Discussion

7.1 Part I: Summary of major achievements and limitations

The ultimate aim of this project was to develop rapid diagnostics for bloodstream infections (BSIs) for the early identification of sepsis and antimicrobial resistance (AMR). Unlike biosensors, which are typically used at the point of care, the focus of this project is on the hospital microbiology lab, specifically on culture, identification (using MALDI), and antimicrobial susceptibility testing (AST). The central role of Toll-like receptors (TLRs) in the innate immune response makes them ideal candidates for rapid pathogen detection. The broad specificity of TLRs 2, 4 and 9 in particular is conferred by their innate repertoire of TLR ligands. Here, I worked towards the development of a bespoke assay to enable the distinction between Gram-status (which antibiotic) and bacterial DNA (not viral) in a multiplexed flow cytometry assay.

The main achievements of the work are as follows:

1. I evaluated the current state of clinical diagnostics in the Glasgow Royal Infirmary (GRI) in order to define key targets for the development and implementation of a novel, alternative sample preparation assay for BSI

diagnostics. In doing so I found evidence that, despite the considerable delay it causes, blood culture nevertheless remains necessary for subsequent pathogen identification using MALDI-TOF MS.

2. I developed and optimised a bespoke, automated gating strategy to accurately quantify the binding capacity of fluorescently labelled receptors to whole bacteria pathogens using imaging flow cytometry and R.

3. As a proof of principle, this method demonstrated fluorescently labelled, recombinant TLR2 was able to bind to 90% of *S. aureus*, at positive-blood culture concentrations in PBS.

4. Building on what was learned in points 2 and 3, an immunomagnetic separation assay was developed to characterise the binding of stained CpG DNA using TLR9-functionalised magnetic beads.

Blood culture is widely regarded as a major bottleneck in the treatment of sepsis, causing significant delays to targeted antimicrobial therapy (Seymour et al. 2017; Mellor 2013). Motivated by the fact that neither the concentration of bacteria after BC incubation (when samples flag positive), nor the limits of detection of the downstream identification processes are particularly clear, I sought to evaluate the current state of the clinical diagnostics workflow to elucidate these key parameters and establish the feasibility of circumventing BC altogether in an NHS hospital. I determined the BC analyser flags a sample as positive once bacterial growth reaches approximately 10^8 CFU/ml. And to complement this, I found that in order to use MALDI-TOF MS for pathogen identification (a process routinely carried out in 80% of UK hospitals (Angeletti 2017)) a bacterial load of approximately 10^7 CFU/ml is required. Additionally these results confirmed that whole pathogens are required, strongly suggesting that total lysis abrogates positive identification. As a follow up study, I tested whether pre-enrichment (*i.e.* initial separation of bacteria from a blood sample) could lead to a faster time-to-positive result on the blood culture analyser. The hypothesis was that by effectively isolating bacteria from growth

inhibitors naturally present in blood, use of a pathogen separation technique could be justified prior to blood culture. Data showed that the presence of inhibitory factors in whole blood significantly delays the time to flag positive for *E. coli* and completely prevents growth in *S. aureus,* however further work will be required to fully determine whether the observed delay to microbial growth in blood was in fact caused by the presence of EDTA in the culture medium. Based on these observations, I concluded that blood culture remains essential with current pathogen identification equipment for a rapid separation method, and that pre-enrichment would likely improve the time to flag positive.

Selective lysis treatment using mammalian cell lysis buffer (MCLB) is presented as a promising method of indirect pathogen enrichment (Trung, Hien, et al. 2016; Trung, Thau, et al. 2019). Prior to a successful characterisation of MCLB-mediated selective lysis, a profound understanding of how to measure the quantity of pathogens was required. Due to the ambiguous approach towards pathogen quantification often found in the literature, I wanted to be able to calculate the number of positive/bound cells as a percentage of the the total with which I started, something which became a recurring theme of each subsequent method I went on to test/develop. Recovery of pathogen DNA at high bacterial concentrations (post BC; ~10^8 CFU/ml), was very good (94%) and in accordance with evidence in the literature (Trung, Hien, et al. 2016; Trung, Thau, et al. 2019). Ultimately however, it was found that a significant proportion of viable bacteria did not grow after treatment, indicating that the LoD of the MALDI-TOF MS could not be met with viable clinical samples. The data ultimately led us to conclude that selective lysis with MCLB is not currently amenable for sample preparation for pathogen ID using MALDI. The study emphasised the importance of considering the entire clinical diagnostic process, including hospital logistics, to have a measurable impact on patient outcomes.

The central role of TLRs in the innate immune response is widely known (Mogensen 2009; Akira and Takeda 2004; Duan et al. 2022; Kumar 2020). As such, the primary goal from the outset of my thesis was to evaluate TLRs as potential candidates for direct pathogen detection or sample preparation in sepsis diagnostics.

Based on the findings from the Glasgow Royal Infirmary, the aim of developing a TLR-mediated approach to sample preparation/enrichment of bacteria from patient blood samples was established. From my extensive review of the literature it was decided that TLRs 2, 4 and 9 would be the primary focus of our tests. As part of this, we planned a 2- to 3-month mobility to work with a group based at the University of Bath who focus on pathogen detection using bespoke printed circuit board (PCB) biosensors and electronic impedance spectroscopy (EIS) (Jolly et al. 2019; Moschou and Tserepi 2017; Dutta et al. 2019; Zupančič et al. 2021). I intended to measure the binding affinity and limit of detection of TLR 2, 4 and 9 with respect to Gram-positive whole bacteria, Gram-negative whole bacteria and non-methylated CpG DNA, respectively. Unfortunately, due to the COVID-19 pandemic, the placement was cancelled and access to the GRI microbiology lab revoked.

Without access to the hospital lab, but with a full immunology/molecular biology suite at the University still at my disposal, my focus turned towards accurate quantification using the equipment available to me at the time, rather than immediate clinical translation. Starting with a typical sandwich ELISA in a 96-well plate, I adapted the protocol to compare different approaches to immobilise TLRs to the surface of the plate as well as other parameters such as whether lysis of bound pathogens improved sensitivity. In the end, limited sensitivity of the detection methods available to us (absorbance, GFP fluorescence and luciferase luminosity) combined with significant background binding of bacteria to the plate in the absence of any receptor, and poor reproducibility of the Anti-E.coli antibody, led to the capture assay being abandoned.

Flow cytometry, although not routinely used for binding characterisation in this way, proved to be a more accurate method for quantifying receptor-bound bacteria compared to the ELISA-style capture assay. Access to a cutting-edge imaging flow cytometer (CYTEK ImageStream) allowed cells to be measured in suspension, overcoming the issues of immobilisation and binding in the absence of a receptor. High throughput, single-cell fluorescence measurements prompted the design and comparison of bespoke, automated gating strategies in R to eliminate

the need for manual gating and provide a more robust method for distinguishing positive and negative cells. The optimised workflow, combining IFC with automated gating, proved to be effective in quantifying the percentage of bacteria cells bound to receptors: 97.01±0.15% of *E. coli* were identified as positive through anti-*E. coli* red fluorescence in a solution of PBS. A suitable proof of principle; the method was reproducible and provided accurate results, especially for samples with faint fluorescence signals, compared to manual gating approaches. Recombinant TLR2 demonstrated a dose-dependent interaction with *S. aureus* and achieved a capture efficiency of up to 90% when tested in PBS. For the first time, this indicates that the extracellular portion of TLR2 (*i.e.* lacking the ability to confer any specificity through downstream signalling pathways) has the potential to effectively bind and detect whole bacteria *in vitro*. Recombinant TLR4 was not able to bind to *E. coli* and, despite several further attempts to optimise the assay, was eventually abandoned in the interest of time. In this case, further investigations are needed to better understand the specific limitations and mechanisms involved.

The implementation of pathogen detection assays in whole blood poses significant challenges, which likely contributes to the scarcity of reports on accurate capture efficiencies in the literature. In experiments where TLR2 binding to *S. aureus* was analysed in whole blood, a notable decrease in binding efficiency was observed. This reduction in efficiency can be attributed to multiple factors. Data suggest the coexistence of recombinant TLR2 with endogenous TLR2 on neutrophils and monocytes, indicating potential homodimerization of the receptors. Additionally, interactions with damage-associated molecular patterns (DAMPs) on cells undergoing apoptosis could also play a role.

These host:recombinant receptor interactions may interfere with the ability of TLR2 to effectively bind to the pathogen, thereby reducing capture efficiency. To address this issue, refined analytical techniques such as improved gating strategies, precise masking, and advanced feature extraction methods could be employed to facilitate the quantification of internalized pathogens and allow for the correlation of cellular features, such as eccentricity, with bacterial internalization.

The use of such techniques could discern whether TLR2 is interacting directly with neutrophils or with bacteria being phagocytosed. These methods have been successfully demonstrated in previous studies, offering a robust framework for further investigation into the complex dynamics of pathogen detection in whole blood (Ploppa et al. 2011; Botha et al. 2021).

TLRs 2 and 4 have the potential to detect whole cells and, when used in parallel, distinguish between Gram-positive and Gram-negative bacteria, but what about DNA? Circulating free DNA (cfDNA) is a promising diagnostic tool for pathogen ID and genomic AST in sepsis (Blauwkamp et al. 2019). Successful pathogen ID and AST are often precluded when bacteriolytic antimicrobial therapy is started prior to blood samples being taken for culture. Furthermore, methods of selective lysis of human material, such as the method tested in this project using MCLB, depletes cfDNA during the wash step which is necessary to remove lysed human cells. I wanted to see if TLR9 could selectively bind and enrich cf-pathogen DNA, first in PBS, then in blood, as a means of reducing the cost of bulk sequencing.

Initially, the TLR9:CpG DNA interaction seemed suitable for biochemical analysis using microscale thermophoresis. Underwhelming results prompted me to adopt a structural biology approach and investigate the 3D protein structure of TLR9 which revealed the proximity of several key lysine residues to CpG DNA. The abundance of lysine residues in the active site suggested an explanation for abrogated binding when TLR9 is fluorescently labelled using NHS-EDC chemistry, which I relied on both for MST analysis and fluorescently labelling TLR2 and 4. This setback was mitigated by re-engineering the IFC assay to work with protein A-coated magnetic microbeads functionalised with FcTLR9. A pull-down assay (immunomagnetic separation) was developed, the beads were stained using a DNA dye and then run directly in the ImageStream. Preliminary experiments demonstrated that TLR9-functionalised magnetic beads are successful in binding CpG DNA, indicating their potential for enriching pathogen-specific DNA sequences. Interestingly, while TLR9-functionalised beads can bind double-stranded DNA from *E. coli*, the binding to double-stranded DNA from *S. aureus* was not detected.

This discrepancy may be attributed to differences in the GC content of the DNA sequences, highlighting the influence of genomic composition on TLR9 binding.

However, an insurmountable obstacle was encountered when it was demonstrated that TLR9 is not able to distinguish between pathogen DNA and human DNA. The experiments show that TLR9 exhibits similar affinity for binding both pathogen and human DNA, suggesting that the external portion of TLR9 alone is unable to differentiate between self and non-self DNA. Furthermore, when tested in whole blood samples, TLR9-functionalised beads did not exhibit any significant binding to DNA at all. This suggests potential limitations in the magnetic separation technique when applied to complex biological samples like whole blood. Further optimisation of the bead system and pre-treatment methods is therefore necessary to improve the efficiency of DNA separation in such samples. Consequently, a pivot towards a recombinant reporter system may allow us to establish whether selectivity between pathogen and host DNA sequences could be achieved. It remains to be tested whether ligand-induced homodimerisation and resultant conformational changes in the TIR domains of TLR9 could result in the quantifiable activation of subsequent downstream signalling pathways.

7.2 Part II: Future state of sepsis diagnostics

Despite many recent advances in our understanding of the immunopathology of sepsis, clinical translation of novel therapies and diagnostics remains a challenge (Cavaillon et al. 2020). All clinical trials designed to temper the so-called cytokine storm - the term given to describe the unrestrained cascade of systemic inflammation responsible for loss of immune regulation in sepsis - have failed (Chousterman et al. 2017; Teijaro 2017; Opal et al. 2014). Indeed, there have been multiple disruptive developments which bring into question the central themes of organ dysfunction in the context of critical illness which have guided sepsis treatment for decades. Organ dysfunction has been shown to arise in sepsis both in the absence of tissue hypoxia and in the absence of significant cell death (Pool et al. 2018). Furthermore, immune

dysfunction appears to be only part of the story; with an ever more complex picture involving endotheliopathy, coagulopathy and metabolic reprogramming beginning to emerge (Chang 2019; Pool et al. 2018; Cavaillon et al. 2020).

From the perspective of this thesis, it draws into question the actual role of the pathogen in sepsis (Gao, Evans, et al. 2008). A significant proportion of sepsis blood samples are culture negative (Lin, McGinley, et al. 2018). However, studies repeatedly show the importance of prompt pathogen identification to facilitate effective antimicrobial therapy (Kumar et al. 2006; Schultz et al. 2017; Niederman et al. 2021) and this is reflected in the most recent guidelines for sepsis treatment (Evans et al. 2021; Singer et al. 2016). Nonetheless, from a causal point of view, there remains a gap in the knowledge. It is accepted that bacteria have the ability to readily change their membrane state between capsule, biofilms, L-form and planktonic states; the latter being the rarest natural form but also the only one we culture in the lab (Minasyan 2019). The dormant blood microbiome is an interesting yet controversial topic (D'Aquila et al. 2021; Païssé et al. 2016; Castillo et al. 2019; Tan et al. 2022) which centres around the theory that LPS shedding by newly resuscitated dormant microbes already present in the blood. The sudden, systemically high concentration of LPS drives the rapid amplification of a cytokine response in absence of high bacterial load (Potgieter et al. 2015; Kell and Pretorius 2015). In parallel, gene expression analysis revealed differential gene signatures in Gram-positive and Gram-negative sepsis in mice (Yu et al. 2004) and in pre-natal cord-blood monocytes (de Jong et al. 2018).

Limitations of sepsis treatment call for a future shift towards precision medicine to consider the heterogeneity of the syndrome (Shankar-Hari, Harrison, et al. 2019b; Russell and Baillie 2017; Leligdowicz and Matthay 2019). Combining biomarkers with electronic medical record data enabled sepsis disease progression to be tracked (Taneja et al. 2017). Transcriptomic analysis of peripheral blood has revealed an immunosuppressed response signature characterised by endotoxin tolerance, T-cell exhaustion, and downregulation of human leukocyte antigen (HLA) class II resulting in higher mortality (Davenport et al. 2016). Single-cell transcriptomics

of sepsis patients revealed a unique CD14+ monocyte state leading to a panel of surface markers characterising epigenomic and functional phenotypes to be designed (Reyes et al. 2020). In general, the landscape of sepsis research appears to predominantly focus on 7-30-day mortality and overlook the long term mortality associated with sepsis survival (Wu et al. 2020), treatment response (Antcliffe et al. 2019) and mortality prediction (Sweeney et al. 2018). In spite of the high mortality rates, more people survive sepsis meaning there are an estimated 200,000 new sepsis survivors in the UK each year (Rudd et al. 2020). Symptoms of post-sepsis syndrome include cognitive dysfunction, amputation, and persistent inflammation, immunosuppression, and catabolism syndrome (PICS) which can last from months to years (Shankar-Hari, Harrison, et al. 2019b; Cavaillon et al. 2020; Sonneville et al. 2013; Bustamante et al. 2020; Mostel et al. 2019). A better understanding of the ways infection heterogeneously drives clinical endotype, based upon the patient's unique epigenome will undoubtedly help to guide treatment response in the future.

TLRs play a central role in the innate immune response (Duan et al. 2022; Mogensen 2009; Akira and Takeda 2004) and expression has been reported to change in sepsis (Tsujimoto et al. 2008; Akira and Takeda 2004; Viemann et al. 2005; Ishii and Akira 2004). Indeed, we are not the first to beg the question as to whether TLRs (2, 4, 9) could serve as biomarkers in sepsis diagnostics (Younis et al. 2018; Lam et al. 2021). Recent research demonstrates that erythrocytes, previously thought the be immunologically inert, act as immune sentinels by expressing TLR9 on their surface as a means of sensing microbial DNA and proposes this role may be leveraged for diagnostic purposes (Lam et al. 2021). Initially seen as a nuisance; over the course of this project the potential strategic value of employing TLRs in a so-called 'double-edged diagnostic' assay became clear. One which could both detect evidence of pathogens in the blood sample (with the granularity of a Gram-stain, or distinction between viral, bacterial or even sterile sepsis; for example) as well as providing a measurement of the host immune response (TLR expression and apoptosis).

Flow cytometry, although not currently used for sepsis diagnostic in the clinic, appears to be gaining translational momentum in this area (Monneret et al. 2019;

Aydin et al. 2017; Marcos-Fernández et al. 2022). Technological advances in full-spectrum flow will likely therefore permeate the clinical diagnostic space in the near future. In addition, it seems we are on the eve of a merger between the fields of flow cytometry and 'omics. As a result of panel sizes growing to the point where high-dimensional analyses can be carried out, flow cytometry will soon catch up to single-cell RNA sequencing analysis. Feature extraction (IDEAS or CellProfiler) has been demonstrated to yield sufficient parameters to perform high dimensional analysis and machine learning prediction to facilitate label-free phenotyping of leukocytes and erythrocytes (Hennig et al. 2017; Lippeveld et al. 2020; Doan et al. 2020; Nassar et al. 2019). Similar approaches have also been applied to real-time deformability cytometry (Donadello et al. 2015). Label-free distinction between B cells and T cells remains challenging (Lippeveld et al. 2020). It is important to appreciate however, to approach this from a diagnostic perspective would need only the ability to distinguish between diseased and healthy states, or Gram-status for instance, thus significantly simplifying the requirements of the assay. Thus, imaging flow cytometry may enable label-free monitoring of changes in erythrocyte morphology in sepsis (Bateman et al. 2017). This would free up additional fluorescent channels – a limiting factor of this technology – to allow the inclusion of broad-spectrum pathogen markers, such as the TLRs investigated here, or even sepsis specific biomarkers such as CD25, CD64 and CD69 (Zhou et al. 2019; Aydin et al. 2017; Verdonk et al. 2022). Furthermore, improvements in image resolution and flow rate could enable TLRs to detect single bacteria in blood using imaging flow cytometry.

In summary, these findings highlight the potential of TLRs as important molecular players in pathogen detection and possible biomarkers of the sepsis immune response. However, they also underscore the challenges in optimising the assay for complex samples like whole blood and addressing the limitations of specific TLRs in accurately detecting intact pathogens. Further investigation to take advantage of recent advantages in flow cytometry and refinement of the assay

are necessary to fully harness the diagnostic capabilities of TLRs 2, 4 and 9 as a double-edged diagnostic in clinical applications.

Appendices

A

The First Appendix (Ch03)

Samples consisted first and foremost of a mixture of positive and negative controls in PBS and whole blood. A total of 53 samples were run, of these only 24 (45.28%) were classed as 'working devices' i.e. having correct positive (P. pan) and negative (E. coli) controls for LAMP/LFT. By calculating the number of correct results as a percentage of the working devices give 54.17% (Figure A.1,A).

Looking at the performance of the individual control LFT strips (Figure A.1,B), 47 (88.68%) devices had either a correct positive or negative control, 84.91% had both negative and positive controls correct. In samples where BRCA was used as a negative control for contamination with human material, 81.82% (n=11) were correct. When BRCA was used as a positive control for selective lysis only 36.36% (n=11) were correct, suggesting treatment with MCLB1 left sufficient host cells to be detected by the LAMP assay. Finally when BRCA acted a positive control for successful DNA extraction from a blood sample, 61.9% (n=21) of LFTs gave the correct result. With the exception of the selective lysis control, the controls performed well in isolation, however taken together only 39.53% of devices had all three controls performing correctly.

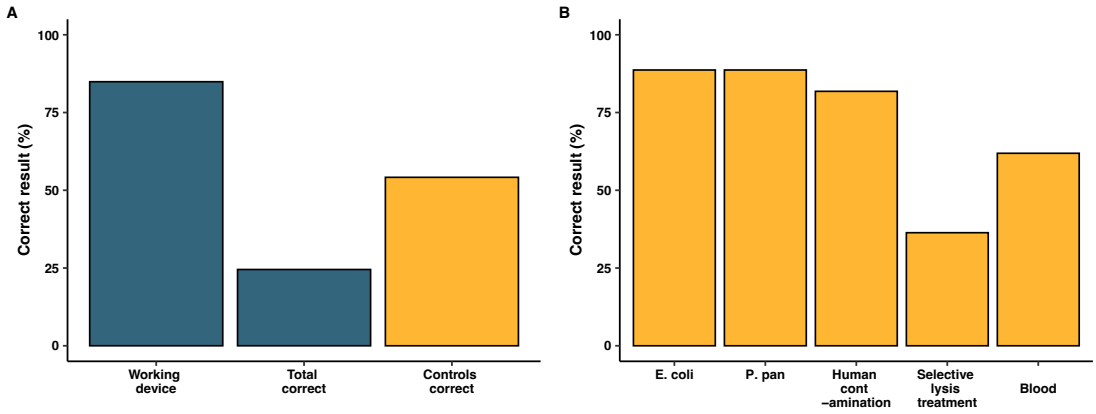

Figure A.1: Point-of-care device performance. **(A)** Overall results. **(B)** Breakdown of the performance of individual controls. BRCA is a sample-dependent control.

B

The Second Appendix (Ch04)

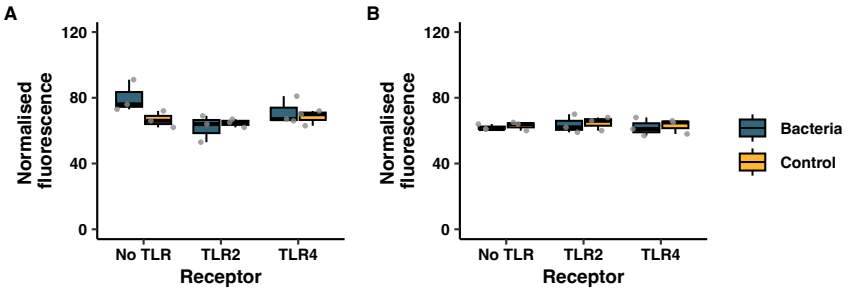

Figure B.1: **A)** Initial test to determine the capture efficiency of TLR2 and TLR4 (at 1 μg/well) incubated with 100 μl of 10^8 CFU/ml bacteria. **B)** The effect of lysing bound bacteria on the GFP fluorescence signal. Negative control (yellow bars) contain no bacteria (n=3 technical replicates).

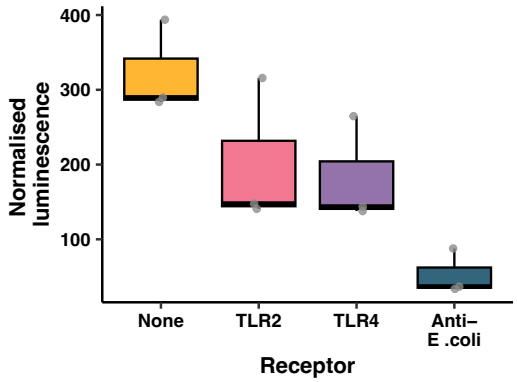

Figure B.2: Capture efficiency of protein A coated plates. 10^7 CFU per sample were added to plates coated with TLR2, 4 and anti-Ecoli at a conccentration of 1 μg per well and compared to wells without any receptor. ATP luminescence was quantified using the BactTiter-Glo kit (Promega), (n=3 technical replicates)

C

The Third Appendix (Ch05)

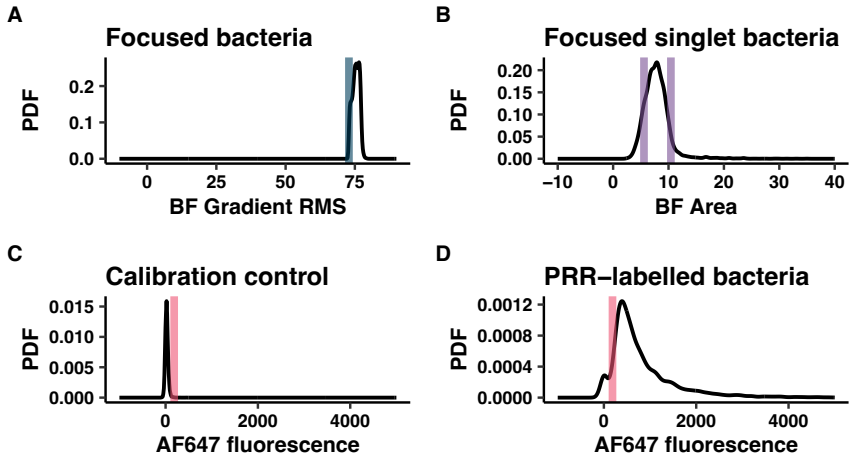

Figure C.1: Appendix. Gating strategy for TLR2 in PBS illustrated by density plots of different exported feature values. **(A)** Cells in focus are gated by taking everything greater than 1 standard deviation (s.d.) less than the mode gradient RMS for BF images of cells. **(B)** Singlets are selected by taking everything ± 1 s.d. of the mode area of BF images. **(C)** A sample containing GFP bacteria only is used as the calibration control. It is used to set a red (AF647) fluorescence intensity threshold (red vertical line) on a sample which should have no red signal. Any cells with a red fluorescence intensity greater than 99.865% of the dataset is classed as positive. **(D)** A sample of GFP *S. aureus* stained with 2 μg/ml AF647-labelled TLR2. The threshold at 99.865 % of data points is represented by the red vertical line, the percent of cells greater than this threshold is then calculated.

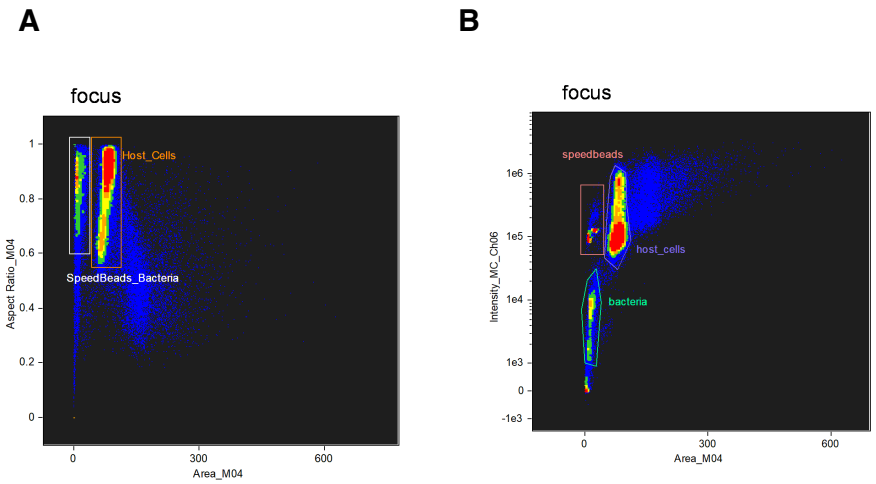

Area_M04

Population	Count	%Gated
focus	73159	100
SpeedBeads_Bacteria & focus	12461	17
Host_Cells & focus	47884	65.5

Area_M04

Population	Count	%Gated
focus	73159	100
speedbeads & focus	5023	6.87
host_cells & focus	47443	64.8
bacteria & focus	7660	10.5

Figure C.2: Appendix. SSC can be used to gate out SpeedBeads in a sample of whole blood stained with AF647:TLR2 gated to select for cells in focus. **A)** Scatter plot showing area *vs.* aspect ratio of BF images, **B)** Scatter plot showing area *vs.* side scatter.

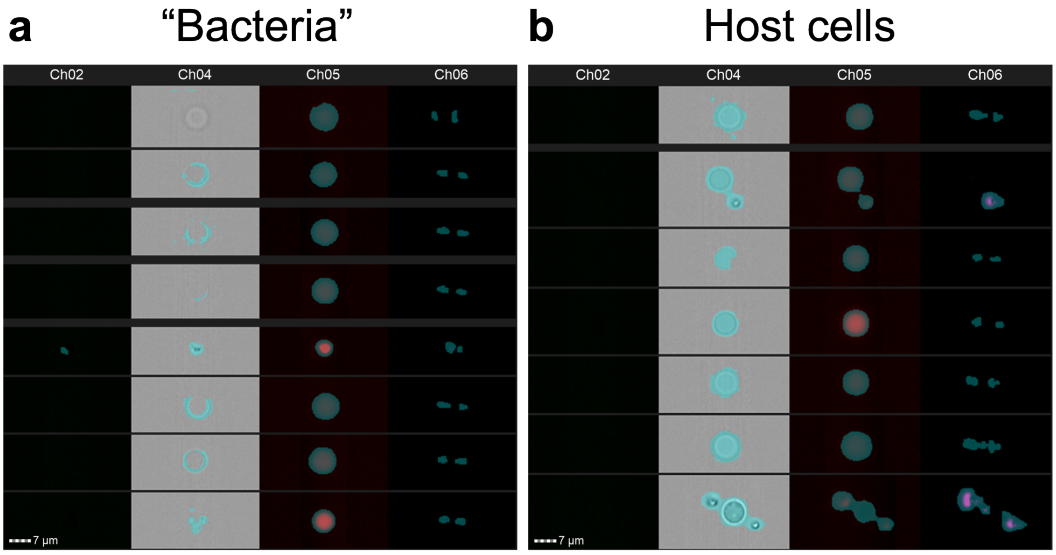

Figure C.3: Appendix. Poorly drawn masks result in mis-characterisation of lymphocytes as bacteria. A RBC-lysed blood which had been sample spiked with GFP-positive *S. aureus*. SSC *vs.* aread of BF images was used to gate populations of **A)** bacteria and **B)** host-cells. Masks in Ch05 (AF647-TLR2) and Ch06 (SSC) appear very similar between the two populations, suggesting they are in fact the same cell type. Ch04 masks, used to calcularte the area feature value, appear fragmentef in the bacteria population.

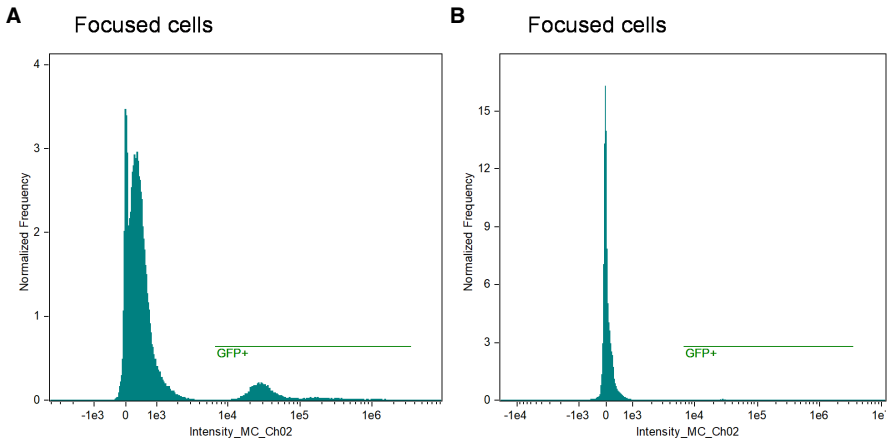

Figure C.4: Appendix. GFP fluorescence intensity in **A)** whole blood and **B)** RBC-lysed blood. The GFP+ gate indicates the protortion of cells in focus which express GFP textiti.e. bacteria. This is used to assign a new threshold for GFP bacteria at 5000 RFU for experiments carried out in blood.

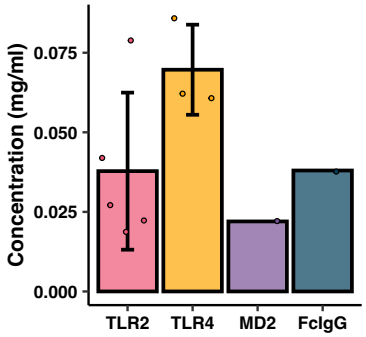

Figure C.5: Appendix. Yield of the Microscale protein labelling kit (ThermoFisher Scientific) measure using NanoDrop. A 50 μg lyophilised aliquots of each PRR was resuspended at 1 mg/ml in PBS and labelled according to the manufacturer's instructions. TLR2 (pink; n=5), TLR4 (yellow; n=3), MD2 (purple; n=1) and FcIgG (blue; n=1). Error bars, where shown, represent standard error of the mean.

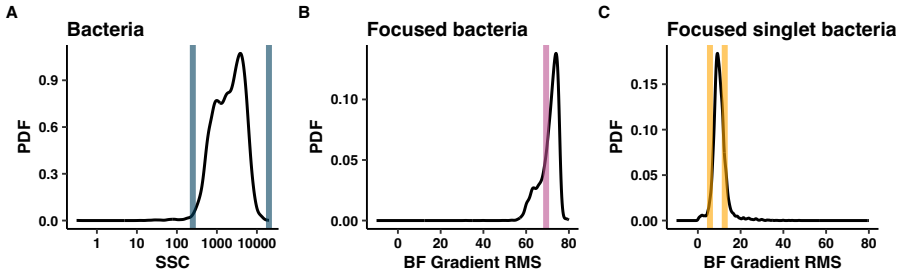

Figure C.6: Appendix. Gating strategy for QD-labelled PRRs in PBS. **(A)** Bacteria are selected by manually gating side-scatter (SSC) intensity values between 250 and 20,000. **(B)** Cells in focus are gated by taking everything greater than 1 standard deviation (s.d.) less than the mode gradient RMS for BF images of cells. **(C)** Singlets are selected by taking everything ± 1 s.d. of the mode area of BF images.

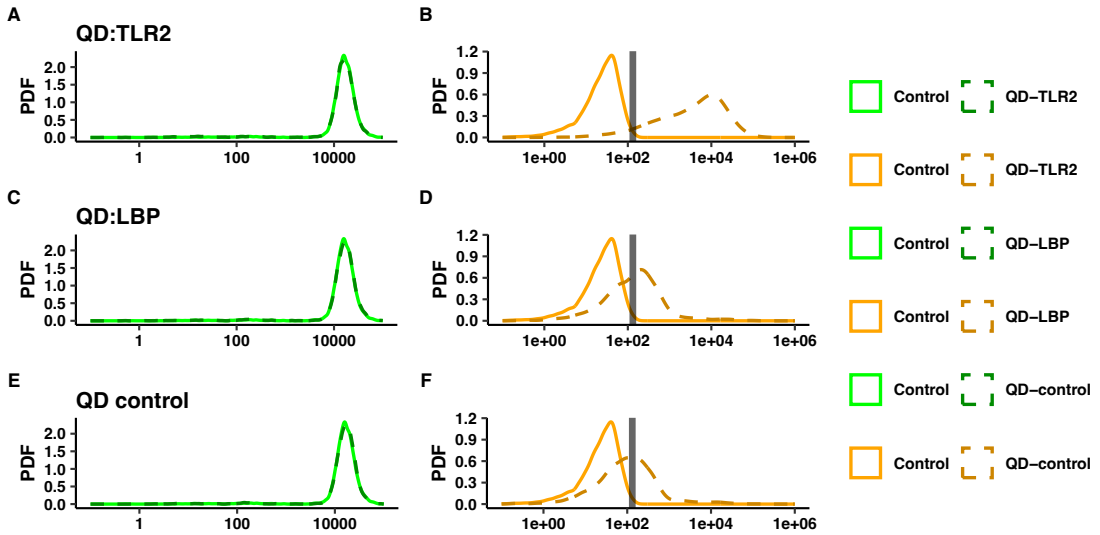

Figure C.7: Appendix. Density plots of GFP (green; left-hand column) and QD (orange; right hand column) fluorescence intensity for QD-labelled TLR2 (**(A, B)**), LPS-binding protein (LBP; **(C, D)**) and free-QDs (QD-control; **(e-f)**). Black vertical lines indicate the threshold for positivity based on QD-fluorescence set at 98.865%. Solid lines show data from the calibration control (same for each sample) and dashed lines represent the stained sample.

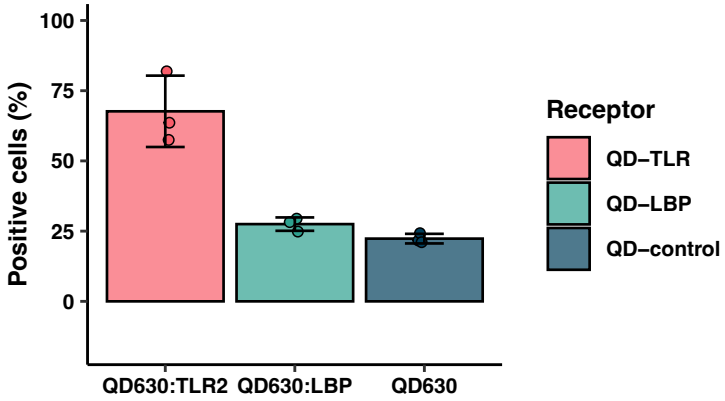

Figure C.8: Appendix. Binding of QD-labelled PRRs to *S. aureus*. PRRs (2 µg/ml) were labelled with QD630 (0.4 µg/ml) at a ratio of 5:1 receptor:QD. Labelled PRRs were then used to stain 10^7 CFU bacteria according to the standard protocol. Error bars show standard deviation of the mean (n=3 technical replicates).

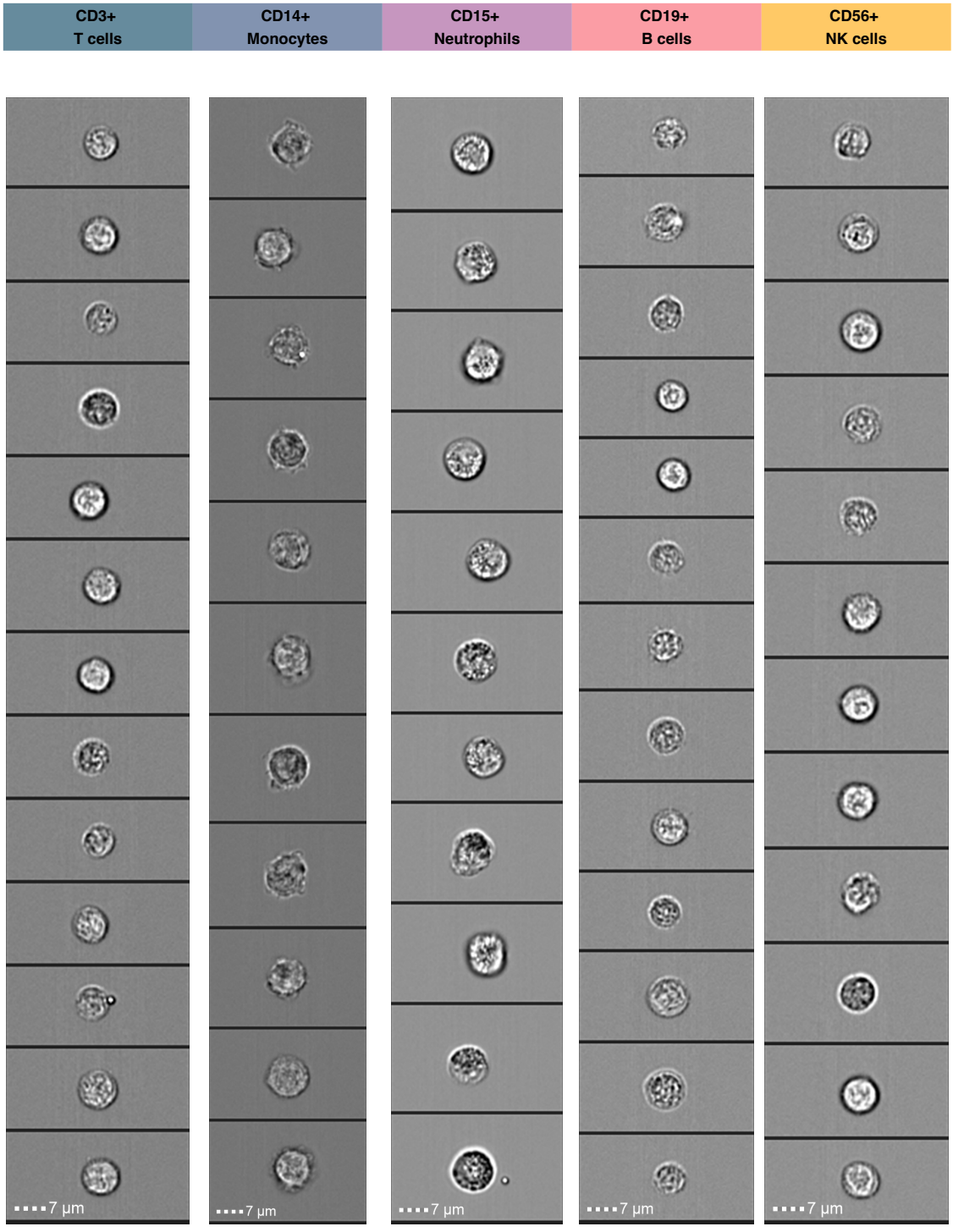

Figure C.9: Appendix. Brightfield images of stained WBCs.

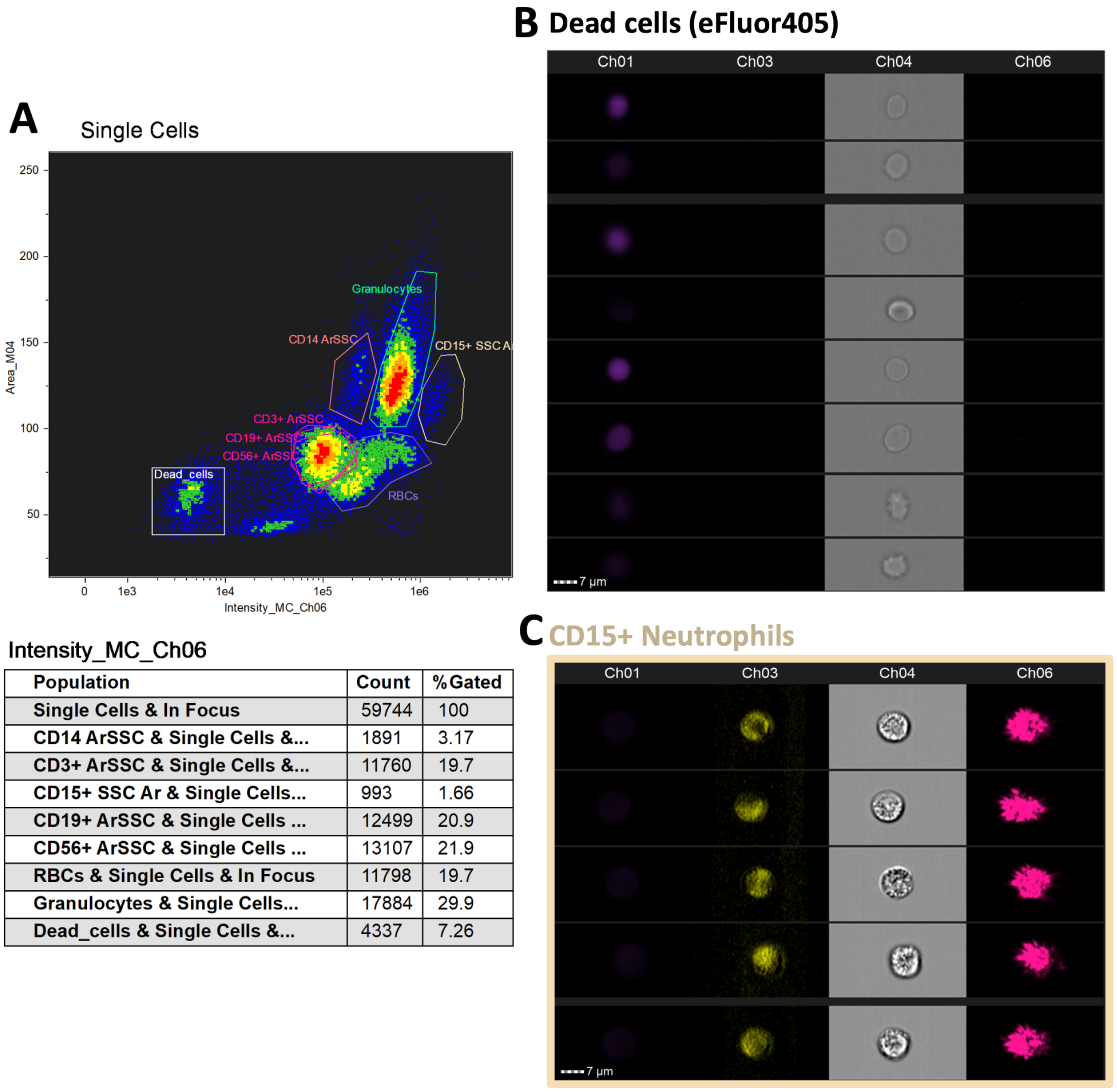

Intensity_MC_Ch06

Population	Count	%Gated
Single Cells & In Focus	59744	100
CD14 ArSSC & Single Cells &...	1891	3.17
CD3+ ArSSC & Single Cells &...	11760	19.7
CD15+ SSC Ar & Single Cells...	993	1.66
CD19+ ArSSC & Single Cells ...	12499	20.9
CD56+ ArSSC & Single Cells ...	13107	21.9
RBCs & Single Cells & In Focus	11798	19.7
Granulocytes & Single Cells...	17884	29.9
Dead_cells & Single Cells &...	4337	7.26

Figure C.10: Appendix. Stained WBC comparison

D

The Fourth Appendix (Ch06)

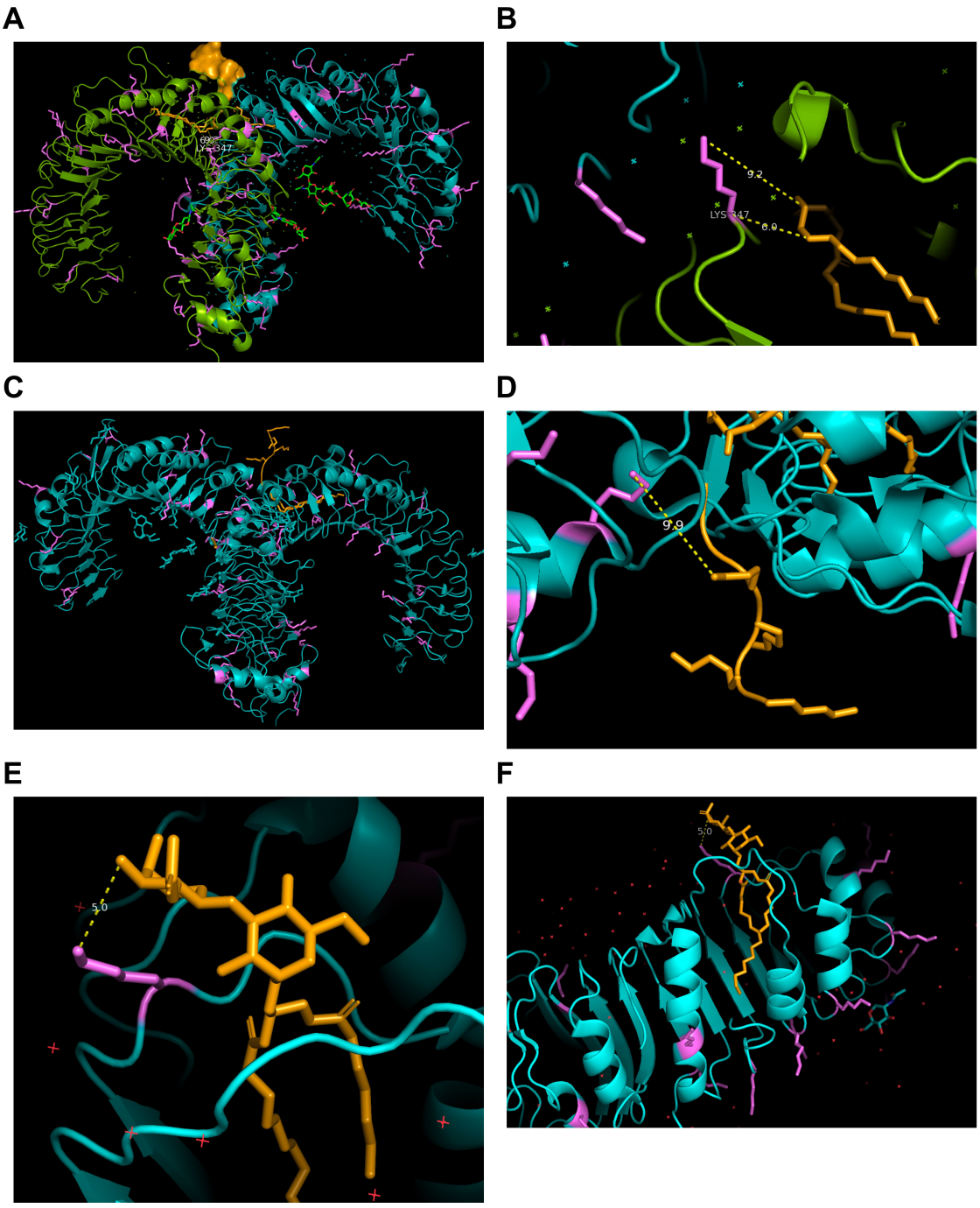

Figure D.1: Crystal structure of TLR2 reveals a significantly shallower active site compared with TLR9, reducing the chance of steric hindrance caused by conjugation to AF647. FcTLR9-functionalised protein A magnetic beads were mixed with 100 ng CpG DNA for 30 min **(a)** DAPI and **(b)** PI 2.0 μg/ml 10^7 CFU/ml

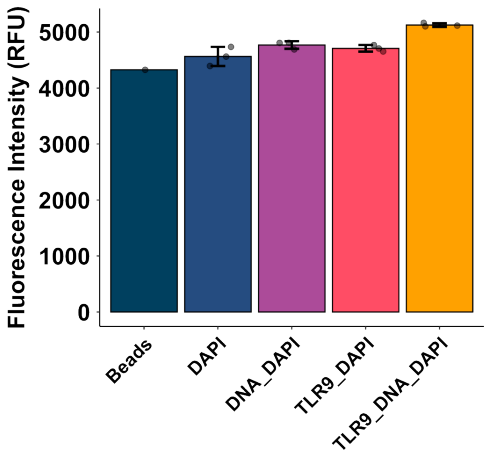

Figure D.2: Appendix. Mean fluorescence was normalised against beads.

Aghaeepour, Nima et al. (Mar. 2013). "Critical assessment of automated flow cytometry data analysis techniques". In: *Nature Methods* 10.3, pp. 228–238. DOI: 10.1038/NMETH.2365.

Akira, Shizuo and Kiyoshi Takeda (2004). "Toll-like receptor signalling". In: *Nature Reviews Immunology* 4.7, pp. 499–511. DOI: 10.1038/nri1391. arXiv: NIHMS150003. URL: http://www.nature.com/doifinder/10.1038/nri1391.

Alexander, Helen K and R Craig MacLean (July 2020). "Stochastic bacterial population dynamics restrict the establishment of antibiotic resistance from single cells". In: *Proceedings of the National Academy of Sciences*, p. 201919672. DOI: 10.1073/pnas.1919672117. URL: http://www.ncbi.nlm.nih.gov/pubmed/32703812%20http://www.pnas.org/lookup/doi/10.1073/pnas.1919672117.

Algar, W. Russ (June 2020). "Heroes or Villains? How Nontraditional Luminescent Materials Do and Do Not Enhance Bioanalysis and Imaging †". In: *Chemistry of Materials* 32.12, pp. 4863–4883. DOI: 10.1021/ACS.CHEMMATER.0C01130/ASSET/IMAGES/LARGE/CM0C01130_0007.JPEG. URL: https://pubs.acs.org/doi/full/10.1021/acs.chemmater.0c01130.

Alliance, Global Sepsis (2017). *Global Sepsis Alliance*. URL: https://www.global-sepsis-alliance.org/%20https://www.global-sepsis-alliance.org/about (visited on 07/04/2023).

Amini, Kaveh, Nora W.C. Chan, and Heinz Bernhard Kraatz (2014). "Toll-like receptor 3 modified Au electrodes: An investigation into the interaction of TLR3 immobilized on Au surfaces with poly(I:C)". In: *Analytical Methods* 6.10, pp. 3322–3328. DOI: 10.1039/c4ay00369a.

Anderson, H. Luke, Igor E. Brodsky, and Nilam S. Mangalmurti (2018). "The Evolving Erythrocyte: Red Blood Cells as Modulators of Innate Immunity". In: *The Journal of Immunology* 201.5, pp. 1343–1351. DOI: 10.4049/jimmunol.1800565.

Anderson, Kathryn V., Gerd Jürgens, and Christiane Nüsslein-Volhard (Oct. 1985). "Establishment of dorsal-ventral polarity in the Drosophila embryo: Genetic studies on the role of the Toll gene product". In: *Cell* 42.3, pp. 779–789. DOI: 10.1016/0092-8674(85)90274-0. URL: http://www.cell.com/article/0092867485902740/fulltext%20http:

//www.cell.com/article/0092867485902740/abstract%20https://www.cell.com/cell/abstract/0092-8674(85)90274-0.

Angeletti, Silvia (July 2017). *Matrix assisted laser desorption time of flight mass spectrometry (MALDI-TOF MS) in clinical microbiology*. DOI: 10.1016/j.mimet.2016.09.003. URL: https://www.sciencedirect.com/science/article/pii/S0167701216302536.

Antcliffe, David B. et al. (2019). "Transcriptomic signatures in sepsis and a differential response to steroids from the VaNISH randomized trial". In: *American Journal of Respiratory and Critical Care Medicine* 199.8, pp. 980–986. DOI: 10.1164/rccm.201807-1419OC.

Arpaia, Nicholas and Gregory M Barton (2013). *The impact of Toll-like receptors on bacterial virulence strategies*. DOI: 10.1016/j.mib.2012.11.004.

Awomoyi, Agnes A. et al. (Sept. 2007). "Association of TLR4 Polymorphisms with Symptomatic Respiratory Syncytial Virus Infection in High-Risk Infants and Young Children". In: *The Journal of Immunology* 179.5, pp. 3171–3177. DOI: 10.4049/jimmunol.179.5.3171. URL: https://pubmed.ncbi.nlm.nih.gov/17709532/.

Aydin, Mustafa et al. (2017). "Application of flow cytometry in the early diagnosis of neonatal sepsis". In: *Annals of Clinical and Laboratory Science* 47.2, pp. 184–190.

Al-Azemi, A. et al. (May 2011). "Effects of chelating agent and environmental stresses on microbial biofilms: Relevance to clinical microbiology". In: *Journal of Applied Microbiology* 110.5, pp. 1307–1313. DOI: 10.1111/j.1365-2672.2011.04983.x. URL: https://dx.doi.org/10.1111/j.1365-2672.2011.04983.x.

Bailey Jila Fazel-madjlessi, James E et al. (Dec. 1977). "Characterization of Bacterial Growth by Means of Flow Microfluorometry". In: *Science* 198.4322, pp. 1175–1176. DOI: 10.1126/SCIENCE.412254. URL: https://www.science.org/doi/10.1126/science.412254.

Balagopalakrishna, Chavali et al. (1996). "Production of superoxide from hemoglobin-bound oxygen under hypoxic conditions". In: *Biochemistry* 35.20, pp. 6393–6398. DOI: 10.1021/bi952875+. URL: https://pubs.acs.org/sharingguidelines.

Banala, Sambashiva et al. (Oct. 2013). *No washing, less waiting: Engineering biomolecular reporters for single-step antibody detection in solution*. DOI: 10.1039/c3ob41315b. URL: https://pubs.rsc.org/en/content/articlehtml/2013/ob/c3ob41315b%20https://pubs.rsc.org/en/content/articlelanding/2013/ob/c3ob41315b%20http://xlink.rsc.org/?DOI=c3ob41315b.

Banerjee, Ritu et al. (2015). "Randomized Trial of Rapid Multiplex Polymerase Chain Reaction-Based Blood Culture Identification and Susceptibility Testing". In: *Clinical Infectious Diseases* 61.7, pp. 1071–1080. DOI: 10.1093/cid/civ447.

Banfi, Giuseppe, Gian Luca Salvagno, and Giuseppe Lippi (May 2007). *The role of ethylenediamine tetraacetic acid (EDTA) as in vitro anticoagulant for diagnostic purposes*. DOI: 10.1515/CCLM.2007.110. URL: https://pubmed.ncbi.nlm.nih.gov/17484616/.

Barbitoff, Yury A. et al. (Feb. 2020). "Systematic dissection of biases in whole-exome and whole-genome sequencing reveals major determinants of coding sequence coverage". In: *Scientific Reports* 10.1, pp. 1–13. DOI: 10.1038/s41598-020-59026-y. URL: https://www.nature.com/articles/s41598-020-59026-y.

Bateman, Ryon M. et al. (Sept. 2017). *The effect of sepsis on the erythrocyte*. DOI: 10.3390/ijms18091932. URL: /pmc/articles/PMC5618581/%20/pmc/articles/PMC5618581/?report=abstract%20https://www.ncbi.nlm.nih.gov/pmc/articles/PMC5618581/.

Beltrán-García, Jesús et al. (2020). "Oxidative stress and inflammation in covid-19-associated sepsis: The potential role of anti-oxidant therapy in avoiding disease progression". In: *Antioxidants* 9.10, pp. 1–20. DOI: 10.3390/antiox9100936.

Bhattacharya, Prasanta Kumar et al. (2022). "Comparison of Systemic Inflammatory Response Syndrome, Sequential Organ Failure Assessment, and Quick Sequential Organ Failure Assessment Scores to predict Mortality in Sepsis". In: *Journal of Association of Physicians of India* 70.8, pp. 14–18. DOI: 10.5005/japi-11001-0062. URL: http://creativecommons..

Bicart-See, A. et al. (June 2016). "Rapid isolation of Staphylococcus aureus pathogens from infected clinical samples using magnetic beads coated with Fc-mannose binding lectin". In: *PLoS ONE* 11.6. Ed. by Cordula M. Stover, e0156287. DOI: 10.1371/journal.pone.0156287. URL: https://dx.plos.org/10.1371/journal.pone.0156287.

Blaskovich, Mark A.T., Mark S. Butler, and Matthew A. Cooper (2017). "Polishing the tarnished silver bullet: the quest for new antibiotics". In: *Essays In Biochemistry* 61.1, pp. 103–114. DOI: 10.1042/ebc20160077. URL: http://www.ncbi.nlm.nih.gov/pubmed/28258234%20http://www.pubmedcentral.nih.gov/articlerender.fcgi?artid=PMC5869247.

Blauwkamp, Timothy A. et al. (Feb. 2019). "Analytical and clinical validation of a microbial cell-free DNA sequencing test for infectious disease". In: *Nature Microbiology 2019*, p. 1. DOI: 10.1038/s41564-018-0349-6. URL: http://www.nature.com/articles/s41564-018-0349-6%20http://www.nature.com/articles/s41564-018-0349-6%7B%5C%%7D0Ahttps://www.nature.com/articles/s41564-018-0349-6.

Bone, R. C. et al. (June 1992). "Definitions for sepsis and organ failure and guidelines for the use of innovative therapies in sepsis". In: *Chest*. Vol. 101. 6. Elsevier, pp. 1644–1655. DOI: 10.1378/chest.101.6.1644. URL: http://journal.chestnet.org/article/S001236921638415X/fulltext%20http://journal.chestnet.org/article/S001236921638415X/abstract%20https://journal.chestnet.org/article/S0012-3692(16)38415-X/abstract.

Bongiorno, Dafne et al. (May 2020). "Detection of methicillin-resistant Staphylococcus aureus persistence in osteoblasts using imaging flow cytometry". In: *MicrobiologyOpen* 9.5. DOI: 10.1002/mbo3.1017. URL: https://onlinelibrary.wiley.com/doi/10.1002/mbo3.1017.

Bonner, W. A. et al. (1972). "Fluorescence activated cell sorting". In: *The Review of scientific instruments* 43.3, pp. 404–409. DOI: 10.1063/1.1685647. URL: https://pubmed.ncbi.nlm.nih.gov/5013444/.

Botha, Jaco, Haley R. Pugsley, and Aase Handberg (Jan. 2021). "Conventional, high-resolution and imaging flow cytometry: Benchmarking performance in characterisation of extracellular vesicles". In: *Biomedicines* 9.2, pp. 1–24. DOI: 10.3390/biomedicines9020124. URL: https://www.mdpi.com/2227-9059/9/2/124/htm%20https://www.mdpi.com/2227-9059/9/2/124.

Bourcier, Simon et al. (June 2017). "Marked regional endothelial dysfunction in mottled skin area in patients with severe infections". In: *Critical Care* 21.1, pp. 1–8. DOI:

10.1186/s13054-017-1742-x. URL: https://ccforum.biomedcentral.com/articles/10.1186/s13054-017-1742-x.

Bouvet, Jean-Pierre (1994). "IMMUNOGLOBULIN Fab FRAGMENT-BINDING PROTEINS". In: *International Journal of Immunopharmacology* 16.5, pp. 419–424. DOI: https://doi.org/10.1016/0192-0561(94)90031-0.

Bustamante, Angela C. et al. (2020). "Transcriptomic profiles of sepsis in the human brain". In: *American Journal of Respiratory and Critical Care Medicine* 201.7, pp. 861–863. DOI: 10.1164/RCCM.201909-1713LE.

By Jennifer Doss et al. (2015). "The Erythrocyte Transcriptome: Global Characterization and Therapeutic Implication". PhD thesis, p. 91. URL: https://dukespace.lib.duke.edu/dspace/bitstream/handle/10161/9812/Doss%7B%5C_%7Dduke%7B%5C_%7D0066D%7B%5C_%7D12742.pdf?sequence=1%7B%5C&%7DisAllowed=y.

Cao, Xiao-guang et al. (Sept. 2022). "The diagnostic value of next-generation sequencing technology in sepsis". In: *Frontiers in Cellular and Infection Microbiology* 12, p. 1361. DOI: 10.3389/fcimb.2022.899508.

Cartwright, Mark et al. (July 2016). "A Broad-Spectrum Infection Diagnostic that Detects Pathogen-Associated Molecular Patterns (PAMPs) in Whole Blood". In: *EBioMedicine* 9, pp. 217–227. DOI: 10.1016/j.ebiom.2016.06.014. URL: https://www.sciencedirect.com/science/article/pii/S2352396416302584.

Cassini, Alessandro et al. (Jan. 2019). "Attributable deaths and disability-adjusted life-years caused by infections with antibiotic-resistant bacteria in the EU and the European Economic Area in 2015: a population-level modelling analysis". In: *The Lancet Infectious Diseases* 19.1, pp. 56–66. DOI: 10.1016/S1473-3099(18)30605-4. URL: http://www.ncbi.nlm.nih.gov/pubmed/30409683%20http://www.pubmedcentral.nih.gov/articlerender.fcgi?artid=PMC6300481.

Castillo, Diego J et al. (2019). "The healthy human blood microbiome: Fact or fiction?" In: *Frontiers in Cellular and Infection Microbiology* 9.MAY, p. 148. DOI: 10.3389/fcimb.2019.00148. URL: http://www.ncbi.nlm.nih.gov/pubmed/31139578%20http://www.pubmedcentral.nih.gov/articlerender.fcgi?artid=PMC6519389.

Cavaillon, Jean-Marc, Mervyn Singer, and Tomasz Skirecki (2020). "Sepsis therapies: learning from 30 years of failure of translational research to propose new leads". In: *EMBO Molecular Medicine* 12.4, pp. 1–24. DOI: 10.15252/emmm.201810128.

Chaichana, Panjaporn et al. (May 2017). "A nonsense mutation in TLR5 is associated with survival and reduced IL-10 and TNF-α levels in human melioidosis". In: *PLoS Neglected Tropical Diseases* 11.5, e0005587. DOI: 10.1371/journal.pntd.0005587. URL: https://journals.plos.org/plosntds/article?id=10.1371/journal.pntd.0005587.

Chan, Mei Po et al. (2015a). "DNase II-dependent DNA digestion is required for DNA sensing by TLR9". In: *Nature Communications* 6.May 2014, pp. 4–6. DOI: 10.1038/ncomms6853.

— (Jan. 2015b). "DNase II-dependent DNA digestion is required for DNA sensing by TLR9". In: *Nature Communications* 6.1, pp. 1–10. DOI: 10.1038/ncomms6853. URL: https://www.nature.com/articles/ncomms6853%20https://www.nature.com/articles/ncomms6853/figures/.

Chang, Jae C. (2019). "Sepsis and septic shock: Endothelial molecular pathogenesis associated with vascular microthrombotic disease". In: *Thrombosis Journal* 17.1, pp. 1–19. DOI: 10.1186/s12959-019-0198-4.

Charalampous, Themoula et al. (June 2019). "Nanopore metagenomics enables rapid clinical diagnosis of bacterial lower respiratory infection". In: *Nat Biotech*, p. 1. DOI: 10.1038/s41587-019-0156-5. URL: http://www.nature.com/articles/s41587-019-0156-5.

Chen, C. H., H. C. Ding, and T. C. Chang (Mar. 2001). "Rapid identification of Bacillus cereus based on the detection of a 28.5-kilodalton cell surface antigen". In: *Journal of Food Protection* 64.3, pp. 348–354. DOI: 10.4315/0362-028X-64.3.348. URL: https://pubmed.ncbi.nlm.nih.gov/11252478/.

Chen, Qi Hong, Jun Shao, et al. (May 2019). "Predictive accuracy of Sepsis-3 definitions for mortality among adult critically ill patients with suspected infection". In: *Chinese Medical Journal* 132.10, pp. 1147–1153. DOI: 10.1097/CM9.0000000000000166. URL: https://journals.lww.com/cmj/fulltext/2019/05200/predictive%7B%5C_%7Daccuracy%7B%5C_%7Dof%7B%5C_%7Dsepsis%7B%5C_%7D3%7B%5C_%7Ddefinitions%7B%5C_%7Dfor.3.aspx.

Chousterman, Benjamin G., Filip K. Swirski, and Georg F. Weber (May 2017). *Cytokine storm and sepsis disease pathogenesis*. DOI: 10.1007/s00281-017-0639-8. URL: https://link.springer.com/article/10.1007/s00281-017-0639-8.

Christiansen, D. et al. (2012). "Differential effect of inhibiting MD-2 and CD14 on LPS-versus whole E. coli bacteria-induced cytokine responses in human blood". In: *Advances in Experimental Medicine and Biology* 946, pp. 237–251. DOI: 10.1007/978-1-4614-0106-3_14. URL: https://link.springer.com/chapter/10.1007/978-1-4614-0106-3%7B%5C_%7D14.

Chu, Ming et al. (Apr. 2018). "Staphylococcus aureus Phenol-Soluble Modulins α1–α3 Act as Novel Toll-Like Receptor (TLR) 4 Antagonists to Inhibit HMGB1/TLR4/NF-κB Signaling Pathway". In: *Frontiers in Immunology* 9.APR, pp. 1–13. DOI: 10.3389/fimmu.2018.00862. URL: http://journal.frontiersin.org/article/10.3389/fimmu.2018.00862/full.

Clark, Stephen R. et al. (Mar. 2007). "Platelet TLR4 activates neutrophil extracellular traps to ensnare bacteria in septic blood". In: *Nature Medicine* 13.4, pp. 463–469. DOI: 10.1038/nm1565. URL: https://www.nature.com/articles/nm1565.

Claushuis, Theodora A.M. et al. (June 2016). "Thrombocytopenia is associated with a dysregulated host response in critically ill sepsis patients". In: *Blood* 127.24, pp. 3062–3072. DOI: 10.1182/blood-2015-11-680744. URL: https://pubmed.ncbi.nlm.nih.gov/26956172/.

Coenye, Tom and Peter Vandamme (2003). "Intragenomic heterogeneity between multiple 16S ribosomal RNA operons in sequenced bacterial genomes". In: *FEMS Microbiology Letters* 228.1, pp. 45–49. DOI: 10.1016/S0378-1097(03)00717-1.

Collins, Bernard and Ian A. Wilson (2014). "Crystal structure of the C-terminal domain of mouse TLR9". In: *Proteins: Structure, Function and Bioinformatics* 82.10, pp. 2874–2878. DOI: 10.1002/prot.24616.

Costa, Ramon T., Antonio P. Nassar, and Pedro Caruso (June 2018). "Accuracy of SOFA, qSOFA, and SIRS scores for mortality in cancer patients admitted to an intensive care unit with suspected infection". In: *Journal of Critical Care* 45, pp. 52–57. DOI: 10.1016/j.jcrc.2017.12.024.

Crippa, Michela et al. (2012). *Occupational diseases due to allergic and toxic chemicals in health care workers: Fitness for work*. URL: https://www.ncbi.nlm.nih.gov/pmc/articles/PMC102748/pdf/gnd064.pdf.

CRUK (2020). *Cancer Statistics for the UK*. URL: https://www.cancerresearchuk.org/health-professional/cancer-statistics-for-the-uk%20https://www.cancerresearchuk.org/health-professional/cancer-statistics-for-the-uk%7B%5C#%7Dheading-Zero (visited on 01/06/2024).

D'Aquila, Patrizia et al. (July 2021). "Microbiome in Blood Samples From the General Population Recruited in the MARK-AGE Project: A Pilot Study". In: *Frontiers in Microbiology* 12.July, pp. 1–9. DOI: 10.3389/fmicb.2021.707515.

Daniels, Ron et al. (June 2011). "The sepsis six and the severe sepsis resuscitation bundle: A prospective observational cohort study". In: *Emergency Medicine Journal* 28.6, pp. 507–512. DOI: 10.1136/emj.2010.095067. URL: http://www.ncbi.nlm.nih.gov/pubmed/21036796.

Davenport, Emma E et al. (2016). "Genomic landscape of the individual host response and outcomes in sepsis: A prospective cohort study". In: *The Lancet Respiratory Medicine* 4.4, pp. 259–271. DOI: 10.1016/S2213-2600(16)00046-1. URL: http://www.ncbi.nlm.nih.gov/pubmed/26917434%20http://www.pubmedcentral.nih.gov/articlerender.fcgi?artid=PMC4820667.

Davey, Hazel M and Douglas B Kell (1996). *Flow cytometry and cell sorting of heterogeneous microbial populations: The importance of single-cell analyses*. DOI: 10.1128/mmbr.60.4.641-696.1996.

Davies, S. C; Grant, Jonathan (2013). *The Drugs Don't Work*. URL: https://blackwells.co.uk/bookshop/product/Drugs-Dont-Work-by-Davies-Professor-Dame-Sally/9780241968888.

De Freitas Caires, Nathalie et al. (Oct. 2018). *Endocan, sepsis, pneumonia, and acute respiratory distress syndrome*. DOI: 10.1186/s13054-018-2222-7.

De Jong, Emma et al. (Feb. 2018). "Identification of generic and pathogen-specific cord blood monocyte transcriptomes reveals a largely conserved response in preterm and term newborn infants". In: *Journal of Molecular Medicine* 96.2, pp. 147–157. DOI: 10.1007/s00109-017-1609-2. URL: https://link.springer.com/article/10.1007/s00109-017-1609-2.

Desjardins, Philippe and Deborah Conklin (Nov. 2010). "NanoDrop microvolume quantitation of nucleic acids". In: *Journal of Visualized Experiments* 45. DOI: 10.3791/2565. URL: http://www.ncbi.nlm.nih.gov/pubmed/21189466%20http://www.pubmedcentral.nih.gov/articlerender.fcgi?artid=PMC3346308.

Dey, Rafik et al. (2019). "Interactions of Pseudomonas aeruginosa with Acanthamoeba polyphaga Observed by Imaging Flow Cytometry". In: *Cytometry Part A* 95.5, pp. 555–564. DOI: 10.1002/cyto.a.23768.

Didar, Tohid F. et al. (2015). "Improved treatment of systemic blood infections using antibiotics with extracorporeal opsonin hemoadsorption". In: *Biomaterials* 67, pp. 382–392. DOI: 10.1016/j.biomaterials.2015.07.046. URL: http://dx.doi.org/10.1016/j.biomaterials.2015.07.046.

Doan, Minh et al. (Sept. 2020). "Objective assessment of stored blood quality by deep learning". In: *Proceedings of the National Academy of Sciences of the United States of America* 117.35, pp. 21381–21390. DOI: 10.1073/pnas.2001227117. URL: https://www.pnas.org/doi/abs/10.1073/pnas.2001227117.

Dodd, Marylin et al. (Mar. 2001). "Advancing the science of symptom management". In: *Journal of Advanced Nursing* 33.5, pp. 668–676. DOI: 10.1046/j.1365-2648.2001.01697.x. URL:

https://onlinelibrary.wiley.com/doi/full/10.1046/j.1365-2648.2001.01697.x%20https://onlinelibrary.wiley.com/doi/abs/10.1046/j.1365-2648.2001.01697.x%20https://onlinelibrary.wiley.com/doi/10.1046/j.1365-2648.2001.01697.x.

Doerr, Allison (June 2011). *A flow cytometry revolution*. DOI: 10.1038/nmeth0711-531. URL: https://www.nature.com/articles/nmeth0711-531.

Dolina, Joseph S. et al. (Apr. 2020). "TLR9 Sensing of Self-DNA Controls Cell-Mediated Immunity to Listeria Infection via Rapid Conversion of Conventional CD4+ T Cells to Treg". In: *Cell Reports* 31.1. DOI: 10.1016/j.celrep.2020.01.040.

Donadello, Katia et al. (2015). "Reduced red blood cell deformability over time is associated with a poor outcome in septic patients". In: *Microvascular Research* 101, pp. 8–14. DOI: 10.1016/j.mvr.2015.05.001. URL: http://dx.doi.org/10.1016/j.mvr.2015.05.001.

Doss, Jennifer F. et al. (2015). "A comprehensive joint analysis of the long and short RNA transcriptomes of human erythrocytes". In: *BMC Genomics* 16.1, pp. 1–16. DOI: 10.1186/s12864-015-2156-2. URL: http://dx.doi.org/10.1186/s12864-015-2156-2.

Duan, Tianhao et al. (Mar. 2022). "Toll-Like Receptor Signaling and Its Role in Cell-Mediated Immunity". In: *Frontiers in Immunology* 13. DOI: 10.3389/fimmu.2022.812774. URL: /pmc/articles/PMC8927970/%20/pmc/articles/PMC8927970/?report=abstract%20https://www.ncbi.nlm.nih.gov/pmc/articles/PMC8927970/%20https://www.frontiersin.org/articles/10.3389/fimmu.2022.812774/full.

Duquenoy, Aurore et al. (June 2020). "Assessment of Gram- and Viability-Staining Methods for Quantifying Bacterial Community Dynamics Using Flow Cytometry". In: *Frontiers in Microbiology* 11, p. 1469. DOI: 10.3389/fmicb.2020.01469.

Dutta, Gorachand et al. (Aug. 2019). "Label-free electrochemical detection of S. mutans exploiting commercially fabricated printed circuit board sensing electrodes". In: *Micromachines* 10.9, p. 575. DOI: 10.3390/mi10090575. URL: https://www.mdpi.com/2072-666X/10/9/575.

Dziarski, R. and D. Gupta (2000). "Role of MD-2 in TLR2- and TLR4-mediated recognition of Gram-negative and Gram-positive bacteria and activation of chemokine genes". In: *Journal of Endotoxin Research* 6.5, pp. 401–405. DOI: 10.1179/096805100101532243. URL: https://pubmed.ncbi.nlm.nih.gov/11521063/.

Dziarski, Roman, Qiuling Wang, et al. (Feb. 2001). "MD-2 Enables Toll-Like Receptor 2 (TLR2)-Mediated Responses to Lipopolysaccharide and Enhances TLR2-Mediated Responses to Gram-Positive and Gram-Negative Bacteria and Their Cell Wall Components". In: *The Journal of Immunology* 166.3, pp. 1938–1944. DOI: 10.4049/jimmunol.166.3.1938. URL: https://pubmed.ncbi.nlm.nih.gov/11160242/.

Evans, Laura et al. (Nov. 2021). "Surviving sepsis campaign: international guidelines for management of sepsis and septic shock 2021". In: *Intensive care medicine* 47.11, pp. 1181–1247. DOI: 10.1007/S00134-021-06506-Y. URL: https://pubmed.ncbi.nlm.nih.gov/34599691/.

Farthing, Andrew G et al. (2021). "Sepsis: When a Simple Infection Becomes Deadly". In: *Frontiers for Young Minds* 9. DOI: 10.3389/frym.2021.639681. URL: https://www..

Federico, Stefano et al. (2020). "Modulation of the Innate Immune Response by Targeting Toll-like Receptors: A Perspective on Their Agonists and Antagonists". In: *Journal of Medicinal Chemistry* 63.22, pp. 13466–13513. DOI: 10.1021/acs.jmedchem.0c01049.

Feehery, George R. et al. (Oct. 2013). "A Method for Selectively Enriching Microbial DNA from Contaminating Vertebrate Host DNA". In: *PLoS ONE* 8.10. Ed. by Sarah K. Highlander, e76096. DOI: 10.1371/journal.pone.0076096. URL: https://dx.plos.org/10.1371/journal.pone.0076096.

Fenollar, Florence and Didier Raoult (Nov. 2007). "Molecular diagnosis of bloodstream infections caused by non-cultivable bacteria". In: *International Journal of Antimicrobial Agents* 30.SUPPL. 1, pp. 7–15. DOI: 10.1016/j.ijantimicag.2007.06.024. URL: https://www.sciencedirect.com/science/article/pii/S092485790700310X?casa%7B%5C_%7Dtoken=EuYq-UPlaAOAAAAA:U5g6VppMo4XfUOZjdng4JyECfyaGJuNo1AdlvAHXOSsWptIYPzQO%7B%5C_%7DP4T47Tvd9Wjzvkb8dQ.

Ferrer-Font, Laura et al. (Sept. 2021). "Panel Optimization for High-Dimensional Immunophenotyping Assays Using Full-Spectrum Flow Cytometry". In: *Current Protocols* 1.9. DOI: 10.1002/cpz1.222. URL: https://pubmed.ncbi.nlm.nih.gov/34492732/.

Fillatreau, Simon, Benoît Manfroi, and Thomas Dörner (Feb. 2021). *Toll-like receptor signalling in B cells during systemic lupus erythematosus*. DOI: 10.1038/s41584-020-00544-4. URL: https://pubmed.ncbi.nlm.nih.gov/33339987/.

Finak, Greg et al. (Feb. 2016). "Standardizing Flow Cytometry Immunophenotyping Analysis from the Human ImmunoPhenotyping Consortium". In: *Scientific Reports* 6.1, pp. 1–11. DOI: 10.1038/srep20686. URL: https://www.nature.com/articles/srep20686.

Francois, Patrice et al. (2003). "Rapid detection of methicillin-resistant Staphylococcus aureus directly from sterile or nonsterile clinical samples by a new molecular assay". In: *Journal of Clinical Microbiology* 41.1, pp. 254–260. DOI: 10.1128/JCM.41.1.254-260.2003.

Fulwyler, M L (Nov. 1965). "Electronic Separation of Biological Cells by Volume". In: *Science* 150.3698, pp. 910–911. DOI: 10.1126/SCIENCE.150.3698.910. URL: https://www.science.org/doi/10.1126/science.150.3698.910.

Gao, Fang, Teresa Melody, et al. (2005). "Open Access R764 The impact of compliance with 6-hour and 24-hour sepsis bundles on hospital mortality in patients with severe sepsis: a prospective observational study". In: *Critical Care* 9.6, R764. DOI: 10.1186/cc3909. URL: http://www.ncbi.nlm.nih.gov/pubmed/16356225%20http://www.pubmedcentral.nih.gov/articlerender.fcgi?artid=PMC1414020%20http://ccforum.biomedcentral.com/articles/10.1186/cc3909%20http://ccforum.com/content/9/6/R764Thisarticleisonlineat:http://ccforum.com/content/9.

Gao, Hongmei, Timothy W. Evans, and Simon J. Finney (May 2008). *Bench-to-bedside review: Sepsis, severe sepsis and septic shock - Does the nature of the infecting organism matter?* DOI: 10.1186/cc6862. URL: /pmc/articles/PMC2481435/%20/pmc/articles/PMC2481435/?report=abstract%20https://www.ncbi.nlm.nih.gov/pmc/articles/PMC2481435/.

Garraud, Olivier and Fabrice Cognasse (Feb. 2015). *Are platelets cells? And if yes, are they immune cells?* DOI: 10.3389/fimmu.2015.00070.

GAWAZ, M. et al. (Nov. 1995). *Platelet activation and interaction with leucocytes in patients with sepsis or multiple organ failure*. DOI: 10.1111/j.1365-2362.1995.tb01694.x. URL: https://onlinelibrary.wiley.com/doi/full/10.1111/j.1365-2362.1995.tb01694.x%20https://onlinelibrary.wiley.com/doi/abs/10.1111/j.1365-2362.1995.tb01694.x%20https://onlinelibrary.wiley.com/doi/10.1111/j.1365-2362.1995.tb01694.x.

Goldenberg, Simon (Oct. 2017). "Molecular-based diagnostics, including future trends". In: *Medicine (United Kingdom)* 45.10, pp. 645–648. DOI: 10.1016/j.mpmed.2017.07.004. URL: https://linkinghub.elsevier.com/retrieve/pii/S135730391730186X%20http://dx.doi.org/10.1016/j.mpmed.2017.07.004.

Gould, Ian M and Abhijit M Bal (Feb. 2013). "New antibiotic agents in the pipeline and how hey can help overcome microbial resistance". In: *Virulence* 4.2, pp. 185–191. DOI: 10.4161/viru.22507. URL: http://www.ncbi.nlm.nih.gov/pubmed/23302792%20http://www.pubmedcentral.nih.gov/articlerender.fcgi?artid=PMC3654619.

Goulopoulou, Styliani, Cameron G. McCarthy, and R. Clinton Webb (Jan. 2016). "Toll-like receptors in the vascular system: Sensing the dangers within". In: *Pharmacological Reviews* 68.1, pp. 142–167. DOI: 10.1124/pr.114.010090. URL: http://dx.doi.org/10.1124/pr.114.010090.

Guo, Xueheng et al. (Feb. 2017). "The novel toll-like receptor 2 agonist SUP3 enhances antigen presentation and T cell activation by dendritic cells". In: *Frontiers in Immunology* 8.FEB. DOI: 10.3389/fimmu.2017.00158. URL: https://pubmed.ncbi.nlm.nih.gov/28270814/.

Halpern, Neil A., Stephen M. Pastores, and Robert J. Greenstein (June 2004). "Critical care medicine in the United States 1985-2000: An analysis of bed numbers, use, and costs". In: *Critical Care Medicine* 32.6, pp. 1254–1259. DOI: 10.1097/01.CCM.0000128577.31689.4C. URL: https://journals.lww.com/ccmjournal/fulltext/2004/06000/critical%7B%5C_%7Dcare%7B%5C_%7Dmedicine%7B%5C_%7Din%7B%5C_%7Dthe%7B%5C_%7Dunited%7B%5C_%7Dstates.2.aspx.

Hanzelmann, Dennis et al. (Nov. 2016). "Toll-like receptor 2 activation depends on lipopeptide shedding by bacterial surfactants". In: *Nature Communications* 7.1, p. 12304. DOI: 10.1038/ncomms12304. URL: http://www.nature.com/articles/ncomms12304.

Haridas, Viraga et al. (Jan. 2017). *Imaging flow cytometry analysis of intracellular pathogens*. DOI: 10.1016/j.ymeth.2016.09.007.

Hatanaka, A. (1993). *The biogeneration of green odour by green leaves*. DOI: 10.1016/0031-9422(91)80003-J.

Havixbeck, Jeffrey J. et al. (Aug. 2015). "Multi-parametric analysis of phagocyte antimicrobial responses using imaging flow cytometry". In: *Journal of Immunological Methods* 423, pp. 85–92. DOI: 10.1016/j.jim.2015.03.016. URL: http://dx.doi.org/10.1016/j.jim.2015.03.016.

He, Weigang et al. (2007). "TLR4 signaling promotes immune escape of human lung cancer cells by inducing immunosuppressive cytokines and apoptosis resistance". In:

Molecular Immunology 44.11, pp. 2850–2859. DOI: 10.1016/j.molimm.2007.01.022. URL: https://pubmed.ncbi.nlm.nih.gov/17328955/.

Headland, Sarah E. et al. (June 2014). "Cutting-edge analysis of extracellular microparticles using imagestreamx imaging flow cytometry". In: *Scientific Reports* 4.1, pp. 1–10. DOI: 10.1038/srep05237. URL: www.nature.com/scientificreports.

Hemmi, Hiroaki et al. (Dec. 2000). "A Toll-like receptor recognizes bacterial DNA". In: *Nature* 408.6813, pp. 740–745. DOI: 10.1038/35047123. URL: https://www.nature.com/articles/35047123.

Hennig, Holger et al. (Jan. 2017). "An open-source solution for advanced imaging flow cytometry data analysis using machine learning". In: *Methods* 112, pp. 201–210. DOI: 10.1016/j.ymeth.2016.08.018.

Henrick, Bethany M. et al. (2019). "TLR10 senses HIV-1 proteins and significantly enhances HIV-1 infection". In: *Frontiers in Immunology* 10.MAR. DOI: 10.3389/fimmu.2019.00482. URL: https://pubmed.ncbi.nlm.nih.gov/30930906/.

Herzenberg, Leonore A et al. (2006). *Interpreting flow cytometry data: A guide for the perplexed*. DOI: 10.1038/ni0706-681. URL: www.TreeStar.com.

Holliman, R. E. (Mar. 1986). "The therapeutic impact of blood culture results". In: *Journal of Hospital Infection* 7.2, pp. 185–188. DOI: 10.1016/0195-6701(86)90062-9. URL: https://www.sciencedirect.com/science/article/pii/0195670186900629.

Holm, Claus and Lene Jespersen (May 2003). "A flow-cytometric gram-staining technique for milk-associated bacteria". In: *Applied and environmental microbiology* 69.5, pp. 2857–2863. DOI: 10.1128/AEM.69.5.2857-2863.2003. URL: https://pubmed.ncbi.nlm.nih.gov/12732558/.

Hornung, Veit et al. (May 2002). "Quantitative Expression of Toll-Like Receptor 1–10 mRNA in Cellular Subsets of Human Peripheral Blood Mononuclear Cells and Sensitivity to CpG Oligodeoxynucleotides". In: *The Journal of Immunology* 168.9, pp. 4531–4537. DOI: 10.4049/jimmunol.168.9.4531. URL: https://pubmed.ncbi.nlm.nih.gov/11970999/.

Huang, Li Yun et al. (2009). "Use of toll-like receptor assays to detect and identify microbial contaminants in biological products". In: *Journal of Clinical Microbiology* 47.11, pp. 3427–3434. DOI: 10.1128/JCM.00373-09.

Hutter, K. J. and H. E. Eipel (Sept. 1978). "Flow cytometric determinations of cellular substances in algae, bacteria, moulds and yeasts". In: *Antonie van Leeuwenhoek* 44.3-4, pp. 269–282. DOI: 10.1007/BF00394305. URL: https://link.springer.com/article/10.1007/BF00394305.

Ibsen, Per H., Jesper W. Petersen, and I. Heron (1993). "Quantification of pertussis toxin, filamentous haemagglutinin, 69 kDa outer membrane protein, agglutinogens 2 and 3 and lipopolysaccharide in the Danish whole-cell pertussis vaccine". In: *Vaccine* 11.3, pp. 318–322. DOI: 10.1016/0264-410X(93)90193-2. URL: https://pubmed.ncbi.nlm.nih.gov/8447160/.

Ishii, Ken J. and Shizuo Akira (2004). "Toll-like receptors and sepsis". In: *Current Infectious Disease Reports* 6.5, pp. 361–366. DOI: 10.1007/s11908-004-0034-1.

Iwasaki, Akiko and Ruslan Medzhitov (Sept. 2004). *Toll-like receptor control of the adaptive immune responses*. DOI: 10.1038/ni1112. URL: https://www.nature.com/articles/ni1112.

Jabbari, Kamel and Giorgio Bernardi (2004). "Cytosine methylation and CpG, TpG (CpA) and TpA frequencies". In: *Gene* 333.SUPPL. Pp. 143–149. DOI: 10.1016/j.gene.2004.02.043.

Jayat, Chantal and Marie Hélène Ratinaud (Jan. 1993). "Cell cycle analysis by flow cytometry: Principles and applications". In: *Biology of the Cell* 78.1-2, pp. 15–25. DOI: 10.1016/0248-4900(93)90110-Z. URL: https://onlinelibrary.wiley.com/doi/full/10.1016/0248-4900%7B%5C%%7D2893%7B%5C%%7D2990110-Z%20https://onlinelibrary.wiley.com/doi/abs/10.1016/0248-4900%7B%5C%%7D2893%7B%5C%%7D2990110-Z%20https://onlinelibrary.wiley.com/doi/10.1016/0248-4900(93)90110-Z.

Jochberger, Stefan et al. (Mar. 2008). "Anesthesia and its allied disciplines in the developing world: A nationwide survey of the Republic of Zambia". In: *Anesthesia and Analgesia* 106.3, pp. 942–948. DOI: 10.1213/ane.0b013e318166ecb8. URL: https://journals.lww.com/anesthesia-analgesia/Fulltext/2008/03000/Anesthesia%7B%5C_%7Dand%7B%5C_%7DIts%7B%5C_%7DAllied%7B%5C_%7DDisciplines%7B%5C_%7Din%7B%5C_%7Dthe.39.aspx%20https://europepmc.org/article/MED/18292444.

Joffre, Jérémie and Judith Hellman (2021). "Oxidative stress and endothelial dysfunction in sepsis and acute inflammation". In: *Antioxidants and Redox Signaling* 35.15, pp. 1291–1307. DOI: 10.1089/ars.2021.0027.

Jolly, Pawan et al. (Jan. 2019). "A PNA-based Lab-on-PCB diagnostic platform for rapid and high sensitivity DNA quantification". In: *Biosensors and Bioelectronics* 123.September 2018, pp. 244–250. DOI: 10.1016/j.bios.2018.09.006. URL: https://linkinghub.elsevier.com/retrieve/pii/S0956566318306924%20https://doi.org/10.1016/j.bios.2018.09.006.

Jude, Brooke A. et al. (2003). "Subversion of the innate immune system by a retrovirus". In: *Nature Immunology* 4.6, pp. 573–578. DOI: 10.1038/ni926.

Kang, Jin Young, Xuehua Nan, et al. (Dec. 2009). "Recognition of Lipopeptide Patterns by Toll-like Receptor 2-Toll-like Receptor 6 Heterodimer". In: *Immunity* 31.6, pp. 873–884. DOI: 10.1016/j.immuni.2009.09.018. URL: http://www.cell.com/article/S1074761309004920/fulltext%20http://www.cell.com/article/S1074761309004920/abstract%20https://www.cell.com/immunity/abstract/S1074-7613(09)00492-0.

Kang, Joo H., Harry Driscoll, et al. (July 2017). "An Engineered Human Fc-Mannose-Binding-Lectin Captures Circulating Tumor Cells". In: *Advanced Biosystems* 1.7, p. 1700094. DOI: 10.1002/adbi.201700094. URL: http://doi.wiley.com/10.1002/adbi.201700094.

Kang, Joo H., Michael Super, et al. (Oct. 2014). "An extracorporeal blood-cleansing device for sepsis therapy". In: *Nature Medicine* 20.10, pp. 1211–1216. DOI: 10.1038/nm.3640. URL: http://www.nature.com/articles/nm.3640.

Kang, Joo H., Eujin Um, et al. (2015). "Optimization of Pathogen Capture in Flowing Fluids with Magnetic Nanoparticles". In: *Small* 11.42, pp. 5657–5666. DOI: 10.1002/smll.201501820.

Kapoor, Garima, Saurabh Saigal, and Ashok Elongavan (2017). *Action and resistance mechanisms of antibiotics: A guide for clinicians*. DOI: 10.4103/joacp.JOACP_349_15. URL: https://www.ncbi.nlm.nih.gov/pmc/articles/PMC5672523/%7B%5C#%7D!po=72.2222.

Kastritis, Panagiotis L and Alexandre M J J Bonvin (2013). "On the binding affinity of macromolecular interactions: daring to ask why proteins interact." In: *Journal of the Royal Society, Interface / the Royal Society* 10.December 2012, p. 20120835. DOI: 10.1098/rsif.2012.0835. URL: http://www.pubmedcentral.nih.gov/articlerender.fcgi?artid=3565702%7B%5C&%7Dtool=pmcentrez%7B%5C&%7Drendertype=abstract.

Kawai, Taro and Shizuo Akira (2011). *Toll-like Receptors and Their Crosstalk with Other Innate Receptors in Infection and Immunity*. DOI: 10.1016/j.immuni.2011.05.006.

Kell, Douglas B (Jan. 2009). "Iron behaving badly: Inappropriate iron chelation as a major contributor to the aetiology of vascular and other progressive inflammatory and degenerative diseases". In: *BMC Medical Genomics* 2, p. 2. DOI: 10.1186/1755-8794-2-2. URL: http://www.ncbi.nlm.nih.gov/pubmed/19133145%20http://www.pubmedcentral.nih.gov/articlerender.fcgi?artid=PMC2672098.

Kell, Douglas B. and Etheresia Pretorius (2015). "On the translocation of bacteria and their lipopolysaccharides between blood and peripheral locations in chronic, inflammatory diseases: the central roles of LPS and LPS-induced cell death". In: *Integrative Biology (United Kingdom)* 7.11, pp. 1339–1377. DOI: 10.1039/c5ib00158g.

Kim, Ho Min et al. (Sept. 2007). "Crystal Structure of the TLR4-MD-2 Complex with Bound Endotoxin Antagonist Eritoran". In: *Cell* 130.5, pp. 906–917. DOI: 10.1016/j.cell.2007.08.002.

Kite, Kerry Anne et al. (2022). "FcMBL magnetic bead-based MALDI-TOF MS rapidly identifies paediatric blood stream infections from positive blood cultures". In: *PLoS ONE* 17.11 November, pp. 1–16. DOI: 10.1371/journal.pone.0276777. URL: http://dx.doi.org/10.1371/journal.pone.0276777.

Konecny, Andrew J et al. (Dec. 2023). "50-color phenotyping of the human immune system with in-depth assessment of T cells and dendritic cells". In: *bioRxiv : the preprint server for biology*. DOI: 10.1101/2023.12.14.571745. URL: https://pubmed.ncbi.nlm.nih.gov/38168221/%20http://www.pubmedcentral.nih.gov/articlerender.fcgi?artid=PMC10760076.

Koymans, Kirsten J et al. (2015). "Structural basis for inhibition of TLR2 by staphylococcal superantigen-like protein 3 (SSL3)". In: *Proceedings of the National Academy of Sciences* 112.35, pp. 11018–11023. DOI: 10.1073/pnas.1502026112. URL: www.pnas.org/cgi/doi/10.1073/pnas.1502026112%20http://www.pnas.org/lookup/doi/10.1073/pnas.1502026112.

Krug, Anne et al. (2001). "Identification of CpG oligonucleotide sequences with high induction of IFN-α/β in plasmacytoid dendritic cells". In: *European Journal of Immunology* 31.7, pp. 2154–2163. DOI: 10.1002/1521-4141(200107)31:7<2154::AID-IMMU2154>3.0.CO;2-U.

Kudla, Grzegorz et al. (2006). "High guanine and cytosine content increases mRNA levels in mammalian cells". In: *PLoS Biology* 4.6, pp. 0933–0942. DOI: 10.1371/journal.pbio.0040180. URL: https://journals.plos.org/plosbiology/article?id=10.1371/journal.pbio.0040180.

Kulkarni, Atul and Jigeeshu Divatia (2013). "A prospective audit of costs of intensive care in cancer patients in India". In: *Indian Journal of Critical Care Medicine* 17.5, pp. 292–297. DOI: 10.4103/0972-5229.120321. URL: www.ijccm.org.

Kumar, Anand Aseem et al. (June 2006). "Duration of hypotension before initiation of effective antimicrobial therapy is the critical determinant of survival in human septic shock". In: *Critical Care Medicine* 34.6, pp. 1589–1596. DOI: 10.1097/01.CCM.0000217961.75225.E9. URL: https://insights.ovid.com/crossref?an=00003246-200606000-00001%20http://www.ncbi.nlm.nih.gov/pubmed/16625125.

Kumar, V. (Dec. 2020). "Toll-like receptors in sepsis-associated cytokine storm and their endogenous negative regulators as future immunomodulatory targets". In: *International Immunopharmacology* 89.October, p. 107087. DOI: 10.1016/j.intimp.2020.107087. URL: /pmc/articles/PMC7550173/%20/pmc/articles/PMC7550173/?report=abstract%20https://www.ncbi.nlm.nih.gov/pmc/articles/PMC7550173/%20https://doi.org/10.1016/j.intimp.2020.107087.

Kuper, Kristi M., Elizabeth A. Coyle, and Audrey Wanger (2012). "Antimicrobial susceptibility testing: A primer for clinicians". In: *Pharmacotherapy* 32.12, pp. 1112–1122. DOI: 10.1002/phar.1146.

Kwizera, Arthur, Emir Festic, and Martin W. Dünser (Dec. 2016). "What's new in sepsis recognition in resource-limited settings?" In: *Intensive Care Medicine* 42.12, pp. 2030–2033. DOI: 10.1007/s00134-016-4222-x. URL: /pmc/articles/PMC5106488/%20https://www.ncbi.nlm.nih.gov/pmc/articles/PMC5106488/.

Ladhani, Husayn A., Charles J. Yowler, and Jeffrey A. Claridge (Feb. 2021). *Burn Wound Colonization, Infection, and Sepsis*. DOI: 10.1089/sur.2020.346.

Lahanas, Sophie et al. (Oct. 2013). "Evaluation of the Alfred 60/AST device as a screening test for urinary tract infections." In: *Journal of clinical microbiology* 51.10, pp. 3406–8. DOI: 10.1128/JCM.01126-13. URL: http://www.ncbi.nlm.nih.gov/pubmed/23885005%20http://www.pubmedcentral.nih.gov/articlerender.fcgi?artid=PMC3811639.

Lam, L. K.Metthew et al. (Oct. 2021). "DNA binding to TLR9 expressed by red blood cells promotes innate immune activation and anemia". In: *Science Translational Medicine* 13.616, p. 1008. DOI: 10.1126/SCITRANSLMED.ABJ1008. URL: https://www.science.org/doi/10.1126/scitranslmed.abj1008.

Lamy, Brigitte et al. (2016). *How to optimize the use of blood cultures for the diagnosis of bloodstream infections? A state-of-the art*. DOI: 10.3389/fmicb.2016.00697. URL: http://www.ncbi.nlm.nih.gov/pubmed/27242721%20http://www.pubmedcentral.nih.gov/articlerender.fcgi?artid=PMC4863885.

Latz, Eicke et al. (Jan. 2004). "TLR9 signals after translocating from the ER to CpG DNA in the lysosome". In: *Nature Immunology* 5.2, pp. 190–198. DOI: 10.1038/ni1028. URL: https://www.nature.com/articles/ni1028.

Lee, Jung-Jae et al. (Jan. 2014). "Synthetic ligand-coated magnetic nanoparticles for microfluidic bacterial separation from blood." In: *Nano letters* 14.1, pp. 1–5. DOI: 10.1021/nl3047305. arXiv: 9809069v1 [arXiv:gr-qc]. URL: https://pubs.acs.org/sharingguidelines%20http://www.ncbi.nlm.nih.gov/pubmed/23367876.

Leligdowicz, Aleksandra and Michael A. Matthay (Mar. 2019). *Heterogeneity in sepsis: New biological evidence with clinical applications*. DOI: 10.1186/s13054-019-2372-2. URL: https://ccforum.biomedcentral.com/articles/10.1186/s13054-019-2372-2.

Lemaitre, Bruno et al. (Sept. 1996). "The dorsoventral regulatory gene cassette spatzle/Toll/Cactus controls the potent antifungal response in Drosophila adults". In: *Cell* 86.6, pp. 973–983. DOI: 10.1016/S0092-8674(00)80172-5.

Levy, Mitchell M. et al. (Apr. 2003). "2001 SCCM/ESICM/ACCP/ATS/SIS International Sepsis Definitions Conference". In: *Intensive Care Medicine*. Vol. 29. 4, pp. 530–538. DOI: 10.1007/s00134-003-1662-x. URL: http://www.ncbi.nlm.nih.gov/pubmed/12664219%20http://link.springer.com/10.1007/s00134-003-1662-x.

Li, Danyang and Minghua Wu (Dec. 2021). *Pattern recognition receptors in health and diseases*. DOI: 10.1038/s41392-021-00687-0. URL: /pmc/articles/PMC8333067/%20/pmc/articles/PMC8333067/?report=abstract%20https://www.ncbi.nlm.nih.gov/pmc/articles/PMC8333067/.

Li, Hui, Liang Liu, et al. (May 2020). *SARS-CoV-2 and viral sepsis: observations and hypotheses*. DOI: 10.1016/S0140-6736(20)30920-X. URL: http://www.thelancet.com/article/S014067362030920X/fulltext%20http://www.thelancet.com/article/S014067362030920X/abstract%20https://www.thelancet.com/journals/lancet/article/PIIS0140-6736(20)30920-X/abstract.

Liang, S. T., M. Ehrenberg, et al. (May 1999). "Decay of rpIN and lacZ mRNA in Escherichia coli". In: *Journal of Molecular Biology* 288.4, pp. 521–538. DOI: 10.1006/jmbi.1999.2710.

Liang, Yitao, Bin Zhang, et al. (2022). "Magnetic Immunosensor Coupled to Enzymatic Signal for Determination of Genomic DNA Methylation". In: *Biosensors* 12.3, pp. 1–12. DOI: 10.3390/bios12030162.

Lin, Donghai, Kenneth D. Harris, et al. (2018). "Nanostructured indium tin oxide electrodes immobilized with toll-like receptor proteins for label-free electrochemical detection of pathogen markers". In: *Sensors and Actuators, B: Chemical* 257, pp. 324–330. DOI: 10.1016/j.snb.2017.10.140. URL: http://dx.doi.org/10.1016/j.snb.2017.10.140.

Lin, Gu Lung, Joseph P. McGinley, et al. (2018). "Epidemiology and Immune Pathogenesis of Viral Sepsis". In: *Frontiers in Immunology* 9.September, pp. 1–21. DOI: 10.3389/fimmu.2018.02147.

Lin, Heng, Jun Yan, et al. (Jan. 2013). "Loss of immunity-supported senescence enhances susceptibility to hepatocellular carcinogenesis and progression in Toll-like receptor 2-deficient mice". In: *Hepatology* 57.1, pp. 171–182. DOI: 10.1002/hep.25991. URL: https://pubmed.ncbi.nlm.nih.gov/22859216/.

Lind, Nicholas A. et al. (2022). "Regulation of the nucleic acid-sensing Toll-like receptors". In: *Nature Reviews Immunology* 22.4, pp. 224–235. DOI: 10.1038/s41577-021-00577-0.

Lippeveld, Maxim et al. (Mar. 2020). "Classification of Human White Blood Cells Using Machine Learning for Stain-Free Imaging Flow Cytometry". In: *Cytometry Part A* 97.3, pp. 308–319. DOI: 10.1002/cyto.a.23920. URL: https://pubmed.ncbi.nlm.nih.gov/31688997/.

Liu, Guohong et al. (2016). "Epigenetic segregation of microbial genomes from complex samples using restriction endonucleases hpaii and McrB". In: *PLoS ONE* 11.1, pp. 1–18. DOI: 10.1371/journal.pone.0146064.

Lizardi, Paul M., Qin Yan, and Narendra Wajapeyee (2017). "Analysis of DNA methylation in mammalian cells". In: *Cold Spring Harbor Protocols* 2017.12, pp. 953–962. DOI: 10.1101/pdb.top094821.

Llor, Carl et al. (2017). "The STOP-AB trial protocol: Efficacy and safety of discontinuing patient antibiotic treatment when physicians no longer consider it necessary". In: *BMJ Open* 7.5, p. 15814. DOI: 10.1136/bmjopen-2016-015814. URL: http://bmjopen.bmj.com/.

Locke, Warwick J. et al. (2019). "DNA Methylation Cancer Biomarkers: Translation to the Clinic". In: *Frontiers in Genetics* 10.November, pp. 1–22. DOI: 10.3389/fgene.2019.01150.

Lopes, Ana Luisa Kalb et al. (Sept. 2016). "Development of a magnetic separation method to capture sepsis associated bacteria in blood". In: *Journal of Microbiological Methods* 128, pp. 96–101. DOI: 10.1016/j.mimet.2016.07.012. URL: https://www.sciencedirect.com/science/article/pii/S0167701216301841.

Lopes-Pires, Maria Elisa, Jéssica Oliveira Frade-Guanaes, and Gregory J. Quinlan (2022). "Clotting dysfunction in sepsis: A role for ros and potential for therapeutic intervention". In: *Antioxidants* 11.1. DOI: 10.3390/antiox11010088.

Luchner, Marina, Sören Reinke, and Anita Milicic (Jan. 2021). *Tlr agonists as vaccine adjuvants targeting cancer and infectious diseases*. DOI: 10.3390/pharmaceutics13020142. URL: https://www.mdpi.com/1999-4923/13/2/142/htm%20https://www.mdpi.com/1999-4923/13/2/142.

Lyngs, Ulrik (2019). "oxforddown: An Oxford University Thesis Template for R Markdown". In: *GitHub*. URL: https://github.com/ulyngs/oxforddown.

Machen, Alexandra, Tim Drake, and Yun F. (Wayne) Wang (Feb. 2014). "Same day identification and full panel antimicrobial susceptibility testing of bacteria from positive blood culture bottles made possible by a combined lysis-filtration method with MALDI-TOF VITEK mass spectrometry and the VITEK2 system". In: *PLoS ONE* 9.2. Ed. by Gilbert Greub, pp. 7–11. DOI: 10.1371/journal.pone.0087870. URL: https://dx.plos.org/10.1371/journal.pone.0087870.

Malek, Mehrnoush et al. (Feb. 2015). "FlowDensity: Reproducing manual gating of flow cytometry data by automated density-based cell population identification". In: *Bioinformatics* 31.4, pp. 606–607. DOI: 10.1093/bioinformatics/btu677. URL: /pmc/articles/PMC4325545/%20/pmc/articles/PMC4325545/?report=abstract%20https://www.ncbi.nlm.nih.gov/pmc/articles/PMC4325545/.

Mansur, Ashham et al. (June 2014). "The regulatory toll-like receptor 4 genetic polymorphism rs11536889 is associated with renal, coagulation and hepatic organ failure in sepsis patients". In: *Journal of Translational Medicine* 12.1, pp. 177–177. DOI: 10.1186/1479-5876-12-177. URL: https://www.ncbi.nlm.nih.gov/pmc/articles/pmid/24950711/?tool=EBI%20https://europepmc.org/article/MED/24950711.

Marcos-Fernández, Raquel et al. (June 2022). "Convergence of flow cytometry and bacteriology. Current and future applications: a focus on food and clinical microbiology". In: *Critical Reviews in Microbiology*, pp. 1–22. DOI: 10.1080/1040841x.2022.2086035. URL: https://www.tandfonline.com/doi/abs/10.1080/1040841X.2022.2086035.

Marsh-Wakefield, Felix M.D. et al. (Aug. 2021). *Making the most of high-dimensional cytometry data*. DOI: 10.1111/imcb.12456. URL: https://onlinelibrary.wiley.com/doi/full/10.1111/imcb.12456%20https:

//onlinelibrary.wiley.com/doi/abs/10.1111/imcb.12456%20https://onlinelibrary.wiley.com/doi/10.1111/imcb.12456.

Marsik, Claudia et al. (May 2003). "Endotoxaemia modulates Toll-like receptors on leucocytes in humans". In: *British Journal of Haematology* 121.4, pp. 653–656. DOI: 10.1046/j.1365-2141.2003.04350.x. URL: https://onlinelibrary.wiley.com/doi/full/10.1046/j.1365-2141.2003.04350.x%20https://onlinelibrary.wiley.com/doi/abs/10.1046/j.1365-2141.2003.04350.x%20https://onlinelibrary.wiley.com/doi/10.1046/j.1365-2141.2003.04350.x.

Mayall, R.M., M. Renaud-Young, N.W.C. Chan, et al. (Jan. 2017). "An electrochemical lipopolysaccharide sensor based on an immobilized Toll-Like Receptor-4". In: *Biosensors and Bioelectronics* 87, pp. 794–801. DOI: 10.1016/j.bios.2016.09.009. URL: https://linkinghub.elsevier.com/retrieve/pii/S0956566316308818.

Mayall, Robert M. M., Margaret Renaud-Young, Erin Gawron, et al. (Jan. 2019). "Enhanced Signal Amplification in a Toll-like Receptor-4 Biosensor Utilizing Ferrocene-Terminated Mixed Monolayers". In: *ACS Sensors* 4.1, pp. 143–151. DOI: 10.1021/acssensors.8b01069. URL: https://pubs.acs.org/doi/full/10.1021/acssensors.8b01069.

McCann, Chase D and Jeanne A Jordan (Apr. 2014). "Evaluation of MolYsis™ Complete5 DNA extraction method for detecting Staphylococcus aureus DNA from whole blood in a sepsis model using PCR/pyrosequencing". In: *Journal of Microbiological Methods* 99.1, pp. 1–7. DOI: 10.1016/j.mimet.2014.01.013. URL: http://www.ncbi.nlm.nih.gov/pubmed/24503182%20http://www.pubmedcentral.nih.gov/articlerender.fcgi?artid=PMC3976640.

Mcfarland, Joseph (Oct. 1907). "The nephelometer: An instrument for estimating the number of bacteria in suspensions used for calculating the opsonic index and for vaccines". In: *Journal of the American Medical Association* XLIX.14, pp. 1176–1178. DOI: 10.1001/jama.1907.25320140022001f. URL: https://jamanetwork.com/journals/jama/fullarticle/444820.

McLeod, Jennifer et al. (Sept. 2020). "Developing a toll-like receptor biosensor for Gram-positive bacterial detection and its storage strategies". In: *Analyst* 145.18, pp. 6024–6031. DOI: 10.1039/d0an01050b. URL: https://pubs.rsc.org/en/content/articlehtml/2020/an/d0an01050b%20https://pubs.rsc.org/en/content/articlelanding/2020/an/d0an01050b.

Mcomber, Ryan (2013). "A Generic Pathogen Capture Technology for Sepsis Diagnosis". PhD thesis.

Medzhitov, Ruslan, Paula Preston-Hurlburt, and Charles A. Janeway (1997). "A human homologue of the Drosophila toll protein signals activation of adaptive immunity". In: *Nature* 388.6640, pp. 394–397. DOI: 10.1038/41131. URL: https://www.nature.com/articles/41131.

Mellor, Julie (2013). *TIME TO ACT: Severe sepsis - rapid diagnosis and treatment saves lives*. Tech. rep.

Messacar, Kevin et al. (2017). "Clinical impact and provider acceptability of real-time antimicrobial stewardship decision support for rapid diagnostics in children with positive blood culture results". In: *Journal of the Pediatric Infectious Diseases Society* 6.3, pp. 267–274. DOI: 10.1093/jpids/piw047.

Miles, A. A., S. S. Misra, and J. O. Irwin (1938). "The estimation of the bactericidal power of the blood". In: *Journal of Hygiene* 38.6, pp. 732–749. DOI: 10.1017/S002217240001158X.

Minasyan, Hayk (Feb. 2019). *Sepsis: Mechanisms of bacterial injury to the patient*. DOI: 10.1186/s13049-019-0596-4. URL: /pmc/articles/PMC6376788/%20/pmc/articles/PMC6376788/?report=abstract%20https://www.ncbi.nlm.nih.gov/pmc/articles/PMC6376788/.

Mogensen, Trine H (2009). *Pathogen recognition and inflammatory signaling in innate immune defenses*. DOI: 10.1128/CMR.00046-08. URL: https://www.ncbi.nlm.nih.gov/pmc/articles/PMC2668232/pdf/0046-08.pdf.

Monneret, Guillaume et al. (2019). "How Clinical Flow Cytometry Rebooted Sepsis Immunology". In: *Cytometry Part A* 95.4, pp. 431–441. DOI: 10.1002/cyto.a.23749.

Moor, Kathrin et al. (July 2016). "Analysis of bacterial-surface-specific antibodies in body fluids using bacterial flow cytometry". In: *Nature Protocols* 11.8, pp. 1531–1553. DOI: 10.1038/nprot.2016.091. URL: https://www.nature.com/articles/nprot.2016.091%20https://www.nature.com/articles/nprot.2016.091/.

Moschou, Despina and Angeliki Tserepi (Apr. 2017). *The lab-on-PCB approach: tackling the μTAS commercial upscaling bottleneck*. DOI: 10.1039/c7lc00121e. URL: http://xlink.rsc.org/?DOI=C7LC00121E.

Mostel, Zachary et al. (Dec. 2019). "Post-sepsis syndrome - an evolving entity that afflicts survivors of sepsis". In: *Molecular medicine (Cambridge, Mass.)* 26.1. DOI: 10.1186/S10020-019-0132-Z. URL: https://pubmed.ncbi.nlm.nih.gov/31892321/.

Moutzouri, Antonia G. et al. (Jan. 2007). "Red blood cell deformability in patients with sepsis: A marker for prognosis and monitoring of severity". In: *Clinical Hemorheology and Microcirculation* 36.4, pp. 291–299.

Müller, Vilhelm and Fredrik Westerlund (2017). "Optical DNA mapping in nanofluidic devices: principles and applications". In: *Lab Chip* 17.4, pp. 579–590. DOI: 10.1039/C6LC01439A. URL: http://xlink.rsc.org/?DOI=C6LC01439A.

Murphy, Kenneth M (2014). *Janeway's Immunobiology*. 8th. Garland Science. DOI: 10.1007/s13398-014-0173-7.2. arXiv: arXiv:1011.1669v3.

Nadkarni, Mangala A et al. (Jan. 2002). "Determination of bacterial load by real-time PCR using a broad-range (universal) probe and primers set". In: *Microbiology* 148.1, pp. 257–266. DOI: 10.1099/00221287-148-1-257. URL: https://www.microbiologyresearch.org/content/journal/micro/10.1099/00221287-148-1-257.

Nakayama, Yuki et al. (2016). "Pitfalls of DNA quantification using dnabinding fluorescent dyes and suggested solutions". In: *PLoS ONE* 11.3. DOI: 10.1371/journal.pone.0150528. URL: http://www.mext.go.jp/.

Nassar, Mariam et al. (2019). "Label-Free Identification of White Blood Cells Using Machine Learning". In: *Cytometry Part A* 95.8, pp. 836–842. DOI: 10.1002/cyto.a.23794. URL: https://pubmed.ncbi.nlm.nih.gov/31081599/.

Neth, Olaf et al. (Feb. 2000). "Mannose-binding lectin binds to a range of clinically relevant microorganisms and promotes complement deposition". In: *Infection and Immunity* 68.2, pp. 688–693. DOI: 10.1128/IAI.68.2.688-693.2000. URL: https://journals.asm.org/journal/iai%20https://journals.asm.org/doi/10.1128/IAI.68.2.688-693.2000.

Ngamsom, Bongkot et al. (Sept. 2017). "A Microfluidic Device for Rapid Screening of E. coli O157:H7 Based on IFAST and ATP Bioluminescence Assay for Water Analysis". In: *Chemistry - A European Journal* 23.52, pp. 12754–12757. DOI: 10.1002/chem.201703487. URL: http://doi.wiley.com/10.1002/chem.201703487.

Ngo, Vu N. et al. (Feb. 2011). "Oncogenically active MYD88 mutations in human lymphoma". In: *Nature* 470.7332, pp. 115–121. DOI: 10.1038/nature09671. URL: https://pubmed.ncbi.nlm.nih.gov/21179087/.

Ngoi, Soo Tein et al. (Mar. 2021). "Genomic analysis revealed a novel genotype of methicillin-susceptible Staphylococcus aureus isolated from a fatal sepsis case in dengue patient". In: *Scientific Reports* 11.1, pp. 1–12. DOI: 10.1038/s41598-021-83661-8. URL: https://www.nature.com/articles/s41598-021-83661-8.

Niederman, Michael S. et al. (Dec. 2021). *Initial antimicrobial management of sepsis*. DOI: 10.1186/s13054-021-03736-w. URL: https://ccforum.biomedcentral.com/articles/10.1186/s13054-021-03736-w.

Nishida, Hiromi (July 2013). "Genome DNA Sequence Variation, Evolution, and Function in Bacteria and Archaea". In: *Current issues in molecular biology* 15.1, pp. 19–24. DOI: 10.21775/cimb.015.019. URL: https://www.mdpi.com/1467-3045/15/1/3.

O'neill, Jim (2016). *TACKLING DRUG-RESISTANT INFECTIONS GLOBALLY: FINAL REPORT AND RECOMMENDATIONS THE REVIEW ON ANTIMICROBIAL RESISTANCE*. Tech. rep. May. DOI: 10.1016/j.jpha.2015.11.005. arXiv: arXiv:1011.1669v3. URL: https://amr-review.org/sites/default/files/160525%7B%5C_%7DFinal%20paper%7B%5C_%7Dwith%20cover.pdf.

Oeschger, Taylor et al. (2019). "Point of care technologies for sepsis diagnosis and treatment". In: *Lab on a Chip* 19.5, pp. 728–737. DOI: 10.1039/c8lc01102h. URL: http://xlink.rsc.org/?DOI=C8LC01102H.

Ohto, Umeharu, Hanako Ishida, et al. (2018). "Toll-like Receptor 9 Contains Two DNA Binding Sites that Function Cooperatively to Promote Receptor Dimerization and Activation". In: *Immunity*, pp. 1–10. DOI: 10.1016/j.immuni.2018.03.013. URL: https://doi.org/10.1016/j.immuni.2018.03.013.

Ohto, Umeharu, Takuma Shibata, et al. (2015). "Structural basis of CpG and inhibitory DNA recognition by Toll-like receptor 9". In: *Nature* 520.7549, pp. 702–705. DOI: 10.1038/nature14138.

Opal, Steven M. et al. (2014). "The next generation of sepsis clinical trial designs: What is next after the demise of recombinant human activated protein C?" In: *Critical Care Medicine* 42.7, pp. 1714–1721. DOI: 10.1097/CCM.0000000000000325. URL: https://pubmed.ncbi.nlm.nih.gov/24717456/.

Opota, O., A. Croxatto, et al. (Apr. 2015). *Blood culture-based diagnosis of bacteraemia: State of the art*. DOI: 10.1016/j.cmi.2015.01.003. URL: https://www.sciencedirect.com/science/article/pii/S1198743X15001834%7B%5C#%7Dfig1.

Opota, O., K. Jaton, and G. Greub (Apr. 2015). *Microbial diagnosis of bloodstream infection: Towards molecular diagnosis directly from blood*. DOI: 10.1016/j.cmi.2015.02.005. URL: https://ac.els-cdn.com/S1198743X15002931/1-s2.0-S1198743X15002931-main.pdf?%7B%5C_%7Dtid=b3c5252c-7228-4c00-b2f7-27450f1785aa%7B%5C&%7Dacdnat=1528036352%7B%5C_

%7D687ef58683e69b13ddf0eccbf7d12379%20https://www.sciencedirect.com/science/article/pii/S1198743X15002931%7B%5C#%7Dfig2%20https://www.sc.

Outterson, Kevin and Anthony McDonnell (Aug. 2016). "Funding antibiotic innovation with vouchers: Recommendations on how to strengthen a flawed incentive policy". In: *Health Affairs* 35.5, pp. 784–790. DOI: 10.1377/hlthaff.2015.1139.

Paau, A. S., J. R. Cowles, and J. Oro (1977). "Flow microfluorometric analysis of Escherichia coli, Rhizobium meliloti, and Rhizobium japonicum at different stages of the growth cycle". In: *Canadian Journal of Microbiology* 23.9, pp. 1165–1169. DOI: 10.1139/m77-175. URL: https://cdnsciencepub.com/doi/10.1139/m77-175.

Paik, Hyojung et al. (2018). "Tracing diagnosis trajectories over millions of inpatients reveal an unexpected association between schizophrenia and rhabdomyolysis". In: *bioRxiv*, p. 473082. DOI: 10.1101/473082. URL: http://dx.doi.org/10.1101/473082%20https://www.biorxiv.org/content/early/2018/11/19/473082.

Païssé, Sandrine et al. (May 2016). "Comprehensive description of blood microbiome from healthy donors assessed by 16S targeted metagenomic sequencing". In: *Transfusion* 56.5, pp. 1138–1147. DOI: 10.1111/trf.13477. URL: http://doi.wiley.com/10.1111/trf.13477.

Paladines, Lucas et al. (May 2022). "Investigation of Conditions for Capture of Live Legionella pneumophila with Polyclonal and Recombinant Antibodies". In: *Biosensors* 12.6, p. 380. DOI: 10.3390/bios12060380. URL: https://www.mdpi.com/2079-6374/12/6/380/htm%20https://www.mdpi.com/2079-6374/12/6/380.

Pan, Xichun et al. (2012). "Leucine-rich repeat 11 of toll-like receptor 9 can tightly bind to CpG-containing oligodeoxynucleotides, and the positively charged residues are critical for the high affinity". In: *Journal of Biological Chemistry* 287.36, pp. 30596–30609. DOI: 10.1074/jbc.M112.396432. URL: http://dx.doi.org/10.1074/jbc.M112.396432.

Park, Beom Seok and Jie Oh Lee (Dec. 2013). *Recognition of lipopolysaccharide pattern by TLR4 complexes*. DOI: 10.1038/emm.2013.97. URL: https://www.nature.com/articles/emm201397.

Park, Lily M., Joanne Lannigan, and Maria C. Jaimes (Oct. 2020). "OMIP-069: Forty-Color Full Spectrum Flow Cytometry Panel for Deep Immunophenotyping of Major Cell Subsets in Human Peripheral Blood". In: *Cytometry Part A* 97.10, pp. 1044–1051. DOI: 10.1002/cyto.a.24213.

Pawaria, Sudesh, Krishna Moody, Patricia Busto, Kerstin Nündel, Chee-Ho Choi, et al. (2015). "Cutting Edge: DNase II Deficiency Prevents Activation of Autoreactive B Cells by Double-Stranded DNA Endogenous Ligands". In: *The Journal of Immunology* 194.4, pp. 1403–1407. DOI: 10.4049/jimmunol.1402893. URL: http://dx.doi.org/10.1016/j.earlhumdev.2015.09.003%7B%5C%%7D5Cnhttp://dx.doi.org/10.1016/j.earlhumdev.2014.01.002%7B%5C%%7D5Cnhttp://dx.doi.org/10.1016/S0378-3782(12)70006-3%7B%5C%%7D5Cnhttp://www.sciencedirect.com/science/article/pii/S2341287914000763%7B%5C%%7D5Cnhttp://dx.doi.org/10.1016/.

Pawaria, Sudesh, Krishna L. Moody, Patricia Busto, Kerstin Nündel, Rebecca Baum, et al. (2015). "An unexpected role for RNA-sensing toll-like receptors in a murine model of DNA accrual". In: *Clinical and Experimental Rheumatology* 33.5, pp. 70–73. URL: http://europepmc.org/backend/ptpmcrender.fcgi?accid=PMC5604322%7B%5C&%7Dblobtype=pdf.

Petrosillo, Nicola et al. (Jan. 2020). *Preventing sepsis development in complicated urinary tract infections*. DOI: 10.1080/14787210.2020.1700794. URL: https://www.tandfonline.com/doi/abs/10.1080/14787210.2020.1700794.

Pham-Ledard, Anne et al. (Nov. 2014). "High frequency and clinical prognostic value of MYD88 L265P mutation in primary cutaneous diffuse large B-cell lymphoma, leg-type". In: *JAMA Dermatology* 150.11, pp. 1173–1179. DOI: 10.1001/jamadermatol.2014.821. URL: https://europepmc.org/article/MED/25055137.

Phanse, Yashdeep et al. (June 2012). "Analyzing cellular internalization of nanoparticles and bacteria by multi-spectral imaging flow cytometry". In: *Journal of Visualized Experiments* 64, e3884. DOI: 10.3791/3884. URL: https://www.jove.com/v/3884/analyzing-cellular-internalization-nanoparticles-bacteria-multi.

Phua, Jason et al. (Sept. 2013). "Characteristics and outcomes of culture-negative versus culture-positive severe sepsis". In: *Critical Care* 17.5, R202. DOI: 10.1186/cc12896. URL: /pmc/articles/PMC4057416/%20/pmc/articles/PMC4057416/?report=abstract%20https://www.ncbi.nlm.nih.gov/pmc/articles/PMC4057416/.

Pinault, Lucile et al. (Apr. 2019). "Direct Identification of Pathogens in Urine by Use of a Specific Matrix-Assisted Laser Desorption Ionization-Time of Flight Spectrum Database". In: *Journal of clinical microbiology* 57.4. DOI: 10.1128/JCM.01678-18. URL: http://www.ncbi.nlm.nih.gov/pubmed/30700506%20http://www.pubmedcentral.nih.gov/articlerender.fcgi?artid=PMC6440795.

Piovesan, Allison et al. (Feb. 2019). "On the length, weight and GC content of the human genome". In: *BMC Research Notes* 12.1, pp. 1–7. DOI: 10.1186/s13104-019-4137-z. URL: https://bmcresnotes.biomedcentral.com/articles/10.1186/s13104-019-4137-z.

Pliakos, Elina Eleftheria et al. (2018). "The cost-effectiveness of rapid diagnostic testing for the diagnosis of bloodstream infections with or without antimicrobial stewardship". In: *Clinical Microbiology Reviews* 31.3, pp. 1–22. DOI: 10.1128/CMR.00095-17. URL: http://www.ncbi.nlm.nih.gov/pubmed/29848775%20http://www.pubmedcentral.nih.gov/articlerender.fcgi?artid=PMC6056844.

Ploppa, Annette et al. (Sept. 2011). "ImageStream cytometry extends the analysis of phagocytosis and oxidative burst". In: *Scandinavian Journal of Clinical and Laboratory Investigation* 71.5, pp. 362–369. DOI: 10.3109/00365513.2011.572182. URL: https://www.tandfonline.com/doi/full/10.3109/00365513.2011.572182%20https://www.tandfonline.com/doi/abs/10.3109/00365513.2011.572182.

Pohar, Jelka et al. (2015). "Minimal Sequence Requirements for Oligodeoxyribonucleotides Activating Human TLR9". In: *The Journal of Immunology* 194.8, pp. 3901–3908. DOI: 10.4049/jimmunol.1402755.

Pool, Rachel, Hernando Gomez, and John A Kellum (Jan. 2018). "Mechanisms of Organ Dysfunction in Sepsis". In: *Critical Care Clinics* 34.1, pp. 63–80. DOI: 10.1016/j.ccc.2017.08.003. URL: http://www.ncbi.nlm.nih.gov/pubmed/29149942%20http://www.pubmedcentral.nih.gov/articlerender.fcgi?artid=PMC6922007%20https://linkinghub.elsevier.com/retrieve/pii/S0749070417300684.

Potgieter, Marnie et al. (July 2015). "The dormant blood microbiome in chronic, inflammatory diseases". In: *FEMS Microbiology Reviews* 39.4. Ed. by

Prof. Antoine Danchin, pp. 567–591. DOI: 10.1093/femsre/fuv013. URL: https://academic.oup.com/femsre/article-lookup/doi/10.1093/femsre/fuv013.

Radstake, Timothy R.D.J. et al. (Dec. 2004). "Expression of toll-like receptors 2 and 4 in rheumatoid synovial tissue and regulation by proinflammatory cytokines interleukin-12 and interleukin-18 via interferon-γ". In: *Arthritis and Rheumatism* 50.12, pp. 3856–3865. DOI: 10.1002/art.20678. URL: https://pubmed.ncbi.nlm.nih.gov/15593217/.

Reboud, Julien et al. (Mar. 2019). "Paper-based microfluidics for DNA diagnostics of malaria in low resource underserved rural communities". In: *Proceedings of the National Academy of Sciences of the United States of America* 116.11, pp. 4834–4842. DOI: 10.1073/pnas.1812296116. URL: http://www.ncbi.nlm.nih.gov/pubmed/30782834%20http://www.pubmedcentral.nih.gov/articlerender.fcgi?artid=PMC6421471.

Reddy, B. et al. (Sept. 2018). "Point-of-care sensors for the management of sepsis". In: *Nature Biomedical Engineering* 2.9, pp. 640–648. DOI: 10.1038/s41551-018-0288-9. URL: http://www.nature.com/articles/s41551-018-0288-9%20http://dx.doi.org/10.1038/s41551-018-0288-9.

Reyes, Miguel et al. (Feb. 2020). *An immune-cell signature of bacterial sepsis*. DOI: 10.1038/s41591-020-0752-4. URL: https://www.nature.com/articles/s41591-020-0752-4.

Robinson, J. Paul et al. (July 2023). *Flow Cytometry: The Next Revolution*. DOI: 10.3390/cells12141875. URL: https://www.mdpi.com/2073-4409/12/14/1875/htm%20https://www.mdpi.com/2073-4409/12/14/1875.

Rodriguez-Emmenegger, Cesar et al. (July 2011). "Polymer brushes showing non-fouling in blood plasma challenge the currently accepted design of protein resistant surfaces". In: *Macromolecular Rapid Communications* 32.13, pp. 952–957. DOI: 10.1002/marc.201100189. URL: http://doi.wiley.com/10.1002/marc.201100189.

Roederer, Mario (Oct. 2002). "Compensation in flow cytometry." In: *Current protocols in cytometry / editorial board, J. Paul Robinson, managing editor ... [et al.]* Chapter 1.1, pp. 1.14.1–1.14.20. DOI: 10.1002/0471142956.cy0114s22. URL: https://onlinelibrary.wiley.com/doi/full/10.1002/0471142956.cy0114s22%20https://onlinelibrary.wiley.com/doi/abs/10.1002/0471142956.cy0114s22%20https://currentprotocols.onlinelibrary.wiley.com/doi/10.1002/0471142956.cy0114s22.

Rosetto, Marco et al. (Apr. 1995). "Signals from the IL-1 receptor homolog, toll, can activate an immune response in a drosophila hemocyte cell line". In: *Biochemical and Biophysical Research Communications* 209.1, pp. 111–116. DOI: 10.1006/bbrc.1995.1477.

Rovas, Alexandros et al. (Nov. 2022). "Microvascular and proteomic signatures overlap in COVID-19 and bacterial sepsis: the MICROCODE study". In: *Angiogenesis* 25.4, pp. 503–515. DOI: 10.1007/s10456-022-09843-8.

Rudd, Kristina E. et al. (2020). "Global, regional, and national sepsis incidence and mortality, 1990–2017: analysis for the Global Burden of Disease Study". In: *The Lancet* 395.10219, pp. 200–211. DOI: 10.1016/S0140-6736(19)32989-7. URL: http://dx.doi.org/10.1016/S0140-6736(19)32989-7.

Russell, Clark D. and J. Kenneth Baillie (2017). "Treatable traits and therapeutic targets: Goals for systems biology in infectious disease". In: *Current Opinion in*

Systems Biology 2, pp. 140–146. DOI: 10.1016/j.coisb.2017.04.003. URL: http://dx.doi.org/10.1016/j.coisb.2017.04.003.

Rutherford, Andrew I. et al. (Dec. 2016). "A population study of the reported incidence of native joint septic arthritis in the United Kingdom between 1998 and 2013". In: *Rheumatology (United Kingdom)* 55.12, pp. 2176–2180. DOI: 10.1093/rheumatology/kew323. URL: https://academic.oup.com/rheumatology/article-lookup/doi/10.1093/rheumatology/kew323.

Rutz, Mark et al. (2004). "Toll-like receptor 9 binds single-stranded CpG-DNA in a sequence- and pH-dependent manner". In: *European Journal of Immunology* 34.9, pp. 2541–2550. DOI: 10.1002/eji.200425218.

Saeys, Yvan, Sofie Van Gassen, and Bart N. Lambrecht (June 2016). *Computational flow cytometry: Helping to make sense of high-dimensional immunology data*. DOI: 10.1038/nri.2016.56. URL: https://www.nature.com/articles/nri.2016.56.

Sankar, Saranya et al. (May 2022). "Global DNA hypomethylation and the expression profile of DNA methyltransferase genes in late-onset neonatal sepsis". In: *Epigenomics* 14.11, pp. 671–682. DOI: 10.2217/epi-2022-0040. URL: https://www.futuremedicine.com/doi/10.2217/epi-2022-0040.

Sansonetti, Philippe J. (2006). "The bacterial weaponry: Lessons from Shigella". In: *Annals of the New York Academy of Sciences*. Vol. 1072. Blackwell Publishing Inc., pp. 307–312. DOI: 10.1196/annals.1326.025.

Scheepers, M. R. W., L. J. van IJzendoorn, and M. W. J. Prins (Oct. 2019). "Single-Dimer Formation Rate Reveals Heterogeneous Particle Surface Reactivity". In: *Langmuir*, acs.langmuir.9b02199. DOI: 10.1021/acs.langmuir.9b02199. URL: https://pubs.acs.org/doi/10.1021/acs.langmuir.9b02199%20https://pubs.acs.org/doi/pdf/10.1021/acs.langmuir.9b02199.

Schmidt, Matthieu et al. (Dec. 2012). "Nosocomial infections in adult cardiogenic shock patients supported by venoarterial extracorporeal membrane oxygenation". In: *Clinical Infectious Diseases* 55.12, pp. 1633–1641. DOI: 10.1093/cid/cis783. URL: /pmc/articles/PMC3888098/%20/pmc/articles/PMC3888098/?report=abstract%20https://www.ncbi.nlm.nih.gov/pmc/articles/PMC3888098/.

Schultz, Marcus J. et al. (May 2017). *Current challenges in the management of sepsis in ICUs in resource-poor settings and suggestions for the future*. DOI: 10.1007/s00134-017-4750-z. URL: https://link.springer.com/article/10.1007/s00134-017-4750-z.

Scicluna, Brendon P. et al. (Dec. 2018). "The search for efficacious new therapies in sepsis needs to embrace heterogeneity." In: *American Journal of Respiratory and Critical Care Medicine*, rccm.201811–2148ED. DOI: 10.1164/rccm.201811-2148ED. URL: https://www.atsjournals.org/doi/pdf/10.1164/rccm.201811-2148ED%20https://www.atsjournals.org/doi/10.1164/rccm.201811-2148ED.

Scotland, Education (2023). *Sepsis – teacher resource and supporting materials | Resources | National Improvement Hub*. URL: https://education.gov.scot/resources/sepsis-teacher-resource-and-supporting-materials/ (visited on 07/04/2023).

Scottish Government (2019). *Raising awareness of sepsis*. URL: https://www.gov.scot/news/raising-awareness-of-sepsis/ (visited on 07/03/2023).

Sepehri, Zahra et al. (July 2016). *Toll-like receptor 2 and type 2 diabetes*. DOI: 10.1186/s11658-016-0002-4. URL: https://pubmed.ncbi.nlm.nih.gov/28536605/.

Sepsis Research FEAT | Sepsis Charity In UK And Awareness (2023). URL: https://sepsisresearch.org.uk/ (visited on 07/04/2023).

Seymour, Christopher W. et al. (June 2017). "Time to Treatment and Mortality during Mandated Emergency Care for Sepsis." In: *The New England journal of medicine* 376.23, pp. 2235–2244. DOI: 10.1056/NEJMoa1703058. URL: http://www.nejm.org/doi/10.1056/NEJMoa1703058%20http://www.ncbi.nlm.nih.gov/pubmed/28528569%7B%5C%%7D0Ahttp://www.pubmedcentral.nih.gov/articlerender.fcgi?artid=PMC5538258.

Shankar-Hari, M., C. Summers, and K. Baillie (2018). "In Pursuit of Precision Medicine in the Critically Ill". In: Springer, Cham, pp. 649–658. DOI: 10.1007/978-3-319-73670-9_48. URL: https://doi.org/10.1007/978-3-319-73670-9%7B%5C_%7D48.

Shankar-Hari, Manu, David A. Harrison, et al. (May 2019a). "Risk factors at index hospitalization associated with longer-term mortality in adult sepsis survivors". In: *JAMA Network Open* 2.5, e194900–e194900. DOI: 10.1001/jamanetworkopen.2019.4900. URL: https://jamanetwork.com/journals/jamanetworkopen/fullarticle/2734808.

— (2019b). "Risk factors at index hospitalization associated with longer-term mortality in adult sepsis survivors". In: *JAMA Network Open* 2.5, pp. 1–14. DOI: 10.1001/jamanetworkopen.2019.4900.

Sheng, Kuo-Ching et al. (May 2013). "Enhanced Dendritic Cell-Mediated Antigen-Specific CD4+ T Cell Responses: IFN-Gamma Aids TLR Stimulation". In: *Journal of Drug Delivery* 2013, pp. 1–9. DOI: 10.1155/2013/516749. URL: https://pubmed.ncbi.nlm.nih.gov/23781340/.

Sheu, Chau Chyun et al. (Jan. 2019). *Infections caused by carbapenem-resistant Enterobacteriaceae: An update on therapeutic options*. DOI: 10.3389/fmicb.2019.00080. URL: https://www.frontiersin.org/article/10.3389/fmicb.2019.00080/full.

Siddiqui, Shoib S. et al. (Mar. 2021). "Sialoglycan recognition is a common connection linking acidosis, zinc, and HMGB1 in sepsis". In: *Proceedings of the National Academy of Sciences of the United States of America* 118.10. DOI: 10.1073/pnas.2018090118. URL: https://pubmed.ncbi.nlm.nih.gov/33658363/.

Singer, Mervyn et al. (2016). "The third international consensus definitions for sepsis and septic shock (sepsis-3)". In: *JAMA - Journal of the American Medical Association* 315.8, pp. 801–810. DOI: 10.1001/jama.2016.0287.

Singh, Ishwar et al. (2021). "N-Heterocyclic carbenes meet toll-like receptors". In: *Chemical Communications* 57.68, pp. 8421–8424. DOI: 10.1039/d1cc03030b.

Sjölinder, Hong et al. (Nov. 2008). "Important role for toll-like receptor 9 in host defense against meningococcal sepsis". In: *Infection and Immunity* 76.11, pp. 5421–5428. DOI: 10.1128/IAI.00615-08. URL: https://pubmed.ncbi.nlm.nih.gov/18794294/.

Skarstad, K., H. B. Steen, and E. Boye (1983). "Cell cycle parameters of slowly growing Escherichia coli B/r studied by flow cytometry". In: *Journal of Bacteriology* 154.2, pp. 656–662. DOI: 10.1128/jb.154.2.656-662.1983. URL: https://pubmed.ncbi.nlm.nih.gov/6341358/.

Song, Qi et al. (May 2021). *Point-of-care testing detection methods for COVID-19*. DOI: 10.1039/d0lc01156h. URL: https://pubs.rsc.org/en/content/articlehtml/2021/lc/d0lc01156h%20https://pubs.rsc.org/en/content/articlelanding/2021/lc/d0lc01156h.

Sonneville, Romain et al. (May 2013). "Understanding brain dysfunction in sepsis". In: *Annals of Intensive Care* 3.1, p. 15. DOI: 10.1186/2110-5820-3-15. URL: http://annalsofintensivecare.springeropen.com/articles/10.1186/2110-5820-3-15.

Sorgenfrei, Michèle et al. (Aug. 2022). *Biomolecules capturing live bacteria from clinical samples*. DOI: 10.1016/j.tibs.2022.03.018.

Steel, Lynsey et al. (2016). "Towards Simple , Rapid Point of Care Testing for Clinically Important Protein Biomarkers of Sepsis". In: *SCIOL Biotechnol* 1, pp. 1–8. URL: https://pure.strath.ac.uk/ws/portalfiles/portal/72281321/Steel%7B%5C_%7Detal%7B%5C_%7DSB%7B%5C_%7D2017%7B%5C_%7DTowards%7B%5C_%7Dsimple%7B%5C_%7Drapid%7B%5C_%7Dpoint%7B%5C_%7Dof%7B%5C_%7Dcare%7B%5C_%7Dtesting%7B%5C_%7Dfor%7B%5C_%7Dclinically%7B%5C_%7Dimportant%7B%5C_%7Dprotein%7B%5C_%7Dbiomarkers%7B%5C_%7Dof%7B%5C_%7Dsepsis.pdf.

Steen, Harald B (2000). "Flow cytometry of bacteria: Glimpses from the past with a view to the future". In: *Journal of Microbiological Methods* 42.1, pp. 65–74. DOI: 10.1016/S0167-7012(00)00177-9. URL: www.elsevier.com/locate/jmicmeth.

Steen, Harald B. et al. (1982). "Applications of flow cytometry on bacteria: Cell cycle kinetics, drug effects, and quantitation of antibody binding". In: *Cytometry* 2.4, pp. 249–257. DOI: 10.1002/cyto.990020409.

Suwannalai, Parawee et al. (Feb. 2012). *Anti-citrullinated protein antibodies (ACPA) in early rheumatoid arthritis*. DOI: 10.1007/s10165-011-0486-8. URL: https://pubmed.ncbi.nlm.nih.gov/21732051/.

Sweeney, Timothy E. et al. (Dec. 2018). "A community approach to mortality prediction in sepsis via gene expression analysis". In: *Nature Communications* 9.1, p. 22. DOI: 10.1038/s41467-018-03078-2. URL: www.nature.com/naturecommunications.

Tan, Cedric C.S. et al. (July 2022). "No evidence for a common blood microbiome based on a population study of 9,770 healthy humans". In: *bioRxiv* 10, p. 2022.07.29.502098. DOI: 10.1101/2022.07.29.502098. URL: https://www.biorxiv.org/content/10.1101/2022.07.29.502098v1%20https://www.biorxiv.org/content/10.1101/2022.07.29.502098v1.abstract%20https://www.biorxiv.org/content/10.1101/2022.07.29.502098v1%7B%5C%%7D0Ahttps://www.biorxiv.org/content/10.1101/2022.07.29.502098v1.abst.

Taneja, Ishan et al. (2017). "Combining Biomarkers with EMR Data to Identify Patients in Different Phases of Sepsis". In: *Scientific Reports* 7.1, p. 10800. DOI: 10.1038/s41598-017-09766-1. URL: http://www.ncbi.nlm.nih.gov/pubmed/28883645%20http://www.pubmedcentral.nih.gov/articlerender.fcgi?artid=PMC5589821.

Tao, Zhi et al. (Aug. 2015). "High-performance Quantum Dots decorated graphene/ZnO-nanowire field-emission type field-effect transistor". In: *IVNC 2015 - Technical Digest: 28th International Vacuum Nanoelectronics Conference*. Institute of Electrical and Electronics Engineers Inc., pp. 138–139. DOI: 10.1109/IVNC.2015.7225559.

Teijaro, John R. (July 2017). *Cytokine storms in infectious diseases*. DOI: 10.1007/s00281-017-0640-2. URL: https://link.springer.com/article/10.1007/s00281-017-0640-2.

Thoendel, Matthew et al. (2016). "Comparison of microbial DNA enrichment tools for metagenomic whole genome sequencing". In: *Journal of Microbiological Methods* 127, pp. 141–145. DOI: 10.1016/j.mimet.2016.05.022. URL: http://dx.doi.org/10.1016/j.mimet.2016.05.022.%20http://dx.doi.org/10.1016/j.mimet.2016.05.022.

To, Eunice E. et al. (Feb. 2019). "Intranasal and epicutaneous administration of Toll-like receptor 7 (TLR7) agonists provides protection against influenza A virus-induced morbidity in mice". In: *Scientific Reports* 9.1, pp. 1–15. DOI: 10.1038/s41598-019-38864-5. URL: https://www.nature.com/articles/s41598-019-38864-5.

Tost, Jörg (Jan. 2010). *DNA methylation: An introduction to the biology and the disease-associated changes of a promising biomarker*. DOI: 10.1007/s12033-009-9216-2. URL: http://link.springer.com/10.1007/s12033-009-9216-2.

Townsend, R. et al. (Jan. 2001). "Differential recognition of obligate anaerobic bacteria by human mannose-binding lectin". In: *Clinical and Experimental Immunology* 124.2, pp. 223–228. DOI: 10.1046/j.1365-2249.2001.01549.x. URL: https://academic.oup.com/cei/article/124/2/223/6461460.

Towse, Adrian et al. (Oct. 2017). "Time for a change in how new antibiotics are reimbursed: Development of an insurance framework for funding new antibiotics based on a policy of risk mitigation". In: *Health Policy* 121.10, pp. 1025–1030. DOI: 10.1016/j.healthpol.2017.07.011.

Tripathy, Archana et al. (Dec. 2017). "Direct recognition of LPS drive TLR4 expressing CD8+ T cell activation in patients with rheumatoid arthritis". In: *Scientific Reports* 7.1. DOI: 10.1038/s41598-017-01033-7. URL: https://pubmed.ncbi.nlm.nih.gov/28424490/.

Trung, Ngo Tat, Tran Thi Thu Hien, et al. (2016). "Enrichment of bacterial DNA for the diagnosis of blood stream infections". In: *BMC Infectious Diseases* 16.1, pp. 1–9. DOI: 10.1186/s12879-016-1568-1. URL: http://dx.doi.org/10.1186/s12879-016-1568-1.

Trung, Ngo Tat, Nguyen Sy Thau, et al. (Dec. 2019). "PCR-based Sepsis@Quick test is superior in comparison with blood culture for identification of sepsis-causative pathogens". In: *Scientific Reports* 9.1, p. 13663. DOI: 10.1038/s41598-019-50150-y. URL: http://www.nature.com/articles/s41598-019-50150-y.

Tsujimoto, Hironori et al. (2008). "Role of toll-like receptors in the development of sepsis". In: *Shock* 29.3, pp. 315–321. DOI: 10.1097/SHK.0b013e318157ee55.

Turley, Shannon J. et al. (Apr. 2000). "Transport of peptide-MHC class II complexes in developing dendritic cells". In: *Science* 288.5465, pp. 522–527. DOI: 10.1126/science.288.5465.522. URL: https://pubmed.ncbi.nlm.nih.gov/10775112/.

Turner, Malcolm W. (Nov. 1996). *Mannose-binding lectin: The pluripotent molecule of the innate immune system*. DOI: 10.1016/S0167-5699(96)80908-X.

Ussery, David W (May 2002). "DNA Structure: A-, B- and Z-DNA Helix Families". In: *Encyclopedia of Life Sciences*. John Wiley & Sons, Ltd. DOI: 10.1038/npg.els.0003122. URL: https:

//onlinelibrary.wiley.com/doi/full/10.1038/npg.els.0003122%20https://onlinelibrary.wiley.com/doi/abs/10.1038/npg.els.0003122%20https://onlinelibrary.wiley.com/doi/10.1038/npg.els.0003122.

Van Andel, Esther et al. (Feb. 2019). "Systematic Comparison of Zwitterionic and Non-Zwitterionic Antifouling Polymer Brushes on a Bead-Based Platform". In: *Langmuir* 35.5, pp. 1181–1191. DOI: 10.1021/acs.langmuir.8b01832. URL: https://pubs.acs.org/doi/10.1021/acs.langmuir.8b01832.

Van Der Pol, E. et al. (May 2012). "Single vs. swarm detection of microparticles and exosomes by flow cytometry". In: *Journal of Thrombosis and Haemostasis* 10.5, pp. 919–930. DOI: 10.1111/j.1538-7836.2012.04683.x. URL: https://pubmed.ncbi.nlm.nih.gov/22394434/.

Vasselon, Thierry et al. (Dec. 2004). "TLR2 Recognizes a Bacterial Lipopeptide through Direct Binding". In: *The Journal of Immunology* 173.12, pp. 7401–7405. DOI: 10.4049/jimmunol.173.12.7401. URL: https://pubmed.ncbi.nlm.nih.gov/15585865/.

Vaure, Céline and Yuanqing Liu (2014). *A comparative review of toll-like receptor 4 expression and functionality in different animal species*. DOI: 10.3389/fimmu.2014.00316. URL: http://www.ncbi.nlm.nih.gov/pubmed/25071777%20http://www.pubmedcentral.nih.gov/articlerender.fcgi?artid=PMC4090903.

Ventola, C Lee (Apr. 2015). "The antibiotic resistance crisis: causes and threats." In: *P & T journal* 40.4, pp. 277–83. DOI: Article. arXiv: /ehis.ebscohost.com/ [http:]. URL: http://www.ncbi.nlm.nih.gov/pubmed/25859123%20http://www.pubmedcentral.nih.gov/articlerender.fcgi?artid=PMC4378521%20http://www.ncbi.nlm.nih.gov/pubmed/25859123%7B%5C%%7D5Cnhttp://www.pubmedcentral.nih.gov/articlerender.fcgi?artid=PMC4378521%7B%5C%%7D5Cnhttp://www.ncbi.nlm.nih.

Verdonk, Franck, Joe L. Hsu, and Brice Gaudilliere (2022). "From Mass to Flow: Emerging Sepsis Diagnostics Based on Flow Cytometry Analysis of Neutrophils". In: *American Journal of Respiratory and Critical Care Medicine* 205.1, pp. 2–4. DOI: 10.1164/rccm.202110-2291ED.

Vergnano, S. et al. (May 2005). *Neonatal sepsis: An international perspective*. DOI: 10.1136/adc.2002.022863. URL: https://fn.bmj.com/content/90/3/F220%20https://fn.bmj.com/content/90/3/F220.abstract.

Verma, Jyoti, Sangeeta Saxena, and Sunil G. Babu (2013). "ELISA-Based Identification and Detection of Microbes". In: pp. 169–186. DOI: 10.1007/978-3-642-34410-7_13.

Viemann, Dorothee et al. (Oct. 2005). "Expression of toll-like receptors in neonatal sepsis". In: *Pediatric Research* 58.4, pp. 654–659. DOI: 10.1203/01.PDR.0000180544.02537.FD. URL: https://www.nature.com/articles/pr2005719.

Viriyakosol, Suganya et al. (Oct. 2001). "MD-2 Binds to Bacterial Lipopolysaccharide". In: *Journal of Biological Chemistry* 276.41, pp. 38044–38051. DOI: 10.1074/jbc.m105228200.

Visintin, Alberto et al. (Jan. 2001). "Regulation of Toll-Like Receptors in Human Monocytes and Dendritic Cells". In: *The Journal of Immunology* 166.1, pp. 249–255. DOI: 10.4049/jimmunol.166.1.249.

Vutukuru, Manjula Ramya et al. (2016). "A rapid, highly sensitive and culture-free detection of pathogens from blood by positive enrichment". In: *Journal of Microbiological Methods* 131, pp. 105–109. DOI: 10.1016/j.mimet.2016.10.008. URL: http://dx.doi.org/10.1016/j.mimet.2016.10.008.

Wagner, Hermann (2004). "The immunobiology of the TLR9 subfamily". In: *Trends in Immunology* 25.7, pp. 381–386. DOI: 10.1016/j.it.2004.04.011.

Walberg, Mette and Harald B. Steen (Jan. 2001). "Flow cytometric monitoring of bacterial susceptibility to antibiotics". In: *Methods in Cell Biology* 64.64, pp. 553–566. DOI: 10.1016/s0091-679x(01)64029-9.

Walsh, Thomas J et al. (Jan. 2023). "Meeting the Challenges of Sepsis in Severe Coronavirus Disease 2019: A Call to Arms". In: *Open Forum Infectious Diseases* 10.1. DOI: 10.1093/ofid/ofac645.

Ward, C. et al. (2015). "Performance evaluation of the Verigene® (Nanosphere) and FilmArray® (BioFire®) molecular assays for identification of causative organisms in bacterial bloodstream infections". In: *European Journal of Clinical Microbiology and Infectious Diseases* 34.3, pp. 487–496. DOI: 10.1007/s10096-014-2252-2.

Waterhouse, Anna et al. (2018). "Advances in Critical Care Medicine Modified Clinical Monitoring Assessment Criteria for Multi-Organ Failure during Bacteremia and Sepsis Progression in a Pig Model". In: URL: http://www.scientificoajournals.org/pdf/ccm.1002.pdf.

Weinbren, M J et al. (2018). "Optimization of the blood culture pathway: a template for improved sepsis management and diagnostic antimicrobial stewardship". In: *Journal of Hospital Infection* 98.3, pp. 232–235. DOI: 10.1016/j.jhin.2017.12.023. URL: https://doi.org/10.1016/j.jhin.2017.12.023.

Wiesinger-Mayr, Herbert et al. (2011). "Establishment of a semi-automated pathogen DNA isolation from whole blood and comparison with commercially available kits". In: *Journal of Microbiological Methods* 85.3, pp. 206–213. DOI: 10.1016/j.mimet.2011.03.003. URL: https://pdf.sciencedirectassets.com/271084/1-s2.0-S0167701211X00064/1-s2.0-S0167701211001023/main.pdf?x-amz-security-token=AgoJb3JpZ2luX2VjEHcaCXVzLWVhc3QtMSJHMEUCIDjyg4CNkLNjGW6jLVgFfzzjmUI96Edi0%7B%5C%%7D2BBtulpfauOhAiEAhKuvmtzdt7%7B%5C%%7D2B7DuSc1ypfBkQbxZ37urheC5H3SdYN.

Wilson, J. et al. (2011). "Trends among pathogens reported as causing bacteraemia in England, 2004-2008". In: *Clinical Microbiology and Infection* 17.3, pp. 451–458. DOI: 10.1111/j.1469-0691.2010.03262.x. URL: http://dx.doi.org/10.1111/j.1469-0691.2010.03262.x.

Wong, Conroy, Lata Jayaram, and Leon Chang (2013). "Mannose-binding lectin and innate immunity in bronchiectasis". In: *The Lancet Respiratory Medicine* 1.3, pp. 179–180. DOI: 10.1016/S2213-2600(13)70010-9.

World Health Organisation (2020). *Global report on the epidemiology and burden of sepsis: current evidence, identifying gaps and future directions*. Tech. rep., p. 56. URL: http://apps.who.int/bookorders.%20http://apps.who.int/bookorders.%7B%5C%%7D0Ahttps://apps.who.int/iris/bitstream/handle/10665/334216/9789240010789-eng.pdf%20http://apps.who.int/bookorders.%7B%5C%%7D0Ahttp://apps.who.int/bookorders.%7B%5C%%7D0Ahttps://apps.who.int/iris/bitstream/handle/.

World Health Organization (2017). "WHO Publishes List of Bacteria for Which New Antibiotics Are Urgently Needed". In: *Saudi Med J* 38.4, pp. 444–445. URL: https://www.who.int/en/news-room/detail/27-02-2017-who-publishes-list-of-bacteria-for-which-new-antibiotics-are-urgently-needed%20https://www.who.int/news/item/27-02-2017-who-publishes-list-of-bacteria-for-which-new-antibiotics-are-urgently-needed.

Wu, Tianzhou et al. (2020). "Comprehensive transcriptome profiling of peripheral blood mononuclear cells from patients with sepsis". In: *International Journal of Medical Sciences* 17.14, pp. 2077–2086. DOI: 10.7150/ijms.46910.

Xagorari, Angeliki and Katerina Chlichlia (2008). "Toll-Like Receptors and Viruses: Induction of Innate Antiviral Immune Responses". In: *The Open Microbiology Journal* 2.1, pp. 49–59. DOI: 10.2174/1874285800802010049.

Yang, Huan, Bo Wang, et al. (2014). "Toll-like receptor 4 prompts human breast cancer cells invasiveness via lipopolysaccharide stimulation and is overexpressed in patients with lymph node metastasis". In: *PLoS ONE* 9.10. DOI: 10.1371/journal.pone.0109980. URL: https://pubmed.ncbi.nlm.nih.gov/25299052/.

Yang, Huan, Huiqin Zhou, et al. (2010). "Reduced expression of Toll-like receptor 4 inhibits human breast cancer cells proliferation and inflammatory cytokines secretion". In: *Journal of Experimental and Clinical Cancer Research* 29.1. DOI: 10.1186/1756-9966-29-92. URL: https://pubmed.ncbi.nlm.nih.gov/20618976/.

Yeaman, Michael R and Nannette Y Yount (2003). "Mechanisms of antimicrobial peptide action and resistance." In: *Pharmacological reviews* 55.1, pp. 27–55. DOI: 10.1124/pr.55.1.2. URL: http://pharmrev.aspetjournals.org.%20http://www.ncbi.nlm.nih.gov/pubmed/12615953.

Younis, Farah Qahtan, Ali Hussein Alwan, and Neihaya Heikmat Zaki (Nov. 2018). "Using of TLR2 and TLR4 as Biomarker of Sepsis Severity Detection". In: *Al-Mustansiriyah Journal of Science* 29.2, pp. 83–92. DOI: 10.23851/mjs.v29i2.370. URL: https://mjs.uomustansiriyah.edu.iq/index.php/MJS/article/view/370.

Yu, Sung Liang et al. (2004). "Differential gene expression in gram-negative and gram-positive sepsis". In: *American Journal of Respiratory and Critical Care Medicine* 169.10, pp. 1135–1143. DOI: 10.1164/rccm.200211-1278oc. URL: www.atsjournals.org.

Zhang, Qi Yu, Zhi Bin Yan, et al. (Sept. 2021). *Antimicrobial peptides: mechanism of action, activity and clinical potential*. DOI: 10.1186/s40779-021-00343-2. URL: https://mmrjournal.biomedcentral.com/articles/10.1186/s40779-021-00343-2.

Zhang, Yubin, Maura Jones, et al. (May 2013). "MyD88 Signaling in CD4 T Cells Promotes IFN-γ Production and Hematopoietic Progenitor Cell Expansion in Response to Intracellular Bacterial Infection". In: *The Journal of Immunology* 190.9, pp. 4725–4735. DOI: 10.4049/jimmunol.1203024. URL: https://dx.doi.org/10.4049/jimmunol.1203024.

Zhao, Yingchi et al. (July 2021). *SARS-CoV-2 spike protein interacts with and activates TLR41*. DOI: 10.1038/s41422-021-00495-9. URL: /pmc/articles/PMC7975240/%20https://www.ncbi.nlm.nih.gov/pmc/articles/PMC7975240/.

Zheng, Min et al. (July 2021). "TLR2 senses the SARS-CoV-2 envelope protein to produce inflammatory cytokines". In: *Nature Immunology* 22.7, pp. 829–838. DOI:

10.1038/s41590-021-00937-x. URL: https://pubmed.ncbi.nlm.nih.gov/33963333/.

Zhou, Yun et al. (Jan. 2019). "Combined CD25, CD64, and CD69 biomarker panel for flow cytometry diagnosis of sepsis". In: *Talanta* 191, pp. 216–221. DOI: 10.1016/j.talanta.2018.08.058.

Zhu, Yingdi et al. (2016). "Sensitive and fast identification of bacteria in blood samples by immunoaffinity mass spectrometry for quick BSI diagnosis". In: *Chemical Science* 7.5, pp. 2987–2995. DOI: 10.1039/c5sc04919a. URL: www.rsc.org/chemicalscience.

Zupančič, Uroš et al. (2021). "Graphene Enabled Low-Noise Surface Chemistry for Multiplexed Sepsis Biomarker Detection in Whole Blood". In: *Advanced Functional Materials* 2010638, p. 2010638. DOI: 10.1002/adfm.202010638.